AI-AEC-13096
NASA-CR-121241

5-kwe REACTOR
THERMOELECTRIC SYSTEM
SUMMARY

AEC Research and Development Report

Atomics International Division
Rockwell International

P.O. Box 309
Canoga Park, California 91304

AI-AEC-13096
SNAP REACTOR
SNAP PROGRAM
M-3679-R69
C-92b
NASA-CR-121241

5-kwe REACTOR

THERMOELECTRIC SYSTEM

SUMMARY

J. H. VAN OSDOL
Editor

Principal Contributors
R. V. ANDERSON
S. BERGER
W. H. DAUTERMAN
J. L. JOHNSON
V. KESHISHIAN
L. D. MONTGOMERY
T. T. SHIMAZAKI
R. J. TUTTLE
J. H. VAN OSDOL

Atomics International Division
Rockwell International

P.O. Box 309
Canoga Park, California 91304

CONTRACT: AT(04-3)-701
ISSUED: JULY 27, 1973

FOREWORD

The work described here was done at the Atomics International Division of Rockwell International Corporation, under the direction of the Space Nuclear Systems Division, a joint AEC-NASA office. Project management was provided by NASA-Lewis Research Center and the AEC-SNAP Project Office.

DISTRIBUTION

This report has been distributed according to the category "Systems for Nuclear Auxiliary Power (SNAP) Reactor – SNAP Program," as given in the Standard Distribution for Classified Scientific and Technical Reports, M-3679, and according to the NASA Supplementary Report Distribution List at the end of this report.

CONTENTS

CONTENTS

CONTENTS

TABLES

TABLES

FIGURES

FIGURES

FIGURES

FIGURES

ABSTRACT

Design of the 5-kwe Reactor Thermoelectric System was initiated in February 1972 and extended through the conceptual design phase into the preliminary design phase. Design effort was terminated in January, 1973. This report documents the system and component requirements, design approaches, and performance and design characteristics for the 5-kwe system. Included is summary information on the reactor, radiation shields, power conversion systems, thermoelectric pump, radiator/structure, liquid metal components, and the control system.

I. INTRODUCTION

Since the start of the U. S. space program, power and lifetime requirements have modestly, but steadily grown. A decade ago, power levels of several watts for durations of 1 or 2 years readily met most mission requirements. However, some DOD and NASA missions in the late 1970's and early 1980's show projected power requirements to 10 kwe and durations to 5 years. In addition, significant potential mission advantages were identified with the use of reactor power systems for some of these missions.

Although the SNAP 10A system flown in 1965 successfully demonstrated all aspects of reactor system operation in space, substantial technology improvements in components and systems have occurred since then. Figure 1 illustrates the gains projected through the use of existing component technology. A 2-kwe system designed to SNAP 10A (1965) technology would weight nearly a ton and require 250 ft^2 of radiator. Using the component technology of the 1970's, the same system would weight 1100 lb and require only 100 ft^2 of radiator area. The gains primarily result from the use of higher efficiency PbTe thermoelectric material, rather than SiGe; and through an increased reactor temperature capability.

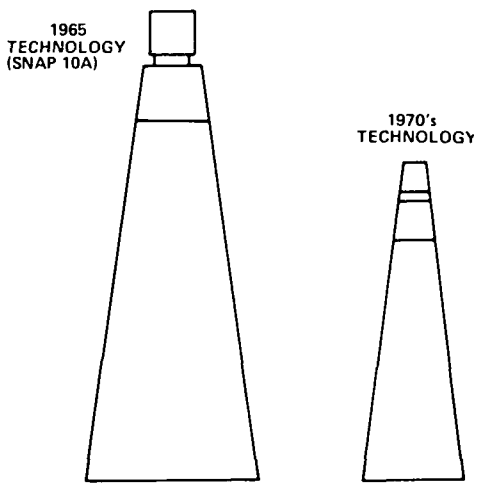

	1965 TECHNOLOGY (SNAP 10A)	1970's TECHNOLOGY
• MAXIMUM COOLANT TEMPERATURE (°F)	1050	1200
• HEIGHT (ft)	21.5	14.5
• BASE DIAMETER (ft)	8	4.5
• RADIATOR AREA (ft)	250	100
• WEIGHT (lb)	1950	1100

Figure 1. 2-kwe System Technology Comparison

The purpose of the 5-kwe Reactor Thermoelectric System Program was to provide potential users with a reactor power system option for future missions and to demonstrate, on a system level, the gains realized in component performance since SNAP 10A. The system was designed to produce 5 kwe for 5 years. Its configuration was consistent with unmanned spacecraft operations and configurations. Shadow shielding was used to reduce radiation levels to 10^{12} nvt and 10^{6} rad at the power system/spacecraft mating plane. Although the demonstration was to be a ground test, the system was designed to meet the requirements for space and to be consistent with all phases of prelaunch operations; to withstand the launch environment of the Titan launch vehicle family; to start up automatically in space; and to operate at full power for 5 years in the vacuum, thermal and meteoroid environment of space.

The program was funded by the joint AEC/NASA Division of Space Nuclear Systems. AEC funding went directly to Atomics International (AI) to support reactor, shield and thermoelectric module engineering and development. NASA funds (NASA Lewis Research Center) were channeled through the AEC to AI for system engineering and all activities relating to liquid metal components. Figure 2 shows the original program schedule. The conceptual design started

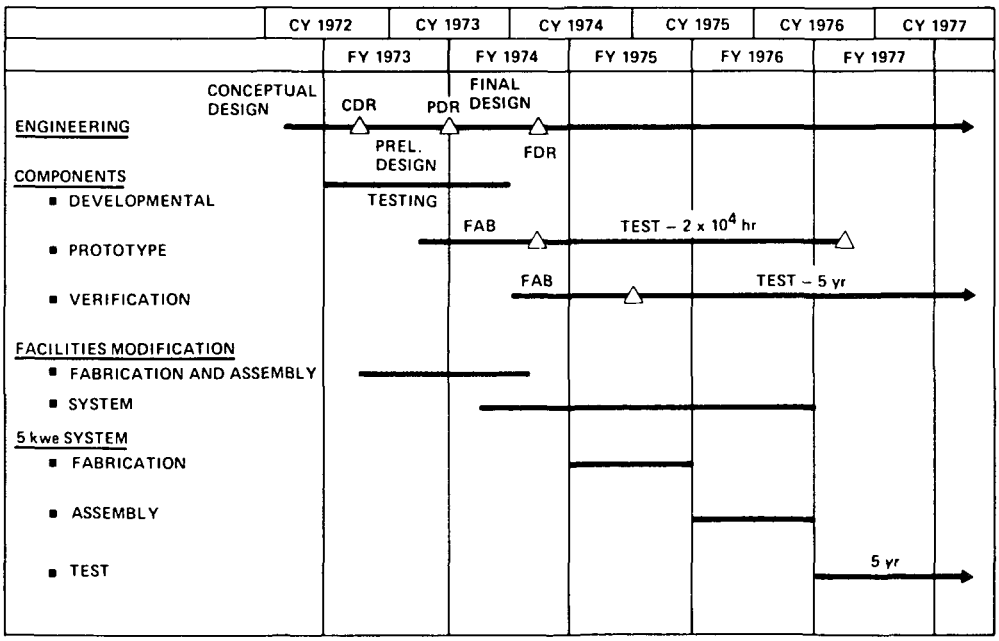

Figure 2. 5-kwe System Program Schedule

in February 1972 and was completed in October 1972, at which time the Preliminary Design Phase was initiated. On January 8, 1973, direction was received to immediately initiate closeout planning and activities relating to the 5-kwe System Program.

The purpose of this report is to summarize the design and performance of the 5-kwe system and components as they existed at the time of program termination.

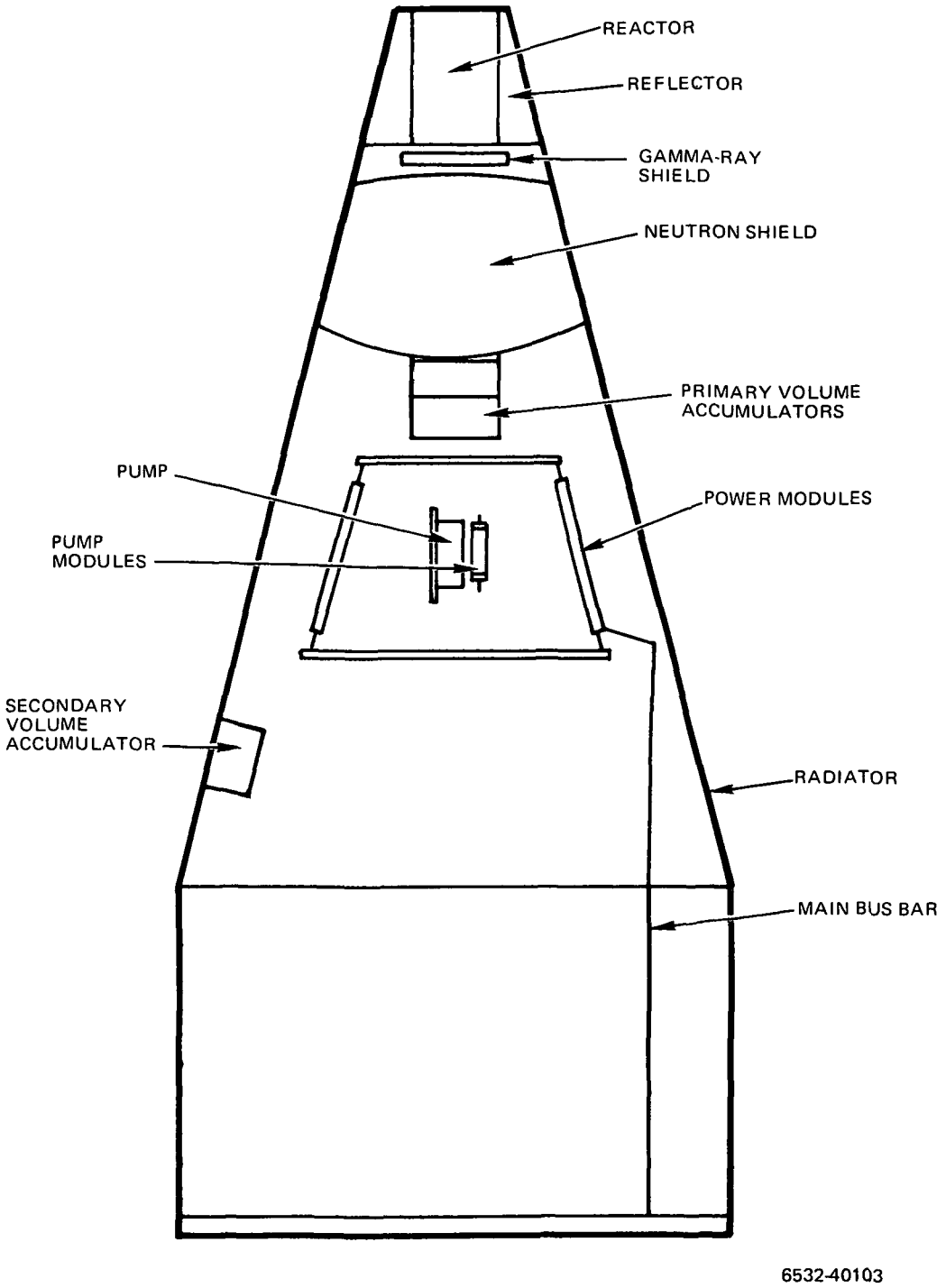

Figure 3. 5-kwe System Schematic

II. DESIGN AND PERFORMANCE SUMMARY

This section presents system design requirements and reference system characteristics, and reviews the trade studies conducted in support of design point selection.

A. SYSTEM REQUIREMENTS AND CONSTRAINTS

In addition to the overall requirements outlined in the preceding section, several other requirements and constraints were placed on the system.

Because a specific application was not defined, specific mission related system weight and size limitations were not established. However, general dimensional limits were established, considering existing Titan launch shroud sizes and typical spacecraft configurations. In addition, the system was configured to be consistent with ground test facility limitations. The results of past application studies were used to establish approximate weight limits with the Titan IIIB-Burner II launch vehicle.

A reactor outlet temperature limit of 1200°F was selected. This limit was selected, not to identify the upper limit of zirconium hydride (ZrH) reactor temperature potential, but to remain well within current state-of-the-art technology.

Component designs were to be tailored specifically to the 5-kwe system; however, the same technology was to be applicable to power systems over a 1- to 10-kwe range.

B. REFERENCE SYSTEM CHARACTERISTICS

This section describes system configuration, performance, design margins and weights.

1. System Configuration and Performance

Figure 3 shows component arrangement schematically, and Figure 4 is a layout drawing of the 5-kwe system. The system has a primary and a secondary, or heat rejection, NaK loop. Primary loop NaK flows into the top of the core vessel through two inlet lines, is heated in the core and flows out through two outlet lines. The NaK then flows through the PbTe thermoelectric modules where it transfers its heat to the hot cladding of the modules. The fluid is then

PAGE INTENTIONALLY LEFT BLANK

SCHEDULE OF PIPING SIZES

SYM.	DWG. ZONE	DESCRIPTION	O.D. (IN.)	WALL (IN.)
1p	16	PUMP DISCHARGE	2.50	.020
2ap	17	REACTOR INLET - BELOW SHIELD	1.50	.020
2bp	19	REACTOR INLET - THRU SHIELD	1.50	.020
3p	19	REACTOR	SEE Rx DWG.	
4ap	19	REACTOR OUTLET - THRU SHIELD	1.50	.020
4bp	18	REACTOR OUTLET - BELOW SHIELD	1.50	.020
5p	16	T/E INLET HEADER	2.00	.020
6p	16 & 14	T/E MODULE PIGTAILS	0.75	.020
7p	14	T/E MODULES	SEE MODULE DWG	
8p	14	T/E OUTLET HEADER	2.00	.020
9p	14	HEADER DISCHARGE LINE	2.50	.020
11p	15	PRIMARY PUMP SUCTION	2.50	.020
12p	17	V.A.U. TO PRIMARY LOOP	0.38	.020
13p	14	PRI. LOOP FILL & CIRCULATE	1.00	.020
14p	20	PRI. LOOP FILL, CIRC. & DRAIN	1.00	.020
1s	16	HRL PUMP DISCHARGE	1.875	.020
2s	17	RADIATOR INLET HEADER FEED	1.250	.020
3s	18	RADIATOR INLET HEADER	1.250	.020
4s	17	RADIATOR TUBES	0.438	.020
5s	7	RADIATOR OUTLET HEADER	1.500	.020
6s	13	RISER (NaK RETURN LINES)	1.250	.020
7s	14	T/E INLET HEADER	1.250	.020
8s	15	T/E MODULE PIGTAILS	.500	.020
9s	15	T/E MODULES	SEE MODULE DWG	
10s	16	T/E OUTLET HEADER	1.500	.020
11s	16	HEADER DISCHARGE LINES	1.250	.020
12s	14	HRL PUMP SUCTION	1.875	.020
13s	13	HRL TO V.A.U.	0.38	.020
14s	18	HRL FILL, CIRC, & DRAIN	.750	.020
15s	8	HRL FILL & CIRC.	1.000	.020
16s	5	HRL FILL, VENT & CIRC.	1.000	.020

Figure 4
5-kwe Reactor Thermoelectric
System Design Layout
(R-N652630001)

PAGE MISSING FROM AVAILABLE VERSION

pumped, by the electromagnetic (EM) pump, back to the reactor core for reheating. Secondary loop NaK picks up the waste heat at the cold cladding of the tubular modules, and is then cooled as if flows through the tubes of the conical/cylindrical radiator. Both loops are pumped by a single dc conduction pump assembly powered by three pump tubular modules. The primary loop requires two volume accumulator units (VAU's) and the secondary loop requires one. All three are of identical design.

Expansion joints are used in the system to permit thermal expansion and contraction of subassemblies. The 16 power tubular modules are arranged in a basket within the radiator. The radiator cools the secondary loop NaK and also acts as primary structural support.

The overall height of the system is 23 ft and it has a maximum diameter of 6 ft. The radiator area is 267 ft^2.

Table 1 is a summary of beginning-of-life (BOL) and end-of-life (EOL) performance. The system is designed to produce 5 kwe for 5 years at a maximum reactor outlet temperature of 1200°F. Because the tubular modules degrade with time at temperature, the maximum reactor outlet temperature occurs at EOL. Consequently, prior to EOL, the temperature is less than 1200°F. At BOL, the temperature is 1148°F, and is gradually increased as degradation occurs.

Figure 5 shows the 5-year variation of reactor outlet temperature, reactor thermal power, and average radiator temperature for a constant electrical power of 5 kwe. Figure 6 illustrates power module thermal input, power degradation rate, and total power degradation as a function of time. The relationship between power module degradation and system performance can be seen by comparing these figures.

The 5-kwe Reactor Thermoelectric System was to be tested in the Building 059 facility at the Santa Susana Field Laboratory of AI. The system was to be operated in an inverted position (reactor down), with a cold wall provided for thermal rejection from the radiator. Detailed analyses were performed to determine the capability of the radiator heat sink utilizing various temperatures and emissive coatings. It was found that an average cold wall temperature of 100°F and an average emissivity of 0.85 provide an environment very similar

TABLE 1
BOL/EOL PERFORMANCE SUMMARY
(Sheet 1 of 2)

Parameters	BOL	EOL
Reactor		
Power (kwt)	95.6	101.3
Outlet Temperature (°F)	1148	1200
Core temperature rise (°F)	88.7	94.8
Power Modules		
Average hot clad temperature (°F)	1091	1140
Average cold clad temperature (°F)	527	543
Thermal input (kwt)	80.36	84.79
Overall efficiency (%)	6.38	6.05
Power degradation (%)	-	6.67
Efficiency degradation (%)	-	4.70
Output power (kwe)	5.13	5.13
Power bus bar losses (I^2R) (kwe)	0.13	0.13
Power at mating plane (kwe)	5.0	5.0
Voltage at mating plane (vdc)	30.0	30.0
Radiator		
Thermal input (kwt)	89.3	94.9
Inlet temperature (°F)	589	611
Temperature drop (°F)	132	144
Average temperature (°F)	522	538
AI-93 emissivity	0.90	0.90
AI-93 absorptivity	0.50	0.50
Fraction bonded fin/tube area (%)	80	72
Direct solar flux (Btu/ft^2-hr)	141.1	141.1
Earth reflected flux (Btu/ft^2-hr)	23.5	23.5
Direct earth flux (Btu/ft^2-hr)	20.17	20.17
NaK Pump		
Primary loop flowrate (lb/sec)	4.87	4.83
Primary loop developed head (psi)	1.11	1.09
Secondary loop flowrate (lb/sec)	3.01	2.94

TABLE 1

BOL/EOL PERFORMANCE SUMMARY
(Sheet 2 of 2)

Parameters	BOL	EOL
Secondary loop developed head (psi)	1.57	1.50
Current input (amp)	1728	1691
Voltage drop (vdc)	0.210	0.209
Primary throat magnet effective field (gauss)	2505	2380
Secondary throat magnet effective field (gauss)	2000	1900
Pump Modules		
Average hot cladding temperature (°)	1079	1128
Average cold cladding temperature (°F)	531	547
Thermal input (kwt)	9.77	10.39
Overall efficiency (%)	3.71	3.41
Power degradation (%)	-	8.13
Efficiency degradation (%)	-	6.75
Output power (kwe)	0.362	0.354
Piping System		
Primary loop flowrate (lb/sec)	4.87	4.83
Primary loop pressure drop (psi)	0.97	0.95
Secondary loop flowrate (lb/sec)	3.01	2.94
Secondary loop pressure drop (psi)	1.37	1.30
Thermal Losses		
Primary loop thermal losses to space (kwt)	1.27	1.43
Primary loop radiative shunt losses to secondary loop (kwt)	3.24	3.71
Primary loop conductive losses to secondary loop through pump bus bar (kwt)	0.97	1.02
System		
Carnot efficiency (%)	36.2	37.2
Overall efficiency (%)	5.23	4.93

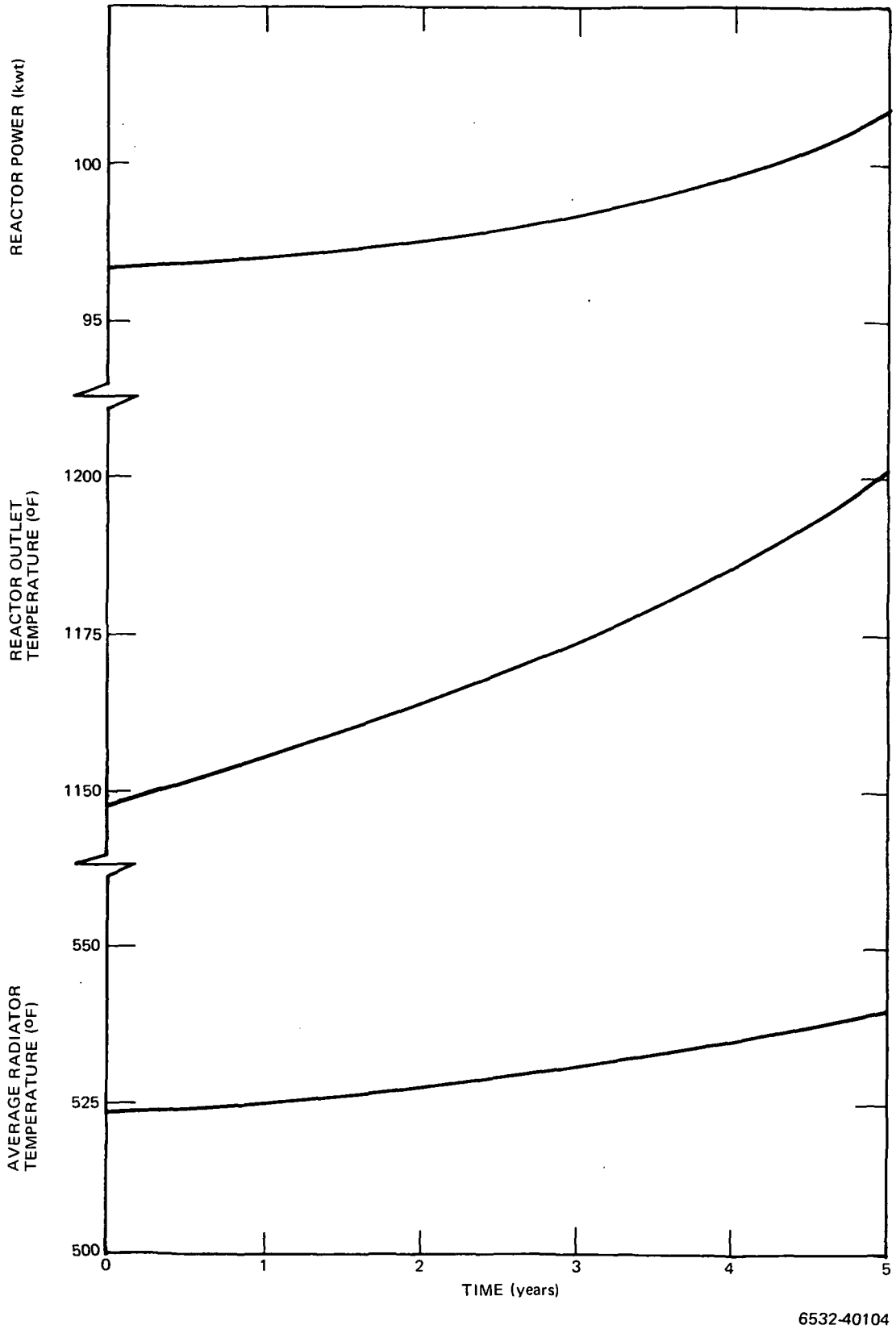

Figure 5. 5-kwe System Performance History

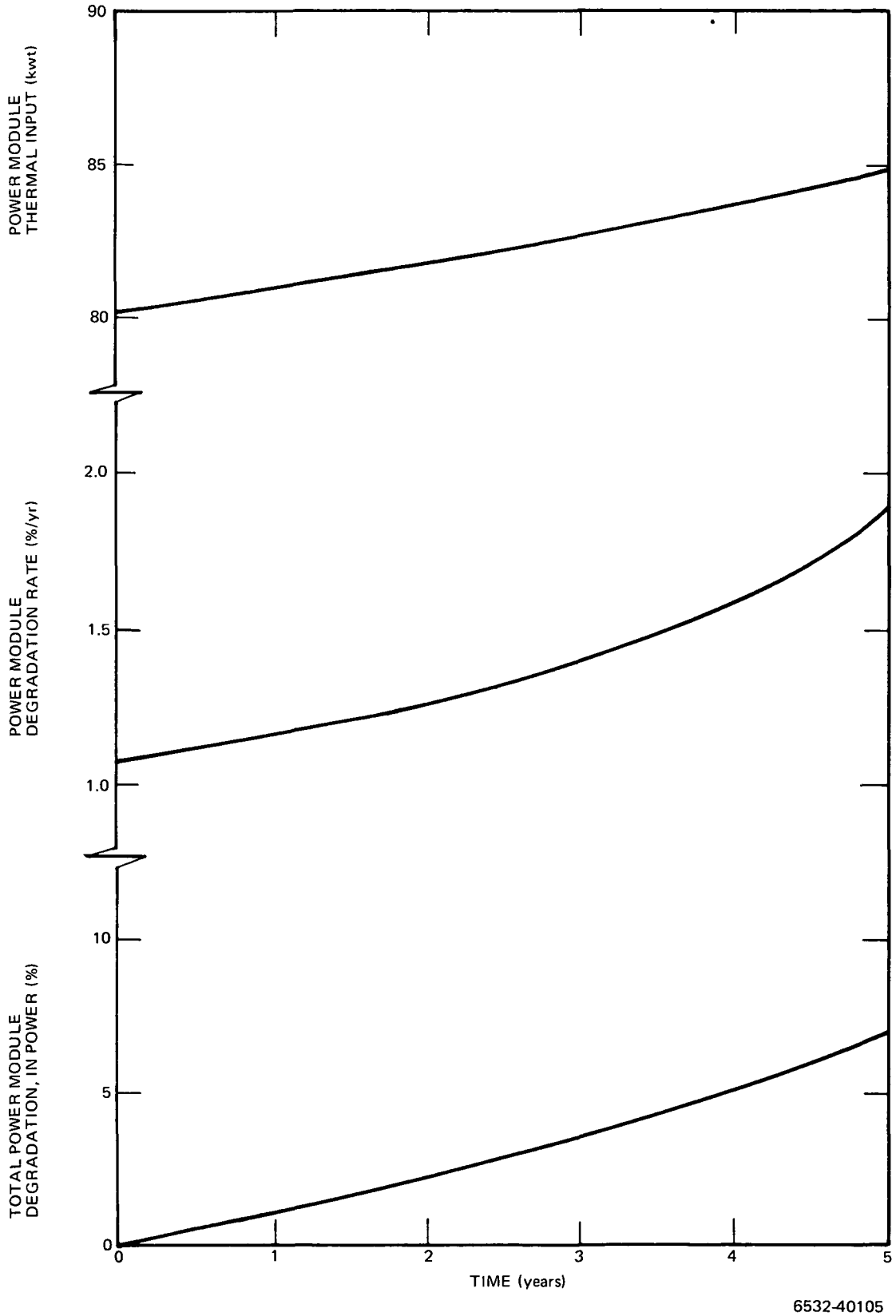

Figure 6. Power Module Performance History

to space. Although the final design of the facility was incomplete, preliminary trade studies indicated that utilization of iron titanate coating (approximate emissivity of 0.90) on most internal sections of the cold wall could easily provide the required average emissivity. The available cooling towers are capable of maintaining the necessary 100°F cold wall temperature. As the ground and space environments are essentially equivalent, the detailed performance of the 5-kwe system remains identical in both situations (although minor second-order variations in the thermal rejection temperature dependence may occur).

2. Design Margin Performance

This section describes the margins applied to each component and their effect on system performance.

Trade studies were performed to analyze those components which should exhibit performance design margins. Four components were selected: (1) the reactor; (2) the EM NaK pump; (3) the radiator; and (4) the VAU's. The power and pump modules were not considered in this analysis because they are developmental items whose performance is currently specified by system requirements.

The ZrH reactor incorporates margins in three areas as it was designed to operate continuously for 5 years at 110 kwt, 1200°F outlet temperature, and 100°F core temperature rise. Comparing these design requirements with the operating requirements of the system indicates the following design margins: (1) 12% on reactor power (average value is 98.5 kwt); (2) 26°F on outlet temperature (average value is 1174°F); and (3) 8°F on core temperature rise (average value is 93°F). These design margins are non-interacting with the system performance statepoints because the reactor is simply the heat source for the power conversion system (PCS), and all thermal requirements are within the design values for the reactor. The system envelope was affected by this margin, however, in that the reactor envelope dimensions were increased to allow for the over-power design requirements.

The EM NaK pump is designed with pressure head capability greater than that required by the piping systems (at a given flowrate). All piping system pressure-drop calculations were done on a worst-case component performance basis. In this way the pressure head design margin was not utilized to neutralize unrealistic pressure drop predictions. Each pump throat exhibits 15% greater head

than is necessary to drive its respective piping loop. These design margins interact with the system performance statepoints because utilization of the additional available pressure head results in: (1) increased flowrates in both loops; (2) increased pressure drop in both loops; and (3) lower temperature differentials in both loops. Thus, analysis of a system which included the pump performance capabilities indicates a more benign operating statepoint.

The radiator design margin was incorporated in three areas: (1) utilization of a lower than measured emissivity for the AI-93 coating; (2) utilization of a higher than measured average solar absorptivity for the AI-93 coating; and (3) utilization of environmental thermal fluxes associated with a worst-case orbit (maximum sun). The AI-93 exhibits an emissivity of 0.92, while the radiator is designed for 0.90. Thus, the design margin is approximately 2% (a value equivalent to approximately 2-kwt rejection capability because emissivity appears directly in the radiation calculation). The solar absorptivity of AI-93 increases during radiator life, being approximately 0.30 at BOL and 0.50 at 5 years (average value is 0.40). The radiator is designed for an absorptivity of 0.50 (continuous, 5-year), and thus exhibits a 67% margin at BOL and no margin at EOL. The expected environmental thermal flux associated with a "nominal" orbit is 64.4 Btu/ft^2-hr (direct solar plus direct earth plus earth reflected). The radiator is designed to accept a flux of approximately 101 Btu/ft^2-hr. This is equivalent to a 57% design margin on environmental input. The combined effects of these margins can be converted to a 6% margin in thermal rejection capability. This margin interacts with the system performance statepoints because utilization of the additional available performance capability would result in a reduced average radiator temperature. All system temperatures are subsequently reduced, thus reducing thermoelectric module degradation rates and increasing reactor lifetime capabilities.

The VAU's are designed to compensate for one-half of the expansion volume of the primary loop at the following temperature condition: EOL average loop temperature plus 50°F to accommodate scram setpoint plus 50°F design margin. Thus each VAU is designed for 191 in^3 of NaK displacement. The expansion volumes associated with the average EOL operating temperatures of the system are 341 in^3 (primary) and 111 in^3 (secondary). Thus the two units in the primary loop exhibit an EOL design margin of 41 in^3 (12%) while the secondary unit

exhibits a design margin of 80 in^3 (72%). This component design margin does not interact with the system performance statepoints because it provides the sink for coolant expansion only. However, the VAU size increase associated with the margin assessment was incorporated in the internal PCS equipment placement.

The additional pumping and heat rejection capabilities of the system can be incorporated into the performance analyses, with the generation of specific statepoints. Table 2 details the BOL and EOL (5 year) performance parameters for the 5-kwe system operated with the design margin capabilities included. Comparison with Table 1 indicates the substantial reductions in component operating requirements.

Note that the reactor outlet temperature at 5 years is well below the 1200°F operating limit. This system is capable of delivering 5.0 kwe over a period significantly longer than the 5-year design lifetime. This period is limited by (1) the reactor outlet temperature (1200°F) or (2) the available control activity. Detailed analyses have shown that the system is reactivity limited rather than temperature limited, as illustrated in Figure 7. No additional control steps are available to the reactor after 7.2 years, while the outlet temperature always remains below 1200°F. It should be noted however that the system is capable of operating at continuously decreasing power levels (less than 5 kwe) while the reactor power and temperature drift down (based on the temperature coefficients). This is indicated schematically by the dotted line in Figure 7.

3. System Weight Summary

Table 3 summarizes component, subassembly and system weights. The total system weight is 1822 lb.

4. System Performance During the 5-Year Mission Lifetime

The following paragraphs are a brief discussion of the 5-kwe system performance over the 5-year operating lifetime. This discussion is included to clarify the difference between BOL and EOL design requirements. The degradation phenomena associated with the system are tabulated to illustrate the conditions which exist causing a change in the design state point over life. An attempt

TABLE 2
UTILIZATION OF COMPONENT DESIGN MARGIN CAPABILITIES
(Sheet 1 of 2)

Parameters	BOL	EOL (5 years)
Reactor		
Power (kwt)	93.8	97.7
Outlet temperature (°F)	1118	1159
Core temperature rise (°F)	84.4	88.3
Power Modules		
Average hot clad temperature (°F)	1063	1102
Average cold clad temperature (°F)	506	523
Thermal input (kwt)	79.00	81.99
Overall efficiency (%)	6.49	6.26
Power degradation (%)	-	4.64
Efficiency degradation (%)	-	3.25
Output power (kwe)	5.13	5.13
Power bus bar losses (I^2R) (kwe)	0.13	0.13
Power at mating plane (kwe)	5.00	5.00
Voltage at mating plane (vdc)	30.0	30.0
Radiator		
Thermal input (kwt)	87.6	91.4
Inlet temperature (°F)	561	584
Temperature drop (°F)	123	131
Average temperature (°F)	501	518
AI-93 emissivity	0.92	0.92
AI-93 absorptivity	0.30	0.50
Fraction bonded fin/tube area (%)	80	72
Direct solar flux (Btu/ft^2-hr	105.4	105.4
Earth reflected flux (Btu/ft^2-hr)	16.5	16.5
Direct earth flux (Btu/ft^2-hr	17.02	17.02
NaK Pump		
Primary loop flowrate (lb/sec)	5.02	5.00
Primary loop developed head (psi)	1.03	1.02

TABLE 2
UTILIZATION OF COMPONENT DESIGN MARGIN CAPABILITIES
(Sheet 2 of 2)

Parameters	BOL	EOL (5 years)
Secondary loop flowrate (lb/sec)	3.16	3.11
Secondary loop developed head (psi)	1.51	1.45
Current input (amp)	1738	1708
Voltage drop (vdc)	0.209	0.209
Primary throat magnet effective field (gauss)	2505	2380
Secondary throat magnet effective field (gauss)	2000	1900
Pump Modules		
Average hot cladding temperature (°F)	1051	1090
Average cold cladding temperature (°F)	510	527
Thermal input (kwt)	9.60	10.01
Overall efficiency (%)	3.79	3.57
Power degradation (%)	-	5.63
Efficiency degradation (%)	-	4.67
Output power (kwe)	0.364	0.357
Piping System		
Primary loop flowrate (lb/sec)	5.02	5.00
Primary loop pressure drop (psi)	1.03	1.02
Secondary loop flowrate (lb/sec)	3.16	3.11
Secondary loop pressure drop (psi)	1.51	1.45
Thermal Losses		
Primary loop thermal losses to space (kwt)	1.19	1.31
Primary loop radiative shunt losses to secondary loop (kwt)	3.04	3.37
Primary loop conductive losses to secondary loop through pump bus bar (kwt)	0.97	1.00
System		
Carnot efficiency (%)	36.4	36.9
Overall efficiency (%)	5.33	5.12

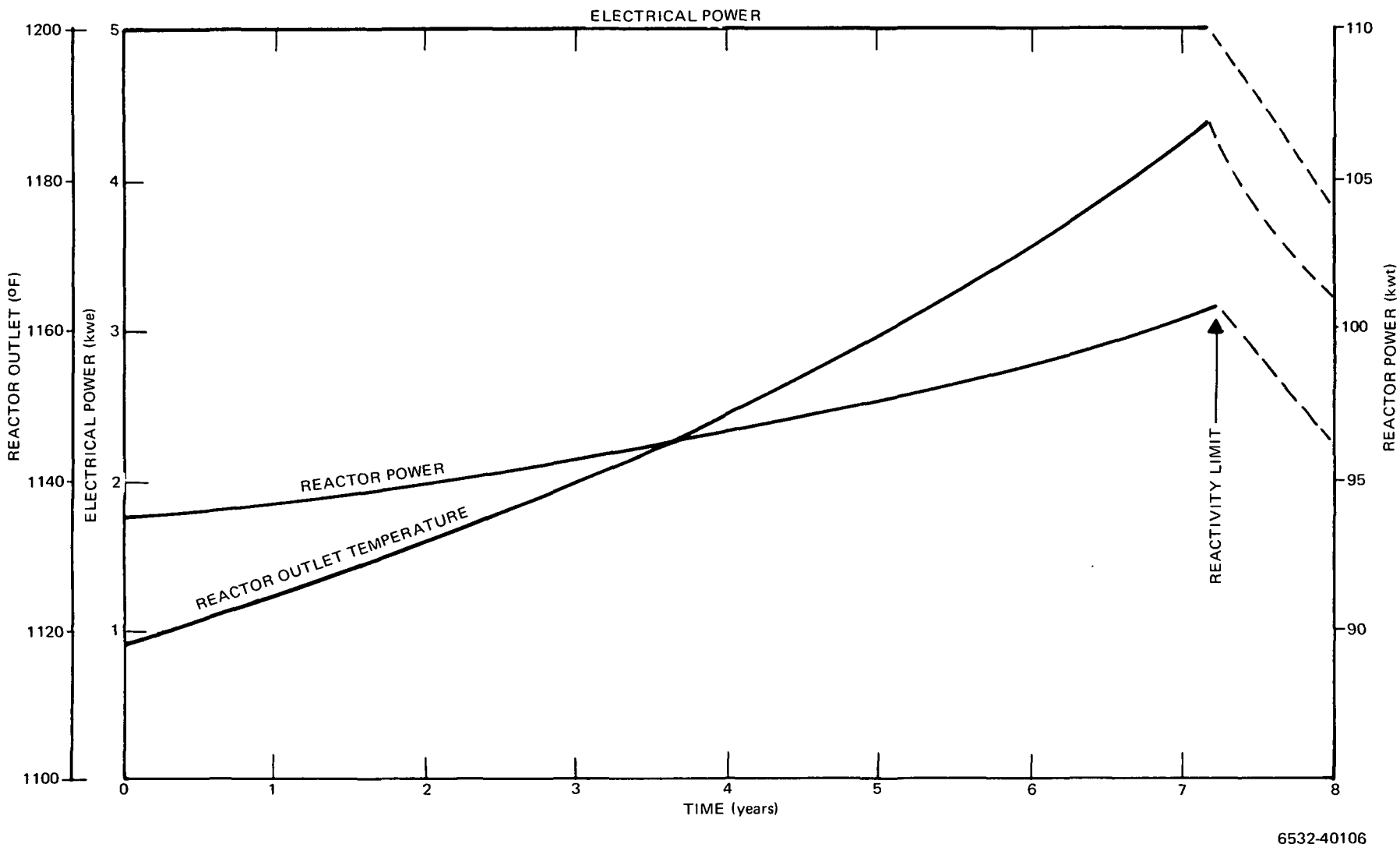

Figure 7. System Performance Utilizing Component Design Margins

TABLE 3
SYSTEM WEIGHT SUMMARY

Component	Weight (lb)	
Reactor		
Core	290	
Reactor vessel	38	
Piping (to shield)	9	
Reflector-control assembly	160	
Total		497
Shielding		
Borated stainless steel gamma-ray shield	98	
LiH neutron shield and honeycomb	195	
Neutron shield casing	59	
Total		352
Power Modules (16)		
Total		192
EM NaK Pump		
Pump throats, magnets, and structure	55	
Pump modules (3)	24	
Total		79
Piping loops		
Primary piping (wet)	62	
Primary loop expansion joints (4)	12	
Primary loop foil insulation	5	
Secondary piping (wet)	70	
Total		149
Volume Accumulators		
Primary units (2)	28	
Secondary unit	14	
Total		42
Radiator		
Fins and armor	179	
Tubes and NaK	124	
Rings and stringers	57	
Pump support flange	9	
Access panels	15	
Rivets	37	
AI-93 surface coating	16	
Support skirt	6	
Thermal baseplane baffle	7	
Miscellaneous bracketry	10	
Total		460
Electrical Wiring		
Power line	11	
Auxiliary pump startup bus bar	10	
Actuator wiring	9	
Instrumentation and wiring	21	
Total		51
System Total		1822

is made to explain the intrinsic coupling between component design margins and system performance.

As was previously discussed, the system is designed to provide a constant 5-kwe output throughout life. However, degradation occurs in the operating characteristics of several components utilized in the 5-kwe system. Because these components exhibit "better" performance at BOL, the BOL reactor outlet temperature is below the operating limit of 1200°F. As degradation occurs during the system life, the outlet temperature is increased to maintain electrical power output. Certain degradation rates are strongly temperature dependent (exponential behavior). This fact complicates prediction of BOL to EOL performance. Table 4 summarizes those components parameters which exhibit degradation.

TABLE 4
SYSTEM COMPONENT PARAMETERS WHICH EXHIBIT DEGRADATION

Parameters	Strongly Temperature Dependent	Temperature Insensitive
Power module efficiency	XX	
Power module power output	XX	
Pump module efficiency	XX	
Pump module power output	XX	
NaK pump magnetic field strengths		XX
NaK pump bus bar braze joints		XX
Radiator coating solar absorptivity		XX
Radiator fin-tube bond thermal resistance		XX

It is thus evident that the EOL operating statepoint is a function of the operating history of the system. In that the system is constrained to operate at 1200°F reactor outlet temperature at EOL (providing 5 kwe at 30 vdc), undegraded system designs (i.e., BOL) must be traced over an assumed operating history. System designs must be rigorously analyzed to couple the component degradation to the system performance, thus arriving at the proper EOL operating statepoint.

C. SYSTEM TRADE STUDIES

This section discusses those trade studies that were performed to arrive at the system design.

1. System Model

The system performance model was incorporated into a time-sharing system computer code described in Reference 1. Modeling was based on component design variables and parametrics which were integrated into a complete time-dependent working model. This code was utilized to predict thermal performance points at several times in the system life. The effects of changing individual component designs can be examined, as can the effects of utilizing the additional performance provided by the component design margins.

A basic modeling technique was coupled to the system performance code to allow calculation of system weight and geometrical characteristics. This analysis technique was used to establish the functional relationships between design variables and system designs. The system was thus parameterized for analytical purposes, with "fine-tuning" of the design point occurring after the final design variables were scoped and fixed.

Two configurations were analyzed for the 5-kwe system: (1) an all-conical system; and (2) a conical-cylindrical system (Figure 8). Analysis was performed to determine which configuration would best satisfy the weight/envelope/performance requirements of the 5-kwe system.

a. Reactor Subsystem

The reactor parametrics were based on an 85-element core design. This constraint was incorporated into the study criteria since previous trade studies had indicated the applicability of the 85-element core to the present system configuration. A two-segment, sliding tapered reflector was incorporated to allow conical shaping of the reactor while providing significant reactivity for control purposes. S8DR and Space Power Facility (SPF) reactor technology was assumed. The reactor outlet temperature was constrained to 1200°F maximum, limiting the hydrogen loss and fuel swelling phenomena effects.

Several auxiliary constraints were applied to the reactor subsystem. Coolant flow through the core assured turbulent flow conditions within the fuel

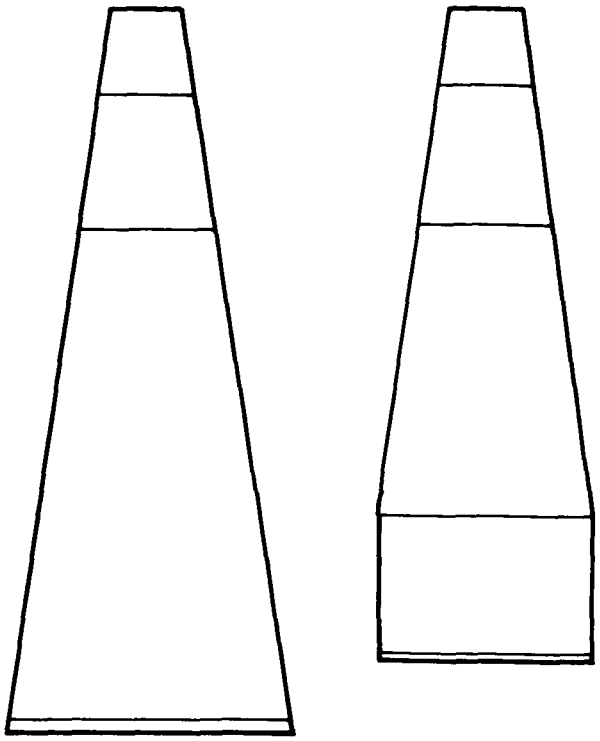

Figure 8. Configuration Schematics

element bundle. Also, the core temperature rise was minimized to limit the temperature gradients developed in the fuel element cladding. These constraints were evaluated for the operating design statepoints of interest, with suitable criteria established for the final design point selection.

The reactor parametrics were modeled as illustrated below:

Reactor Weight Reactor Dimensions	As a Function Of	Reactor Power Conical Half-Angle Fuel Length Core Temperature Rise Design Margins

Typical reactor parameters are illustrated in Figure 9.

b. Shield Subsystem

The shield subsystem consists of a gamma-ray shield (below the reactor) and a neutron shield (truncated conical design). Encased lithium hydride was

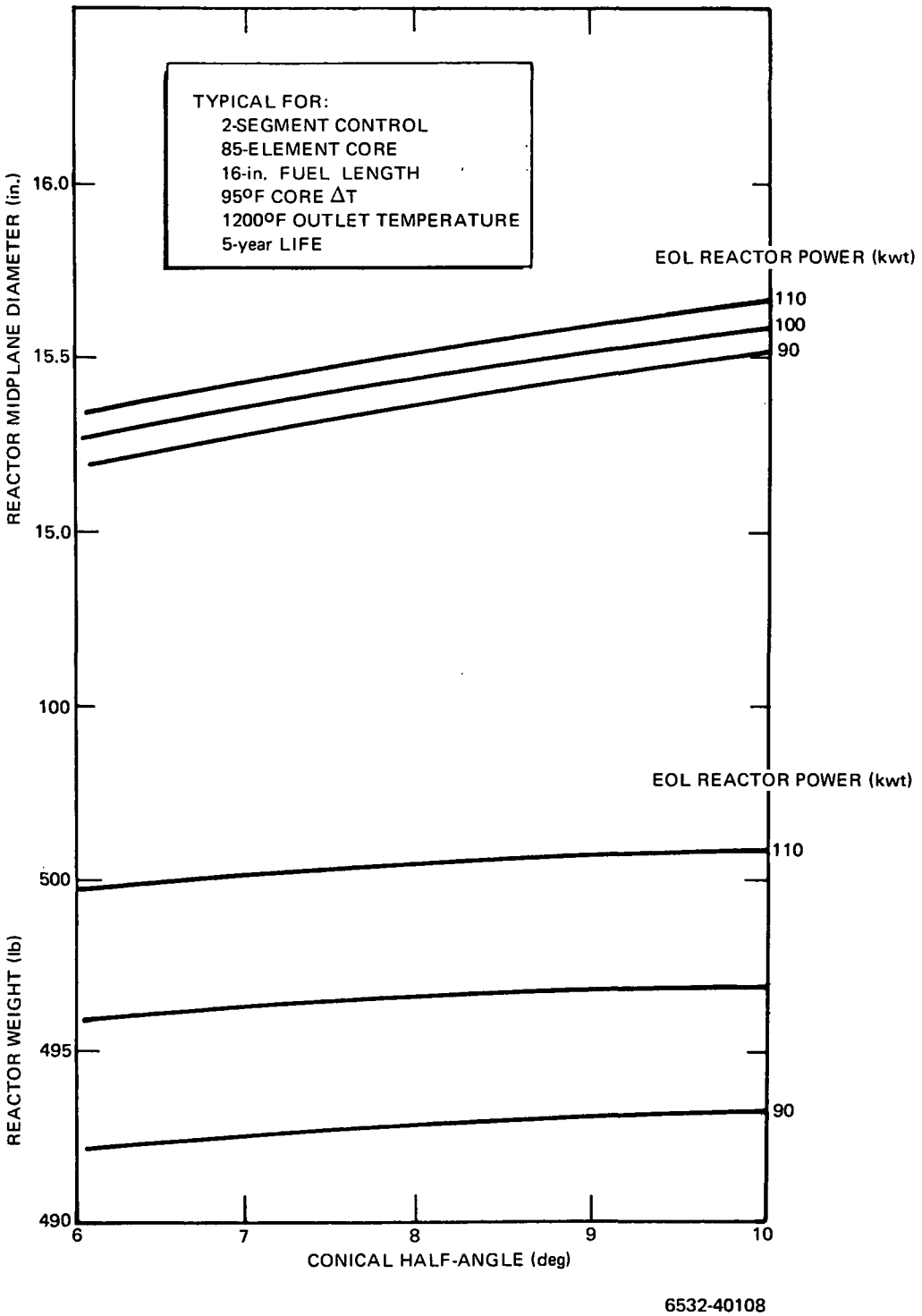

Figure 9. Reactor Parametrics

the material chosen for use in the neutron shield. Previous shield designs (SNAP 10A and S8DR) have shown the applicability of this design to space reactor systems. Several materials were investigated for utilization in the gamma shield, with borated stainless steel chosen from considerations of weight.

External constraints were placed on the shield design. The neutron shield must be an integral structural design capable of supporting the reactor subsystem. Several internal structures for this shield were investigated, with the related additional weights being considered in the system calculations.

Typical shield parametrics for system studies are illustrated below:

Shield Weights Shield Dimensions	As a Function Of	Reactor Power Conical Half-Angle Reactor Dimensions Separation Distance System Base Diameter PCS Attenuation Factors

The PCS attenuation factors (gamma and neutron) are additionally a function of the number of power modules, the pump weight, the volume accumulator weight, and the conical half-angle (as it affects the PCS "density packing factor" within the conical radiator upper section). The gamma and neutron shield PCS factors were critically analyzed by the Oak Ridge National Laboratory (ORNL) and the shields were tailored to the specific power system design. Typical shield parametrics are illustrated in Figure 10.

c. Power Modules

The power module design utilized in the 5-kwe Reactor Thermoelectric System was based on predictable relative performance improvements for the TEM-X modules. These performance improvements are defined in Section IV - Power Conversion System.

The system design was constrained to utilize even integral numbers of thermoelectric power modules. This constraint results from the voltage requirement for the system, the state-of-the-art knowledge on thermoelectric couple design, and the desire for module electric circuit redundancy.

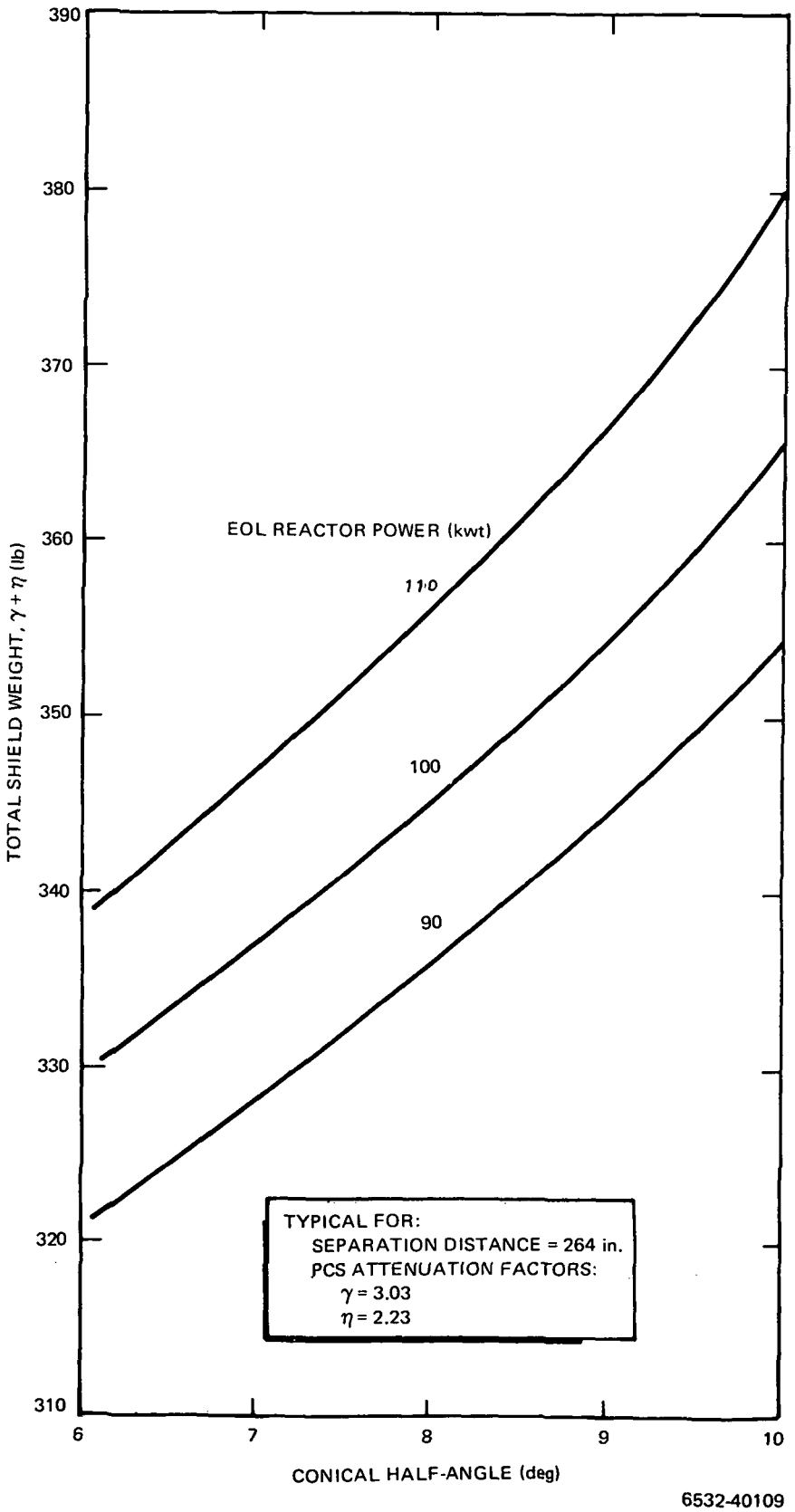

Figure 10. Shield Parametrics

Utilization of two parallel strings of modules results in a thermoelectric couple washer thickness which is compatible with current TEM-X designs.

The power module parametrics were modeled as illustrated below:

Module Efficiency Module Power Output Module Load Voltage	As a Function Of	Average Hot Clad Temperature Average Cold Clad Temperature Number of p-n Couples Power Degradation Load Conditions

Typical power module parameters are illustrated in Figure 11.

d. Pumping Subsystem

The pumping subsystem consists of the EM pump and associated thermoelectric pump modules.

The EM NaK pump is defined as the primary and secondary throats, associated magnets, copper bus bar, and related structure. All analysis of the pump was based on utilization of a two-throat pump (primary and secondary throats sharing common current path and structure). Previous trade studies indicated the applicability of this design to present system goals.

Auxiliary constraints were placed on the pump design. The current requirement for the dual-throat pump was not to exceed 1800 amp to retain compatibility with a maximum of three thermoelectric pump modules (state-of-the-art design). The pump was to be connected with the pump modules via a minimum length bus bar. Pump performance was based on computer predictions which were correlated to experimental data. The design specifies effective magnetic fields, because the actual field is perturbed significantly by the high current flow in the bus bar.

The EM NaK pump parametrics were modeled as shown below:

Pump Weight Pump Efficiency Secondary Throat Hydraulic Power	As a Function Of	Primary Flowrate Primary Pressure Head Pressure Head Design Margin Effective Magnet Field Strengths Pump Current Input

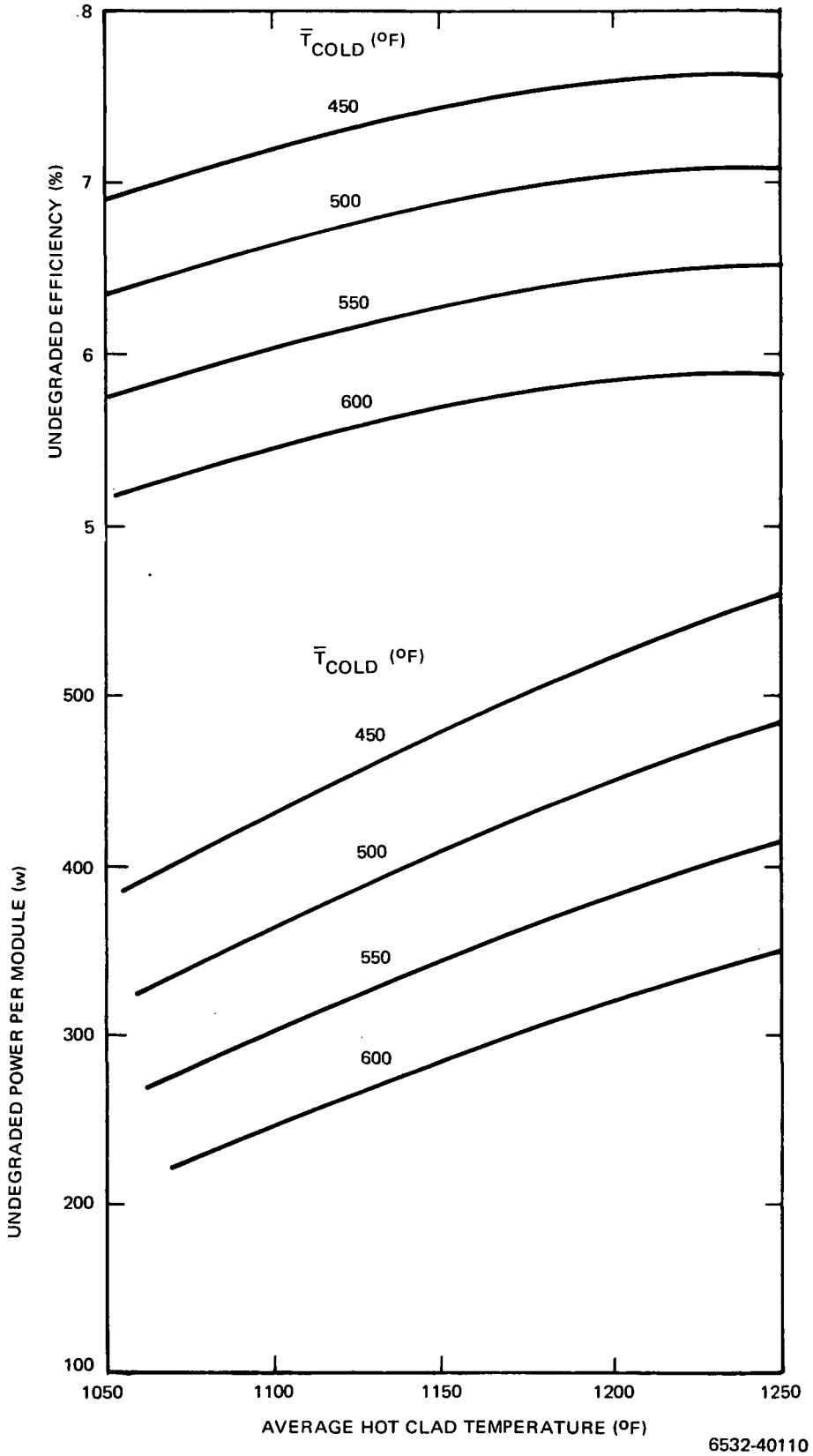

Figure 11. Power Module Parametrics

The pumping requirements imposed by the primary loop dictate the pump design because the hydraulic power requirement for this loop exceeds that for the secondary loop in all useful system designs. This results from the minimization of the core temperature rise (because it affects fuel element cladding stresses). Typical pump parameters are illustrated in Figure 12.

The pump module design utilized in the 5-kwe Reactor Thermoelectric System was based on the existing TEM-14A pump modules. Modification to the TEM-14A design was allowed to provide proper electrical coupling characteristics between the pump and modules. Improvements in performance which could be realized by utilization of ternary materials were not considered; however, improvements in power degradation rate were permitted resulting from the incorporation of EBVD tungsten diffusion barriers.

The pump module design was constrained to use integral numbers of thermoelectric couples with the couple washer thickness comparable to that utilized in the TEM-14A design. In addition, the module design utilized nickel-clad copper conduction pins to minimize voltage drops (and power losses). These pins are brazed to the conduction rings of the copper bus bar.

The pump module parametrics were modeled as illustrated below:

Module Efficiency	As a	Pump Current Requirement
Module Weight	Function	Pump Voltage Requirement
Module Length	Of	Average Hot Clad Temperature
		Average Cold Clad Temperature
		Number of p-n Couples
		Power Degradation
		Couple Washer Radial Thickness

Typical pump module parametrics are shown in Figure 13.

e. Radiator Subsystem

The radiator subsystem is defined as the radiating fins, meteoroid protection armor, stainless steel coolant tubing, radiator coolant (NaK), structural rings and stringers, mating plane interface, PCS access paneling, and associated bracketry and fasteners. The subsystem acts as thermal rejector for the

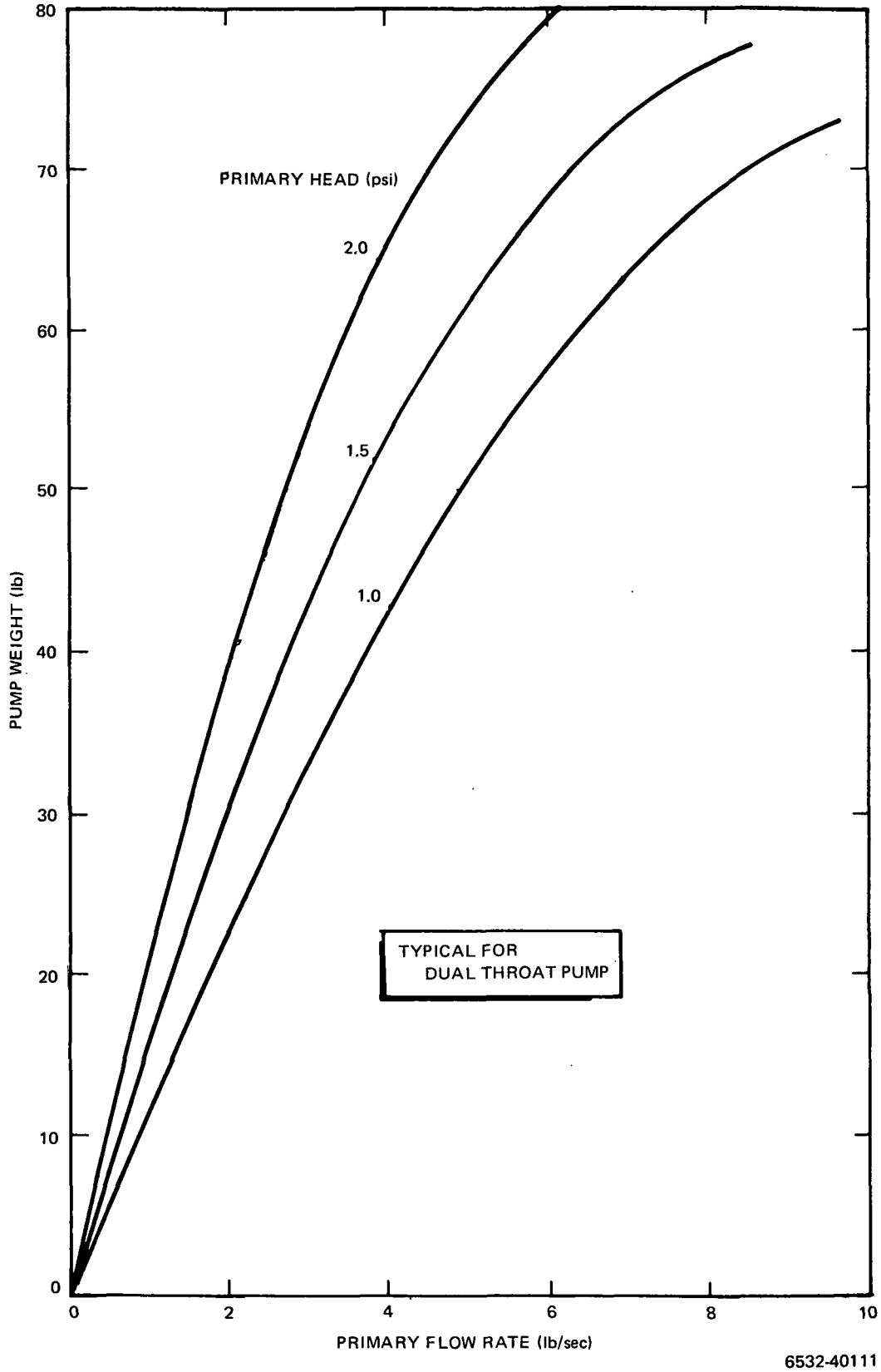

Figure 12. Pump Weight Parametrics

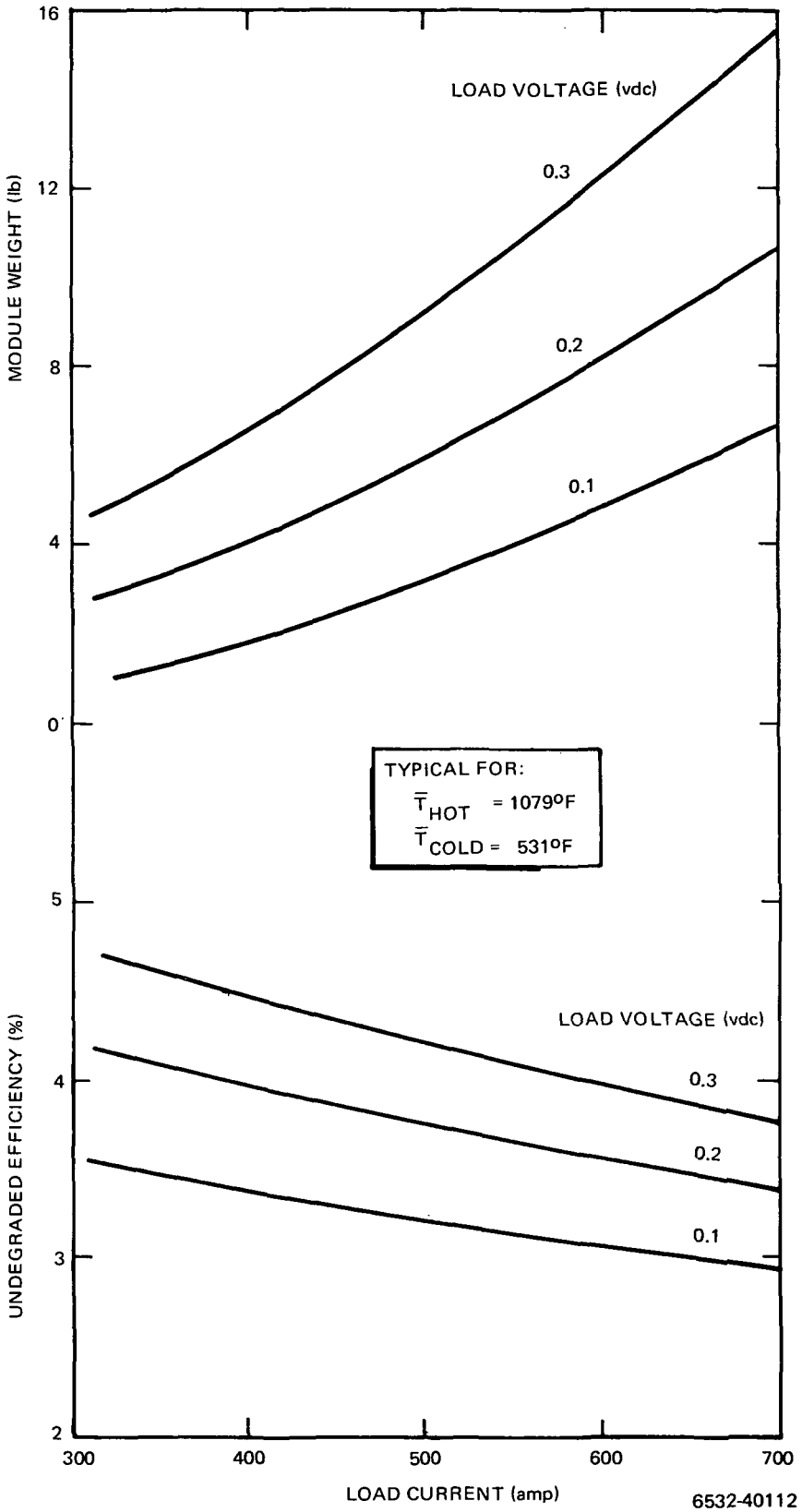

Figure 13. Pump Module Parametrics

PCS, and structural support for the system components during launch and operation. Thus the radiator must satisfy combined thermal performance and structural requirements.

The design of the radiator was constrained to a bonded fin-tube cross-section. Previous trade studies have indicated the applicability of this design to space power systems. Stainless steel is used for the coolant containment in all designs. A high emissivity coating is applied to the radiator to maximize performance. AI93 coating was utilized in all designs because it previously demonstrated its applicability to radiators in space environments. Armor requirements were based on a 99% noncritical damage probability, which was deemed to be an optimal value from consideration of reliability and fin design. The radiating fin (and structural) material was evaluated from several viewpoints: ease of fabrication, thermal stresses, weight, and bond reliability. Trade studies were performed to select the most suitable material. Aluminum, stainless steel, copper, and Lockalloy were considered, with the latter being chosen for the final design.

The radiator subsystem dual parametrics were modeled as follows:

1) Thermal performance

Fin Design Number of Coolant Tubes Armor Requirements Subsystem Weight	As a Function Of	Radiator Inlet Temperature Radiator Temperature Drop Radiator Configuration Heat Input Radiator Area Fin Material Emissivity Design Margin Absorptivity Design Margin

2) Structural subsystem

Fin Design Number of Coolant Tubes Armor Requirements Subsystem Weight	As a Function Of	Radiator Configuration Radiator Dimensions Applied Component Loads

The greater of these two weight requirements was utilized in the system weight summation. The radiator will thus exhibit a minimum weight for a design which compromises the thermal and structural requirements. Typical thermal requirement parameters are illustrated in Figure 14.

f. Piping Subsystem

The primary and secondary piping system designs were based on maximum utilization of the PCS for shielding. The piping systems were compatible with fill-and-drain operations and non-nuclear system testing.

The piping systems were constrained to utilize standard size tubing with a minimum 0.020-in. wall thickness. Trade studies were performed indicating that expansions joints should be used in critical lines to limit the thermally induced stresses. All piping system pressure drops were computer calculated based on worst-case design parameters.

The piping parametrics for each loop were modeled as follows:

Piping Weight Expansion Joint Weight NaK Weight	As a Function Of	Loop Flowrate Loop Pressure Drop System Design Dimensions

Typical primary loop piping parameters are illustrated in Figure 15.

g. Volume Accumulation Subsystem

Trade studies were performed to select the basic design concept for the VAU's. These studies indicated that the redundant gas-backed formed-bellows units proved most desirable within the scope of maximized reliability and ease of fabrication. The VAU's were designed for utilization of two units in the primary loop and one unit in the secondary loop. This approach maximizes the design concept and minimizes fabrication costs.

The VAU parametrics were modeled as below:

Total Weight (three units)	As a Function Of	Primary Loop NaK Weight Secondary Loop NaK Weight Loop Design Pressures

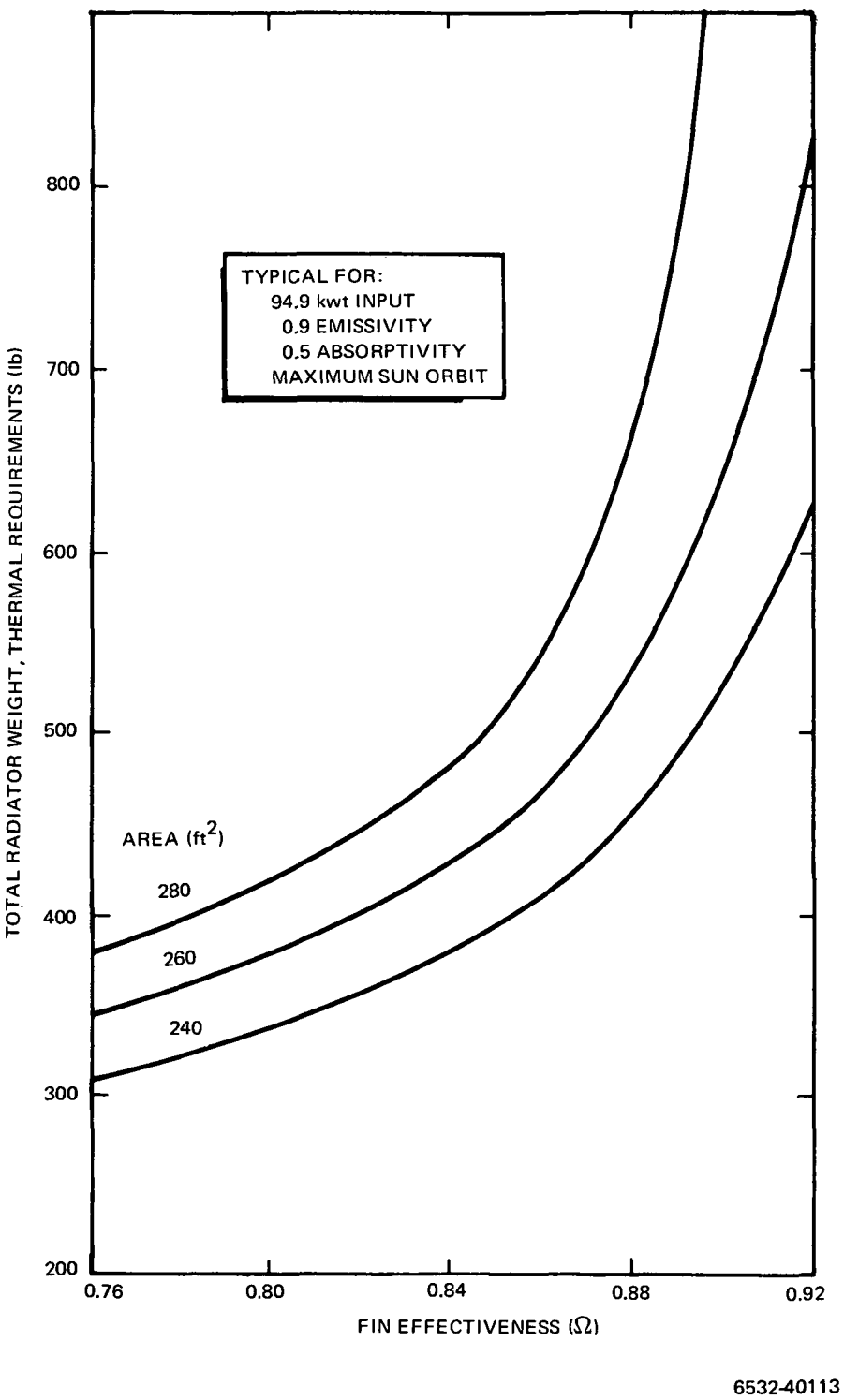

Figure 14. Radiator Parametrics

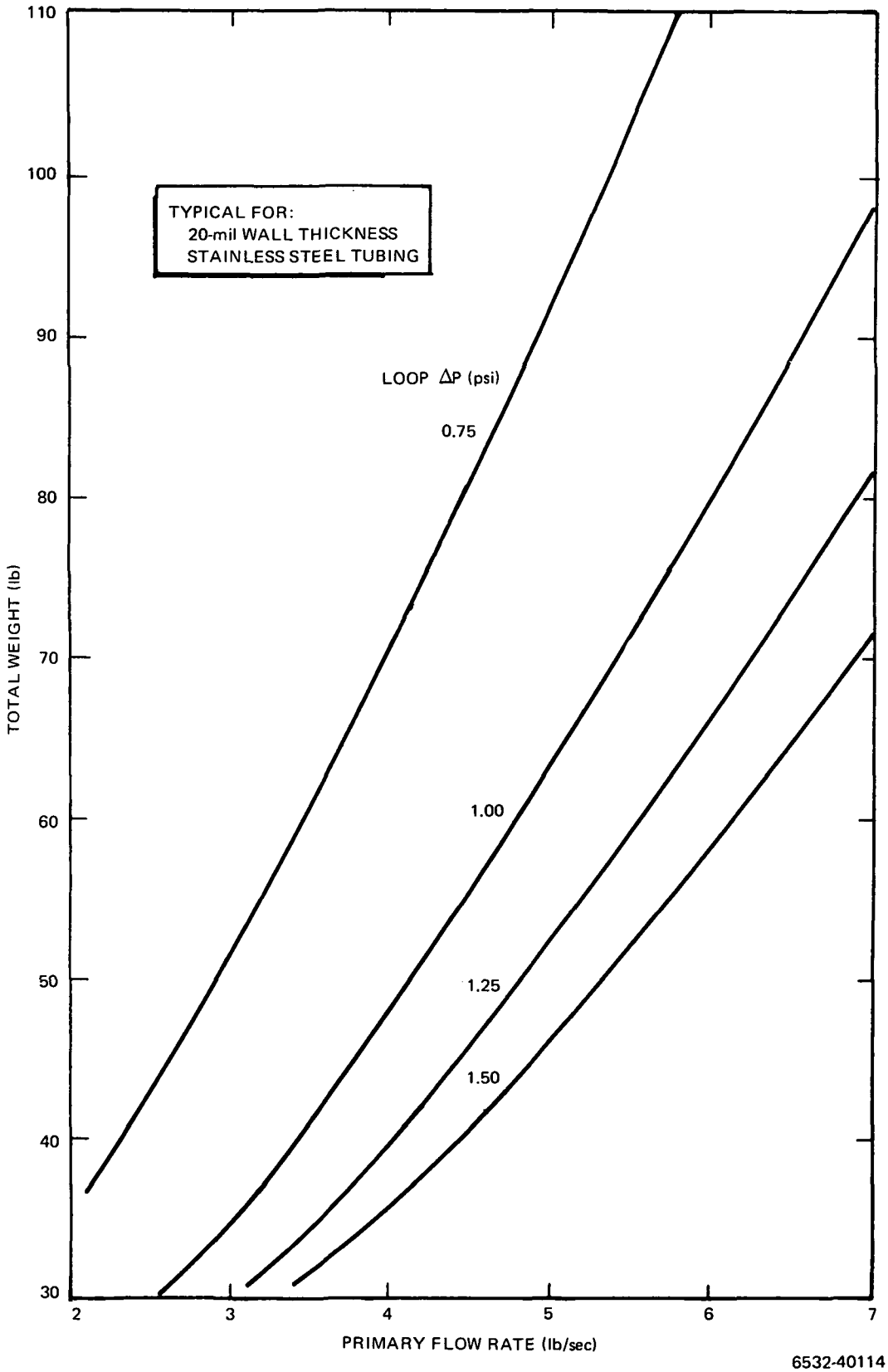

Figure 15. Primary Piping Loop Parametrics

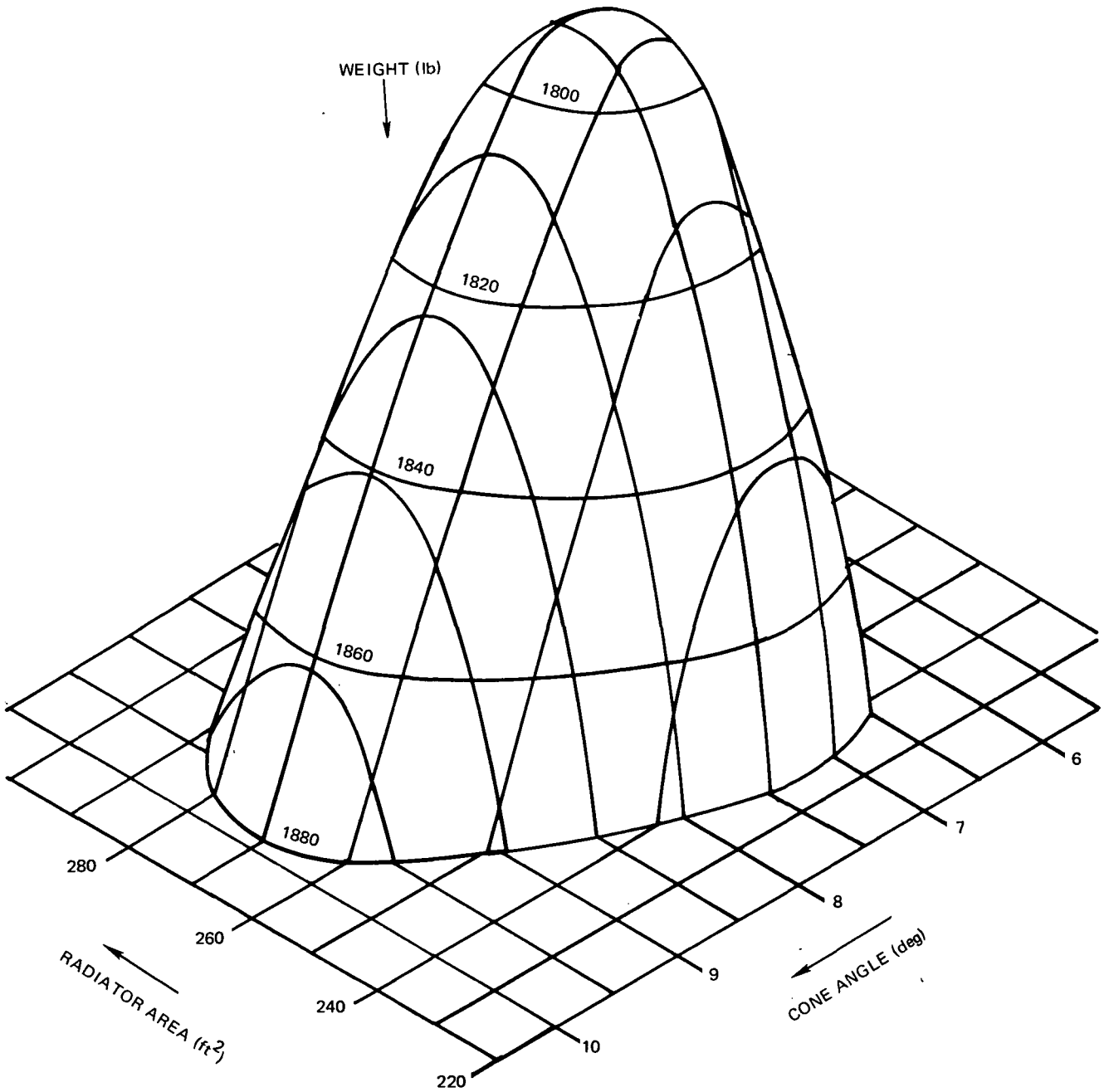

Figure 16. Conical System Weight

h. Wiring Subsystem

The wiring subsystem consists of the main power bus bars, pump startup power bus bars, and control wiring harnesses. The power transmission line design was based on utilization of insulated aluminum wiring. This type of line was also employed to provide startup pumping power. Control wiring was assumed to be high-temperature stainless steel sheathed cable.

The wiring subsystem parametrics were modeled as follows:

Power Line Weight Startup Pump Line Weight Control Harness Weight	As a Function Of	System Design Dimensions Allowable Power Losses Allowable Voltage Drops

2. Configuration Selection

Trade studies were performed to select that system configuration which was the best compromise between weight, envelope dimensions, and performance. Several systems were analyzed which represented conical and conical-cylindrical versions of a specific performance point. Selection of the configuration includes geometry (conical or conical-cylindrical), cone half-angle, and base diameter (for conical-cylindrical).

The system design point geometry selection was conical-cylindrical. As shown in comparing Figures 16 and 17, the conical system exhibits the lowest weight for a specific area (and performance). The system weight penalty associated with the conical-cylindrical geometry choice is approximately 0.5%. However, the envelope minimization resulting from this weight penalty encompasses a 3% reduction in system height and a 10% reduction in system base diameter. Since the design configuration is a compromise between minimization of weight and envelope, selection of the conical-cylindrical configuration seems best suited to a flight-oriented system. Its ability to be integrated with several spacecraft configurations is assured.

Additional benefits arise from use of conical-cylindrical geometry. Since the shielded angle includes the entire conical section, an area larger than the base mating plane lies in the shield shadow angle. This additional shielded area provides improved vehicle integration capabilities. Ease in fabrication

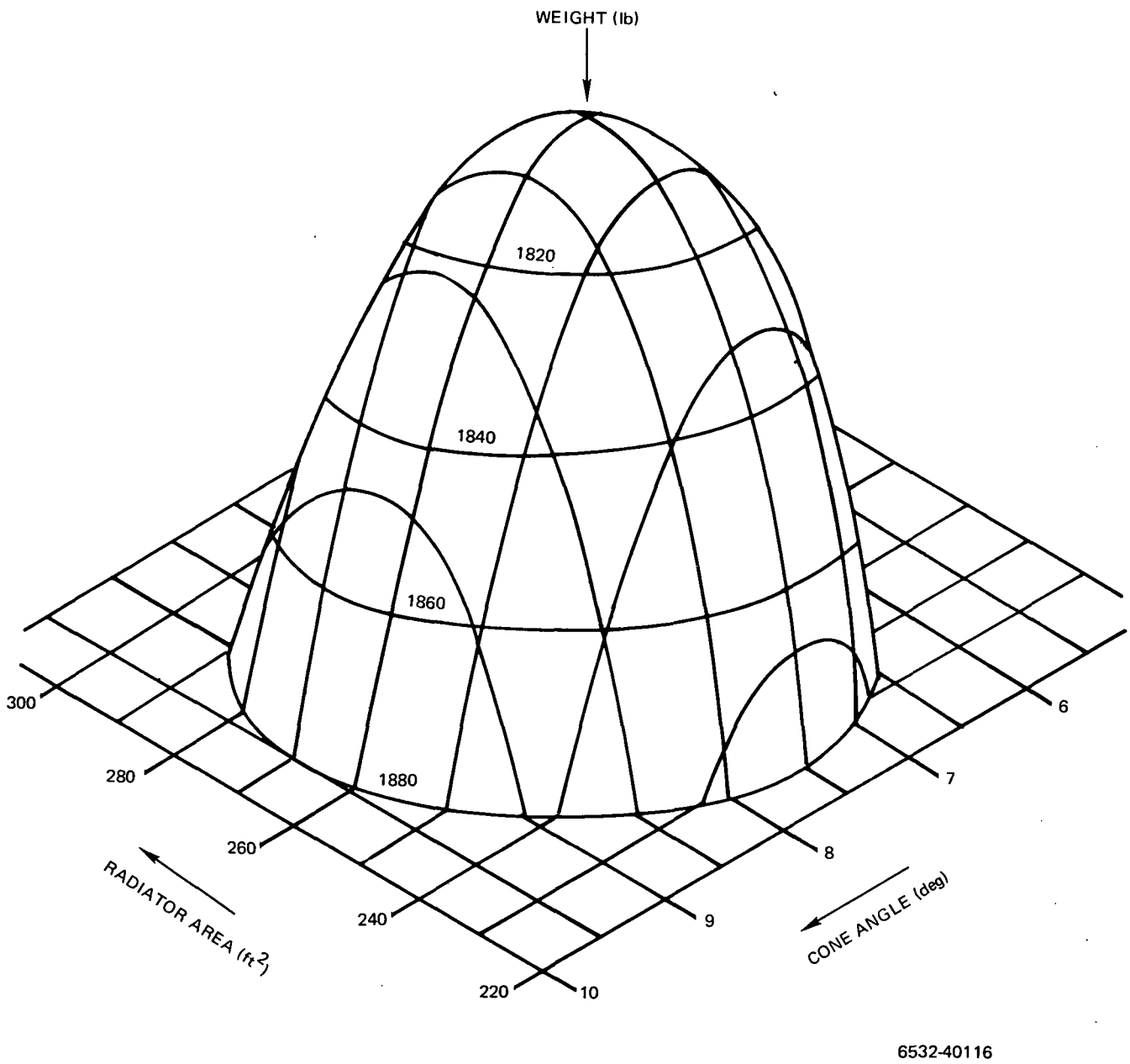

Figure 17. Conical-Cylindrical System Weight

of the radiator fin sections also results from conical-cylindrical geometry selection because the top-to-bottom tapering of the conical section fins is minimized. An ideal location for joining two sublength fin sections is also provided at the conical-to-cylindrical transition point.

The cone half-angle selection for the system design point was 8.5 degrees. As illustrated in Figure 17, minimum conical-cylindrical system weight occurs with approximately a 7.5 degree half-angle. The selection is again a compromise between minimum system envelope and minimum system weight. A 2.5% reduction in height is realized for a 0.50% increase in weight.

The choice of this larger cone half-angle results in a longer radiator cylindrical section. Therefore, ease in fabrication is realized as an additional benefit from the selection. Also, the volume for placement of the PCS equipment near the shield is greater for a larger angle, increasing the PCS packing density.

A cylindrical section base diameter of 6 ft was selected for the 5-kwe Reactor Thermoelectric System. This selection was made on a weight minimization basis; however, the resultant system envelope exhibits excellent compatibility to launch vehicles and potential spacecraft. The system height and weight variation with base diameter are illustrated in Figure 18. Note that system height varies inversely in a one-to-one ratio with base diameter.

3. Component Design Variables Studies

Analysis and final specification of the design variables for the 5-kwe system determines a unique system statepoint within the scope of the system design requirements and component parametrics. The following sections detail those studies which were conducted to derive the final specification of the performance design point.

a. Primary Loop Piping Heat Losses

Analyses were performed to detail the heat losses from the primary loop piping to the space environment. These parasitic losses occur from:

1) The reactor inlet plenum to space.

2) The reactor inlet piping to space.

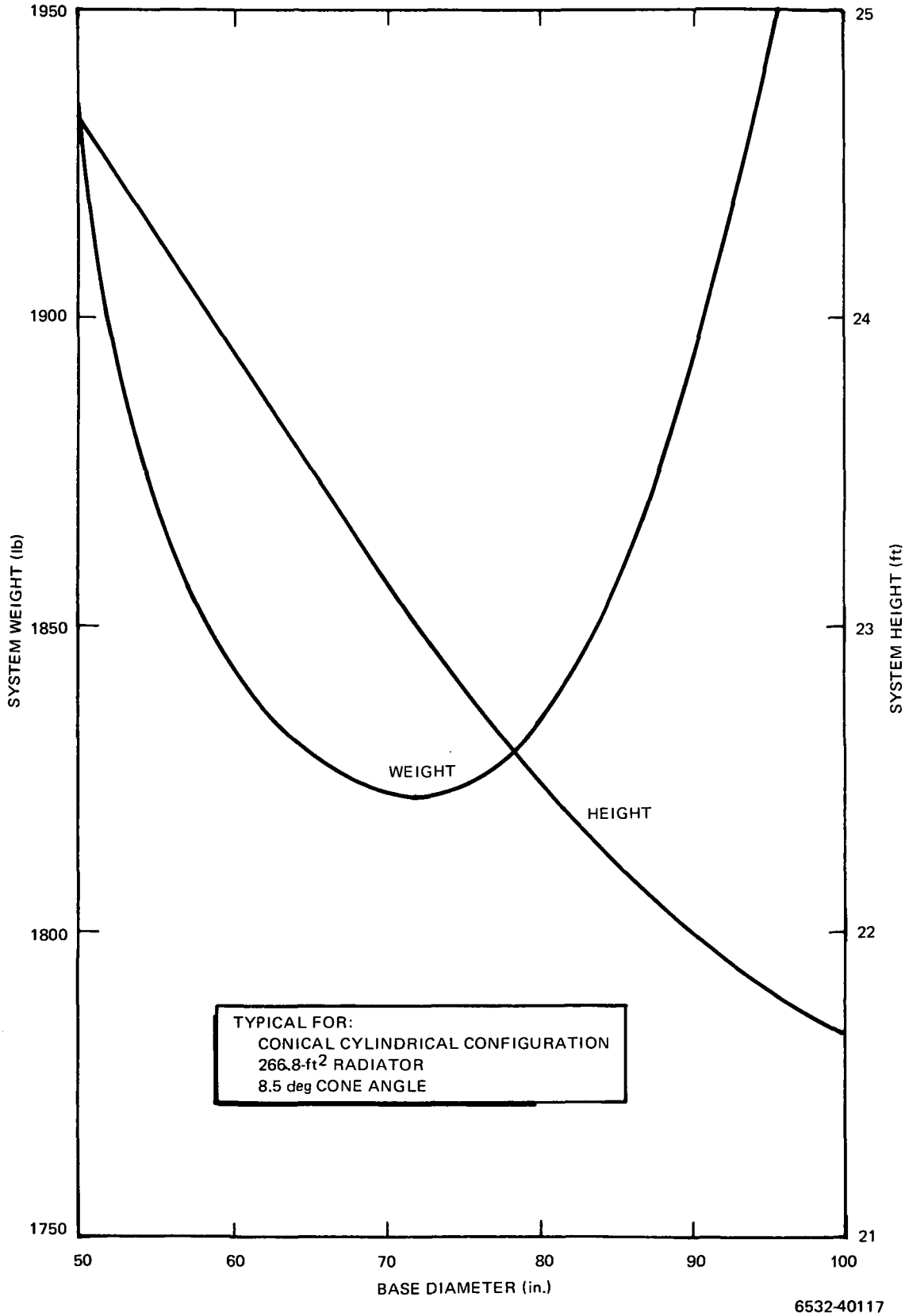

Figure 18. System Weight versus Base Diameter

3) The reactor outlet plenum to space.

4) The reactor outlet piping to space.

5) The reactor outlet plenum to the shields.

6) The inlet and outlet piping (in the shield) to the neutron shield.

Previous trade studies indicated that utilization of single layers of gold-flashed molybdenum foil can minimize the radiative losses from the components. All radiative space losses were thus assumed to occur from a foiled surface exhibiting an emissivity of 0.05 (with 95% coverage). Radiative and conductive losses to the neutron shield were analyzed with the aid of multinodal computer techniques. It should be noted that the piping to shield heat losses must be maintained at a level which will hold the minimum shield temperature above that necessary for annealing of the lithium hydride. Thus, these latter parasitic losses are used for internal heating of the shielding material, with the heat loss occurring from the outer shield can.

b. Primary Loop Piping Shunt Heat Analysis

Parasitic thermal losses exist between the primary piping loop and the secondary piping loop. These shunt losses consist of: (1) radiative losses between the exposed primary piping and the interior of the radiator, and (2) conductive losses between the primary and secondary NaK pump throats (via the large area of the copper bus bar).

Previous trade studies indicated that utilization of multiple wraps (maximum of three wraps) of dimpled gold-flashed molybdenum foil can significantly lower the emissivity of the radiating surfaces. All radiative shunt loss analysis was based upon the primary piping surface exhibiting an emissivity of 0.045 (with 95% coverage). Conductive pump shunt losses were analyzed using a multinodal computer technique.

c. Power Module/Pump Module Flow Distribution Analysis

A trade study was performed to assess the system sensitivity to variations between the power and pump module operating temperatures. The overall system efficiency (thermal to electrical) might be increased by operating the power modules at greater hot-to-cold cladding temperature differentials than

the pump modules, thus utilizing the inherently higher efficiency of the power modules. Several systems were investigated in which the axial temperature gradients through the modules were varied (in both the primary and secondary loops by varying the flow distribution between the sets of modules). The results of this analysis are shown in Figure 19. Note that system weight and radiator area requirements are quite insensitive to this variation. The selected design point utilizes equal temperatures and axial gradients in the power and pump modules, and thus exhibits minimum weight with respect to temperature variation.

d. Power Module/Pump Module Series/Parallel Plumbing Analysis

A trade study was performed to analyze the effects of installing the pump modules hydraulically in series with the power modules. The power modules would thus operate at a higher hot-to-cold cladding temperature differential (with the power modules "first" in the plumbing arrangement), or at a lower temperature differential ("second" in the plumbing arrangement). This investigation indicated that the required modifications to the primary and secondary piping systems would create severe additional pressure drops in these loops. A modification of the pump module inner cladding and mandrel would also be necessary to accommodate the full loop flowrates. No benefits exist for the series plumbing design, in that the higher hydraulic power requirements cause significant increases in system weight, reactor power, and radiator area. The selected design point utilizes a parallel plumbing arrangement.

e. Power Module Radial Dimensions Trade Study

A complex analysis which evaluated the effects of 80 different combinations of power module radial dimensions was conducted. System weight sensitivity to the module radial dimensions was studied on two comparative bases: (1) minimum weight system, and (2) constant area system. The results of both studies were equivalent. The study most applicable to the 5-kwe design was that based on systems exhibiting minimum weight versus area characteristics (for a given module design). The results of this trade study are illustrated in Figure 20. System weight is shown as a function of module radial dimensions. All systems considered in this analysis utilized radiator areas between 265 and 275 ft^2 (the system design point area is 266.8 ft^2).

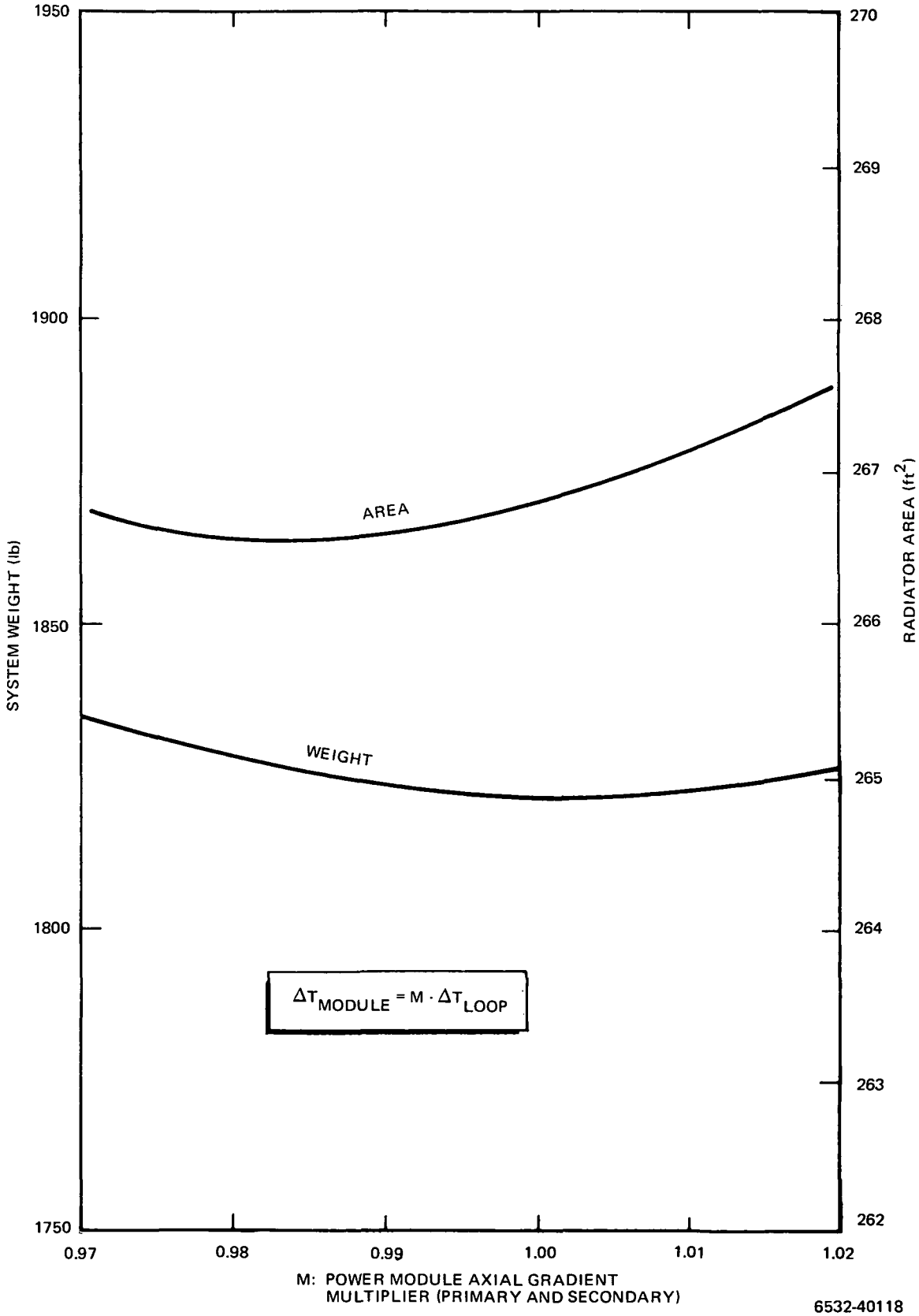

Figure 19. System Weight versus Axial Module ΔT

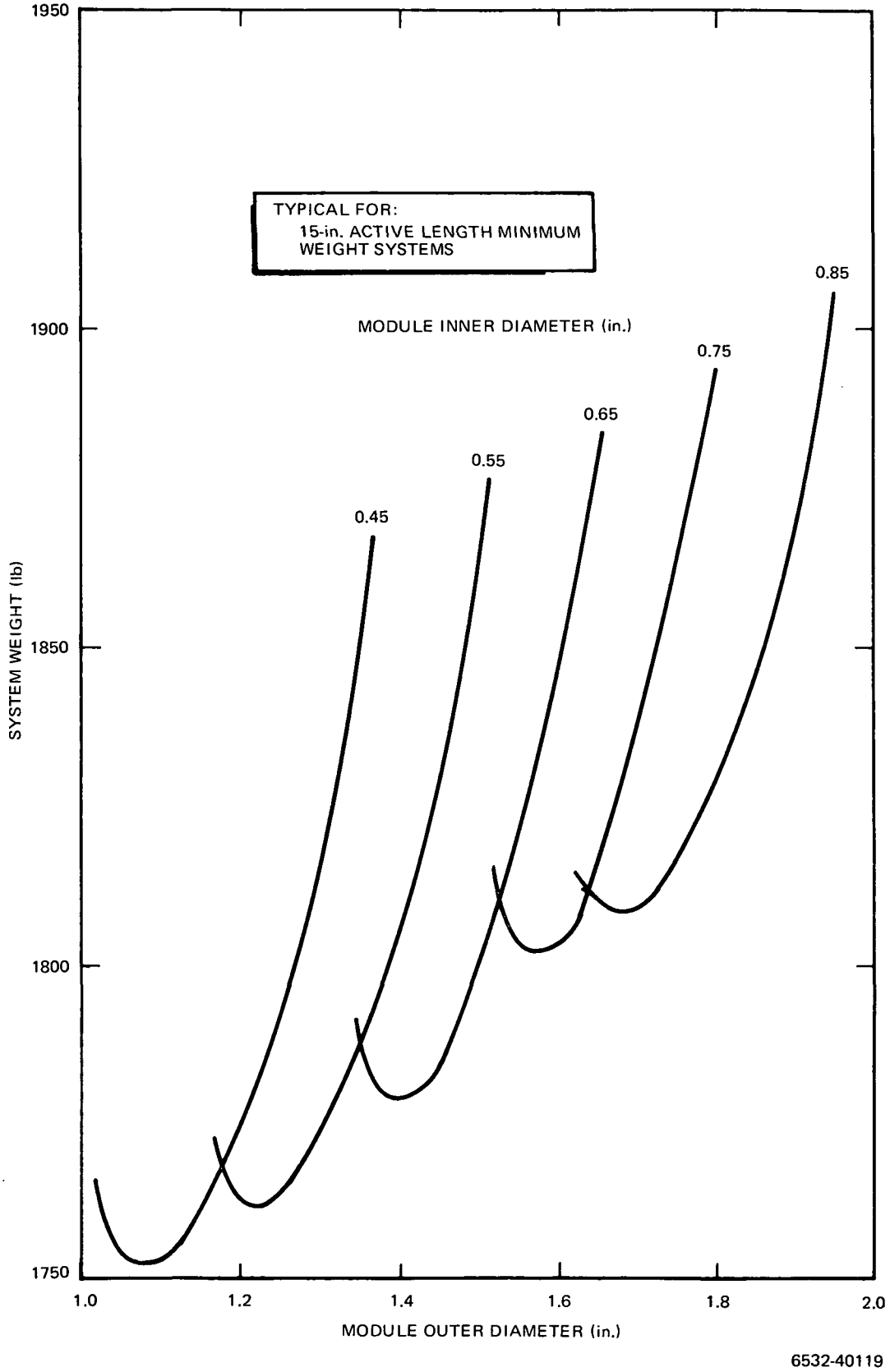

Figure 20. System Weights versus Power Module Radial Dimensions

As shown in Figure 20, a 50 to 60 lb weight savings can be realized through the use of 18 modules with radial dimensions: 0.450-in. ID/1.110-in. OD (as compared to the design point system utilizing 16 modules with dimensions: 0.750-in. ID/1.660-in. OD). However, this dramatic change in module design could result in unknown changes in module fabrication, performance, and degradation. In that the 5-kwe system should utilize current state-of-the-art fabrication procedures and test data, a major modification seems outside the intent of the design. The design point selection is thus based upon 16 modules with TEM-X radial dimensions.

f. Power Module Axial Dimension Trade Study

A system was investigated which utilized TEM-X type power modules with an active circuit length of 20 in. (compared to the reference module with 15 in.). This length modification caused only minor perturbations in the system thermal performance, in that the number of modules is decreased (from 16 to 12) to compensate for the length increase. A slight increase in module efficiency was realized by this modification because of the reduced end losses (25% fewer "ends"). However, changes in shielding and piping which result from this modification tend to negate the weight savings from the efficiency increase. Thus no weight penalty or benefit exists for the axial length increase. A possible cost savings for the power modules could be offset by future developmental and testing costs. The design point selection was based on utilization of modules with a 15-in. active circuit length.

g. Primary Loop ΔT Trade Study

A trade study was performed to assess the impact of primary loop ΔT on system weight. The selection is actually an evaluation of the pumping power requirements versus the reactor core temperature gradient limitations. As illustrated in Figure 21, system weight is minimized for the maximum possible core temperature rise (minimum possible flowrate and pumping power). However, the reactor flowrate must be maintained above that value necessary to assure proper flow distribution throughout the core. An additional limiting factor results from stress analysis of the fuel elements, which indicates that the core temperature rise should be limited to assure a proper margin of safety for cladding stresses.

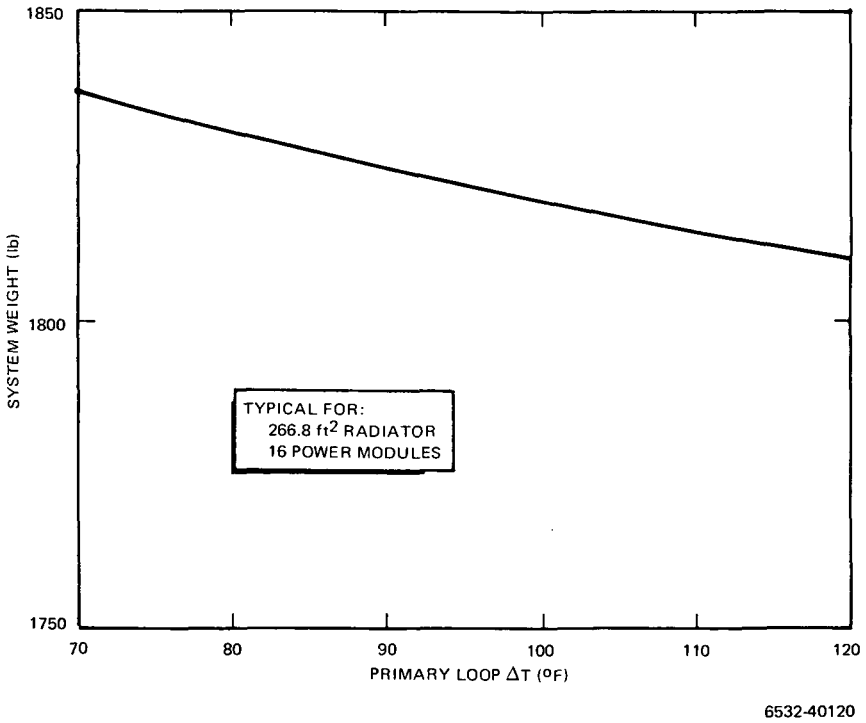

Figure 21. System Weight versus Primary Loop ΔT

The system design point primary loop temperature differential was based on the above limitations. The maximum temperature differential occurs at the system EOL because: (1) the pump modules have degraded, supplying less power to the pump; (2) the pumping magnets have degraded, reducing the pumping capability of the pump; and (3) the power modules have degraded requiring increased reactor power. Thus the primary loop design point EOL ΔT was selected as 95°F, with the assurance that lower values will occur during all previous operation.

h. Primary Loop Pressure Drop Trade Study

A trade study analysis was performed to determine the effects of variation of the primary loop pressure drop. The selection study is equivalent to an evaluation of the pumping power requirements compared to the piping size requirements. Referring to Figure 22, it can be noted that the system weight increases with increasing pressure drop. Thus weight minimization requires utilization of the largest practical piping diameters.

The system design point primary loop pressure drop was selected as 0.97 psi (EOL: at the flowrate required by the selected ΔT). This selection is based on the following considerations:

1) System weight minimization.

2) Piping size limitations as determined from stress analyses.

3) Power module pressure drops sufficient to assure minimal flow maldistribution between modules.

4) Reactor core pressure drops sufficient to minimize flow maldistribution in the core and plenums.

5) Pump current requirements compatible to the utilization of three TEM-14C type pump modules (1800 amp. maximum). The design parameter selection is again an EOL performance statepoint requirement in that component degradation minimizes flow (and thus pressure drop at EOL.

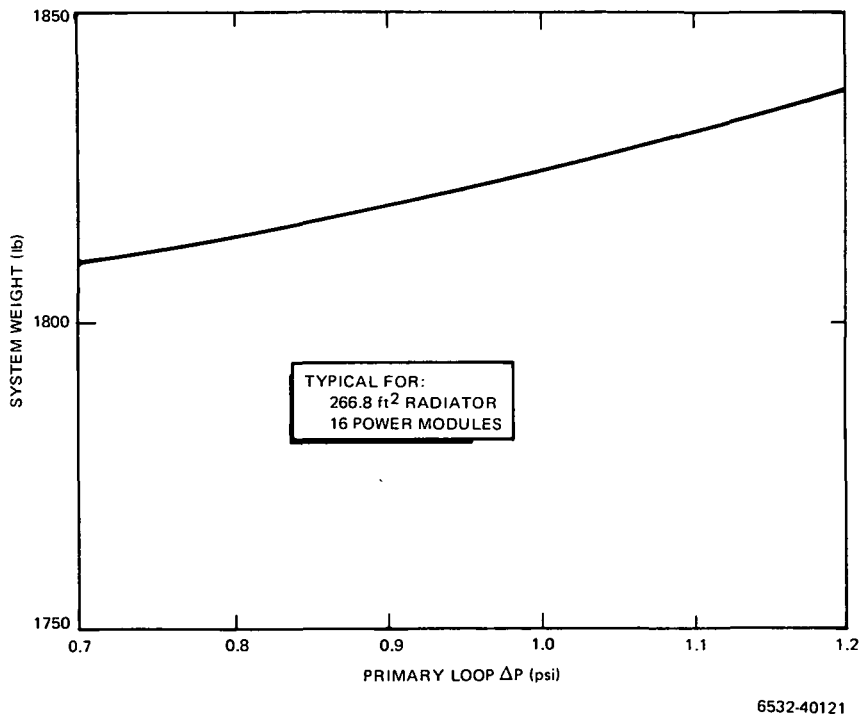

Figure 22. System Weight versus Primary Loop ΔP

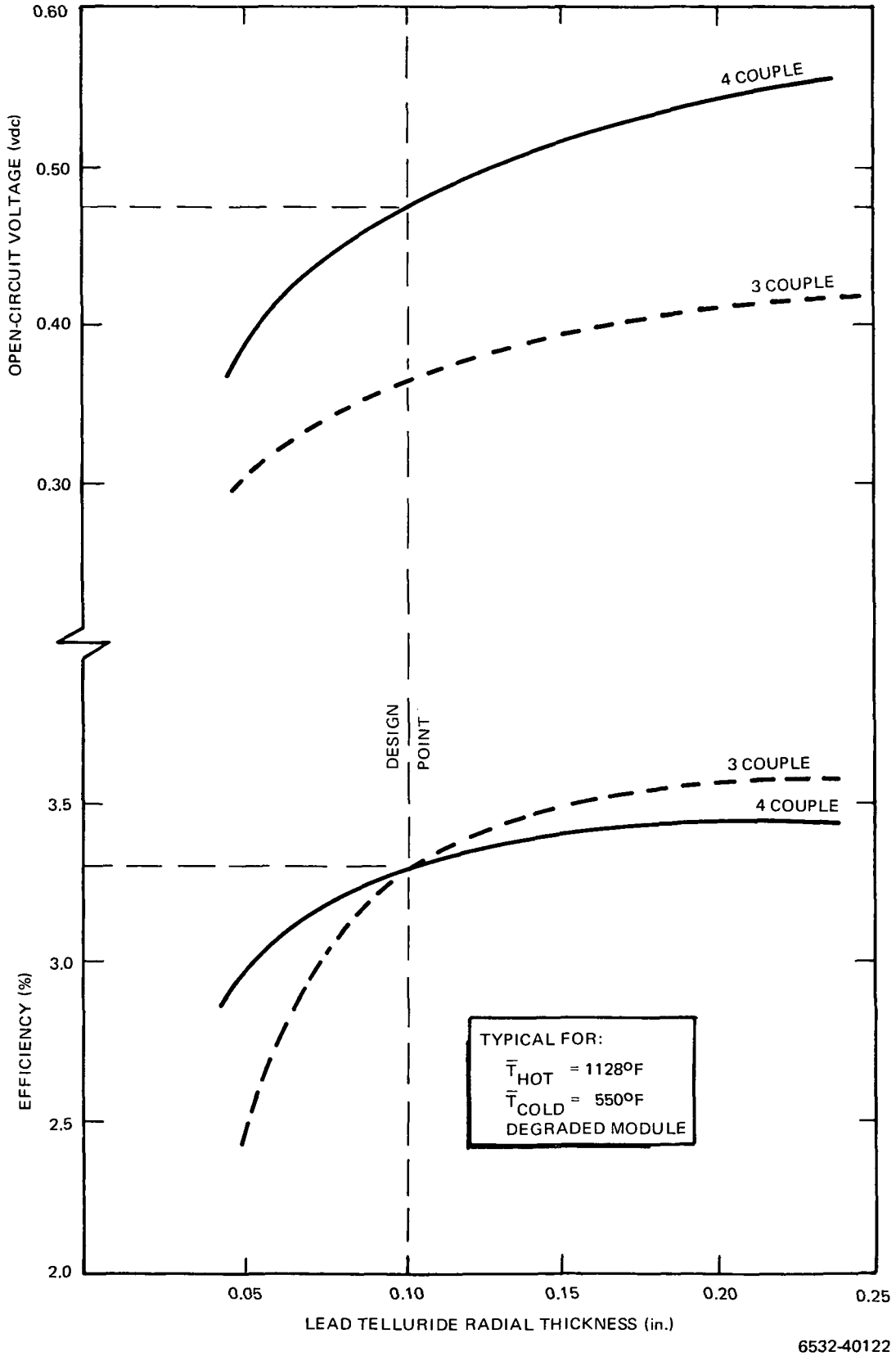

Figure 23. Pump Module Design Parametrics

i. Pump Module Design Analyses

All EM NaK pump analyses were performed in conjunction with the design selection analysis for the pump modules. This design analysis encompassed determination of the optimum couple washer radial thickness and the most suitable number of couples (three or four per module). The module performance analysis was performed by Westinghouse Astronuclear Laboratory, with the system integration studies performed at AI. Results of the analysis which was performed to select the design point pump module are illustrated in Figure 23. This module was designed for the specific performance requirements of the EM NaK pump (based on previous design iterations). The design point selection is indicated on this figure. The washer radial thickness is 0.100 in. (equal to the washer radial thickness in TEM-14A). The module utilizes four thermoelectric couples. This design was chosen because

1) The resultant EOL operating statepoint for the pump/pump module combination is near matched load (thus providing minimum performance sensitivity to degradation phenomena).

2) The module length is compatible with pump integration.

3) The pump module efficiency is maximized within the constraints of module weight.

4) The module design closely resembles that of TEM-14A (thus providing proven performance and fabrication capabilities.

This pump module is designated TEM-14C.

j. Radiator Fin Effectiveness Trade Study

Analyses were performed to determine the fin geometry which achieved the best compromise between system performance, weight, and ease of fabrication. The average fin effectiveness was chosen as that parameter which most uniquely described the design geometry. Within the constraints of fabricability and materials utilization, several values of average radiator fin effectiveness were investigated. The results of this study are indicated in Figure 24, for the design performance statepoint. Note that system weight increases drastically with high values of fin effectiveness.

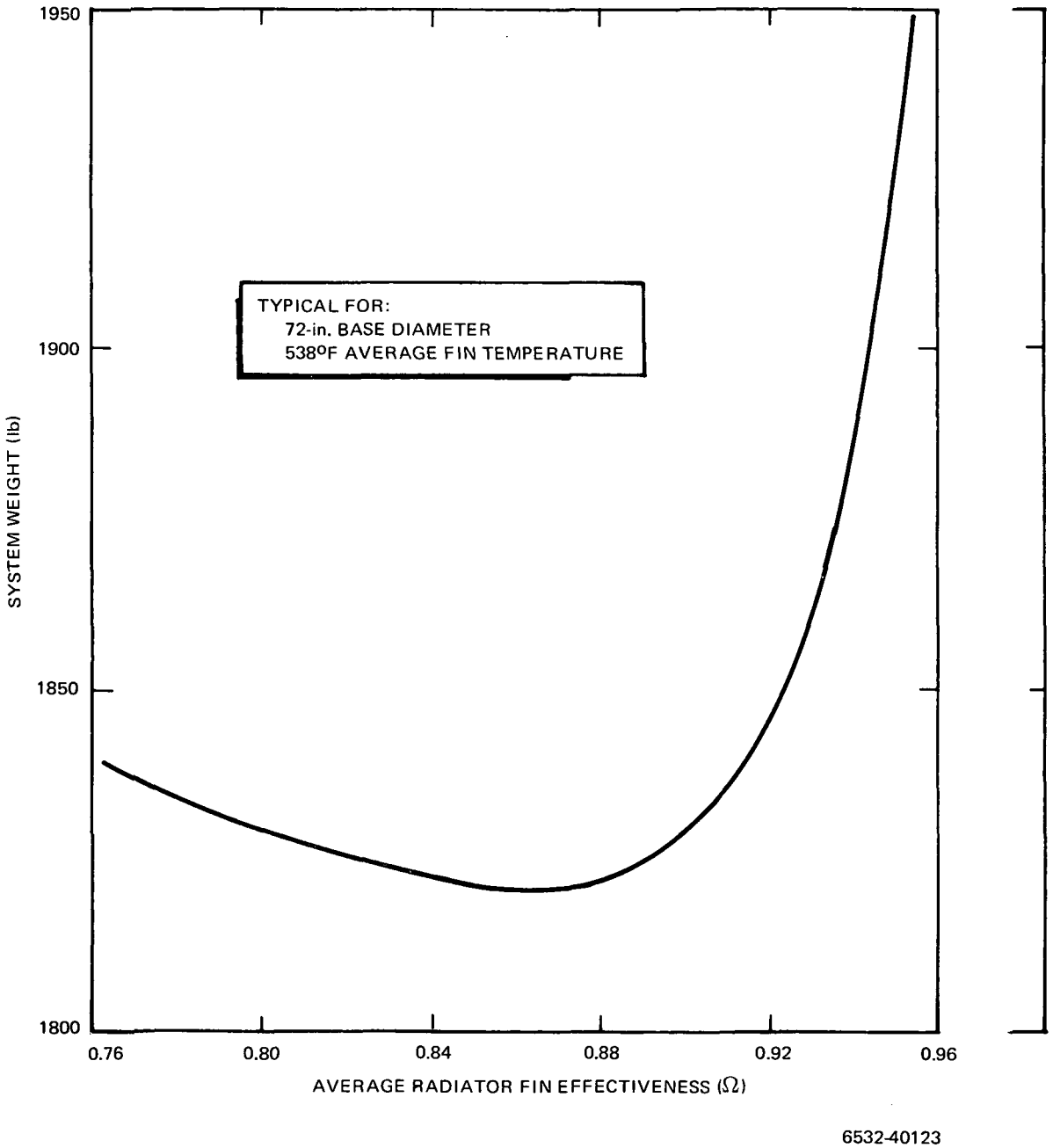

Figure 24. System Weight versus Radiator Fin Effectiveness

The design point fin effectiveness selection was made in the insensitive (flat) portion of the fin effectiveness-weight curve, thus allowing for design variation without possible severe weight penalty. The selected value is 0.85 which minimizes weight and provides a suitable fin design (with respect to fabrication and materials selection).

k. Power Module Utilization Trade Study

Within the design constraints imposed by all previous performance parameter selections, utilization of a given even integral number of power modules totally specifies the system performance statepoint. A trade study was performed to determine the optimum operating statepoint within the constraints of system weight and system envelope. This study involved the analyses of several systems utilizing different numbers of power modules, with subsequent determination of the necessary system performance point and design requirements. System weight and envelope were calculated from these results, and were crossplotted as illustrated in Figure 25.

The design point system uses 16 thermoelectric power modules. As shown in Figure 25, this system exhibits minimum weight with respect to the number of power modules. System envelope is additionally constrained, and handling and testing requirements are satisfied.

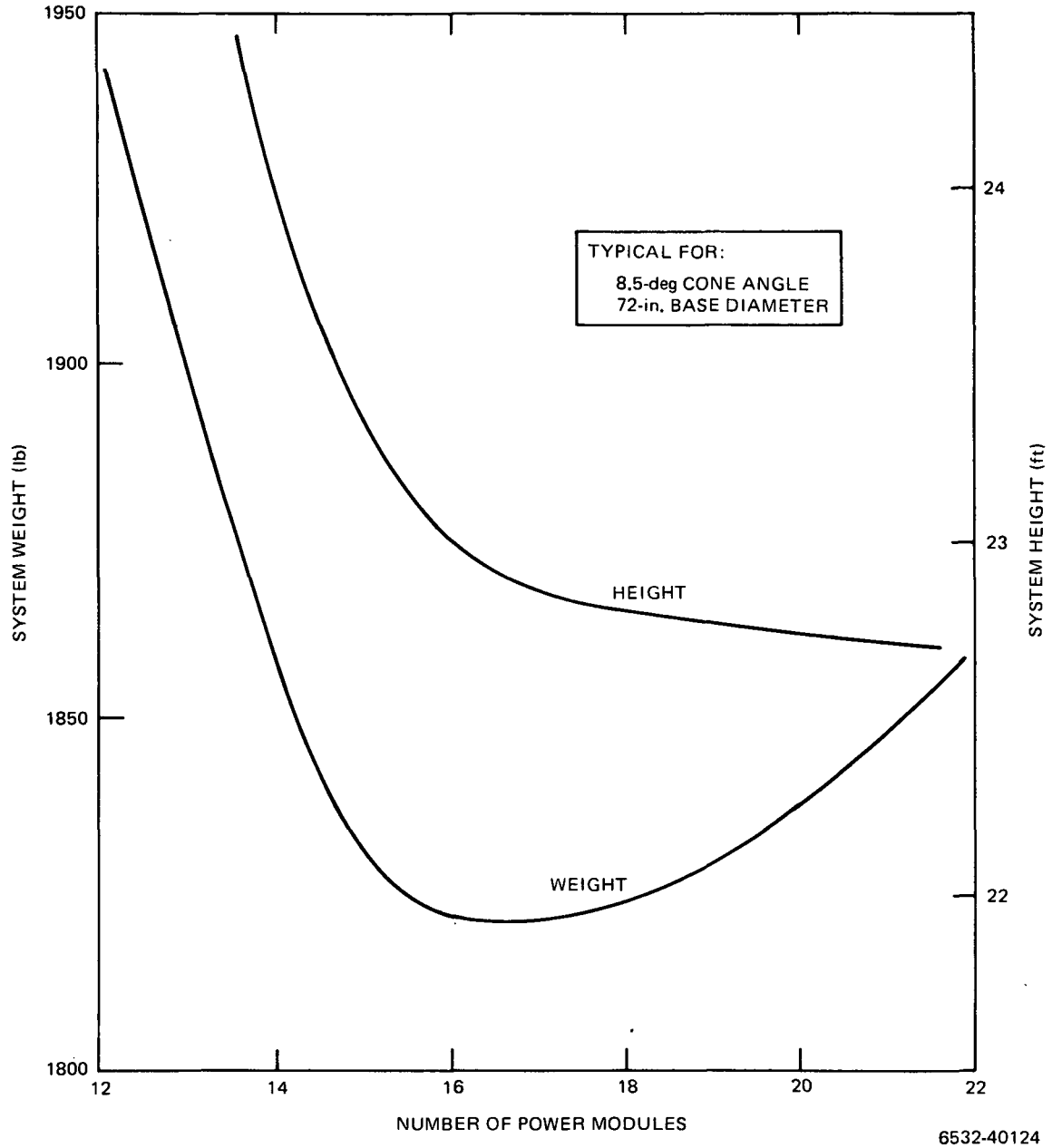

Figure 25. System Weight versus Number of Modules

III. REACTOR

A. REACTOR DESCRIPTION

1. Reactor Configuration

The reactor designed for integration into the 5-kwe Reactor-Thermoelectric System is illustrated in Figure 26. It consists of:

1) A core 10.5 in. in diameter by 16 in. long (fuel-length) made up of 85 1-in. diameter fuel elements packed in a triangular array, plus 12 internal reflector segments (stainless steel clad BeO) to fill the void space between the periphery of the fuel element array and the circular reactor vessel.

2) Inlet and outlet grid plates plus a corner liner to support the fuel elements within the vessel and properly control the flow through the element array.

3) The reactor vessel which is the containment for the NaK coolant and serves as the basic structure of the reactor assembly.

4) The reflector-control assembly, a tapered beryllium reflector assembled in two identical halves, each having an axially sliding control segment associated drive and actuator. The reflector mounting hardware allows the reflector halves to rotate 15 degrees outward for EOL shutdown.

The NaK coolant is fed to the reactor through the two pipes which traverse the reflector through grooves in the outer face at the split line between the two halves. Flow is directed within the inlet plenum by vanes and baffling to produce a flat pressure profile over the inlet grid plate. After passing through the core the flow exits from the outlet plenum through two nozzles oriented 15 degrees off the reflector split-line axis.

A unique aspect of this reactor, relative to all previous SNAP reactors, is the tapered reflector with sliding control segments. All previous SNAP reactors used rotating drums for control. The primary advantage of this new design is the minimization of the diameter of the neutron shield required to shadow the payload.

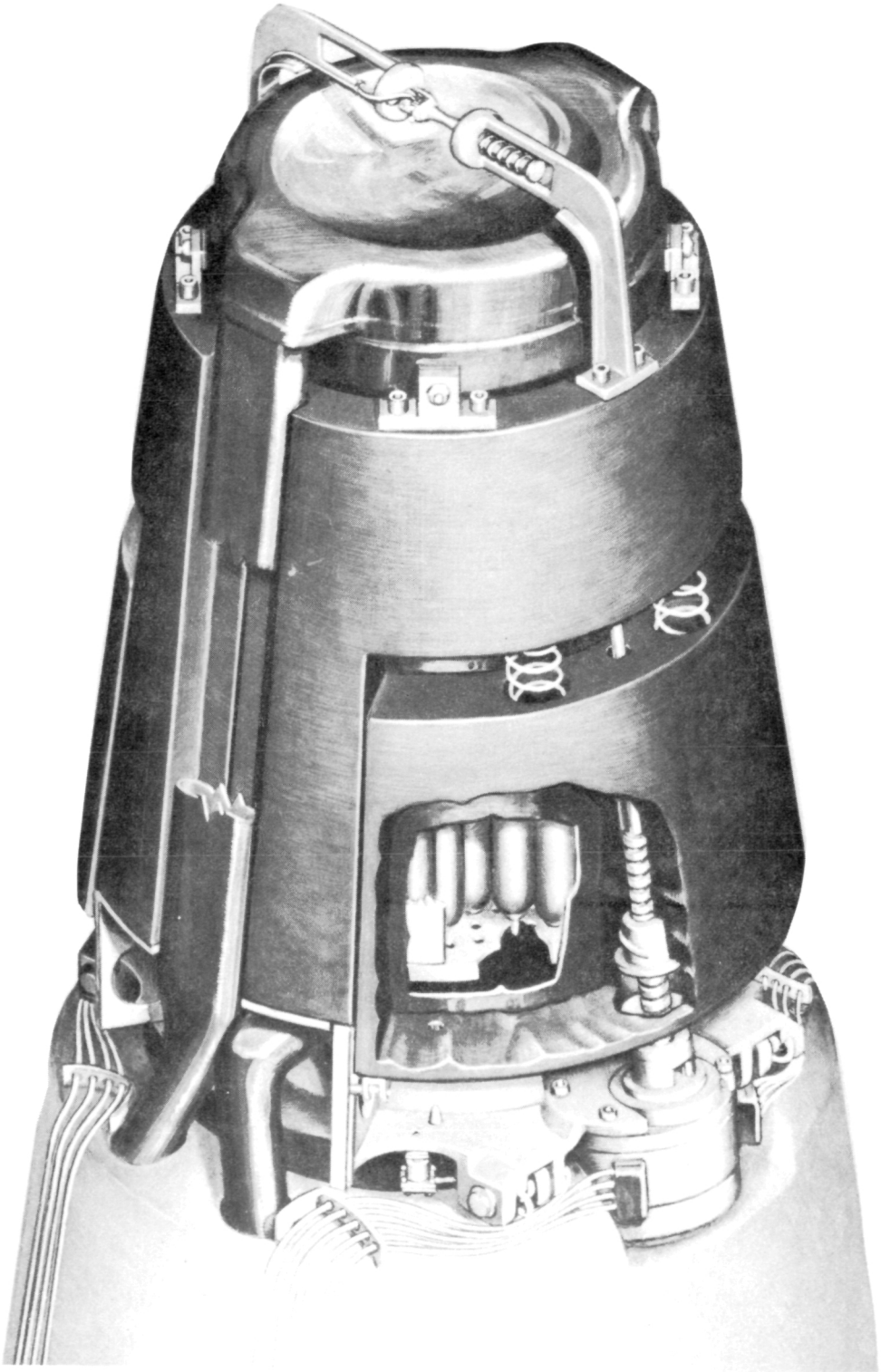

72-JU1-15-60

Figure 26. 5-kwe Reactor Thermoelectric System

2. Core Assembly

The core is designed as a unitized assembly of the 85 fuel elements, inlet and outlet grid plates, fuel element locking rods, internal reflectors and a core liner. The unit is bench assembled, with poison splines in the coolant channels to insure subcriticality, and then inserted into the reactor vessel. Figure 27 illustrates the component arrangement.

Of the 85 fuel elements in a core assembly, 27 are right hand finned (similar to a right hand screw), 27 are left hand and 31 are unfinned (neutral). The elements are arrayed in a triangular lattice as shown on Figure 28. Figure 29 shows the details of the array and the basic dimensional data for the core.

a. Fuel Element

Each fuel element consists of a segmented (5 piece) fuel rod of hydrided 10% uranium-zirconium alloy sealed within a Hastelloy-X cladding. A burnable poison is included as a vapor deposited coating of gadolinium oxide applied to the radial surface of the fuel slugs. A ceramic coating on the inside surfaces of the cladding is the primary hydrogen retention barrier. Basic dimensional data for the fuel element are given in Table 5.

The finned elements have three fins, spaced 120 degrees apart, which spiral through three turns on a 5-in. pitch. The fins, 0.12 in. wide, are formed by hobbing a heavy wall starting tube; the hobbing leaves a fin height of 0.050 in., and then 6 flats are milled to a fin height of 0.010 in., giving a cross section as shown in Figure 30.

A vibration suppressor is installed between the fuel and the cold end cap as illustrated in Figure 30. This device, which resembles a collar button, prevents axial movement of the fuel rod under the dynamic loadings incurred during launch. It is designed to yield by collapse of the prekinked column to accommodate axial fuel growth during reactor operation, without overstressing the cladding tube.

The hot end cap is basically a spherical head closure, butt welded to the cladding tube. The end pins have a 15-degree chamfer to provide a lead-in for the grid plate during core assembly. The pin diameter on all finned elements and on the 12 outer neutral elements is sized for 0.020-in. (nom.) diametral

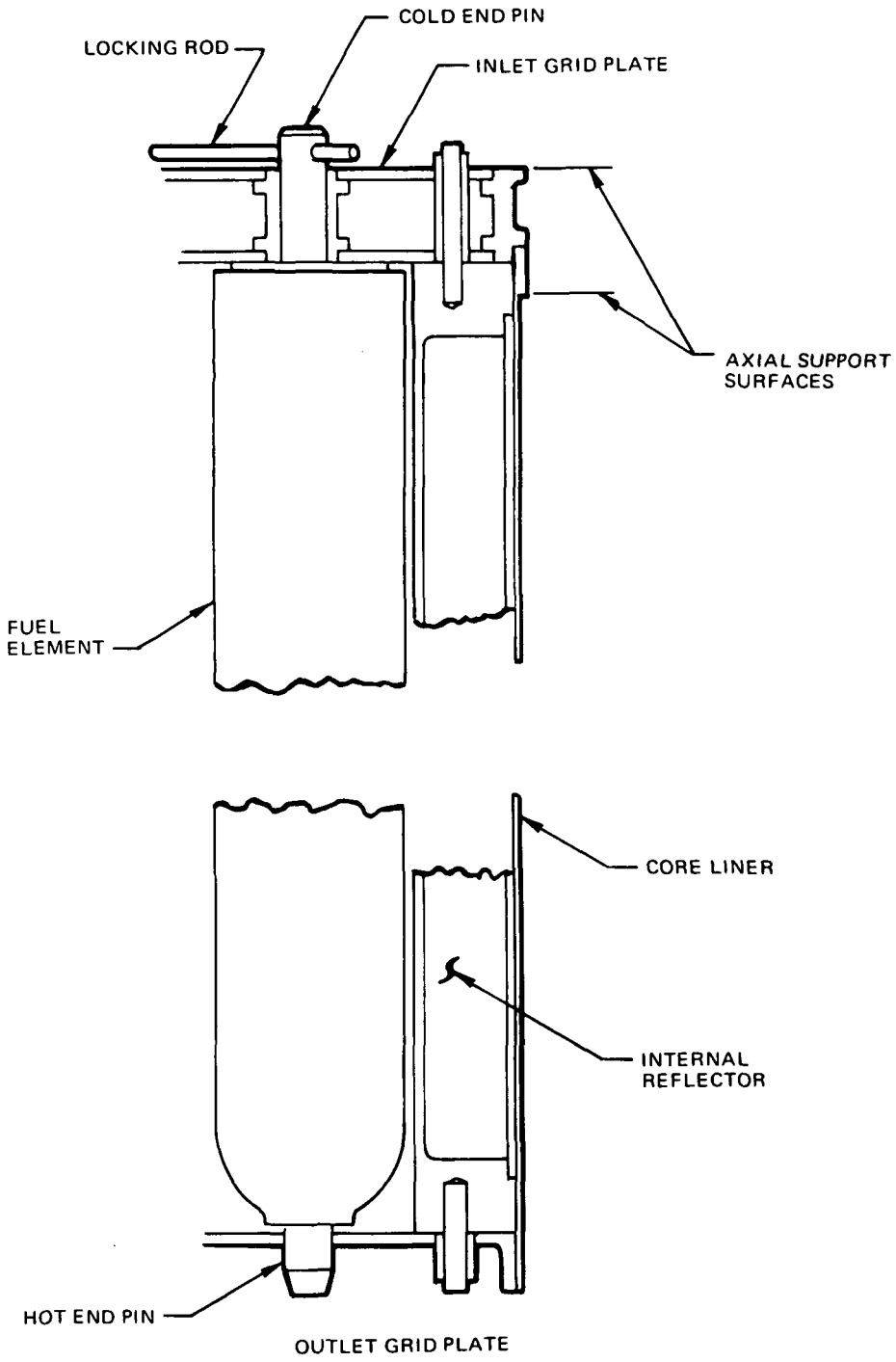

Figure 27. Core Section Details

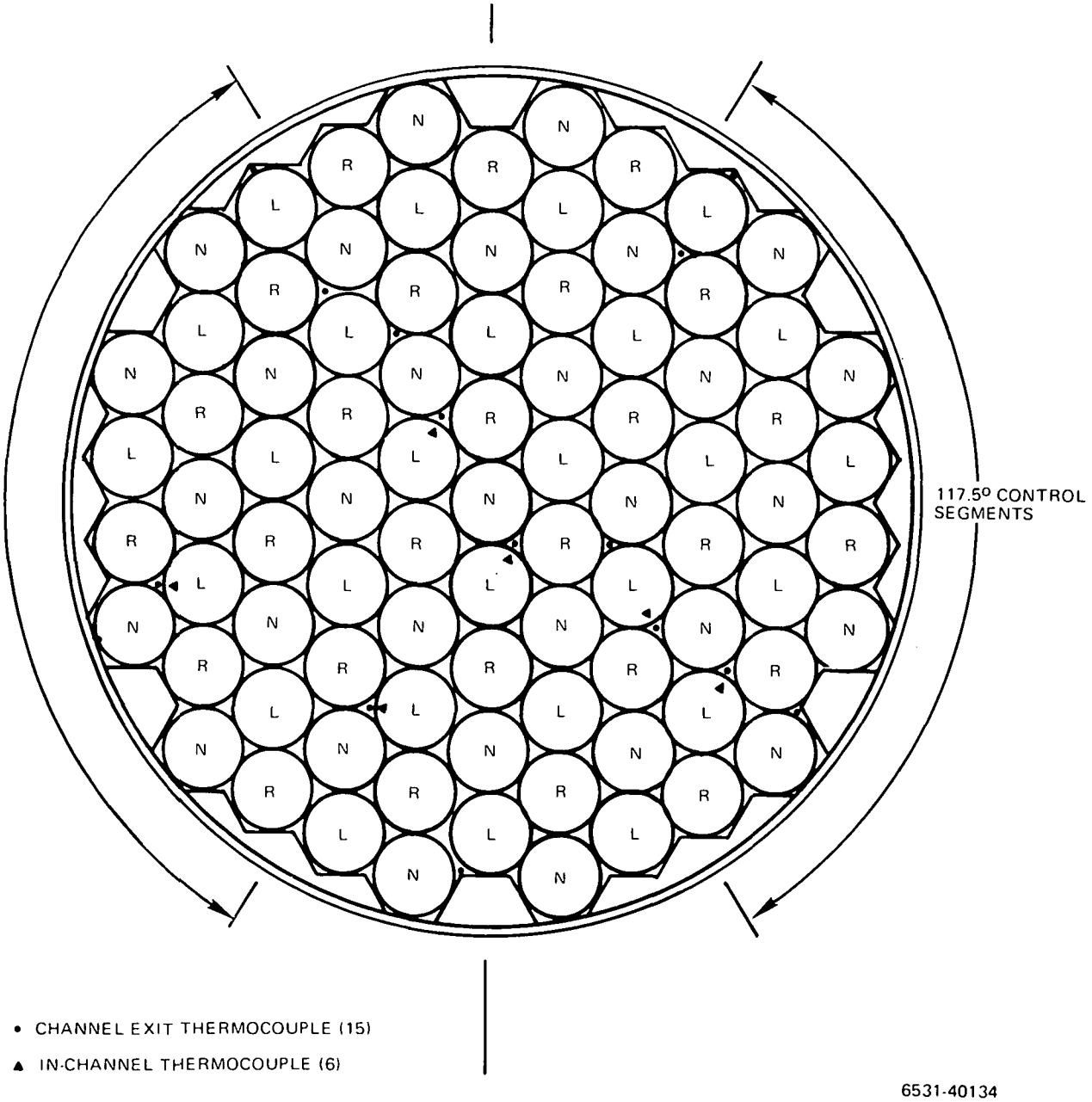

Figure 28. Core Plan

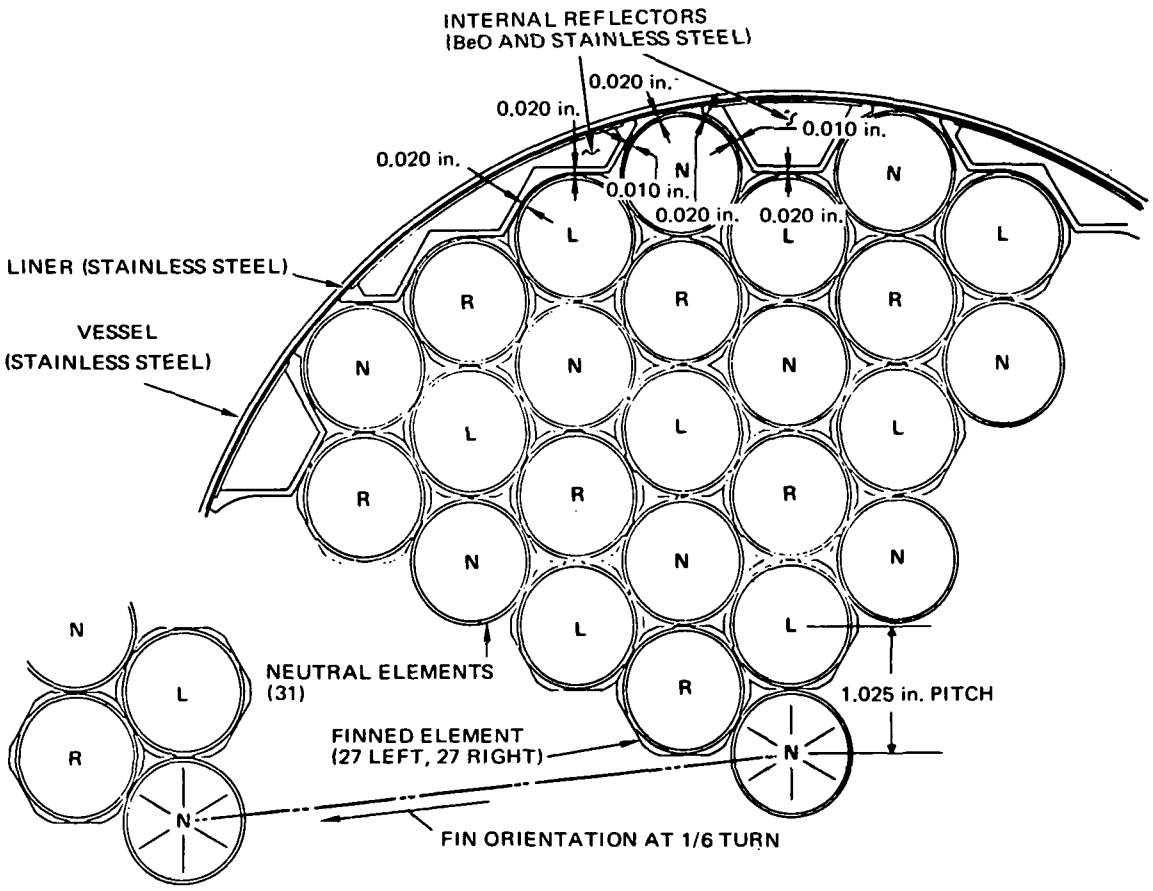

BASIC DATA	
85 ELEMENTS:	1.025 in. PITCH
LINER ID:	10.450 in.
LINER THICKNESS:	0.015 in. (x2)
CLEARANCE:	0.010 in. (x2)
VESSEL ID:	10.500 in.
VESSEL WALL:	0.050 in. (x2)
VESSEL OD:	10.600 in.
FUEL LENGTH:	16.00 in.
FUEL ELEMENT SPACING	
CLAD-CLAD:	0.020 in.
FIN-CLAD	0.010 in.
CLADDING TO INTERNAL REFLECTOR	AS SHOWN

72-JU6-12-10C

Figure 29. Core Plan Details

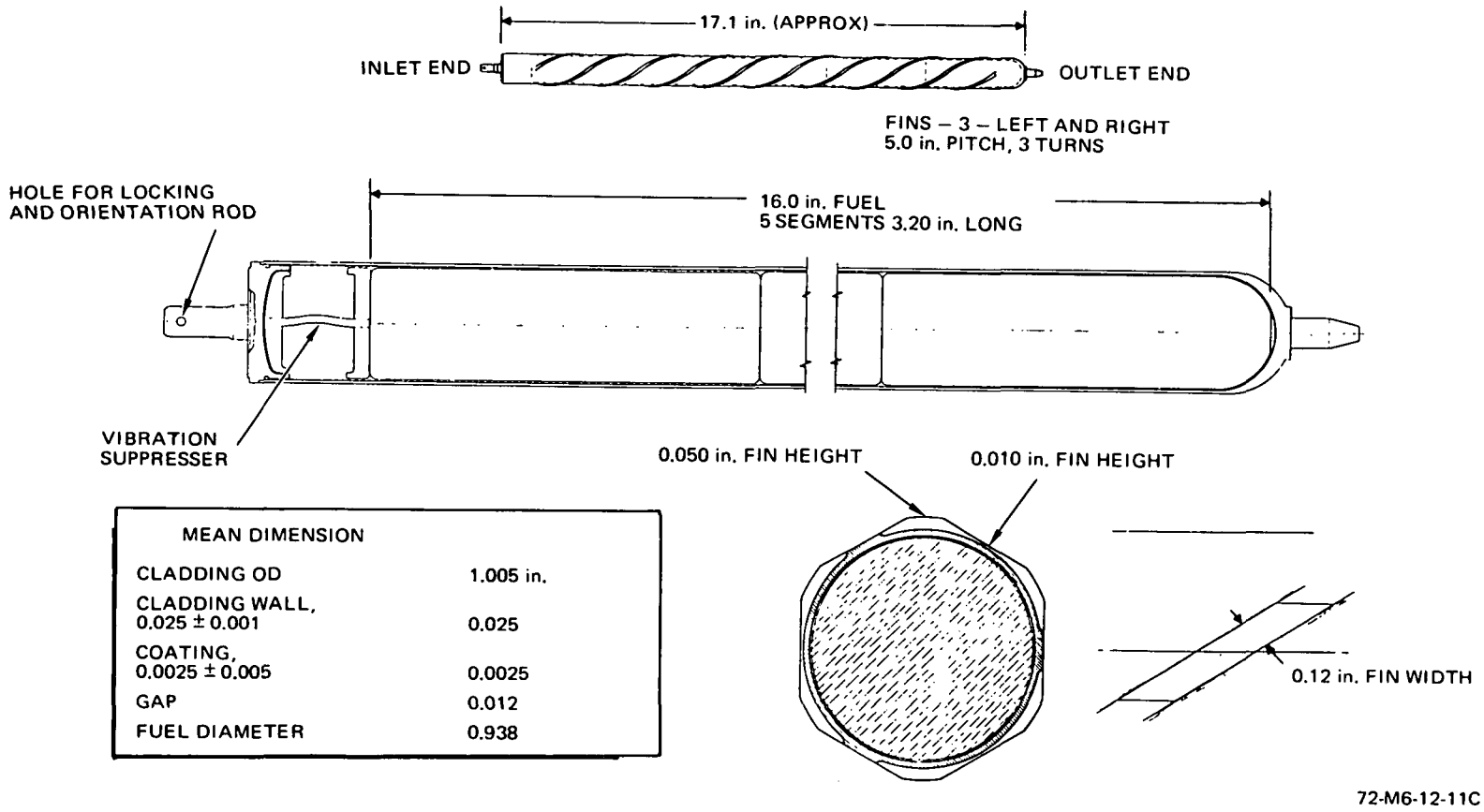

MEAN DIMENSION	
CLADDING OD	1.005 in.
CLADDING WALL, 0.025 ± 0.001	0.025
COATING, 0.0025 ± 0.005	0.0025
GAP	0.012
FUEL DIAMETER	0.938

Figure 30. Fuel Element Cross Section

TABLE 5
FUEL ELEMENT DIMENSIONS
(85-Element, 1.025-in. Pitch Reactor)
(All Dimensions in Inches)

	Lower Limit	Mean	Upper Limit
Pitch, 1.025		1.025	
Spacing		0.020	
Cladding OD	1.002	1.005	1.008
Cladding Wall, 0.025 ± 0.001	0.024	0.025	0.026
(x 2)	0.048	0.050	0.052
Cladding ID, 0.955 ± 0.001	0.954	0.955	0.956
Glass Thickness, 0.0025 ± 0.0005	0.002	0.0025	0.003
(x 2)	0.004	0.005	0.006
Glass ID	0.948	0.950	0.952
Diametral Gap, 0.011 to 0.013*	0.011	0.012	0.013
Fuel Diameter, 0.9xx ± 0.0005†	0.935	0.938	0.941
Fuel Length (nominal)		16.0	
Straightness (TIR)		0.012	

*Specified Dimensions — all others are reference
†Fuel diameter ground and/or selected to give 0.011 to 0.013 in. diameter gap

clearance in the grid plate hole, and on the inner neutral elements the pin is sized for a close fit (0.002- to 0.005-in. diametral clearance).

The cold end cap is a flat head closure with an interference fit between the coated tube ID and the coated OD of the engaging socket portion of the cap. After the cap is inserted, the engaged section of the cap and tube is heated to the softening temperature of the ceramic to blend the coating into a continuous hydrogen barrier. The cold end pins are all sized for a close fit (0.002- to 0.005-in. diametral clearance) engagement in the grid plate holes. This close fit engagement is limited to a 0.125-in. length engagement adjacent to the end surface of the cap. The remainder is reduced in diameter to facilitate assembly of finned elements adjacent to finned elements.

b. Grid Plates

As illustrated in Figure 27, the inlet grid plate is the basic structural element of the core assembly. The fuel elements are secured to the grid plate by the locking rods which are threaded through holes in the fuel element and pins. Each locking rod secures a complete row of elements across the core and thereby also performs a fuel element orientation function: maintains the correct relationship between the flatted fins and the clad OD of adjacent elements.

The inlet grid plate is designed as a brazed sandwich structure made up of two 0.062-in. thick facing sheets, an outer rim, and 85 spacer posts located at the fuel element axis positions. The spacer posts and the outer rim act as shear transfer elements and thereby cause the two facing sheets to function as though they are integral parts of a solid plate. This sandwich, with a 0.376-in. separation between the facing sheets, has a strength equivalent to a 0.38-in. thick solid plate, and a stiffness equivalent to a 0.41-in. thick solid plate. The sandwich plate approach thereby produces a significant weight saving.

The outlet grid plate provides only lateral spacing and support for the fuel elements. This plate is, therefore, of minimum thickness (0.062 in.). An integral rim at the outer edge (0.062 thick by 0.025 in. long) is included in the design to give the plate flatness stability and to provide a larger engagement with the core liner.

Both grid plates are fabricated from Type 316 SS; the upper grid plate assembly is furnace brazed using a nickel base braze alloy. The fuel element positioning holes are precision located (within 0.001 in. of true position) and reamed to a tolerance of ±0.0005 in. The coolant passage holes are 0.25 in. in diameter, except for 12 of the outer boundary channel holes, which are 0.190 in. in diameter due to space limitations. Each plate also has 12, 0.170-in.-diameter holes near the periphery for engagement of internal reflector positioning pins.

The use of the brazed sandwich structural grid plate is based on experience on almost identical designs in the SNAP 10A and SNAP 2 DRM reactors. This covers fabrication of over 20 grid plate assemblies and experimental tests which verify the strength and deflection characteristics of the concept.

c. Internal Reflectors

As shown in Figures 28 and 29, 12 internal reflector segments fill the spaces between the noncircular boundary of the fuel element array and the cylindrical core liner. These consist of BeO shapes contained in sealed stainless steel enclosures. The surfaces which face the boundary fuel elements are configured to provide flowrates in individual boundary channels, which minimizes the possible temperature difference across the boundary fuel elements.

Fast neutron irradiation of BeO causes material swelling and helium generation, which produces a pressure buildup within the stainless steel container. The design therefore includes a 1.5-in. axial gas space to limit the pressure at EOL to 18 psi, equal to the NaK coolant pressure if both NaK volume accumulator bellows fail. The internal reflectors, initially evacuated, therefore have a negative internal pressure throughout reactor lifetime.

Each internal reflector is held in position by a pin at each end which engages the grid plates. Because reflector location relative to the boundary elements is critical in establishing the boundary channel flow areas, these pins are custom located during the core assembly sequence.

d. Core Liner

The core liner is a 0.015-in. thick stainless steel cylinder closely fitted around the internal reflectors. Its primary function is to limit core bypass flow to a very low value (less than 0.5%) to minimize the bowing stresses induced in the boundary fuel elements by cross-element temperature differentials, while still allowing a generous clearance for insertion of the unitized core assembly into the reactor vessel.

The liner has an external support flange at the core inlet end which fits between a step in the reactor vessel ID and the grid plate. The clamping pressure induced by the weld shrinkage, when the vessel closure weld is made, prevents coolant leakage from the core inlet area into the clearance between the liner and the reactor vessel. The outlet grid plate fits into the liner and is secured axially by a weld to the liner.

The clearance between the liner and the reactor vessel is open to the outlet plenum. The liner therefore operates under a low internal pressure,

starting at zero at the outlet end and increasing almost linearly to the core pressure drop (0.19 psi) at the inlet end.

B. NUCLEAR PERFORMANCE

From the results of the reactor parametric studies and the reactor thermoelectric system optimization studies, the reactor design summarized in Table 6 was selected as the conceptual design. The reactor was designed for continuous operation for 5 years at 110 kwt. The thermoelectric system power requirements to produce 5 kwe do not exceed 102 kwt. This has the effect of providing additional EOL reactivity margins.

TABLE 6
REACTOR DESIGN SUMMARY

Thermal power (kwt)	110
Number of fuel elements	85
Active fuel length (in.)	16
Lattice pitch (in.)	1.025
Inter-element spacing (mils)	20
Cladding thickness (mils)	25
Glass thickness (mils)	2.5
Gap thickness (mils)	6.0
Fuel diameter (in.)	0.938
Active core diameter (in.)	9.920
Active core volume (liters)	20.3
Core vessel OD (in.)	10.600
Vessel-reflector clearance (in.)	0.060
Reflector midplane thickness (in.)	2.386
Reactor midplane envelope (in.)	15.492
Taper angle (degree)	8.5
Segment stroke (in.)	4.0
Movable angle (degree)	235
Fissile mass (kg U^{235})	9.0
N_H in Fuel (10^{22} at/cc)	5.72

1. Reactivity and Reactivity Lifetime

The reactivity requirements for the design power level and the operating power level are shown in Table 7. The reactor nuclear characteristics are shown in Table 8. As may be seen, a cold, unpoisoned reactivity of $7.74 is needed to provide the reactivity requirements for 5-years' operation at 110 kwt with a $0.50 EOL reactivity margin. At the operating power level the EOL reactivity margin increases to $1.26. The reactivity as a function of time at the design power level is shown in Figure 31. Also shown is the cold, shutdown reactivity with the control segments fully open.

2. Prepoison Selection and Loading

The nuclear parameters which influence the selection of a prepoison material are the burnout rate, the effect on the prompt temperature coefficient, and the specific worth ($/gm). The non-nuclear parameters are the compatibility of

TABLE 7
REACTIVITY REQUIREMENTS
($)

	Design		Operating	
Temperature defect	2.18		2.09	
Power defect	0.04		0.03	
Equilibrium Xe^{135}	0.18		0.15	
Hydrogen redistribution	0.10		0.09	
Total recoverable losses		2.50		2.36
U^{235} burnout	0.82		0.69	
U^{236} buildup	0.31		0.26	
U^{238} burnout	-0.02		-0.02	
Gross fission products	0.92		0.78	
Equilibrium Sm^{149}	0.94		0.90	
Hydrogen loss	1.16		0.75	
Residual prepoison	0.61		0.76	
Total nonrecoverable losses		4.74		4.12
Total requirements		7.24		6.48

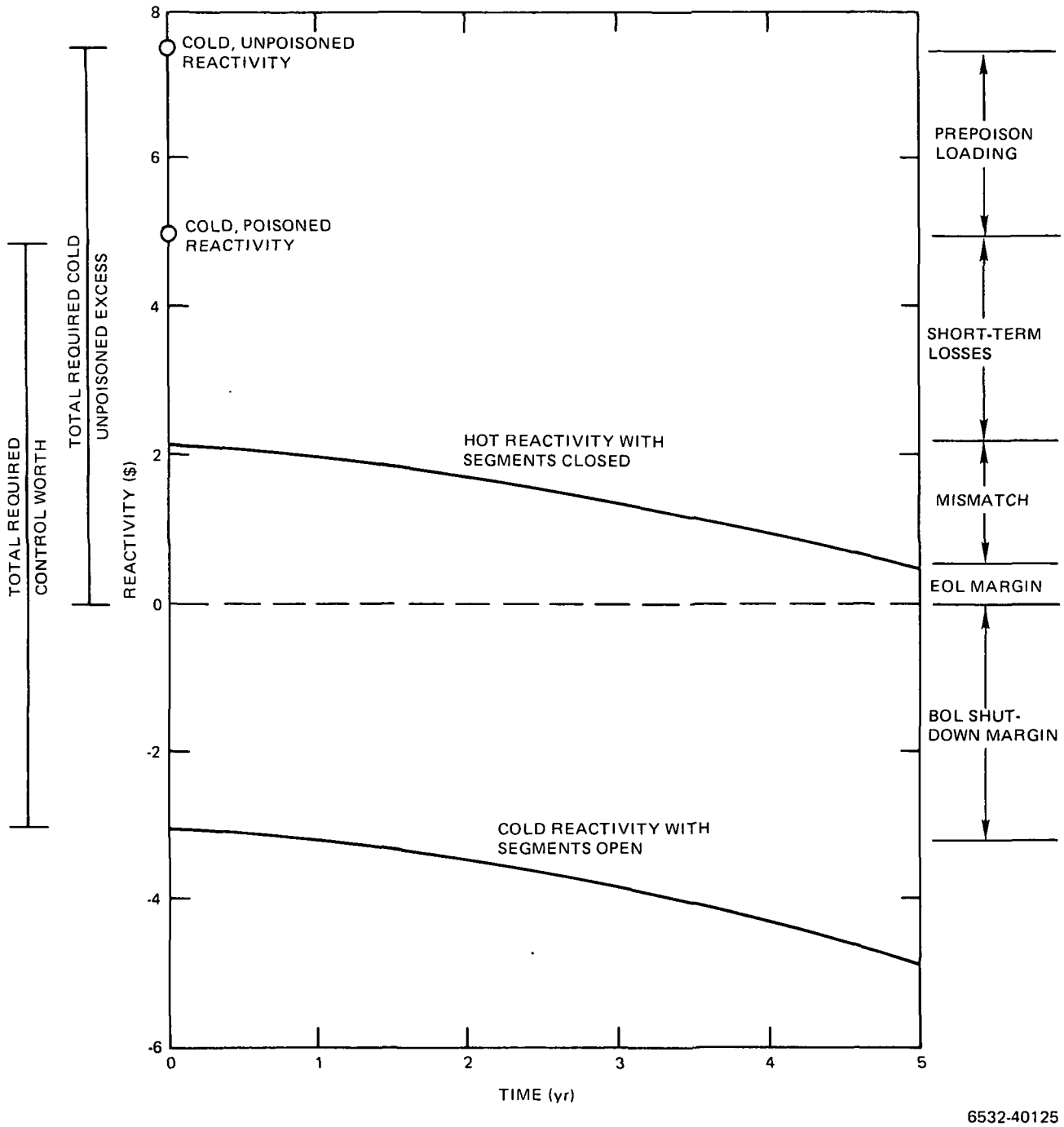

Figure 31. 5-kwe Reactor-Reactivity versus Time

the poison with other core materials, the availability and cost of the poison, and the method of depositing the poison in the core.

The reason for including a prepoison in the reactor is to reduce the control requirements by reducing the reactivity loss over life. The burnout of the prepoison helps to offset the losses from fuel depletion, fission product buildup, and hydrogen loss.

The poisons which have both nuclear and physical properties which make them suitable for use in SNAP reactors are samarium, gadolinium, gadolinium enriched in Gd^{155}, europium enriched in Eu^{151}, and erbium.

TABLE 8

NUCLEAR CHARACTERISTICS
($)

	Design	Operating
Cold, unpoisoned reactivity	7.74	7.74
Hot prepoison loading	3.00	3.00
Recoverable losses	2.50	2.36
Hot, poisoned reactivity	2.24	2.38
Nonrecoverable losses	4.74	4.12
Prepoison burnout	2.39	2.24
EOL reactivity margin	0.50	1.26
Control worth	7.74	7.74
BOL shutdown margin	3.00	3.00

3. Control Worth

Reactivity control is provided by two sliding reflector segments. The movable segments subtend 235 degrees of the reactor circumference and open 4-in. windows about the vertical center of the core. The sliding segments move along the 8.5-degree taper angle rather than parallel to the core vessel surface. This also opens gaps between the reflector and core vessel and between the sliding segment and fixed reflector which enhance the control worth.

A reliability analysis indicated that more than two segments did not yield a significant increase in reliability. Two segments were selected from the standpoint of simplicity and cost.

A total control worth of $7.74 was determined from two-dimensional DOT calculations in R, Z geometry. In the DOT calculations, it was necessary to assume that the segments subtend the full 360 degrees. The worth obtained from the DOT calculations was multiplied by 235/360 to obtain the worth of the 235-degree segments. Calculations were made with the segments closed, 2-in. open, and 4-in. open. The worth of the first 2-in. opening was $3.95, and the worth from 2 - to 4-in. open was $3.79. This indicates that the control worth is very nearly linear over the 4-in. stroke.

4. Temperature Coefficients

Partial temperature coefficients of reactivity are shown in Table 9. The fuel coefficient is made up of the spectral, Doppler, and axial fuel expansion coefficients. The isothermal coefficient is the sum of the fuel, grid, and reflector coefficients. The isothermal coefficient is used to determine the reactivity loss in going from ambient to operating temperatures. The partial temperature coefficients are used to predict the kinetic behavior of the reactor.

TABLE 9

PARTIAL TEMPERATURE COEFFICIENTS
(¢/°F)

Spectral	+0.007
Doppler	-0.022
Fuel axial expansion	-0.051
Fuel coefficient	-0.066
Inlet grid	-0.060
Outlet grid	-0.020
Reflector heating	-0.034
Isothermal	-0.18

The coefficients were determined using the k-difference method. The various effects which cause the reactivity to change with temperature, such as Doppler broadening of cross sections and thermal expansion of the different reactor components, were evaluated individually using the APC code. The calculations were performed at BOL conditions. The gadolinium prepoison loading has a positive effect on the spectral component of the fuel coefficient. As the gadolinium burns

out over life, the fuel coefficient becomes more negative. The effect of the burnout of gadolinium is partially offset by the buildup of Sm^{149} fission product. The fuel coefficient at EOL was evaluated to be -0.108¢/°F.

C. THERMAL HYDRAULIC PERFORMANCE

1. Core Thermal Performance

The core power requirements vary over the lifetime of the reactor because of the degradation of the thermoelectric components of the total system. To provide margins for uncertainties, the reactor is designed to operate at a level somewhat more severe than system requirements. The design-to conditions are applied with the BOL configuration when the fuel-cladding gas gap is largest and, thus, the thermal gradients are somewhat higher than the EOL configuration. Because the exact manufactured configuration of each individual element is not known, other than that its dimensions are within a specified tolerance range, nominal operational conditions must be calculated for an "ideal" average element. The ideal is primarily the assumption that the element is perfectly straight and that the fuel segments are all centered in the clad. The calculational methods used are described in Reference 2. Table 10 shows nominal operating conditions for design-to, BOL and EOL conditions.

TABLE 10

NOMINAL OPERATING CONDITIONS

Parameter	Design*	BOL	EOL
Thermal power (kwt)	110	95	101
Coolant outlet temperature (°F)	1200	1148	1200
Coolant temperature rise, (°F)	100	88	95
Peak fuel centerline temperature (°F)	1310	1247	1286
Peak fuel average temperature (°F)	1292	1232	1270
Maximum cross element ΔT (°F)	21.4	18.8	17.2
Core flowrate (lb/hr)	17900	17500	17400
Average channel velocity (fps)	1.71	1.67	1.66
Average Reynolds number	6940	6760	6740
Minimum Reynolds number	2990	2910	2900
Core pressure drop (psi)	0.19	0.18	0.18

*BOL power distribution

Hot channel factors have been calculated to take into account the expected range of uncertainties involved in the calculation of reactor power and temperatures. The uncertainties are divided into tolerance effects, property effects, and power and flow effects. The parameter values assumed are the maximum expected variations, or tolerances, and are thus considered 3σ limit values. The uncertainty factors are listed in Tables 11, 12, and 13 for design-to, BOL, and EOL conditions.

The tolerance effects have to do with the allowable range of parameters during the manufacture of the fuel element. The property effects are concerned with uncertainties in the material properties. The power and flow effects are concerned with the uncertainty in calculated power profile and with the possible variations in flow and heat flux distributions from fuel element clustering and fuel slug asymmetry in the cladding tube.

For the design conditions, Table 11, the coolant outlet temperature uncertainty is 18.5°F and the maximum fuel temperature uncertainty is 20.8°F. The maximum fuel temperature, after adding the 20.8°F uncertainty and a 5°F allowance for control band, is 1318°F.

2. Hydraulic Performance

The reactor coolant flow, supplied by the primary thermoelectric pump, is 17,500 lb/hr initially and 17/400 lb/hr after 5 years. The design-to-flow is 17,900 lb/hr, which corresponds to a 100°F core ΔT at the design-to reactor power of 110 kw.

The 85-element core has 204 coolant channels. At the design flow, the average coolant channel velocity is 1.71 fps and the core bundle pressure drop (plenum-to-plenum) is 0.19 psi. The fuel element spacing in the core is 0.020 in. The finned elements have three fins each, which extend 0.050 in. into the coolant channel, but are cut down to 0.010 in. between fuel elements. An average fin height of 0.030 in. has been used for interchannel mixing calculations. The interchannel mixing factor for a typical coolant channel is 27%/in.

In addition to the regular coolant channels in the core there are four types of different sized channels at the core periphery (Figure 32). Each regular (Type 1) coolant channel is bounded by two finned and one neutral fuel element. Each of the three fins on a finned element must be in one of the six channels surrounding

TABLE 11

HOT CHANNEL FACTORS, CENTER ELEMENT, DESIGN-TO CONDITIONS

	Uncertainty	ΔT_{cool} (°F)	ΔT_{fuel} (°F)
Tolerance Effects			
Gas gap thickness	±0.001 in.	--	±9.9
Hydrogen barrier thickness	±0.0005 in.	--	±1.0
Cladding thickness	±0.0015 in.	--	±0.2
Fuel uranium content	±0.3%	±2.5	±3.8
Fuel hydrogen content	±0.15 x 10^{22} atoms/cc	±1.7	±2.8
Property Effects			
NaK film heat transfer	±20%	--	±2.9
Fuel thermal conductivity	±12%	--	±1.9
Gas gap conductivity	±14%	--	±8.8
Gas gap accommodation	±30%	--	±1.5
Power and Flow Effects			
Channel flow distribution	±6.4%	±8.9	±6.5
Element/element power distribution	±5%	±7.0	±9.7
Fuel slug asymmetry	variable	±14.0	+6.0 -24.0
Thermocouple error	1/2%/thermocouple (4 are averaged)	±3.0	±3.0
Statistical Sum		±18.5	+20.8 -31.2
		Nominal	Hot Channel
Nominal Operation-Maximum Values			
Channel outlet temperature (°F)		1229	1247.5
Fuel temperature (°F)		1292	1312.8
Top of Control Band Values (+5°F)			
Channel outlet temperature (°F)		--	1253.5
Fuel temperature (°F)		--	1317.8

9.4

TABLE 12

HOT CHANNEL FACTORS, CENTER ELEMENT, BOL

	Uncertainty	ΔT_{cool} (°F)	ΔT_{fuel} (°F)
Tolerance Effects			
Gas gap thickness	±0.001 in.	--	±8.6
Hydrogen barrier thickness	±0.0005 in.	--	±0.8
Cladding thickness	±0.0015 in.	--	±0.2
Fuel uranium content	±0.3%	±2.2	±3.0
Fuel hydrogen content	±0.15 x 10^{22} atoms/cc	±1.5	±2.4
Property Effects			
NaK film heat transfer	±30%	--	±2.5
Fuel thermal conductivity	±12%	--	±1.7
Gas gap conductivity	±14%	--	±7.6 — 8.1
Gas gap accommodation	±30%	--	±1.3
Power and Flow Effects			
Channel flow distribution	±6.4%	±7.7	±5.6
Element/element power distribution	±5%	±6.1	±8.4
Fuel slug asymmetry	variable	±12.1	+5.7 -22.9
Thermocouple error	1/2%/thermocouple (4 are averaged)	±3.0	±3.0
Statistical sum		±16.1	+18.1 -28.7
		Nominal	Hot Channel
Nominal Operation - Maximum Values			
Channel outlet temperature (°F)		1173	1189.1
Fuel temperature (°F)		1232	1250.1
Top of Control Band Values (+5°F)			
Channel outlet temperature (°F)			1195.1
Fuel temperature (°F)			1255.1

TABLE 13

HOT CHANNEL FACTORS, CENTER ELEMENT, EOL

	Uncertainty	ΔT_{cool} (°F)	ΔT_{fuel} (°F)
Tolerance Effects			
Gas gap thickness	±0.001 in.		±8.2
Hydrogen barrier thickness	±0.0005 in.		±0.9
Cladding thickness	±0.0015 in.		±0.2
Fuel uranium content	±0.3%	±2.4	±2.8
Fuel hydrogen content	±0.15 x 10^{22} atoms/cc	±1.6	±2.1
Property Effects			
Fuel swelling	0.0038 in. ΔD		±16.0
NaK film heat transfer	±30%		±2.6
Fuel thermal conductivity	±12%		±1.6
Gas gap conductivity	±14%		±5.6
Gas gap accommodation	±30%		±0.8
Power and Flow Effects			
Channel flow distribution	±6.4%	±8.2	±5.9
Element/element power distribution	±5%	±6.5	±7.8
Fuel slug asymmetry	variable	±13.0	+5.1 -20.3
Thermocouple error	1/2%/thermocouple (4 are averaged)	±3.0	±3.0
Statistical Sum		±17.2	+23.2 -30.4
		Nominal	Hot Channel
Nominal Operation - Maximum Values			
Channel outlet termperature (°F)		1225	1242.2
Fuel temperature (°F)		1270	1293.2
Top of Control Band Values (+5°F)			
Channel outlet temperature			1248.2
Fuel temperature (°F)			1298.2

8.5

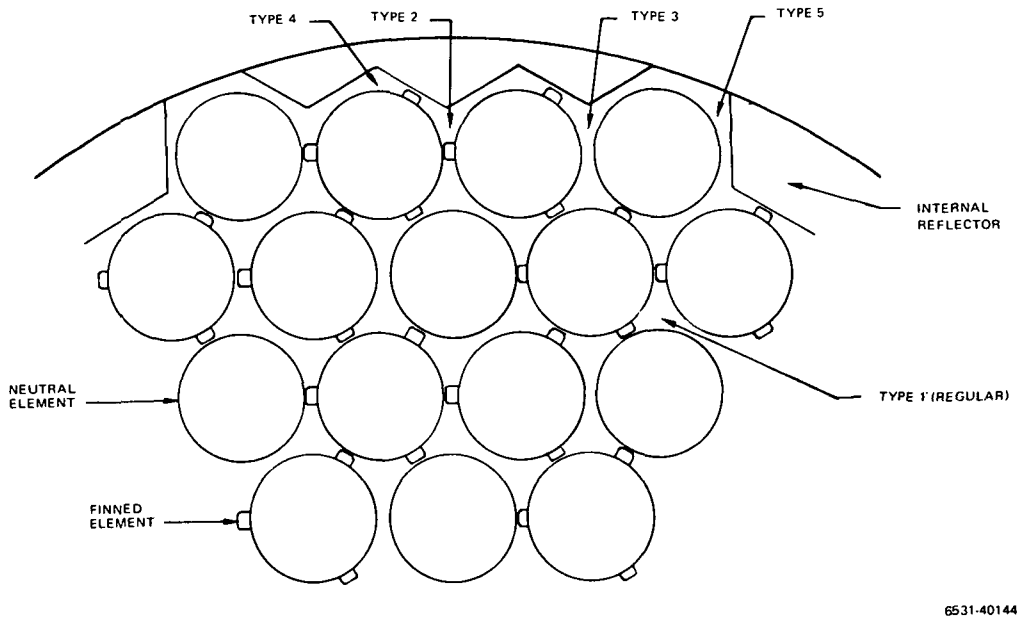

Figure 32. Flow Channels at Edge of Core

TABLE 14

COOLANT CHANNEL DATA

Channel Type	Number	Area* ($in.^2$)	Velocity (ft/sec)	N_{Re}	Fin Area ($in.^2$)	Flow (lb/hr)
1	138	0.0583	1.80	8300	0.0038	110.5
2	6	0.0402	1.09	3225	0.0038	44.7
3	24	0.0375	1.29	3790	0.0019	51.6
4	12	0.0249	1.08	2995	0.0019	27.9
5	24	0.0179	1.62	3580	0.0000	32.5
Average	204 total	0.0486	1.71	6940	0.0030	87.6

*Channel cross-sectional area before subtracting the fin area.

that element at any given time, so that a finned element contributes 3/6 or 1/2 to each channel. Thus, a Type 1 coolant channel has an average of one fin in it throughout its length. Similarly, Type 2 edge channels (Figure 32) contain an average of one fin. Edge channel types 3 and 4 average 1/2 fin. Channel Type 5 is between a neutral element and the core edge. It contains no fins. Hydraulic information for the various channel types is shown in Table 14. The edge channels purposely have less area than a normal channel since the edge channels service only one or two fuel elements instead of three as the inner channels do. Any variation in lower plenum pressure at the grid plate is small enough in comparison with the fuel bundle pressure drop that it need not be considered.

Core bypass flow around the grid plates has been eliminated by the sealed liner around the internal reflectors. Leakage along any gap between the liner and the internal reflectors will be less than 0.5% of the flow by keeping the gap at 0.010 in. or less.

D. FUEL ELEMENT CHARACTERISTICS

The reactor fuel element is manufactured with a 12-mil (diametral) gap inside the cladding for fuel swelling. Based upon the design operating conditions and the current fuel growth data, the predicted fuel growth in the peak rated element[3] is 6.3 mils (diametral), 4.7 mils at offset with an additional 1.6 mils occurring during the 5-year lifetime. This allows a 5.7-mil margin for fuel segment bowing and swelling uncertainty.

The hydrogen retention capabilities of the SCB (ceramic) hydrogen barrier, attached to the internal surfaces of the cladding, are described by the dimensionless parameter, A_D. This parameter defines the fractional internal surface area of the cladding which is effectively bare metal. The leak rate is, typically, made up of about three parts due to metal leakage and one part due to SCB leakage, so that the magnitude and timewise variation of A_D pretty much determine the hydrogen retention characteristics of a fuel element. Evaluation of available test data[3] indicate that A_D for the 5-kwe system will be of the order of 0.15% and will remain constant throughout the life of the core. The integral hydrogen loss over the design life of the reactor core results in a reactivity loss of $0.75.

The margin of safety for the cladding stresses was always greater than one except for cases where the element manufacturing bow was assumed to be greater than the expected 6 mils. However, even for an assumed 10-mil manufacturing bow, the margin of safety was still positive. The cladding stress margin is based on that stress at which hydrogen leakage from the fuel element increases significantly.

E. STRUCTURAL ANALYSIS

1. Reactor Vessel Structural Design Status

Preliminary analyses were performed to scope the structural aspects of the reactor vessel assembly. The basic structural requirements of the vessel include support of the core within the vessel, coolant pressure containment, support of the reflector-control assemblies externally, and support of the entire reactor assembly through its attachment to the neutron shield. Other structural considerations involve stresses induced in vessel components by temperature gradients that occur during reactor startup and shutdown, external piping reactions, etc.

a. Design Criteria

The design basis structural criteria were formulated using the requirements of Section III of the ASME Boiler and Pressure Vessel Code (BPVC) (for Class 2 nuclear components) as guidelines. The ASME BPVC was not intended for application to space power systems, and it was considered unrealistic to adopt the Code structural requirements in total. The nature of the operating conditions to which each type of system is subjected differ sufficiently to warrant modification to the design basis. In particular, the 5-kwe Reactor Thermoelectric System is not subjected to the many cycles of severe thermal transients which are so critical in the design of high-temperature stationary nuclear systems. Further, Code requirements do not consider the penalties associated with weight in a space system. The requirements for Section III Class 2 nuclear components were, therefore, adopted with modifications based on consideration of specific requirements.

The criteria were based on the use of elastic structural analysis methods, but do not preclude rigorous inelastic analysis of individual component areas as required to satisfy good engineering practice and/or specific functional limits.

Table 15 presents the reactor vessel structural design data applicable to defining the stress intensities and applying the design criteria.

TABLE 15

REACTOR VESSEL STRUCTURAL DESIGN DATA

Reactor Weight (lb)		497
Core	290	
Vessel	38	
Piping	9	
Reflector	160	
Launch Loads, Equivalent Static (g)		
Limit axial		11
Limit lateral		8
Ultimate axial		16.5
Ultimate lateral		12
Coolant Pressure		32
Design Temperature (°F)		1250
Design Lifetime (hr)		50,000
Material		Type 316 SS
Startup Cycles		50
Coolant Flow, NaK 78 (lb/hr)		16,800
Inlet Temperature, BOL/EOL (°F)		1057/1110
Radiation (nvt)		1.7×10^{20} (E>1 Mev)
		4.0×10^{20} (E>0.1 Mev)
		(Maximum in vessel shell)

b. Analyses Performed

The structural analyses performed during the conceptual design were those required to define critical dimensions, such as where component-to-component interfaces were involved, and to verify the basic feasibility of the concept. In areas where adjustments in details of configuration and dimension could be made later without causing major changes in the design, the structural analyses were scheduled for subsequent phases of the design effort.

(1) Vessel Shell Thickness

The inside diameter of the vessel was defined by the core design and internal clearance requirements. The thickness and thereby the outside diameter had to be established so that the design of the reflector assembly, which surrounds the vessel, could proceed on a firm basis.

The controlling criterion for the reactor vessel shell thickness is the 32-psi internal pressure at a temperature of 1250°F for 50,000 hr. The ASME code allowable membrane stress (S_{mt}) for these design conditions is 4900 psi; and thereby, a minimum shell thickness of 0.035 in. would normally be specified.

The ASME code does not limit creep strain as such but does specify that the designer verify that creep distortions do not destroy functional aspects of the components and that he modify the design if necessary. The vessel shell is surrounded by the reflector control assembly with the initial clearance set at 0.060 in. If the radial deformation of the vessel was to equal the clearance, reflector ejection for EOL shutdown of a flight system or backup scram of the ground test system would be impaired. A large margin of safety against reflector contact is, therefore, necessary.

The ASME creep data do not include the effect of radiation on creep. Although the code requires that radiation effects be considered, it does not provide any design criteria or guidelines, leaving it to the designer to determine the required allowances.

In AI work related to fast breeder reactor core design, irradiation creep prediction equations have been developed. One evaluation[4] indicates that the AI creep equation overestimates irradiation creep at high temperatures (>1100°F) and low stresses (less than stresses causing substantial thermal creep). The reference recommends that for the 5-kwe reactor conditions, the upper limit estimate of total creep be taken as the sum of ASME thermal creep data at 1250°F plus a radiation creep prediction using the AI equation at 1100°F.

Based on the above, the creep prediction curves of Figure 33 were developed. Figure 33 includes three curves of creep strain in 50,000 hr (in./in.) versus stress for: (1) thermal creep at 1250°F based on data for Type 316 SS from the ASME Code for Nuclear Vessels (Code Case 1331-6); (2) radiation-induced creep

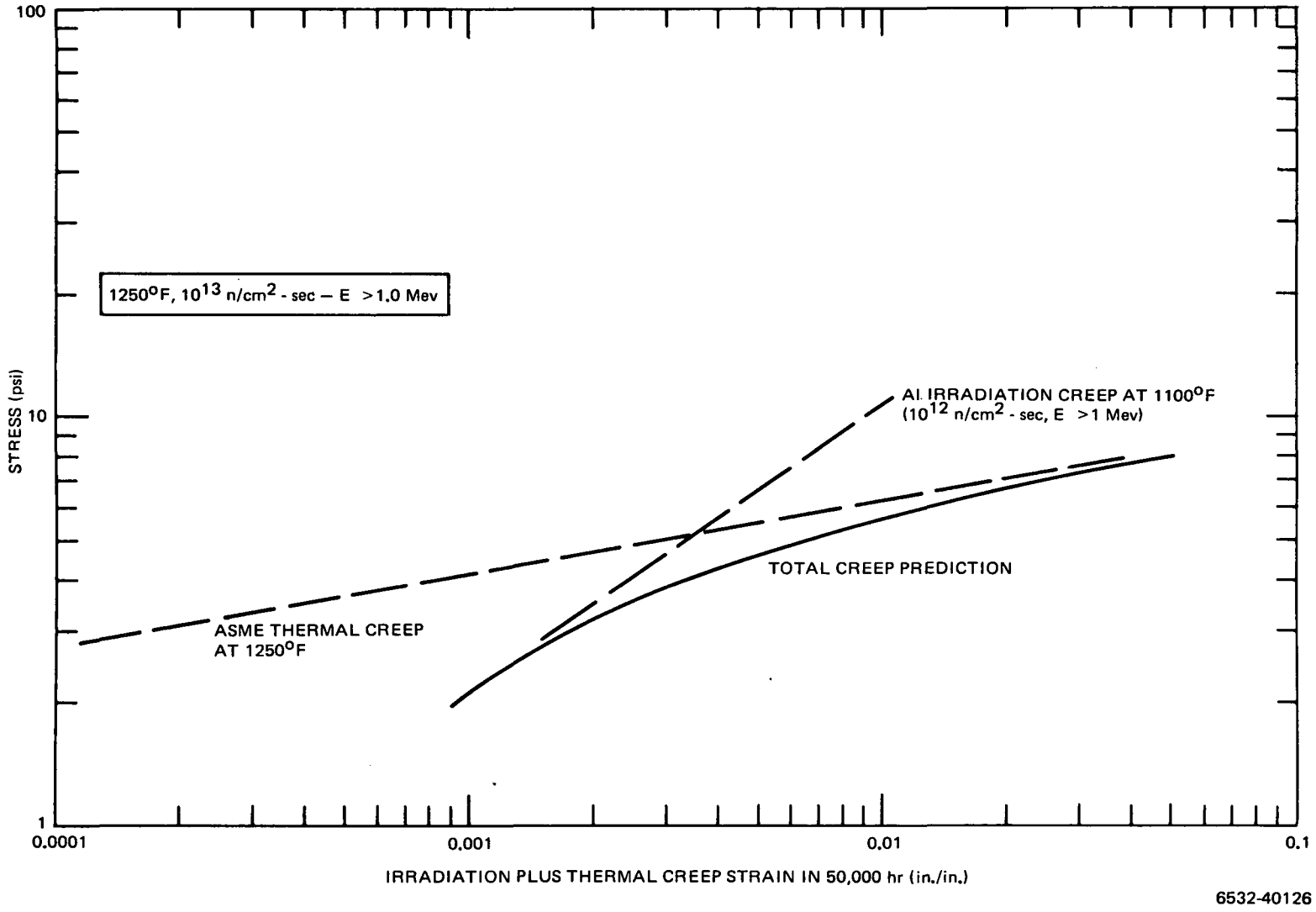

Figure 33. Upper Limit Creep Prediction

based on the AI prediction equation applied at 1100°F at the dose rate of 10^{12} n/cm^2-sec (E > 1 Mev); and (3) a total creep prediction which is the sum of thermal plus radiation creep.

From Figure 33, a limit of 3700 psi was selected for the primary general membrane stress in the vessel shell. The upper limit creep prediction (thermal plus radiation) is 0.0027 in./in. in 50,000 hr giving a radial displacement for the 5.25-in. vessel radius of 0.142 in. The elastic displacement is about 0.001 giving a total EOL displacement of 0.015 in.

(2) Vessel Heads

The vessel plenum heads are spherically dished, both having a dish radius of 18 in. The inlet head is dished outward and has a knuckle radius of 1.00 in. The outlet head is dished inward and has a knuckle radius of 0.50 in.

The outlet head is completely axisymmetric and therefore amenable to analysis by a straightforward computerized finite element technique. The maximum calculated stress intensity of 6900 psi versus a design allowable of 8200 psi at 1250°F. Figure 34 shows the network used for the analysis and includes a tabulation of the principle stresses at selected locations.

The inlet head is not axisymmetric, due to the two projections which extend outward to cover the projections from the vessel where the inlet pipes connect. An initial scoping anslysis was performed, in which the head was assumed to be axisymmetric, and then a detailed analysis of the nonsymmetric areas of the head was performed.

The analysis of the nonsymmetric areas of the head, using the most advanced finite element techniques available, determined that the thickness in these areas should be increased to a minimum of 0.193 in., and that the other areas of the head are acceptable with a 0.125-in. thickness.

(3) Reactor Support Skirt

The reactor is supported through a cylindrical skirt, approximately 3 in. long, which is brazed to the outlet end plenum of the vessel and has the other end flanged for a bolting attachment of the reactor to the top of the neutron shield. Cutouts are required at two places in the skirt for the control segment drive motors.

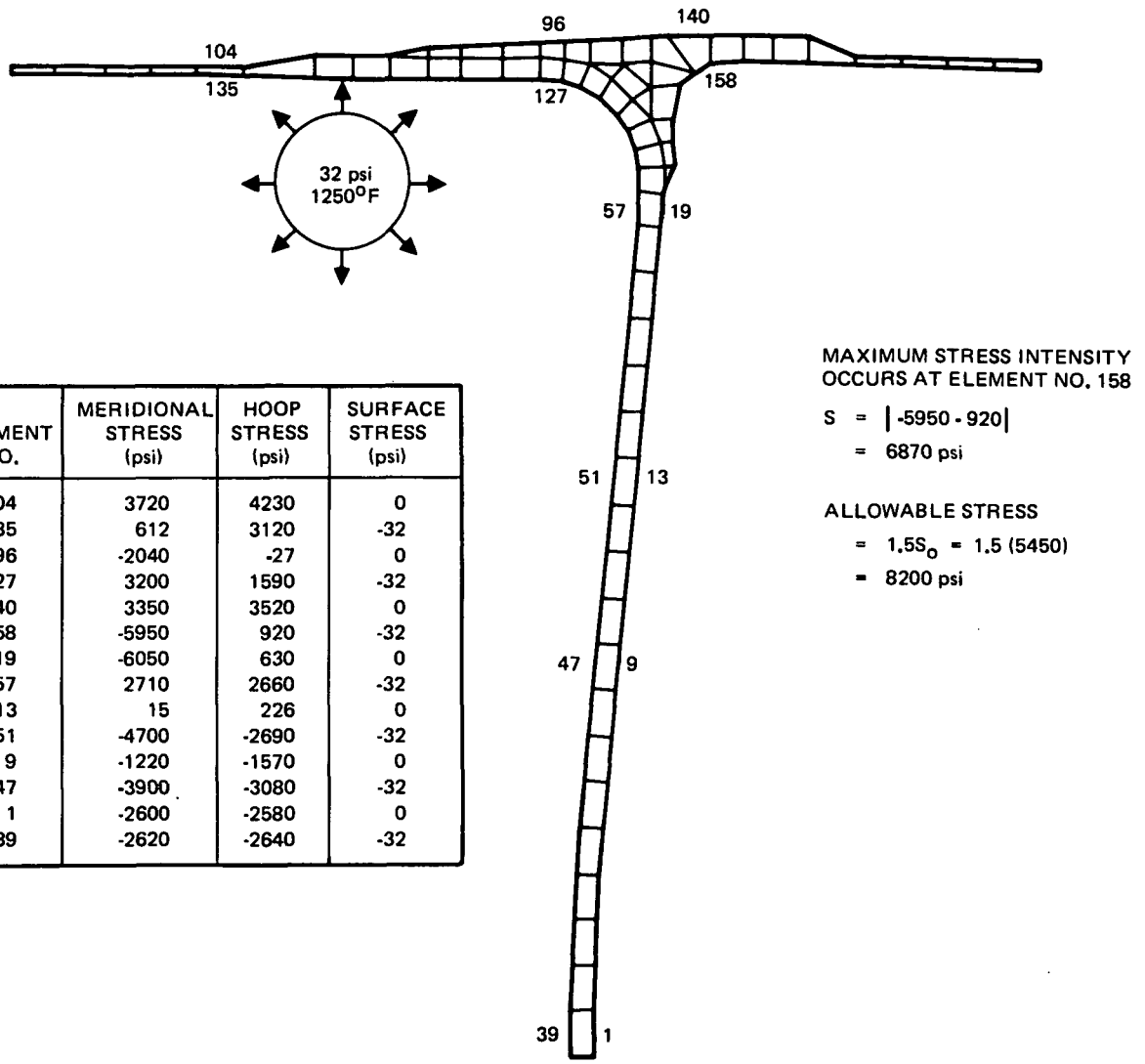

ELEMENT NO.	MERIDIONAL STRESS (psi)	HOOP STRESS (psi)	SURFACE STRESS (psi)
104	3720	4230	0
135	612	3120	-32
96	-2040	-27	0
127	3200	1590	-32
140	3350	3520	0
158	-5950	920	-32
19	-6050	630	0
57	2710	2660	-32
13	15	226	0
51	-4700	-2690	-32
9	-1220	-1570	0
47	-3900	-3080	-32
1	-2600	-2580	0
39	-2620	-2640	-32

Figure 34. Outlet Plenum Head Finite Element Analysis

A plain cylinder analysis indicates that a skirt thickness of 0.40 in. is required to accommodate the loading imposed by the axial and transverse accelerations of the reactor mass. The limiting condition is based on material stress allowable rather than the elastic stability limit of the cylinder, not considering the cutout edges. Local reinforcement is required at the edges of the cutouts.

The neutron shield has a very large heat capacity, approximately 100,000 Bt for a 500°F temperature change. In the startup sequence, the reactor outlet temperature rises from approximately 100°F to 1140°F (BOL) over a period of about 2 hr. Even with this relatively slow reactor startup, the heat capacity of the shield is so large that when the reactor has reached its operating temperature, the shield temperature will have changed very little. The result is a large temperature gradient across the reactor support skirt, approximately 1000°F when the reactor first reaches power, which decreases slowly as the shield temperature rises. When the shield temperatures reach equilibrium, many hours after startup, the top of the shield where the reactor support skirt is attached will be in the range of 800° to 900°F, giving a temperature gradient of 300° to 400°F across the support skirt during operation.

The current design criteria require a capability of 50 startup-shutdown cycles, For a plain cylinder with fixed ends, having a linear axial temperature gradient, the maximum strain, E_m, is equal to $1.41\,\alpha\Delta T/L\sqrt{Rt}$.

With the 0.40-in. thickness the design fatigue limit, based on Section III of the ASME Code is 100 cycles of application of the 1000° temperature gradient to the cylinder. If tolerances allow the thickness to increase to 0.050 in., the design limit is reduced to 75 cycles.

Because the 50% margin on cycles was considered low, due to questions about the adequacy of the 50-cycle requirement, design modifications that would increase the cyclic capability of the support cylinder were studied. These included: (1) axial profiling of the thickness of the cylinder (a number of profiles were analyzed) to locally decrease the temperature gradient at the vessel end of the cylinder; and (2) a beam-ended cylinder connection at the vessel end, thereby removing the circumferential restraint and reducing the stresses induced by axial flexure at this critical end.

A stepped-thickness cylinder was selected as the reference concept for the conceptual design of the reactor support skirt. The thickness of the cylinder is increased over a 0.75-in. length at the vessel end. An optimization study showed that with a 0.040-in-thick cylinder, increasing the thickness of the vessel end of the cylinder to 0.150 in. raised the design cyclic limit from 100 to 500 cycles. If tolerances allow the 0.040 in. to increase to 0.050 in. the limit is reduced to 300 cycles.

(4) Coolant Inlet Pipes

The reactor inlet pipes traverse the reflector through grooves at the split plane. To reduce the depth of the grooves, and to keep the pipes within the shield shadow cone, the pipes are flattened. Three basic options were considered: (1) flattened tube (flat sides with radiused ends), (2) flattened tube with internal support web, and (3) eliptical tube.

Although the internally supported flat tube offered a potential 2-lb weight advantage (neglecting meteoroid nonpuncture requirements) it was not considered worth the added difficulty and cost of installing the central support bar, i.e., obtaining and verifying a high integrity connection. The eliptical tube showed no advantage.

The basic flattened tube was selected for the reference conceptual design. Finite element analysis established that an 0.080 in. minimum thickness is required to keep the stresses, induced by the 32-psi internal pressure within limits allowed by the ASME Code.

IV. POWER CONVERSION SYSTEM

The reference design of the thermoelectric power conversion module was selected through a series of trade studies and system performance evaluations described in Section II - Design and Performance Summary. The initial design of the power conversion module was specified as a fractional performance improvement above that measured for the current TEM-X modules. The final design of the module was based on a detailed evaluation by Westinghouse Astronuclear Laboratory (WANL),[5] utilizing specific performance improvements from achievable TEM-X design modifications.

This section discusses the detailed performance requirements and physical design of the power module. Performance expectations of the module are included, and integration into the 5-kwe Reactor Thermoelectric System is discussed.

A. DESIGN GOALS

The goals for the Compact Thermoelectric Development Program were established at WANL. These goals are consistent with achievable improvements in module performance which result from modifications to currently tested designs.

The comparative base performance for the power conversion modules was derived from that chosen for the TEM-X S/N-3 series of power conversion modules. These modules were tested at WANL and at the Santa Susana Field Laboratory of AI. Their performance is considered the best current example of state-of-the-art thermoelectric power module technology. The following performance goals were specified for the reference power conversion modules:

1) The reference power module shall have an undegraded, matched load efficiency of 6.50% at the following average cladding temperatures: $\overline{T}_{hot}$ = 1085°F and $\overline{T}_{cold}$ = 507°F. These temperatures correspond to those utilized during the majority of TEM-X module testing. The 6.50% efficiency represents a 30% improvement over the TEM-X S/N-3 series of modules, resulting from utilization of ternary thermoelectric materials and design modifications.

2) The reference power conversion module shall have a matched load power degradation of 1.00%/year at 1085°F. Degradation rate is here defined as the percentile decrease in module matched load power (per year) at an average hot clad temperature of 1085°F. Additionally, this degradation shall have the following temperature dependence:

$$\text{Rate} = Ae^{-Q/RT}$$

where

Rate = matched load power degradation rate (%/year)

A = Frequency factor (%/year) ($\sim 7.84 \times 10^7$)

Q = Activation energy of degradation phenomenon (cal/gm-mole) ($\sim$31,000 based on TEM-X data)

R = Boltzman gas constant (1.1038 cal/gm-mole-°R)

T = Absolute average temperature of module hot clad (°R)

The effects of the axial temperature gradient variation (on the primary, hot side) has not been considered in the performance analysis. The degradation rate as specified is that for a 100°F average axial gradient throughout the 5-year module operating period.

B. POWER MODULE PERFORMANCE REQUIREMENTS

The performance requirements for the power conversion modules were established through system optimization analysis of the 5-kwe Reactor Thermoelectric System. The power output and voltage output requirements for the power conversion modules were specified for the system EOL conditions. Analyses have demonstrated that module efficiency varies with the module-to-load voltages slightly greater than one-half of the module open-circuit voltage (defined as the optimized-load condition). The electrical power transfer is maximized for load voltages exactly one-half of the open-circuit module voltage (defined as the matched-load condition).

The module is designed to operate very near the matched-load condition at the EOL (degraded) performance statepoint. Systems analyses have

subsequently shown that the BOL module performance statepoint is very near the optimized-load condition. Thus, the module nominally operates in the maximum efficiency-to-maximum power transfer regime during its 5-year lifetime.

The 5-kwe system utilizes 16 power conversion modules. The "load" for these modules is defined as the system load (5 kwe at 30 vdc) plus the load imposed by the electrical power transmission line. This total module load is 5.13 kwe at 30.8 vdc. Thus, each module must supply 320.6 w to the total load at a voltage of 3.85 vdc (two parallel strings of eight modules in series are used to satisfy the voltage requirement).

The degradation phenomenon is understood as a diffusion of tellurium from the P-type washer to the N-type washer, increasing the material resistivity of the latter. Thus, analytic predictions of EOL (degraded) performance are made by artificially increasing the N-leg washer resistivity (until the expected decrease in matched load output power is achieved). The module thermoelectric couple washer thicknesses are concurrently optimized for maximum efficiency (with the N-leg washer in the degraded state). This maximization is performed by varying the relative thicknesses of the two washers, thus matching their total electrical resistance.

The developmental program goals specify undegraded performance requirements, while the system integration analyses specify degraded (EOL) performance requirement. Evaluations of the module operating statepoints throughout the 5-year system lifetime have indicated that the total degradation in matched load power should be approximately 6.5 to 7.5% (depending on the specific system design). To facilitate selection of the final reference power module design and to minimize the effects of system design perturbations on this module, the degraded (EOL) design point was defined to occur with a 7.0% decrease in matched load module power. The system shall, therefore, operate near the matched load condition at EOL.

The EOL module temperatures (average hot clad, $\overline{T}_{hot}$, and average cold clad, $\overline{T}_{cold}$) are determined by iterative systems analyses. The EOL temperatures are calculated concurrently with the EOL performance statepoint.[1] Table 16 summarizes the degraded and undegraded performance requirements for the reference power conversion module.

TABLE 16

POWER CONVERSION MODULE PERFORMANCE REQUIREMENTS

Degraded (EOL) requirements at specific $\overline{T}_{hot}$ and $\overline{T}_{cold}$ with 7.0% decrease in matched load power ouput:

320.6 w/module (power output)

3.85 vdc volts per module (at total load)

P-leg and N-leg thermoelectric couple washer thickness ratio optimized for maximum module efficiency with increased N-leg washer resistivity (artificially degraded module)

Undegraded requirements:

6.50% overall efficiency at $\overline{T}_{hot}$ = 1085°F and $\overline{T}_{cold}$ = 507°F (at matched load, utilizing washer thickness ratio established for degraded operation).

1.00%/year degradation rate (in matched load power output) at $\overline{T}_{hot}$ = 1085°F.

It should additionally be noted that the degradation in matched load power output is accompanied by a degradation in the module thermal-to-electrical efficiency. Efficiency degrades at a rate of ~70% of that for matched load power. The rates are thus linearly proportional in the first approximation. Negligible degradation occurs in the module open-circuit voltage, as indicated by analysis and TEM-X S/N-3 test data.

C. MODULE DESIGN AND PCS PERFORMANCE CHARACTERISTICS

The design of the power conversion modules has been detailed by WANL.[5] The module performance associated with this design was calculated at distinct operating conditions and temperatures. Existing performance predictions were fitted accurately to these discrete operating points, and the resulting module characteristics are included in the following sections.

The reference power conversion module design (Figure 35) is based on the TEM-X S/N-3 series of modules with the following improvements:

1) Utilization of ternary thermoelectric materials for the N and P washers (97% achievement of predicted available performance).

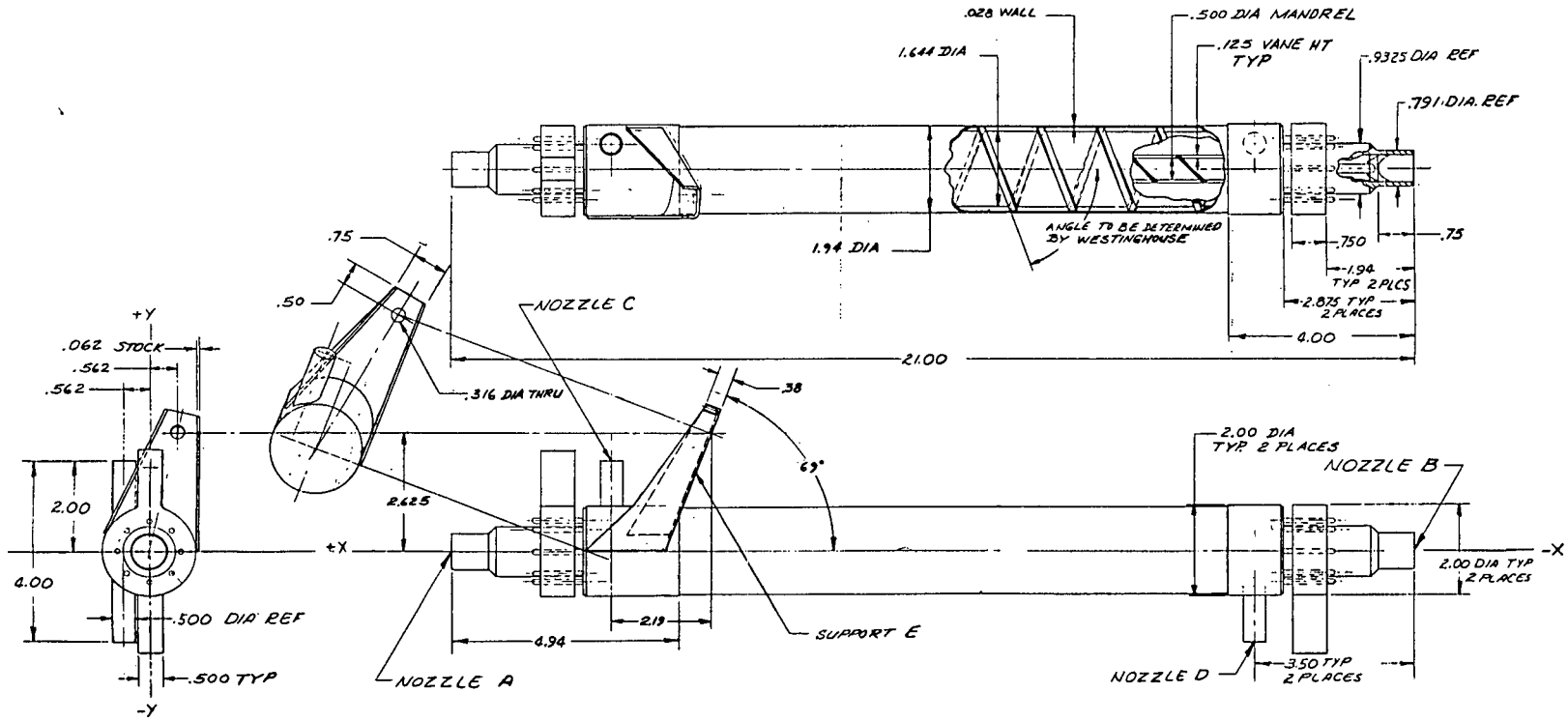

NOZZLE	ID +.002 -.000	OD ±.006 -.000
A	.751	.791
B	.751	.791
C	.460	.500
D	.460	.500

Figure 35. Thermoelectric Converter Module — WANL (N652420004)

2) Utilization of EBVD tungsten on the thermoelectric couple faces and on the mica intercouple washers as a diffusion barrier against tellurium migration.

3) Incorporation of 0.0015-in. -thick mica insulating washers to minimize the thermal shunting path through these washers.

4) Utilization of tungsten inner conduction ring interface shoes on both the P and N washers to minimize tellurium diffusion.

The pertinent design information for the reference module is presented in Table 17.

TABLE 17

REFERENCE POWER CONVERSION MODULE DESIGN INFORMATION

Inner clad diameter, ID (in.)	0.750
Outer clad diameter, OD (in.)	1.644
Number of thermoelectric couples	48
Active circuit length (in.)	15.024
N-type ternary thermoelectric washer thickness (in.)	0.161
P-type ternary thermoelectric washer thickness (in.)	0.149
Mica intercouple insulator thickness (in.)	0.0015

The design performance of the reference power conversion module is presented in Table 18, as reported by WANL.[5] The temperatures reported are those existing in the 5-kwe system at EOL conditions. The matched load performance characteristics for this reference module are illustrated in Figure 36.

It should be noted that the efficiency degrades approximately 70% of the matched load power degradation. The small increase in load voltage (a result of decreased current flow in the module) is considered negligible.

TABLE 18

REFERENCE POWER CONVERSION MODULE PERFORMANCE
($\overline{T}_{hot}$ = 1140°F, $\overline{T}_{cold}$ = 542°F at matched load conditions)

	Undegraded	Degraded
Load voltage (vdc)	3.86	3.87
Power output (w)	345	321
Power input (kwt)	5.420	5.300
Overall efficiency (%)	6.37	6.06
Matched load power degradation (%)	0	6.96
Efficiency degradation (%)	0	4.87

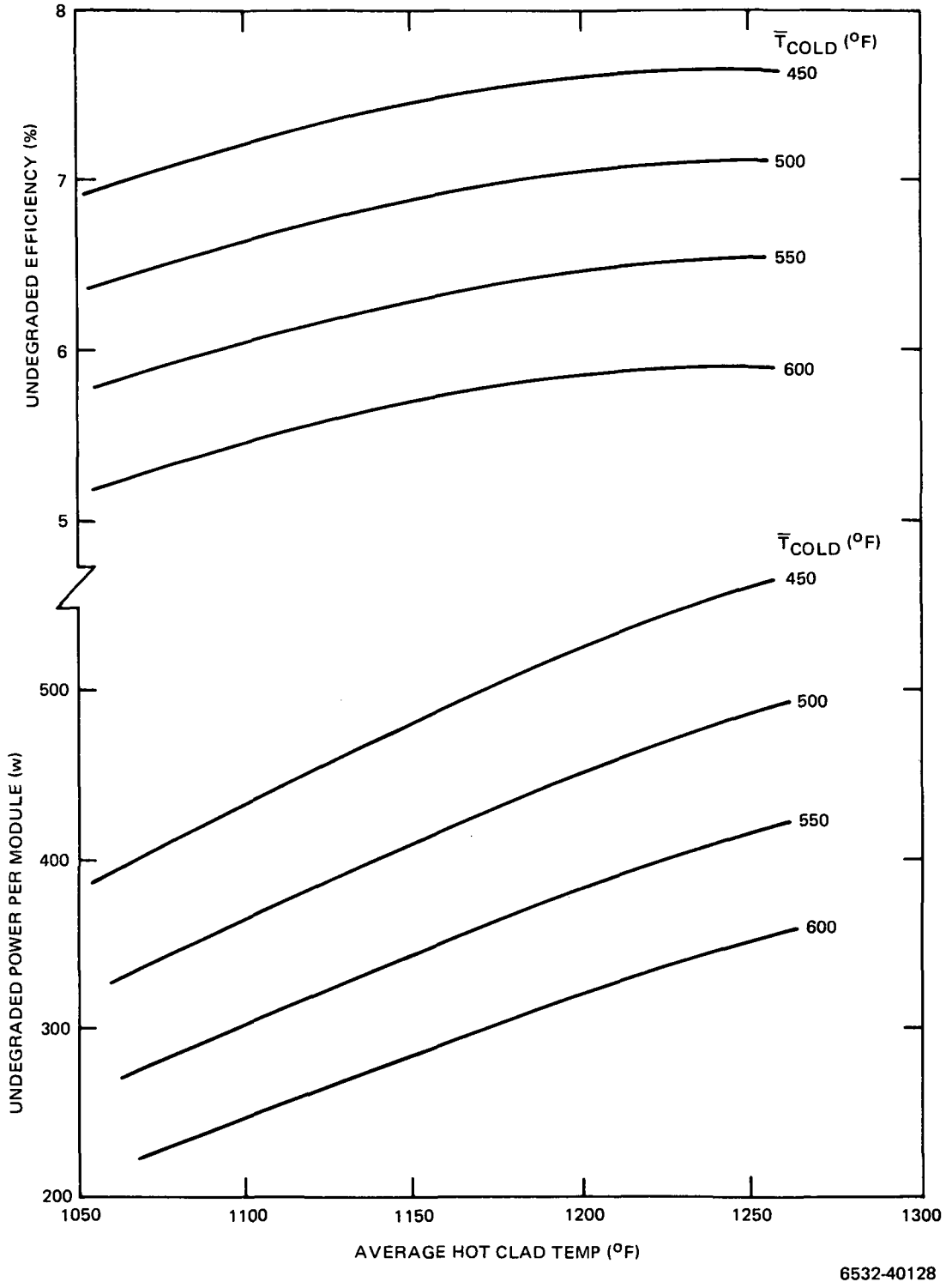

Figure 36. Power Output and Efficiency - Power Conversion Module

V. THERMOELECTRIC PUMP

This section describes the requirements, design and performance of the thermoelectric pump, which includes the dc conduction pumps and thermoelectric modules.

A. DESIGN DESCRIPTION

The configuration of the prototype thermoelectric pump assembly is shown in Figure 37. The overall pump assembly dimensions are 21 in. long (direction of NaK flow) by 13 in. wide (direction of magnetic flux) by 10 in. high as shown in Reference 6. The materials of construction and the typical dimensions of each throat section are shown in Figure 38. This design incorporates many of the features of the developmental thermoelectric pump assembly that has been successfully tested in a NaK test loop installation. The thermoelectric modules are located as close as practicable to the pump throats to keep electrical power losses low. The buses, between the throats and between the pump module and the throat, are fabricated of multiple, separated strips of copper to provide flexibility and minimize thermal stresses. A thermal reflective barrier covers the flexible bus between the throats to reduce magnet temperatures and to reduce the amount of thermal energy that escapes the pump assembly and, ultimately, is shunted to the radiator. The direction of current flow (module to primary throat to secondary throat) is such that the magnetic field established by the current does not interfere with the magnetic field across the primary throat. The present configuration causes some magnetic field losses in the secondary throat but since the hydraulic pumping requirements are lower in that loop, these losses can be tolerated. The transition between the rectangular throat and the round system piping is made as uniformly and smoothly as possible and with a cone angle of $\sim$12 degrees, which keeps the transition piece length within reason and does not provide intolerable entrance and exit hydraulic losses. All joints in the pump-module electrical circuit are of the metallurgical type (welded, brazed or diffusion bonded). The wall thickness of throats (0.028 in.) and pipe transitions (0.025 in.) is greater than that of the system piping (0.020 in.).

The objective of the prototype thermoelectric pump design was to provide a minimum weight pumping system (pump, power source, heat rejection system) that would satisfy 5-kwe system pumping requirements (see Table 19).

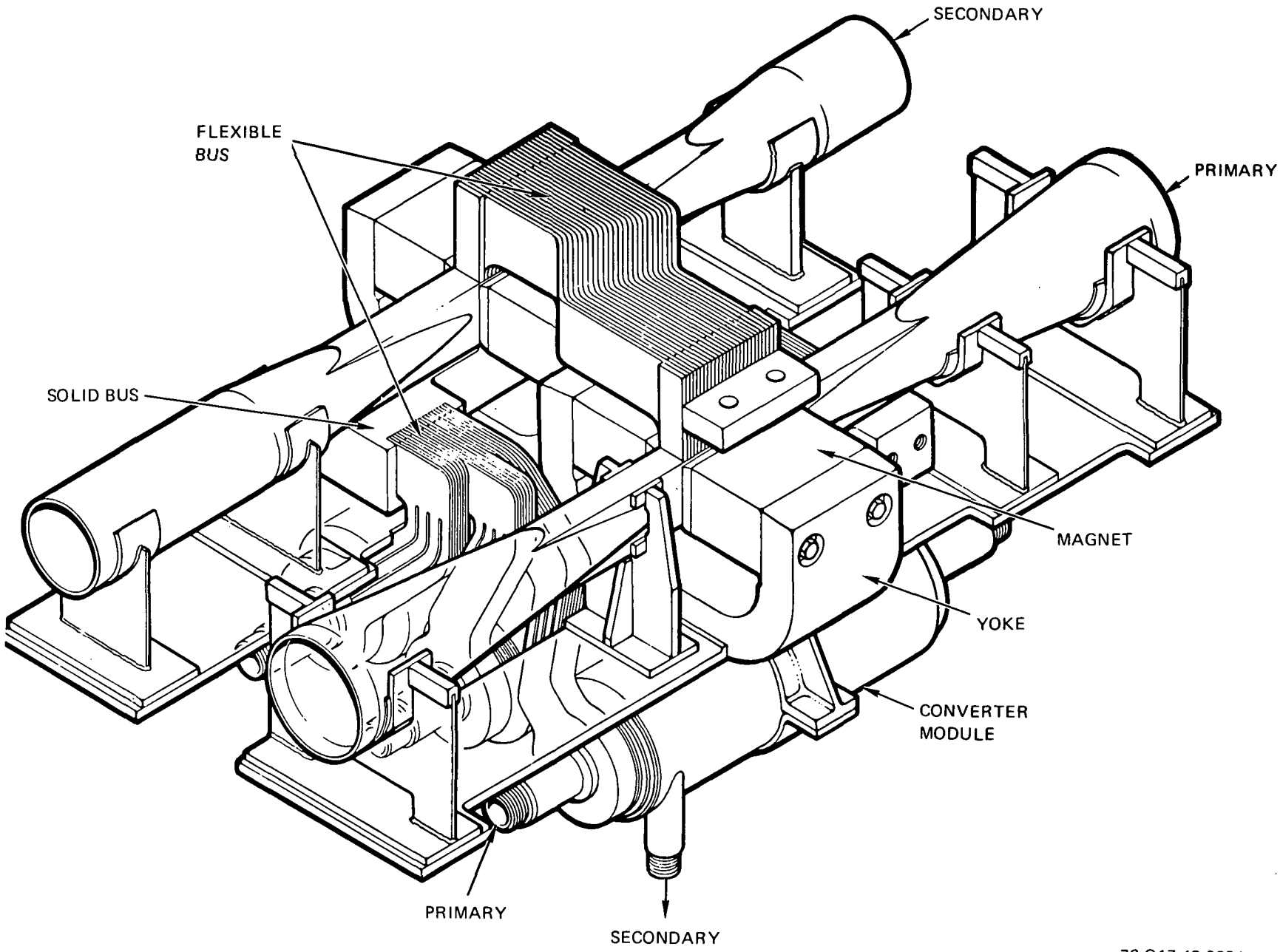

Figure 37. Prototype Thermoelectric Pump Assembly

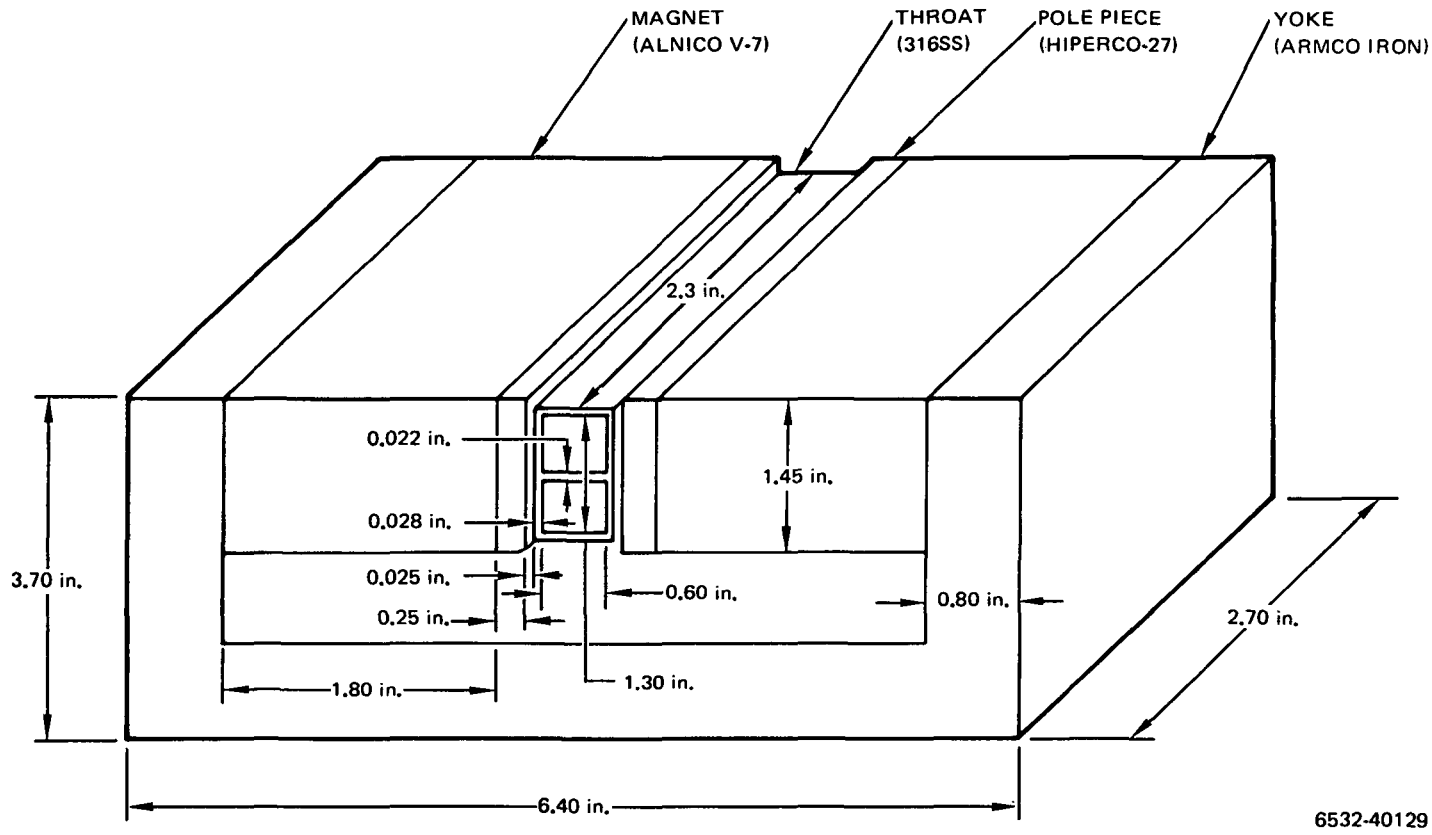

Figure 38. Prototype dc Pump – Materials and Dimensions

TABLE 19

5-KWE SYSTEM PUMPING REQUIREMENTS

	BOL	EOL
Primary Loop		
Flow (lb/sec)	4.87	4.83
*Pressure drop (psi)	1.11	1.09
Temperature (°F)	1059	1105
Secondary Loop		
Flow (lb/sec)	3.01	2.94
*Pressure drop (psi)	1.57	1.50
Temperature (°F)	589	611

*A 15% design margin is incorporated into these pressure drop requirements.

The operating life of the system is 5 years with the temperatures increasing uniformly from the BOL temperature to the EOL temperature of Table 19 during this period. The pump shall be capable of providing from 1 to 100% of design flow in the primary loop with an external power source, and there shall be a continuous progressive relationship between applied electrical current and flowrate. Voltage taps shall be located on the throats in the fringe flux region and will be calibrated to measure NaK flowrate.

The pump must be capable of withstanding the 5-kwe system environmental requirements as specified in Reference 7, including the following:

	Pressure (psig)	Temperature (°F)
Primary Throat	+50	50 to 150
	-15 to +30	70 to 1100
Secondary Throat	+50	50 to 150
	-15 to +30	70 to 700
Thermal Cycles	100 thermal cycles between operating temperatures and 70°F	
Radiation Levels		
Fast Neutrons (>0.1 mev)	1×10^{14} nvt	
Gamma	5×10^{9} rad	

B. PUMP SELECTION

Early in the conceptual design phase of the 5-kwe Reactor Thermoelectric System Program, a trade study[8] was performed to evaluate a number of types of pumping systems considered for use on the program. This trade study provided an evaluation of two basic methods of providing system pumping requirements: (1) ac pump systems versus dc pump systems, and (2) an evaluation of three variations of dc pumping systems (dual-throat, single-throat and multipass pump configuration).

Factors which were considered in this trade study evaluation are listed in Table 20.

TABLE 20

TRADE STUDY FACTORS

Factor	Desired Characteristics
Reliability	Maximum
Power	Minimum, matched to pump
Current	Minimum (dc pumps)
*Pump system weight	Minimum
Pump weight and size	Minimum
Costs and schedule	Minimum
Performance predictability	High accuracy
Fabrication process development	State-of-the-art
Startup	Low power and power supply weight

*Includes pump, power supply, power conversion equipment, interconnecting wiring, structure and all equipment associated with heat supply and heat rejection for pump power supply.

These evaluations were performed for a two-loop system, with one loop at ~1100°F, the other loop at ~600°F and hydraulic pumping power requirements of ~30 w per loop. The power source available to these systems consisted of either the regular thermoelectric power modules, which would require voltage inversion for the ac pumps and voltage reduction for dc pumps, or a special low-voltage thermoelectric pump power module (TEM-14A) that had been developed for ZrH reactor thermoelectric system dc pumps. The results of these

evaluations on three dc-type pumping systems showed that the dual-throat dc pump concept was clearly superior to the single-throat and multi-pass concepts as regards weight, efficiency and cost.[8] All of the dc pump concepts are superior to an ac-type pump for the 5-kwe system when considering costs, schedule, reliability, weight, efficiency, etc.

The prototype pump size and power requirements were determined with the dc pump computer code[9] using the design performance requirements as inputs with the following constraints and assumptions:

1) Configuration, as shown in Figure 37
2) Materials
   a) Bus, OFHC copper
   b) Yoke, ARMCO iron
   c) Magnet, Alnico V-7
   d) Throat, Type 304 SS
   e) Pole piece, Hiperco 27
3) Bus length, 32 in.
4) Bus efficiency, 67% (about optimum for this configuration)
5) Identical dimensions in both throats
6) Pump voltage and current match to TEM-14A type pump converter (355 w at 0.210 v)
7) Thermoelectric pump converter efficiency = 3.4%
8) Converter power-to-weight ratio of 15 w/lb.
9) Associated system heat supply and rejection weight of 8 lb/kw of heat rejected.

Determination of the pump design point was an iterative process. Pump performance characteristics and weights for a dual-throat pump configuration, as shown in Figure 37, were computed for many throat sizes. The minimum current necessary to obtain the required pressure at a selected flowrate was determined for a given set of throat dimensions. Magnet area and length were

determined at the maximum magnet energy product as this provides the smallest magnet and, therefore, the lightest pump. For this program, the pump design selected was that which provided the minimum pumping system weight for a pumping system comprised of the dual-throat pump, pump power supply (thermoelectric module) interconnecting buses, associated heat supply and rejection weights and the structure required for these components.

The determination of a best pump configuration was made by varying the throat dimensions (length, height, and width) over a range of values such that the end points selected always provided higher weight pumping systems than the intermediate values. An examination of performance and weight data enabled the selection of a configuration that satisfies the above requirements. Figures 39, 40, and 41, in which pump voltage, current, power, pump weight and pump system weight were plotted as a function of the throat dimensions, illustrate how changing throat dimensions affect various parameters and how the pump design was selected. Throat width is the distance between the bus electrodes, throat height is the distance across the throat between the magnets, and throat length is the distance across the bus-throat joint in the direction of NaK flow. In Figure 39, the selection of throat height at 0.60 in. was principally a compromise between minimum current and minimum system weight. In Figure 40, the selection of throat width at 1.3 in. was for minimum system weight and power. In Figure 41, the selection of throat length at 2.3 in. was for minimum pump system weight and current. In selecting the design point in the three figures, it is desirable to pick the lightest pump as weight is indicative of size and larger pumps result in greater integration problems in the system. In the region of the pump design point selections shown here, slight variations in throat dimensions can be made to provide an optimum pump-thermoelectric converter electrical load match. This is important as operation of the converter at match load conditions provides most efficient use of the heat energy available and best overall pump system performance.

C. THERMOELECTRIC PUMP MODULES

The reference design of the thermoelectric pump supply modules was selected through a series of trade studies and system performance evaluations. The final design of the pump supply modules was based on dimensional modifications to the current state-of-the-art TEM-14A design.

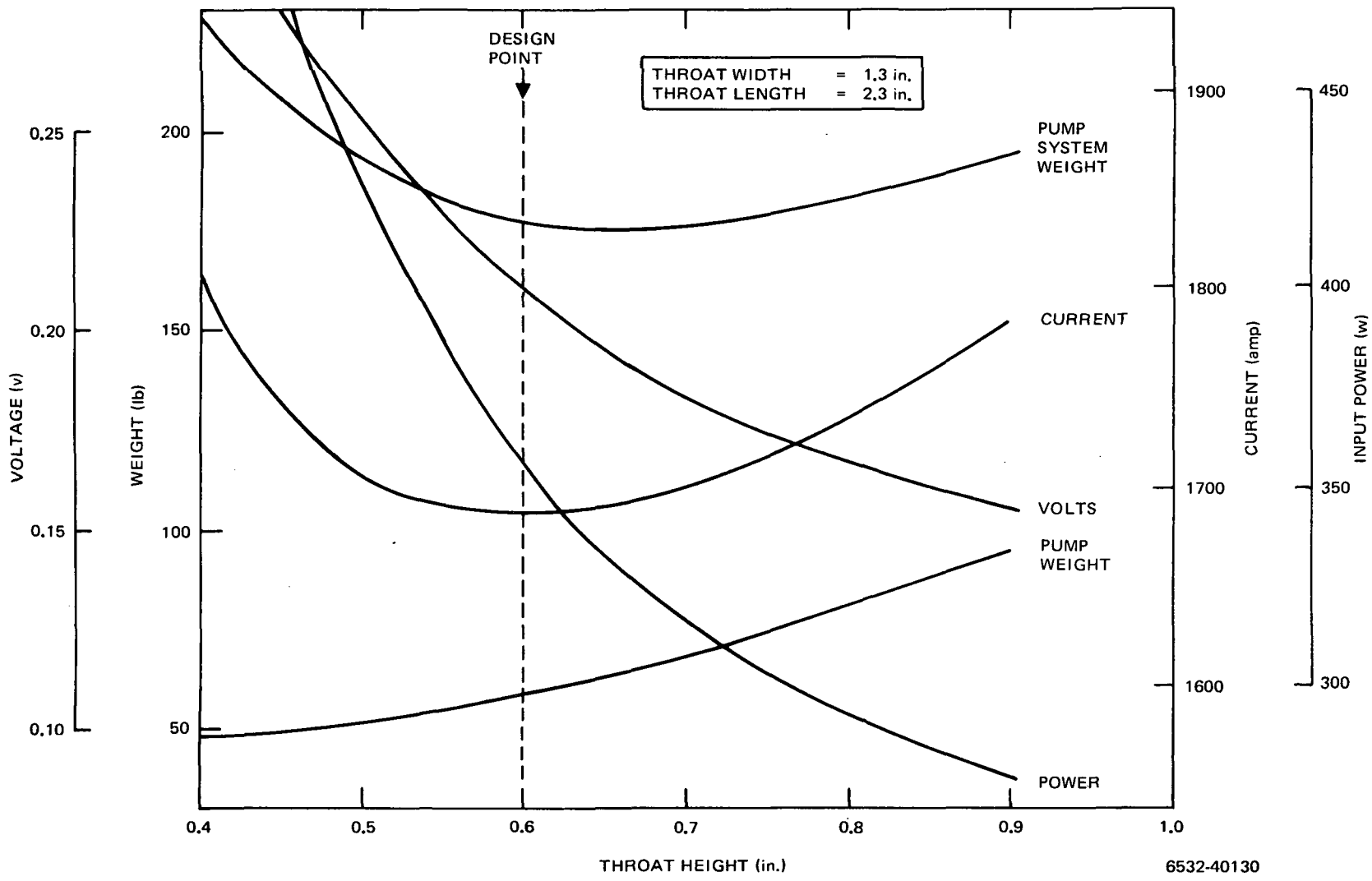

Figure 39. DC Pump Performance versus Throat Height

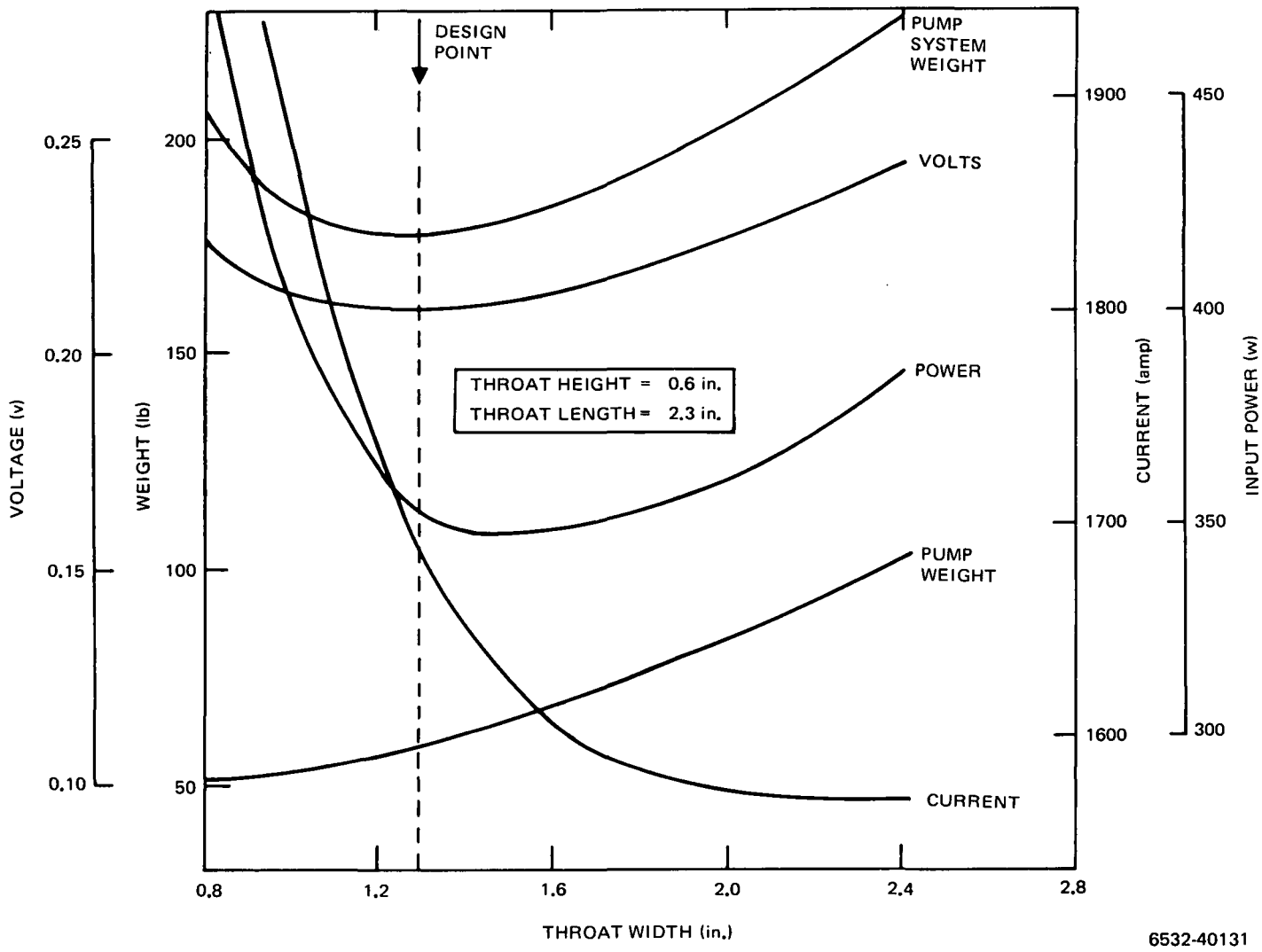

Figure 40. DC Pump Performance versus Throat Width

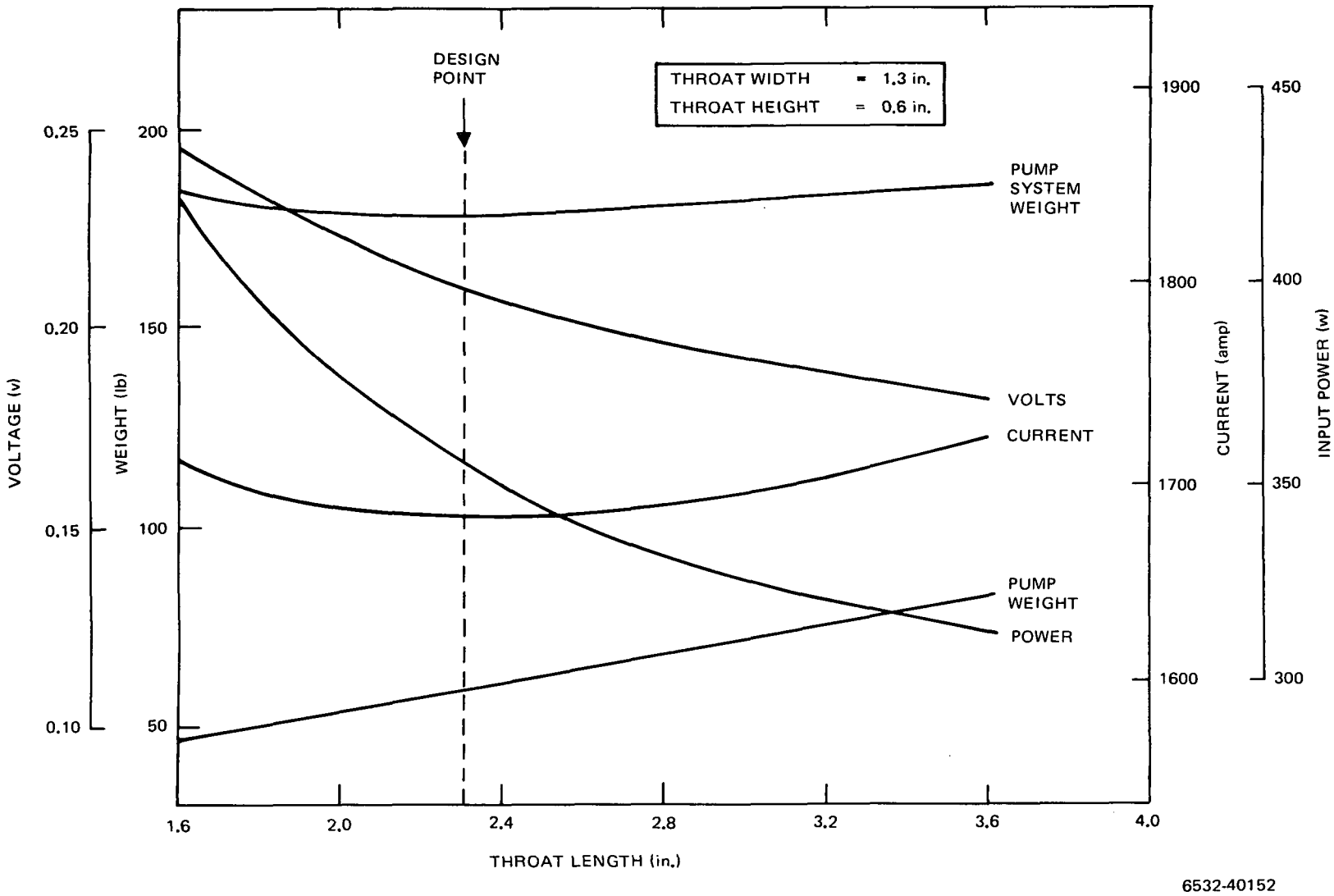

Figure 41. DC Pump Performance versus Throat Length

This section discusses the detailed performance requirements and physical design of the pump modules. Performance expectations of the module are included, and integration into the 5-kwe system pump is discussed.

1. Pump Thermoelectric Module Developmental Goals and Requirements

The pump supply module design is based on dimensional modifications to the existing TEM-14A pump module design. This design is considered the best current example of state-of-the-art thermoelectric pump module technology. The following performance goals were established for the reference pump modules:

1) The reference pump supply module shall have an undegraded, matched-load efficiency approximately 20% greater than that exhibited by the TEM-14A series of modules. This performance improvement results from replacing the nickel electrical access pins with nickel-clad-copper electrical conduction pins.

2) The reference pump supply module shall have a matched load power degradation rate of 1.40%/year at 1085°F. Degradation rate is here defined as the percentile decrease in module matched load power (per year) at an average hot clad temperature of 1085°F. This corresponds to a 50% reduction in degradation rate over that demonstrated in the TEM-14A series of modules. Additionally, this degradation shall have the following temperature dependence:

$$\text{Rate} = A_e^{-Q/RT}$$

where

Rate = matched load power degradation rate (%/year)

A = frequency factor (%/year) ($\sim 1.10 \times 10^8$)

Q = activation energy of degradation phenomenon (cal/gm-mole) (31,000 based on TEM-X data)

R = Boltzman gas constant (1.1038 cal/gm-mole-°R)

T = Absolute average temperature of module hot cladding (°R)

The effects of the axial temperature gradient variation (on the primary, hot side) has not been considered in the performance analysis. The degradation rate as specified is that for a 100°F average axial gradient throughout the 5-year module operating period.

The current and voltage requirements for pump supply modules were specified for the system EOL conditions. The pump supply module was designed to operate as close to the matched load power transfer condition as possible within the constraints imposed by the pump design. System integration studies were performed to optimize the interface between the pump modules and the pump (see Section II).

The 5-kwe system utilizes three pump modules which share a common pump bus bar. Therefore, the module current output is additive into the pump, while the voltage is constant. The "load" for the pump supply modules is defined as the sum of the voltage drops in the two pump throats plus the voltage drop in the bus bar and the copper electrical connection ring (which is mounted to the pump electrical access pins). Each module must supply one-third of the pump current requirement at the desired pump load voltage drop.

The pump supply module degradation phenomenon is also understood as a diffusion of tellurium from the P-type washer to the N-type washer (in the thermoelectric couple). The material resistivity of the N-leg is thus increased, resulting in increased internal power losses and reduced efficiency. Degraded module performance calculations are performed by artificially increasing the resistivity of the N-type washer material (until the expected decrease in matched load power output is achieved). The module thermoelectric couple washer thickness ratio is concurrently optimized for maximum performance.

Evaluation of the module operating statepoints throughout the 5-year system lifetime has indicated that the total degradation in matched load power is approximately 8.0 to 9.0% (depending on the specific system design). To facilitate selection of the final reference design and to minimize the effects of system design perturbations on this module, the degraded (EOL) design point was defined to occur with an 8.5% decrease in matched load power. (During actual calculations, any value of degradation in the range of 8.25 to 8.75% was acceptable, in that the pump module design has only slight impact on the system performance points.)

The EOL module temperatures (average hot clad, $\overline{T}_{hot}$, and average cold clad, $\overline{T}_{cold}$) are determined by iterative systems analyses. The BOL temperatures are calculated concurrently with the end-of-life temperatures (see Section II and Reference 1).

It should additionally be noted that the degradation rate in matched load power output (1.4%/year at 1085°F) is accompanied by a degradation in the module thermal-to-electrical efficiency. Efficiency degrades at a rate approximately 83% of that for matched load power. The two rates are thus linearly proportional in the first approximation. Negligible degradation occurs in the module open circuit voltage, as indicated by analysis and TEM-14a test data.

2. Pump Thermoelectric Module Design and Performance Characteristics

The design of the pump supply modules has been detailed by WANL.[5] The module performance associated with this design was calculated at distinct operating conditions and temperatures. Existing performance predictions were fitted accurately to these discrete operating points, and the resulting module characteristics follow.

The reference pump supply module (Figure 42) design is based on the TEM-14A series of modules with the following improvements:

1) Utilization of EBVD tungsten on the thermoelectric couple washer faces and on the mica intercouple washers as a diffusion barrier against tellurium migration.

2) Utilization of tungsten inner conduction ring interface shoes on both the P and N washers to minimize tellurium diffusion.

3) Utilization of nickel-clad copper electrical access pins to reduce power losses and improve efficiency.

The pertinent design information for the reference pump module is presented in Table 21.

The design performance of the reference pump supply module is presented in Table 22, as reported by WANL.[5] The temperatures reported are approximately those existing in the 5-kwe system at EOL conditions. The matched load performance characteristics of this module are illustrated in Figure 43.

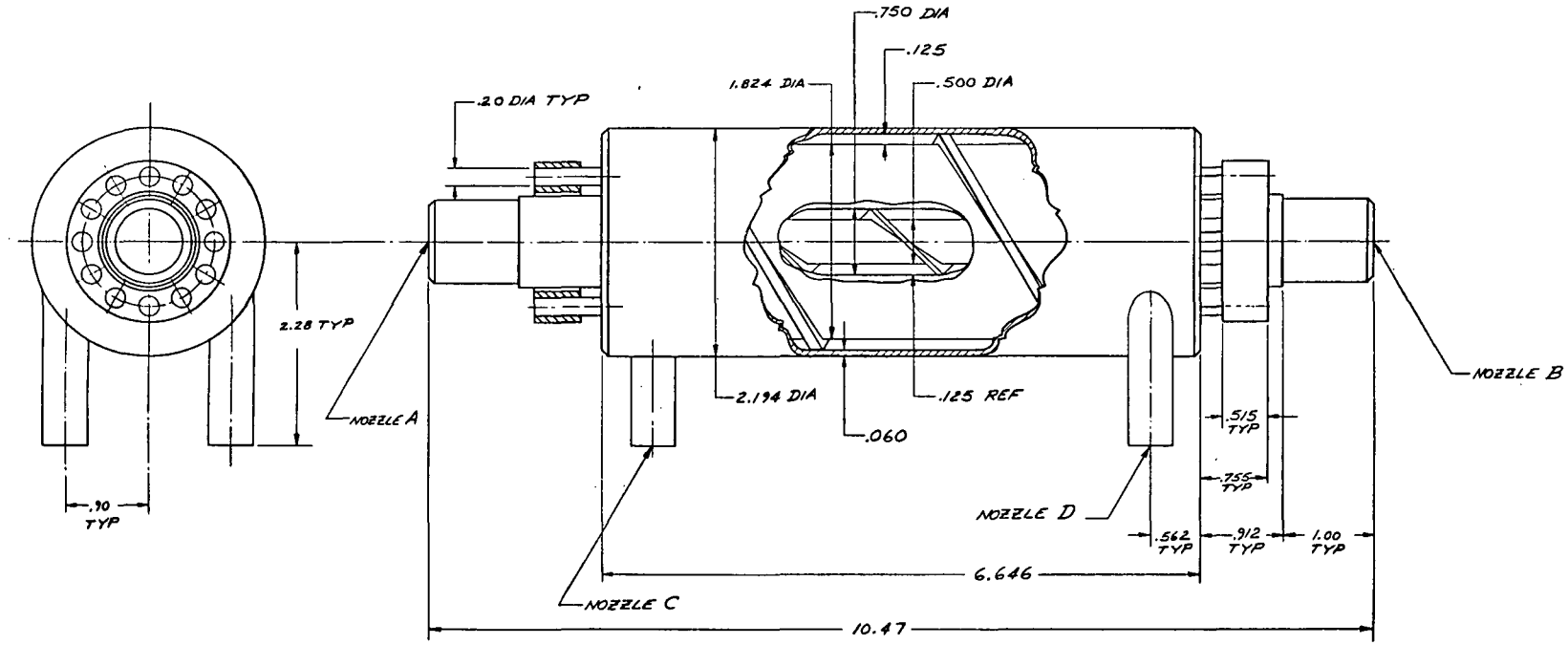

NOZZLE	I.D. +.002 −.000	O.D. +.006 −.000
A	.750	.870
B	.750	.870
C	.430	.500
D	.430	.500

Figure 42. Thermoelectric Converter Module – Pump Power, WANL TEM (N652420008)

TABLE 21

REFERENCE PUMP MODULE DESIGN INFORMATION

Inner clad diameter, ID (in.)	0.750
Outer clad diameter, OD (in.)	2.194
Number of the thermoelectric couples	4
Active circuit length (in.)	5.420
N-type thermoelectric washer thickness (in.)	0.712
P-type thermoelectric washer thickness (in.)	0.622
Mica intercouple insulator thickness (in.)	

TABLE 22

REFERENCE PUMP MODULE PERFORMANCE
($\overline{T}_{hot}$ = 1128°F, $\overline{T}_{cold}$ = 550°F at matched load)

	Undegraded	Degraded
Load voltage (vdc)	0.237	0.238
Module internal resistance (mΩ)	0.4343	0.480
Power output (w)	128.8	118.0
Power input (kwt)	3.435	3.378
Overall efficiency (%)	3.75	3.49
Matched load power degradation (%)	0	8.39
Efficiency degradation (%)	0	6.39

The efficiency of this module degrades approximately 83% of the matched load power degradation. The small increase in load voltage (a result of decreased current flow in the module) is considered negligible.

D. PUMP PERFORMANCE

The performance of the prototype pump design was evaluated at the nominal operating temperatures and at 100°F to determine startup characteristics.

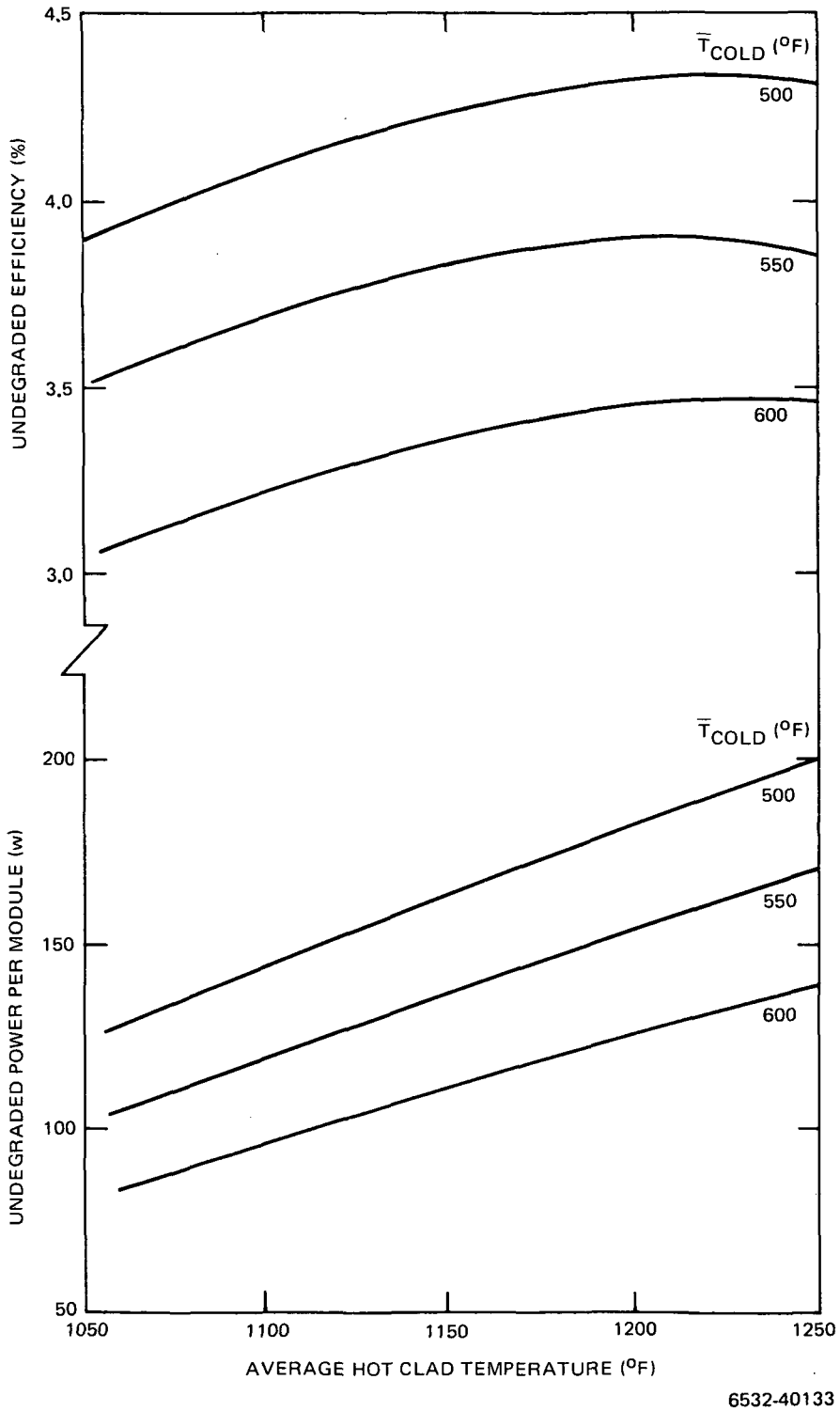

Figure 43. Power Output and Efficiency – Pump Module

Anticipated performance at design temperatures is best shown in Figures 44, 45 and 46. Figure 44 shows the pressure developed in each throat as a function of flowrate at BOL and EOL conditions. Figures 45 and 46 show the relationship between pump current and individual loop pressure drop as a function of flowrate at EOL conditions, for the primary and secondary throat, respectively. For example, 24% drop in current from 1690 amp to 1290 amp results in about a 16% drop in flowrate in each loop. Figure 47 shows the effect on pump performance (pressure developed at EOL conditions as a function of throat magnetic flux density) at several values of current. Performance of the pump is less affected by loss in magnetic flux density than loss in current. A 20% drop in flux density in the primary throat results in about a 9% drop in developed pressure; and from Figure 45, about a 4 to 5% drop in flowrate. From Figure 47 it is seen that a 100-amp loss in current (6%) has almost the same effect. Magnetic losses have a greater influence on performance in the secondary throat, but since its physical size is the same as the primary throat and its operating temperature is lower, it could easily be magnetized to a higher level initially to accommodate such degradation.

Prior to startup of the reactor in space it is necessary to provide flow in the system to prevent local freezing of the NaK. An evaluation was performed to determine the current required to provide low flowrates in each loop during this period. Figure 48 shows the relationship between the current applied across each throat and flowrate. Also, shown are the pressure losses in each loop as a function of flowrate, assuming pressure is proportional to the square of the flowrate ($P = K Q^2$). Providing reasonable currents across the throats is difficult because of the metallurgically bonded low-resistance circuit depicted in Figure 49, a circuit that cannot be broken.

If current is applied across points 1 and 4 the effective current through the throat is

$$\frac{R_{B2} + R_{B3} + R_C}{R_T} \times I = \frac{40}{115} \times I \simeq \frac{1}{3} I.$$

Therefore, only 1/3 of the current supplied is providing useful work, and pre-startup hydraulic pumping requirements could be fairly high depending on flow

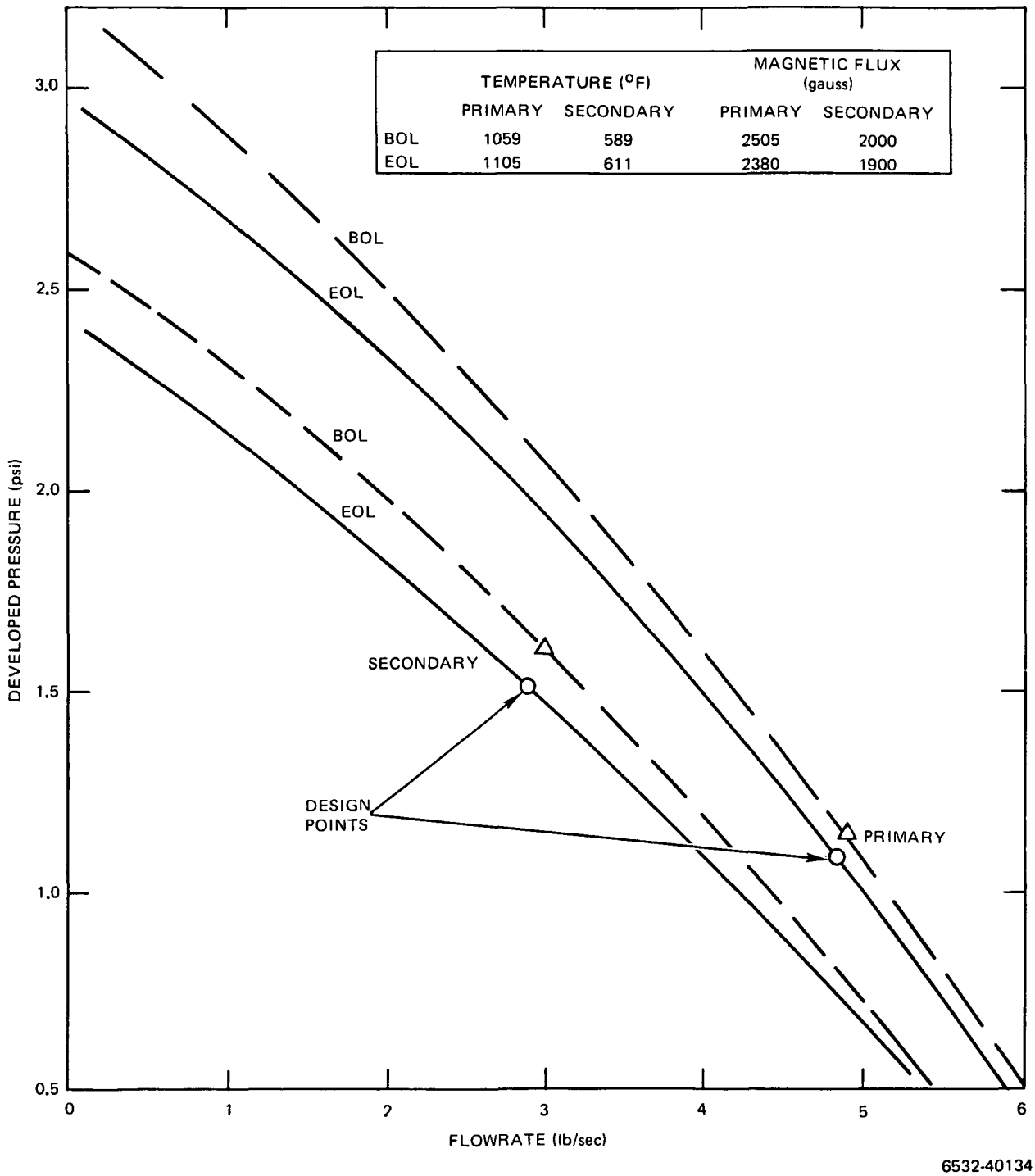

Figure 44. Prototype Pump Performance

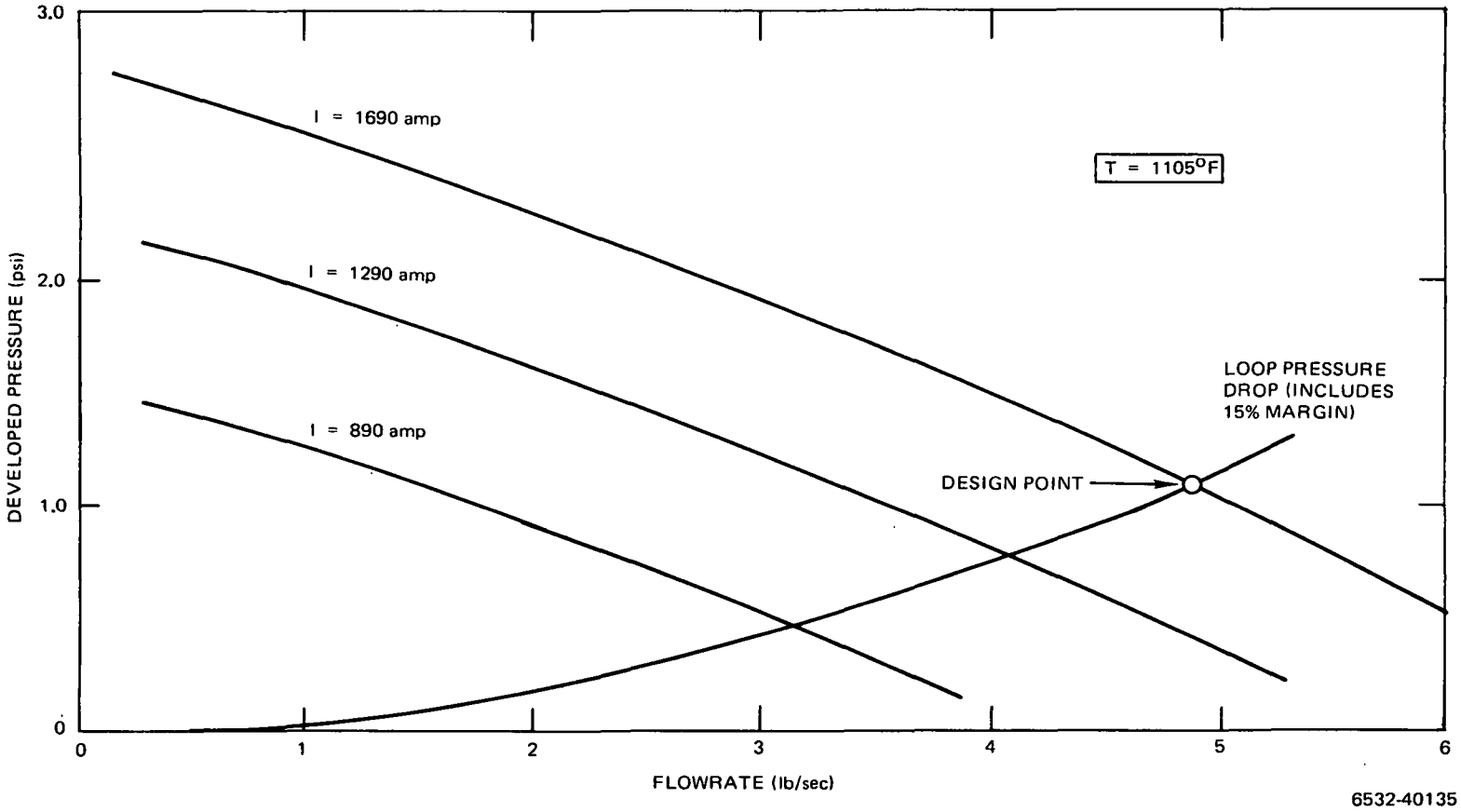

Figure 45. Primary Throat – Loop Characteristics

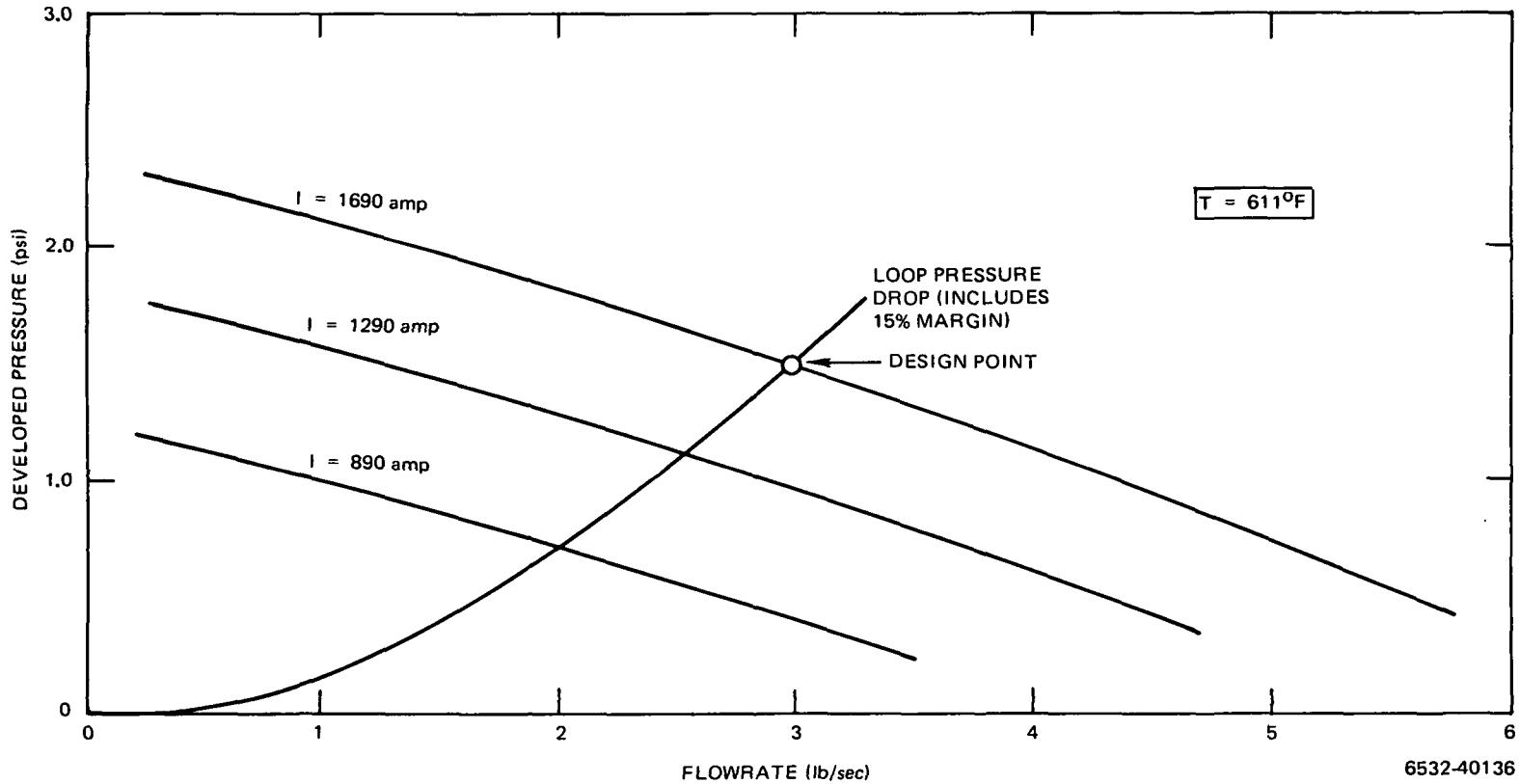

Figure 46. Secondary Loop – Throat Characteristics

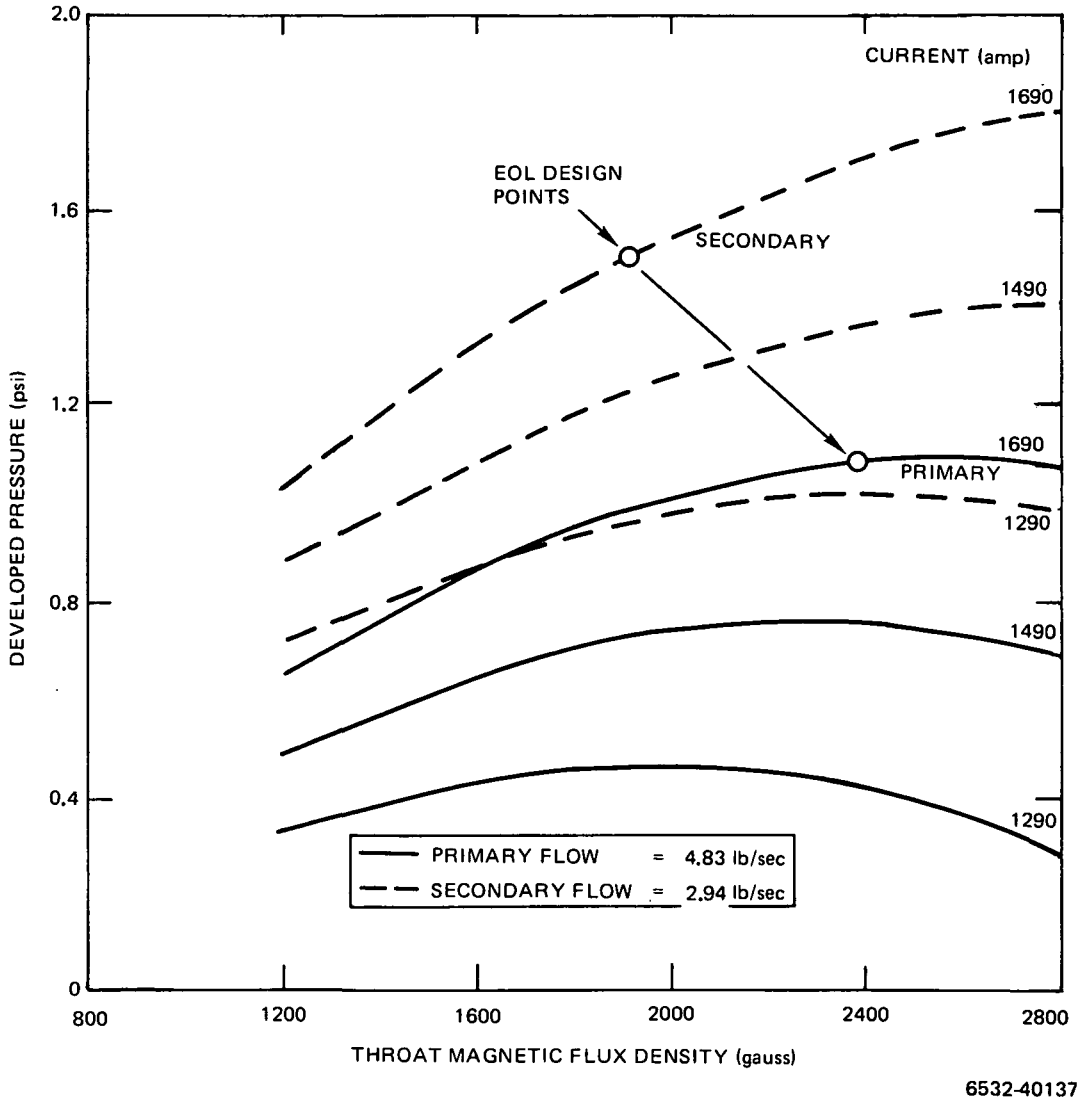

Figure 47. Pump Performance – ΔP versus Flux Density

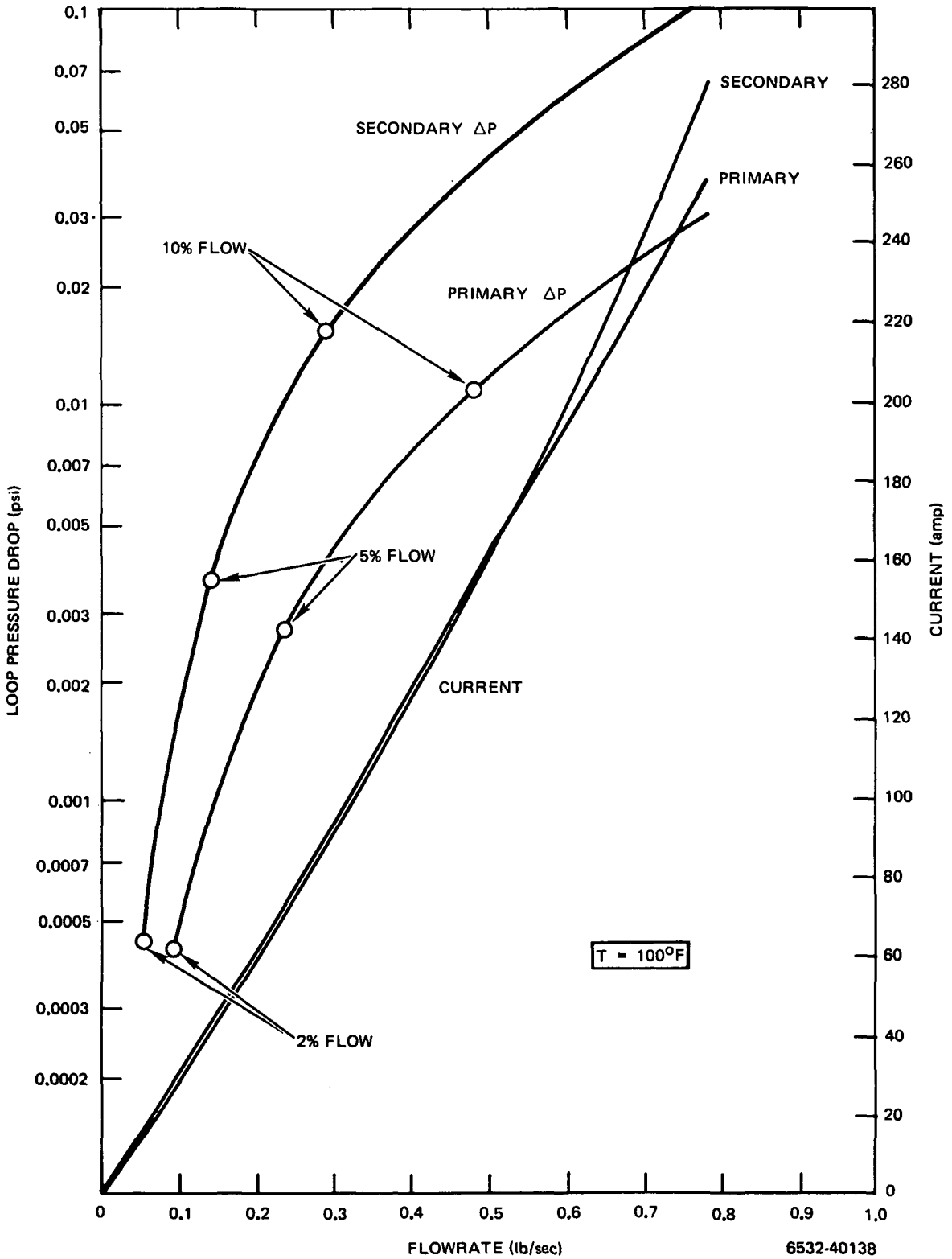

Figure 48. DC Pump Startup Characteristics

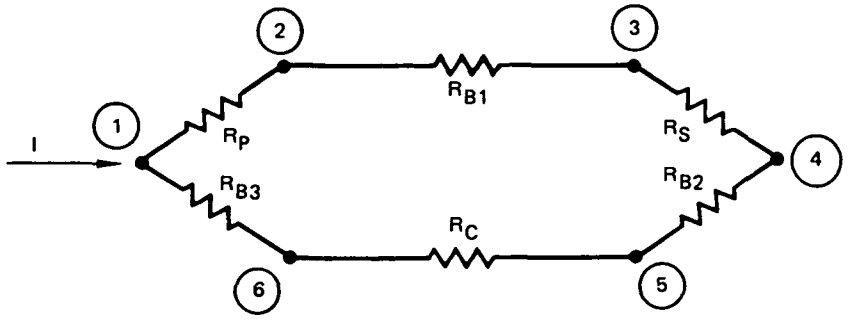

R_P	= PRIMARY THROAT	~ 35 microhms	
R_{B1}	= FLEX BUS	~ 5 microhms	
R_S	= SECONDARY THROAT	~ 35 microhms	
R_{B2}	= FLEX BUS	~ 5 microhms	
R_C	= TE CONVERTER	~ 30 microhms	(WITH N_1 END RINGS)
R_{B3}	= FLEX BUS	~ 5 microhms	

$R_T = R_P + R_{B1} + R_{B2} + R_{B3} + R_S + R_C$ = TOTAL CIRCUIT RESISTANCE

6532-40139

Figure 49. Thermoelectric Pump Assembly Electrical Schematic

and length of time before reactor startup. If current can be applied across points 1 and 2 then about 2/3 of the current will pass through the primary throat,

$$\frac{R_T - R_P}{R_T} \times I = \frac{80}{115} \times I \quad \frac{2}{3} I,$$

and about 1/3 will pass through the secondary throat, resulting in a lesser flow in the reverse direction in the secondary loop. This may or may not be acceptable, depending on system operating characteristics and requirements, and would need to be evaluated.

VI. RADIATOR/STRUCTURE

The radiator/structure performs two separate functions: first, it must reject system waste heat to maintain the thermoelectric converter cold junction temperature; second, it acts as the primary support structure for all components in the power system. It must withstand prelaunch handling, launch, and orbital operation, including micrometeoroids and the thermal/vacuum environment of space. This section describes the characteristics of the radiator/structure for the 5-kwe Reactor Thermoelectric System.

A. REFERENCE DESIGN

Figure 50 shows the configuration of the reference radiator/structure. The overall height is 19.2 ft. The 72 in. diameter radiator base is designed to mate with the reactor/shield assembly. The radiator area is 266.8 ft^2. All other components are located within the radiator. The radiator has Lockalloy fins and stainless steel tubes, stringers and rings. There are 48, equally spaced, NaK coolant tubes. Two supply lines deliver NaK from the thermoelectric converter manifolds to the header at the top of the cone. The NaK flows down through the coolant tubes and is gathered in a header at the base of the cylinder. Two lines then return the cooled NaK to the thermoelectric converters.

Figure 51 shows fin/tube cross sections at two locations. The fins are uniform thickness and vary in width from 1.944 in. at the top of the core to 4.712 in. on the cylinder. The 0.060-in. Lockalloy fins are attached to D-shaped stainless steel tubes. An armor thickness of 0.075 in. is required to provide a meteoroid noncritical damage probability of 0.99 for 5 years.

Table 23 shows the radiator/structure characteristics, and Table 24 shows a detail weight breakdown.

Figure 52 shows how fin base temperature and effectiveness vary over the length of the radiator. The fin effectiveness ranges from nearly 92% to 81%. Figure 53 shows fin temperature level and distribution at three locations. The maximum gradient occurs in the cylinder, where the fins are the widest.

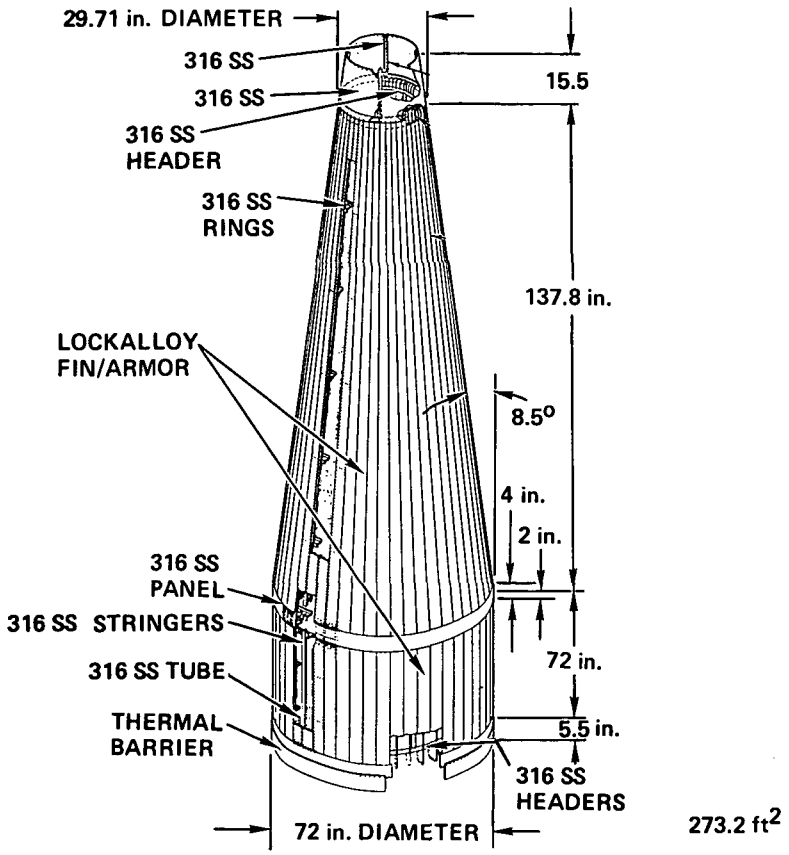

Figure 50. Radiator Dimensions

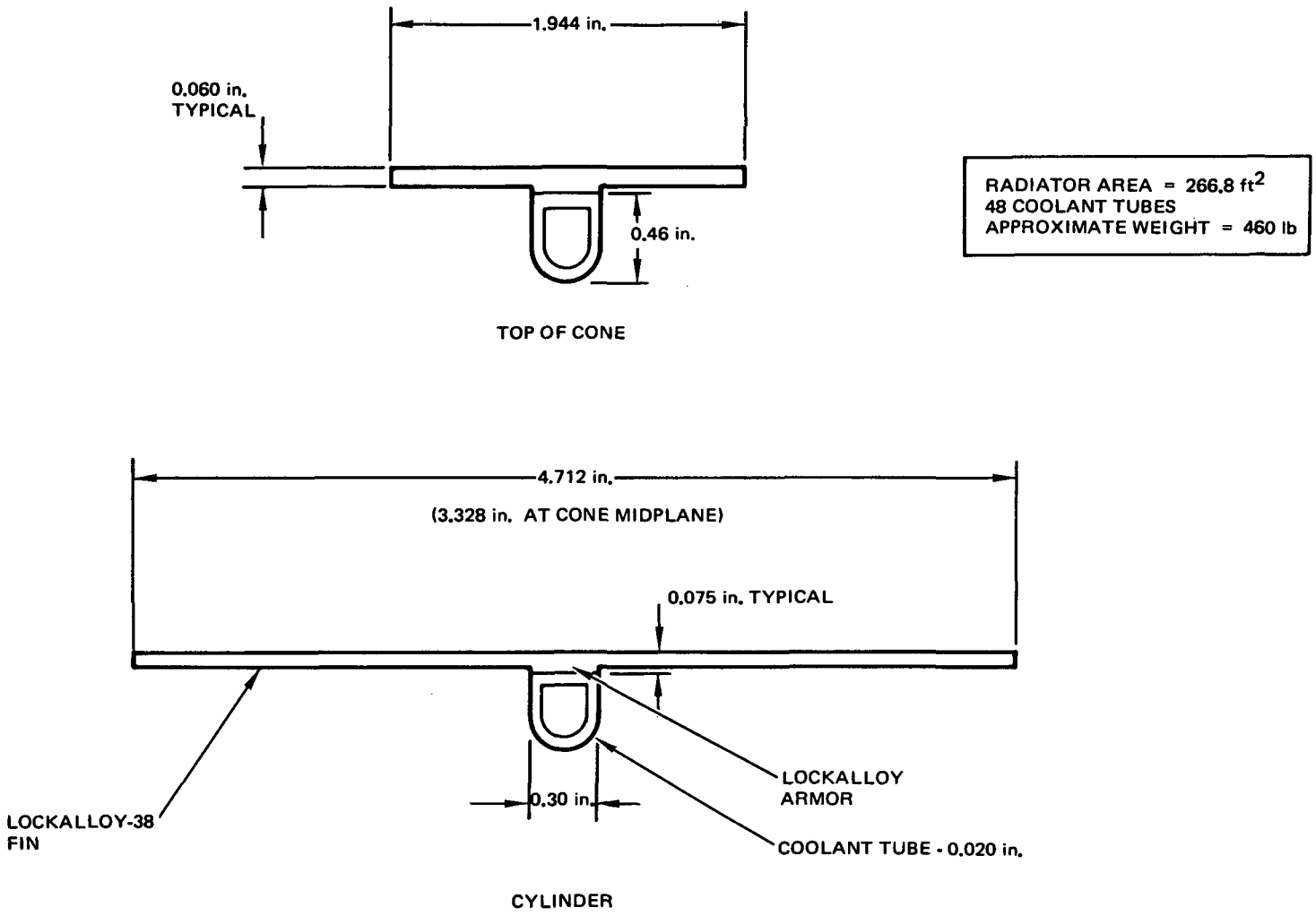

Figure 51. Reference Lockalloy-38 Radiator

TABLE 23

RADIATOR/STRUCTURE CHARACTERISTICS

Thermal power rejected (kw)	94.9
NaK temperatures (°F)	
Inlet	611
Outlet	467
Environmental heat input (Btu/ft^2-hr)	102
Emissivity	0.90
Solar absorptivity	0.50
Average fin effectiveness	0.835
Coolant pressure drop (psi)	0.2
Coolant flowrate (lb/sec)	2.9
Radiator area (ft^2)	266.8
Total Weight (lb)	460

TABLE 24

WEIGHT SUMMARY
(lb)

Fin/Armor	179
Tubes (wet)	124
AI-93 emissivity coating	16
Rings and stringers	57
Support skirt	6
Rivets	37
Access panels	15
Thermal baffles	7
Pump support flange	9
Miscellaneous bracketry	10
Total	460

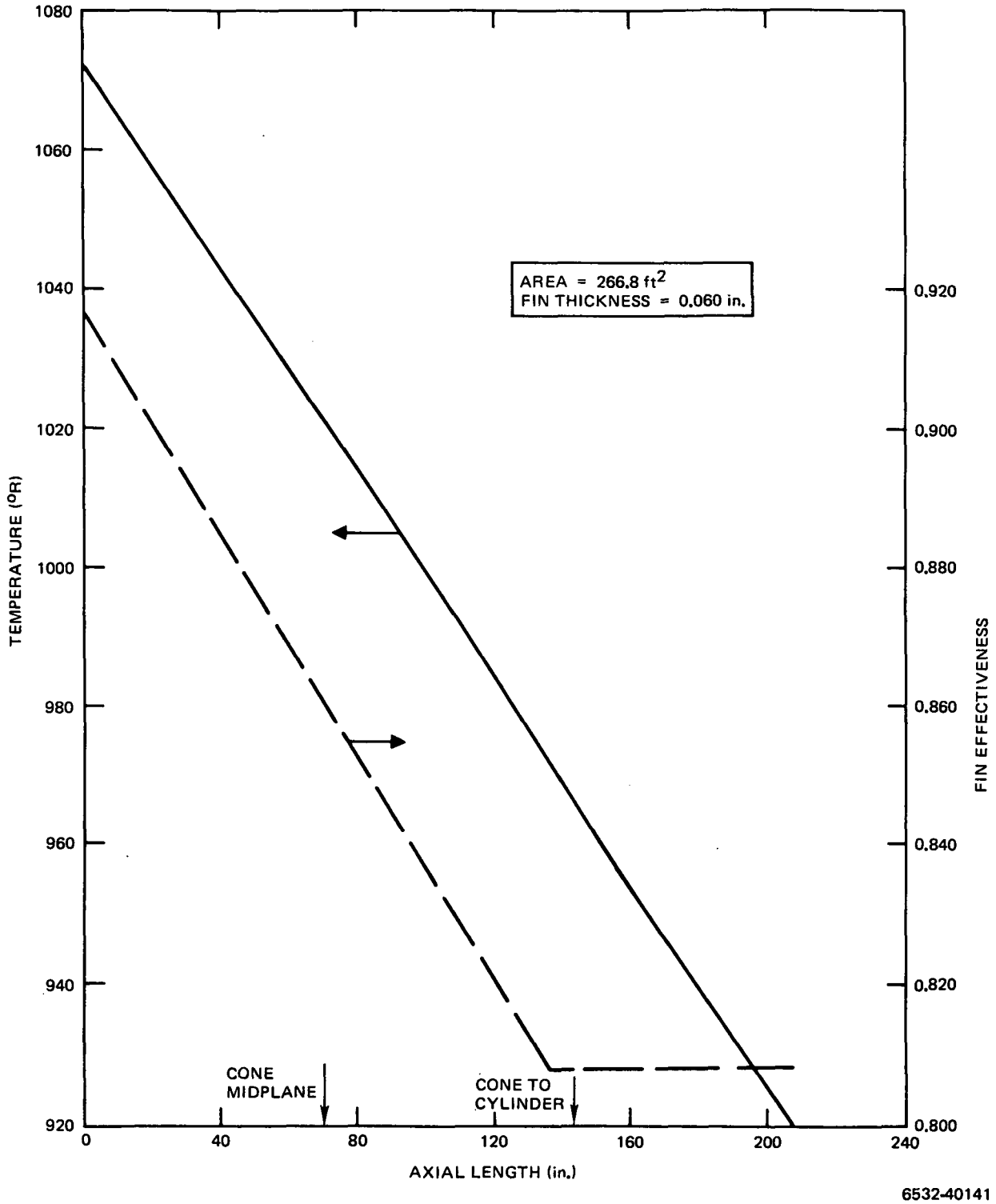

Figure 52. Temperature and Fin Effectiveness versus Axial Length

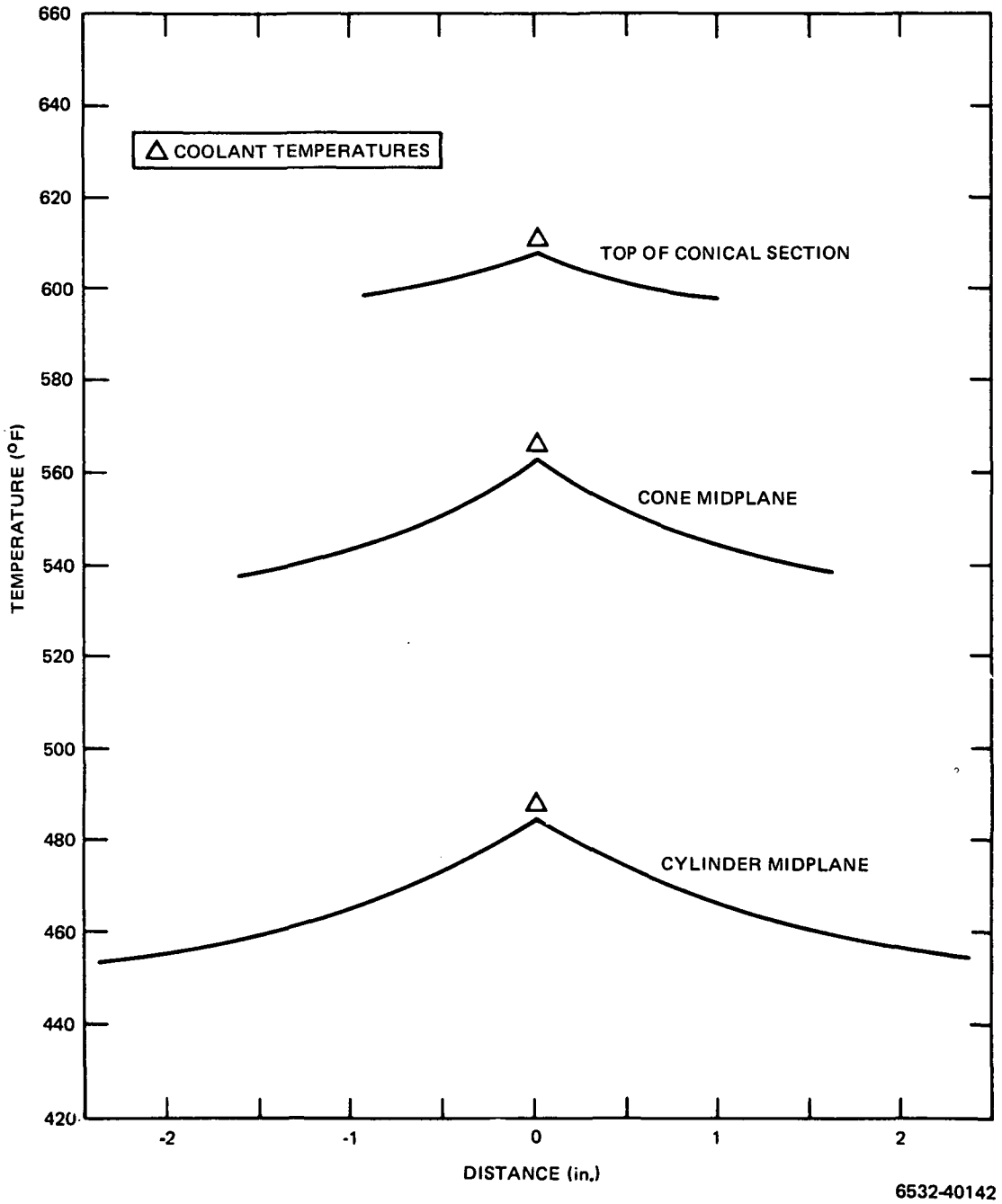

Figure 53. Lockalloy Radiator Fin Thermal Profiles

B. INDUCED ENVIRONMENT

This section describes the thermal and mechanical environments to which the radiator/structure would be subjected during: (1) fabrication, (2) ground handling, (3) orbit operation, and (4) ground test.

1. Mechanical Environment

The loads which have an influence on the structural characteristics of the radiator exist throughout the life of the radiator and begin with its fabrication. Both mechanical and thermal loads are imposed on the system. Aside from a 1-g axial load in conjunction with the ground test and prelaunch thermal environment, the mechanical and thermal loads do not occur simultaneously. With this one exception, the loads can be treated separately.

The most significant mechanical loads occur during the launch. Although the 5-kwe system was not designed for a specific application, a reference spacecraft design and launch vehicle were established. The spacecraft was estimated to weight 1350 lb and have a length of 12 to 14 ft with a diameter equal to that of the 5-kwe system radiator. It was assumed that the orbit would be polar, circular, and 600 mi. With a system of approximately 1850 lb, the total orbital weight would be about 3200 lb and would require a TITAN launch vehicle.

The launch-induced loads can be categorized as follows:

1) Low frequency and sustained accelerations

2) Acoustic

3) Shock

4) Thermal.

Non-launch-induced thermal loads are results of system operating characteristics.

a. Ground Handling Loads

These loads occur while moving the various segments of the radiator during the fabrication phase and moving the completed radiator and system. Packaging, handling, and hoisting equipment must be designed in such a manner that ground handling loads do not govern the structural design of the system or its

components. Ground handling loads, therefore, do not constitute a limiting design condition.

b. Launch Accelerations

The TITAN IIIB/Burner II was selected as the most probable launch vehicle. However, to accommodate potential variations in payload weight and system weight, the TITAN IIIB and the TITAN IIIC with Transtage were also considered.

The accelerations of design significance occur during the maximum q α transonic phase, first-stage burnout, and second-stage burnout. Table 25 shows the anticipated accelerations associated with these three conditions. An ultimate factor of safety of 1.25 is used in conjunction with the design loads.

TABLE 25

LAUNCH ACCELERATIONS

Case	Design Load (g)		Ultimate Load (g)	
	Axial	Transverse	Axial	Transverse
Transonic	6.0	1.6	7.5	2.0
Uncontrolled First-Stage Burnout	8.0	1.0	10.0	1.25
Second-Stage Burnout	13.0	0.5	16.25	0.625

Figure 54 shows the axial accelerations of the potential launch vehicles as a function of time from lift-off. A TITAN system without a third stage and with a low mass payload can reach 13.25 g's at the end of Stage II burn. The acceleration of Stage II and a 3200-lb payload can reach 12.6 g's. With a Burner II and a 3200-lb payload, the Stage II maximum acceleration is 9.1 g's.

The loading in the radiator from the launch environment is a function of the system weight distribution and the configuration. Table 26 shows the radiator panel loads for a system of 1800 lb, 72-in. -diameter cylinder, 236 in. from the base of the neutron shield to the base of the reactor, and 8.5 degree cone. The panel loads are derived from the shear (thrust) and moment curves. For the full panel, defined as one tube and the fin and armor between tube centerlines, the radiator loads are the unit loads times the panel width.

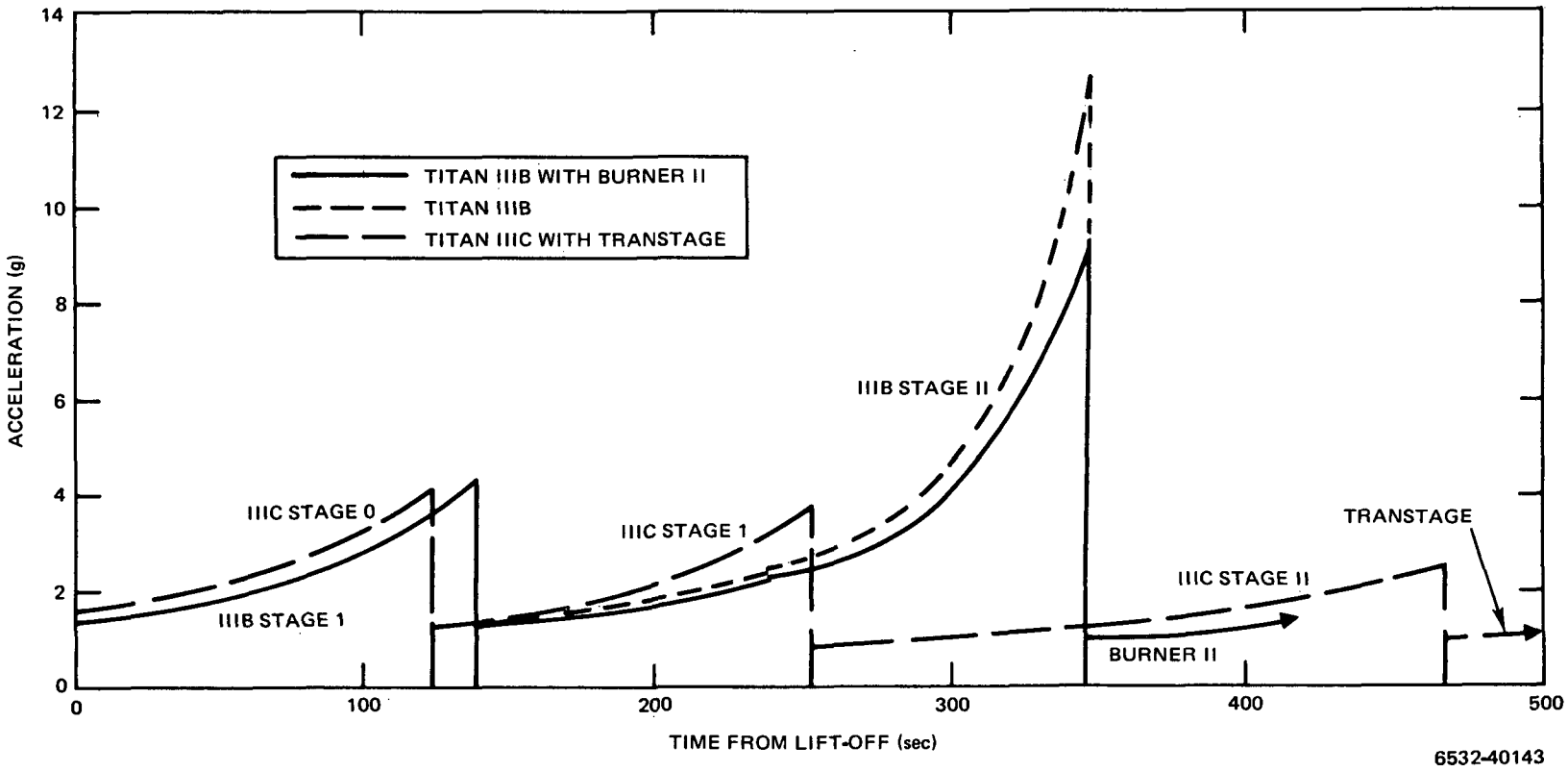

Figure 54. TITAN Sustained Acceleration

TABLE 26

UNIT PANEL LOADS FOR LAUNCH ACCELERATIONS

Station	1-G Shear (lb)	1-G Moment (lb)	Radius (in.)	Membrane (Thrust) (lb/in)	Membrane (Bending) (lb/in)	1-G Shear (lb/in)
0	1800	330000	36	- 7.97	±81.05	15.9
61.3	1660	225000	36	- 7.34	±55.26	14.7
80	1620	196000	33.2	- 7.77	±56.64	15.5
120	1530	130000	27.8	- 8.76	±53.54	17.5
150	1430	85000	22.0	-10.35	±55.90	20.7
182	1030	52000	17.9	- 9.16	±51.66	18.3
212	880	25000	12.4	-11.31	±51.75	22.6
236	620	11000	9.9	-10.02	±35.73	19.9

Station	Maximum $q\alpha$			Stage I Burnout			Stage II Burnout		
	Maximum (lb/in)	Minimum (lb/in)	Shear Flow (lb/in)	Maximum (lb/in)	Minimum (lb/in)	Shear Flow (lb/in)	Maximum (lb/in)	Minimum (lb/in)	Shear Flow (lb/in)
0	102.3	-221.9	31.8	+21.6	-181.0	19.9	- 78.9	-180.1	9.9
61.3	55.4	-165.6	29.4	- 4.3	-142.5	18.4	- 84.8	-153.8	9.2
80	55.0	-171.6	31.0	- 6.9	-148.5	19.4	- 90.9	-161.7	9.7
120	31.4	-172.8	35.0	-20.7	-154.5	21.9	-108.9	-175.9	10.9
150	34.2	-189.4	41.4	-33.6	-173.4	25.9	-133.3	-203.1	12.9
182	34.6	-172.0	36.6	-27.0	-156.2	22.9	-116.6	-181.1	11.4
212	18.7	-188.3	45.2	-48.4	-177.8	28.3	-151.5	-216.1	14.2
236	- 3.7	-146.7	39.8	-55.5	-144.9	24.9	-140.5	-185.1	12.4

c. Acoustic Loads

There are essentially two sources of acoustic excitation during the TITAN launch. At lift-off and for approximately 5 sec., engine noises reflect off the launch pad and couple with direct excitation of the nose shroud. At Mach 1 through maximum $q\alpha$, there is aerodynamic turbulence for approximately 55 sec. TITAN nose shrouds are designed to attenuate acoustic fields of this type to 145 db or less inside the nose fairing.

Typically, a 145-db sound pressure level does not excite large payload masses. However, thin panels and components with large surfaces can be subjected to detrimental displacements. The nature of the 5-kwe radiator suggests that it will not be excited to the extent that it will sustain damage in this acoustic environment but that masses mounted on it will require evaluation. This is particularly true of the reactor which contains the fuel elements, and which supports the reflector drive mechanism.

d. Launch-Induced Shock

Shock loads generated in a TITAN system have two primary sources. The first occurs when stages are separated. The shock stems from the pyrotechnic splitting of the seam at the stage fairings and also from the nose shroud split and separation. The second source occurs when the payload is ejected from the final stage.

All of these events occur at high altitude in a near vacuum that will not transmit shock pressure waves. Consequently, the shock can only be transmitted mechanically through the structure.

The 5-kwe system will be no closer than 12 ft to a shock source. Since these waves attenuate rapidly in a structure, there are no requirements for shock in the radiator design.

e. Orbital Mechanical Loads

During orbit, the system will be at an essentially 0-status. Small orientation engines on the payload may induce short-time accelerations, however, there is no requirement for structural consideration in the radiator of these loads.

f. Ground Test Mechanical Loads

The 5-kwe system was to be oriented with the reactor down during the 5-year ground operation test, with the support point at the base of the radiation shield with several "steady-rest" points at the base of the radiator. Thus, the radiator would be subjected to a sustained -1.0-g load.

2. Thermal Environment

a. Fabrication

Fabrication of the radiator would involve various heating steps, depending on the materials used. In all cases, the tube/fin assemblies would be in the fully annealed condition after fabrication.

The type 304L SS tubing, when used with the Lockalloy fin material, would require the deposition of a layer of titanium which would act as a diffusion barrier to prevent the formation of brittle intermetallics between the stainless and the braze (BAl-Si4). Deposition of the titanium is performed on the stainless tubing at a temperature of approximately 1400°F. Vacuum brazing of Lockalloy stainless steel would occur at a temperature of approximately 1120°F using BAl-Si4, the aluminum-silicon eutectic composition.

Thermal cycling of the radiator assembly would also be required during the application of the AI-93 emissivity coating. Oxidation of the entire radiator assembly at 650°F for 15 min. would be required prior to coating. Application of AI-93 would then require three separate coatings, each of which must be baked at a temperature of 600°F for 15 min.

b. Startup and Shutdown

The thermal design objectives for the reactor during startup have been established on the basis of operational requirements, engineering analyses of the system, and safety guides and standards. These objectives are:

1) Temperature rise through the core limited to less than 150°F.

2) Rate of temperature change in the inlet plenum limited to less than 150°F/min.

Limiting the temperature rise through the core to less than 150°F prevents generation of excessive thermal stresses in the fuel, cladding, internal reflector,

and core vessel. This temperature rise is affected mainly by the reactor power and its rate of increase, and by the primary NaK flowrate.

Limiting the rate of temperature change to 150°F/min avoids severe thermal shock. This startup results in a rate of temperature increase in the radiator of less than 50°F/min. During the simulated normal and emergency reactor scrams, the maximum rate of radiator temperature drop is also less than 50°F/min.

The 50°F/min temperature rise during startup may result in critical stress levels in the cold regions between the individual radiator coolant tubes. A 30 to 50°F thermal lag may exist between the fin root and fin tip. This lag will produce a differential thermal expansion and consequently an increase in stress level between the fin root and tip. Additional analyses will be required to assess the degree of this thermally induced stress during system startup.

c. Space Operation

A 600 n. mi constant sun-shade polar orbit was used to determine the environmental heat input to the radiator surface in space. This orbital attitude is considered to provide the maximum environmental thermal flux to the radiator surface as follows:

Direct solar = 146 Btu/ft^2-h4

Direct earth = 13.8 Btu/ft^2-h4

Earth reflected = 9.5 Btu/ft^2-h4

Using these input parameters with $\alpha_s = 0.5$ and $\epsilon = 0.90$ the environmental heat flux absorbed by the radiator fin is 102 Btu/ft^2-hr.

C. MATERIAL SELECTION

1. Fin/Tube

The development of the radiator structure was based on the use of established techniques for its design, analysis and fabrication. It was to be fabricated by brazing aluminum fins to stainless steel tubes and edge riveting these assemblies to form an integral heat rejection/structural support radiator. Joining of aluminum to stainless steel had apparently been successfully achieved by several fabricators.

The technical requirements for the radiator fin material were:

1) Service temperature: 490°F to 618°F over 5 years in space vacuum (600 n. mi orbit), 50 thermal cycles
2) Ground checkout: Thermal excursions to 618°F in vacuum
3) Manufacture: Braze cycle exposure to 1100°F
4) Coating application: 450°F for 45 min
5) NaK fill: 600°F for 100 hr
6) Mechanical and physical properties:
   a) High thermal conductivity
   b) Moderate strength
   c) Low vaporization of alloying elements in space
   d) Brazeable to austenitic stainless
   e) Low density
7) Availability and low cost.

It was found that magnesium was undesirable as an alloying element due to its high vapor pressure.

A number of aluminum alloys were considered. In general it was found that the higher strength alloys contained magnesium in unacceptable quantities. A discussion of each of the aluminum alloys follows:

1100 An alloy having high thermal conductivity, a high melting range, is brazeable and available but has low mechanical strength.

2011 A magnesium-free alloy but available only as bar stock and having lead, zinc and bismuth as additions for free machining purposes and considered not suitable.

2024 A high strength alloy susceptible to stress corrosion and containing magnesium.

2219 A low magnesium alloy that maintains mechanical strength at temperatures up to 600° F; better than 1100 or 3003 but due to its low melting range would not be suitable for brazing.

3003 An alloy with thermal conductivity slightly inferior to 1100 but with higher mechanical strength.

3004 An alloy similar to 3003 but with higher mechanical strength and 1% nominal magnesium content.

5052 A high strength work hardening alloy that contains magnesium.

6061 A high strength heat treatable alloy that contains magnesium.

7075 An alloy that can be heat treated to high strengths but is susceptible to stress corrosion and contains magnesium.

The manufacturing, prelaunch, and space service conditions imposed requirements on the material selection that exceeded the conventional range of properties developed for engineering purposes. The specific selection of the materials was, of necessity, a compromise of a number of applicable factors. For these reasons, alloy 3003 condition "O" was originally selected for the radiator fin material. This alloy possessed the high thermal conductivity required for the component but had low mechanical strength. The selection was based on the assumption that the aluminum radiator panels would be brazed to the stainless steel Nak tube and then the assembly of the panels and support structure would be accomplished by mechanical fasteners. The outer surface of the assembled radiator would then receive the emittance coating.

Concurrent with the materials and process development effort, stress analysis was being performed on the fin-tube assembly. A basic problem with the bonded aluminum/stainless steel is the great differential in their thermal expansion rates. The aluminum will contract about 25% more than the stainless steel on cooling from 600° F to room temperature. This amounts to approximately 0.5 in.of mismatch over the total length of the radiator. Although the analysis showed that the aluminum could be made to yield and recover in a stable manner (i. e. , always returning to the same position) if the stainless were thick enough, differential yielding and creep of the fin from root to tip would probably cripple it as a load-carrying member. The residual stresses imposed on the

stainless steel tubes and aluminum sections would be nearly impossible to analyze since the local yielding of the aluminum would depend upon local temperatures and the direction of the ripples being formed.

With the disappointing thermal cycling tests and the detailed stress analysis results, it was evident that the aluminum/stainless steel radiator design was the wrong approach. A search for alternate materials combinations was made to alleviate the differential thermal expansion mismatch problem.

After an extensive materials survey, a Lockalloy (Be-38% Al) 304L combination was selected for further evaluation since a nearly perfect match in thermal expansions was obtained. The Lockalloy compared to 3003 aluminum has lower density, higher stiffness and higher strength, which makes it suitable as a radiator fin material. Although its conductivity is higher than that of 3003 aluminum at room temperature, it is lower at 600°F.

Stress analysis of the Lockalloy-stainless steel fin-tube assembly showed that both materials remained in the elastic range through thermal cycling. These materials eliminated the stress problems resulting from differential thermal expansion because both materials remained in the elastic range during subsequent thermal cycling.

Lockalloy could be machined, drilled, and riveted by techniques approaching standard aluminum and magnesium alloys. Rockwell International is presently using Lockalloy as stringers in a riveted missile application, and no special procedures are followed except that all chips are picked up with a vacuum cleaner during drilling of holes. Lockalloy has been successfully bonded to aluminum, beryllium and itself using aluminum-silicon braze alloys, but any braze alloy used to join Lockalloy must have a melting point below the 1193°F Al-Be eutectic melting point.

In addition to the Lockalloy stainless steel, other materials combinations considered were copper stainless steel and boron filament impregnated aluminum. Both of the above combinations essentially solved the thermal expansion mismatch problem, and indications were that the bonding problems could be readily solved. However, the copper fins would result in a significant weight penalty, and handling of the thin annealed copper would be difficult during assembly. Also, the application of the AI-93 emissivity coating to copper is more of an unknown

than applying it to aluminum or Lockalloy, as continued oxidation of the copper during radiator operation could result in spalling of the coating. The boron aluminum appeared to be too far in advance of the state-of-the-art and the cost would be excessive. Both approaches were abandoned.

2. Emissivity Coating

The radiator fin surface requires a coating system which is effective in rejecting heat and reflecting solar input. The coating must operate in space in the temperature region of 500 to 700°F for 5 years.

During the SNAP 10A program, two thermal coatings were considered for use on the system radiator, Z-93 and AI-93. Z-93 is a zinc oxide coating with a potassium silicate binder. AI-93 consists of a top coat of stannic oxide, a subcoat of Cr-Co-Ni and a binder of aluminum phosphate.

Early screening tests included many of the basic metal oxides, with particular interest devoted to the whites oxides. These tests were begun with an evaluation of the spectral reflectance and total normal emittance of candidate metallic oxides including the oxides of Ba, Ce, Sb, Si, Ti, Zn, and Zr. From this study it was found that:

1) The thermal emittance at 600°F for coatings with the aluminum phosphate binder was consistently 3 to 5% higher than coatings with the potassium silicate binder.

2) The solar absorptance for coatings with the aluminum phosphate binder was consistently 10 to 20% higher than coatings with the potassium silicate binder.

3) The white pigment which exhibited the highest thermal emittance at 600°F was stannic oxide.

Because the optimum thermal effectiveness of the radiation control coating is determined primarily by the thermal emittance, further coating experimentation emphasized use of the stannic oxide pigment and an aluminum phosphate binder. Total hemispherical emittance measurements of the stannic oxide coating system yield a value of $\epsilon = 0.88$ at 600°F.

Many black coatings have a high thermal emittance in the short wavelength infrared region (1 to 4 μ). To further increase the bulk emittance, a composite

coating system was devised in an effort to maximize the spectral emittance throughout the infrared region. This was accomplished by utilizing a high thermal emittance, black subcoat and the stannic oxide as a topcoat. Total hemispherical emittance measurements of the two-layer composite coating (AI-93) yielded a value of $\epsilon = 0.91$ at 600° F.

Long-term emittance stability tests of AI-93 were made at 600° F in vacuum. Prior to the test, the emittance of the tailored coating as adaptable to aluminum substrates was 0.90. Subsequent to the 4900-hr test the emittance of the sample was 0.92. The results of these tests, taken at 10^{-5} torr, are shown in Figure 55 as a function of time. The 3000-hr stability tests of the AI-93 coating system in a simulated space ultraviolet environment resulted in a 30% increase in solar absorptance. The tests were performed utilizing an AH6 mercury lamp for exposure and the vacuum attained during irradiation was 10^{-7} torr. Samples were irradiated at two solar factors; i. e., 5 and 10. Degradation results were similar for each of these accelerated exposures. These tests were also run at 600° F.

From the results of these tests, AI-93 was selected as the reference radiator emissivity coating. The values of solar absorptivity = 0.5 and emissivity = 0.9 were used as conservative values in the radiator analyses.

D. METEOROID PROTECTION ANALYSES

The equation used to calculate the meteoroid armor requirements is:

$$\delta = \gamma_R{}^a \left(\frac{\rho P}{\rho a}\right)^{1/2} \left(\frac{V_p}{C_a}\right)^{2/3} \left(\frac{6}{\pi \rho p}\right)^{1/3} \left(\frac{E\alpha A_v t}{-\ln P_o}\right)^{1/3B} \left(\frac{2}{3n\theta B+2}\right)^{1/3B} \left(\frac{T}{T_R}\right)^{1/6}$$

where:

δ	=	armor thickness
γ_R	=	room temperature cratering coefficient,
a	=	rear surface damage thickness factor,
ρ_P	=	meteroid average density, 0.5 g/cm^3
ρa	=	armor density
V_p	=	meteroid average velocity, 20 km/sec
C_a	=	sonic velocity in armor

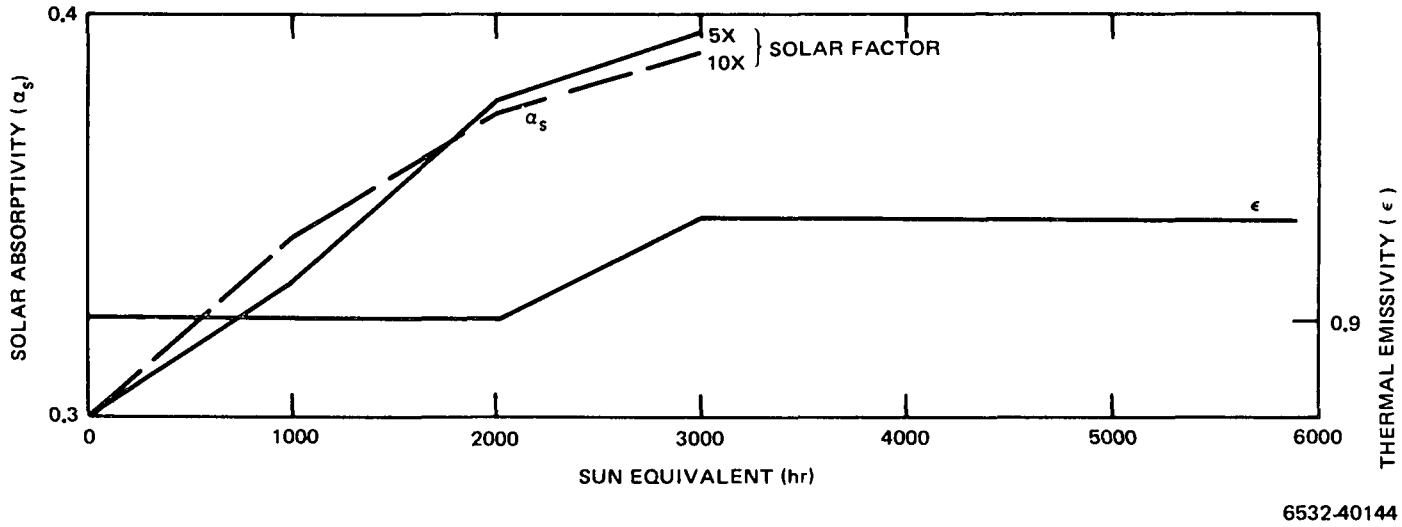

Figure 55. AI-93 Stability in High Vacuum

E	=	armor earth shielding factor, 0.7631
α	=	meteroid flux constant, $10^{-14.37}$ gm^{B}/$_{m}$2 sec
A_v	=	vulnerable area
t	=	mission time
P_o	=	design probability of no critical damage
n	=	damage factor for oblique impact, 1.0
θ	=	penetration constant, 0.667
B	=	meteroid flux constant, 1.213
T	=	armor temperature
T_R	=	room temperature

The cratering coefficients, γ_R, and the rear surface damage factors, a, in the meteoroid armor equation vary for different armor materials and as a function of temperature. The cratering coefficient for Be is 2.28 and the value for aluminum is 1.70. These values were percentage composition weighted to obtain a γ_R value for Lockalloy-38 of 2.06. The value of "a" used for the asymmetric fin/tube radiator cross section was 0.9.

The armor equation was used to determine the required thickness of Lockalloy armor that must be provided to protect the front side of the thermal radiator coolant tubes. Figure 56 shows Lockalloy armor thickness as a function of the noncritical damage probability. The critical event for these calculations was a 0.99 probability of not receiving a 0.75 in. dimple of the coolant tube during the 5-year mission lifetime. As shown in the figure, a 0.075-in. thickness of Lockalloy is required. This is the total material thickness between the outer edge of the coolant tubes and the outer surface of the radiator fin, as shown in Figure 51.

E. STRUCTURAL ANALYSES

A braze process is used for the basic fabrication of the aluminum fin/stainless tube panel assembly. As illustrated, free contraction of the aluminum will be greater than that of the steel while cooling to room temperature. The fin and tube are bonded, however, and the combination will contract an intermediate amount based on the relative areas, modulus of elasticity and expansion rates.

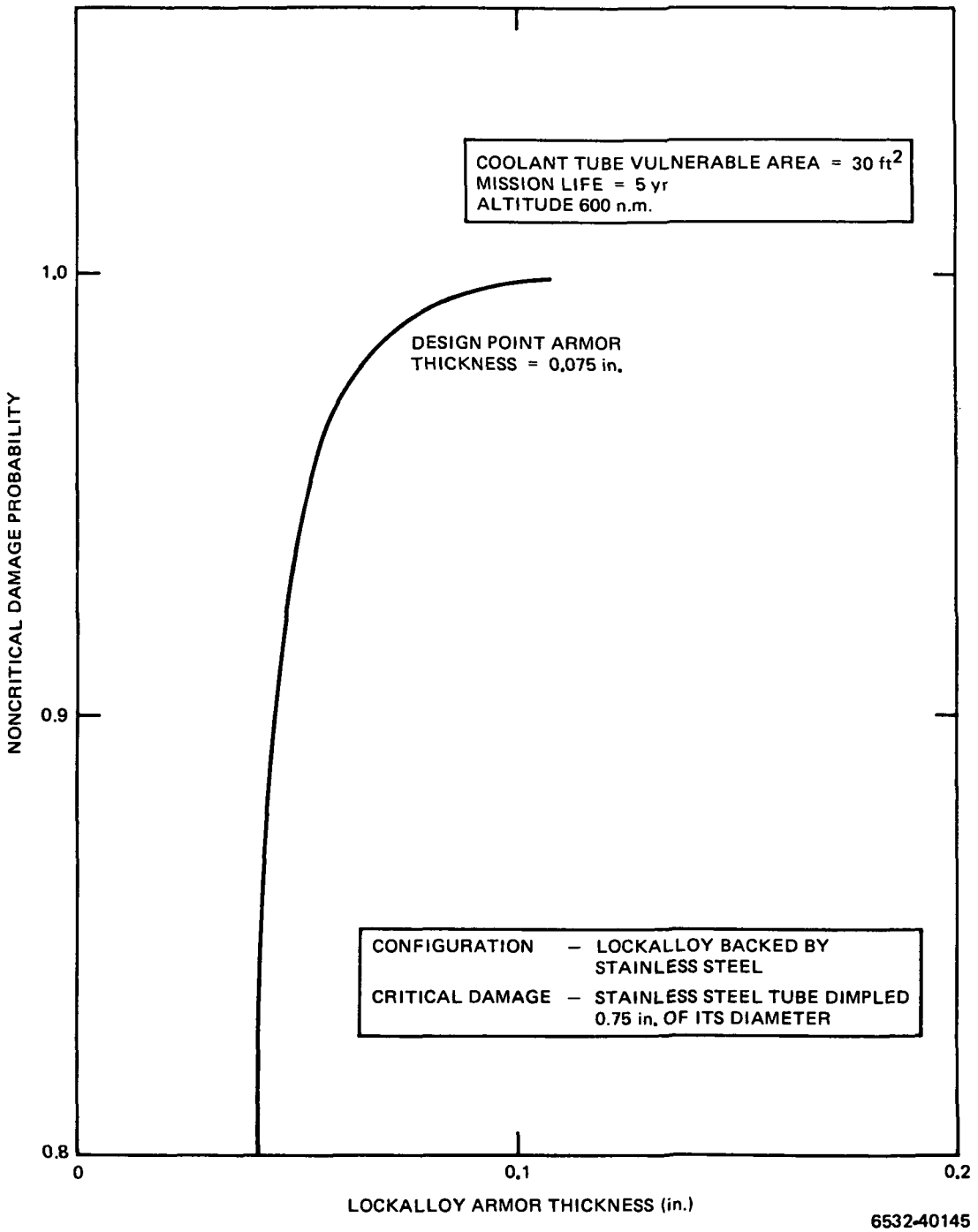

Figure 56. Lockalloy Armor versus Noncritical Damage Probability

$$\epsilon_R = \Delta T \left[\alpha_F - \frac{(\alpha_F - \alpha T)(A_T E_T)}{(A_T E_T + A_F E_F)} \right]$$

where

ϵ_R = net contraction of fin/tube composite
α_F = coefficient of expansion of fin
αT = coefficient of expansion of tube
A_F = cross-section area of fin
A_T = cross-section area of tube
E_F = modulus of elasticity of fin
E_T = modulus of elasticity of tube
ΔT = temperature change.

The strain in each metal is the difference between their free contraction and that of the composite. With a bond solidification at 775° F, and the ratio of aluminum-to-stainless in the original cross section, the strain in the steel is 0.32% and that in the aluminum is 0.04%. It is evident that the tube is far into the plastic range and an alternate braze process was required. It was then proposed that soaking at 600° F would allow the aluminum to relax and create a stress-free condition at that temperature. The residual strains when cooled to room temperature were +0.05% in the aluminum fin and 0.21% in the tube. Although this was still in the plastic range, an evaluation of the cross section was made to determine the effect of subsequent thermal cyling to determine if the configuration would ratchet. If the radiator would reach a shakedown relationship such that subsequent thermal cycles would not create additional plastic strain, aluminum would gain as a potential radiator material.

As the temperature increases from 75° F, the material tends to return to the original stress-free state at 600° F, however, there is a 0.10% permanent strain in the tube. Figure 57 shows the complete cycle of strain versus temperature starting with equal length, stress-free material at 600° F. Both fin and tube are essentially stress-free and of equal length at point 0.

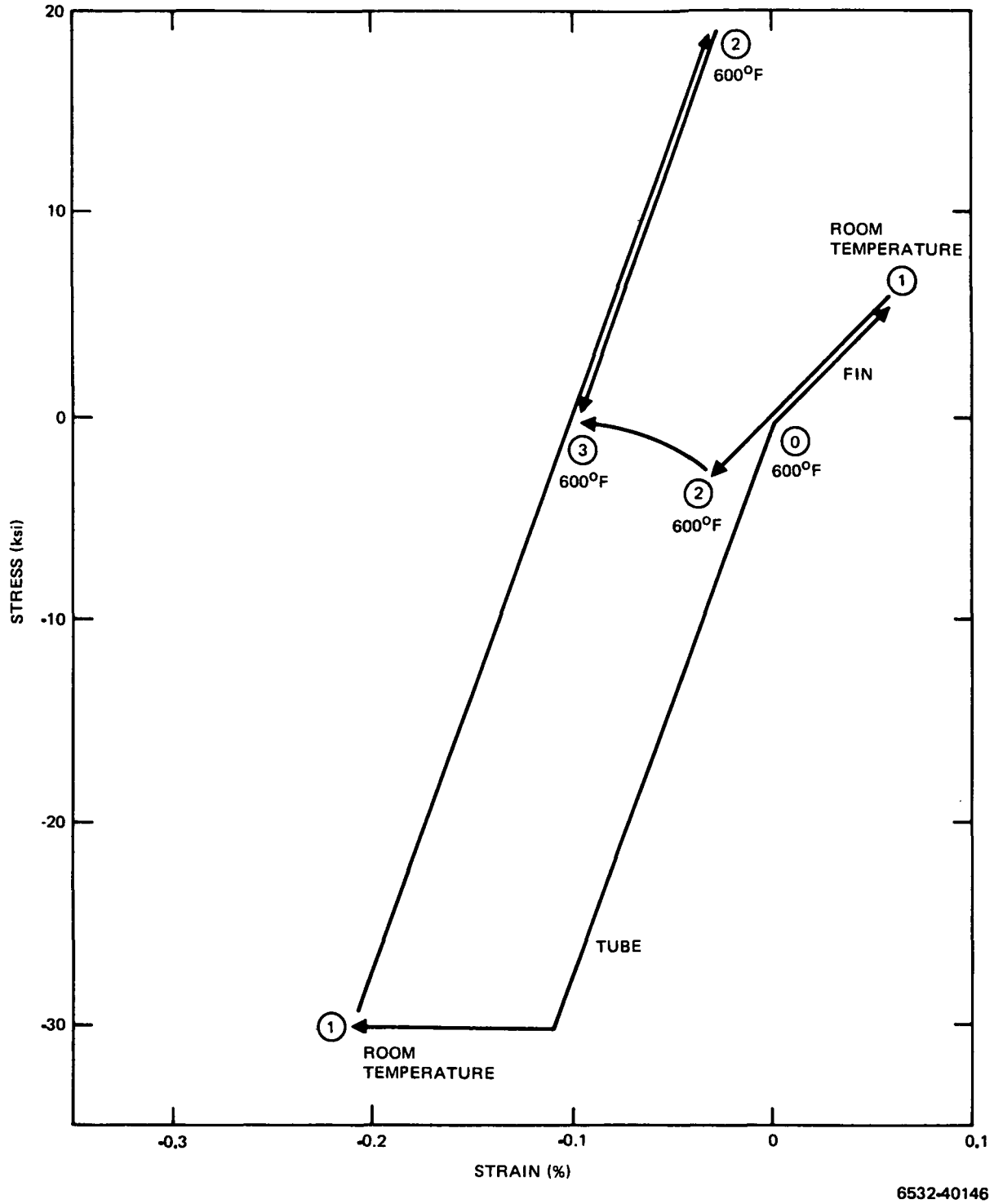

Figure 57. Thermal Cycle

As cooling begins, the strain is elastic; but at about 270°F, the tube enters the plastic range and continues to strain without increased stress to room temperature (Points 1 on the curve). The tube has undergone 0.10% plastic strain but the fin is still elastic.

On reheat from room temperature to the 600°F operating temperature, (Point 1 to Point 2), the stresses are relieved elastically and a new position is reached about 0.03% shorter than the original position. Note that the aluminum and stainless have opposing forces at 600°F and that the strains have not followed a line of plasticity. With sustained 600°F conditions, the aluminum tends to relax or anneal and conforms to the stainless by virtue of 0.10% strain. Since the stainless does not relax appreciably at 600°F and has not entered the plastic range of positive strain, it unloads elastically to the -0.1% strain Point 3. Now, both materials have undergone a 0.10% permanent strain in the cycle, the tube during the cooling and the fin in reheating. Both materials are of equal length and if the bond were broken, would not assume a new length. This represents a new starting point for subsequent thermal cycles but is 0.10% shorter than the previous starting point. Each repeat of this cycle would produce an additional 0.10% strain and with sufficient cycles, rupture would occur. Therefore, the assembly was shown to encounter thermal ratcheting and was not satisfactory.

Stresses related to the operationally induced circumferential gradients were evaluated at 48 θ values (Table 27). At any cross section, stresses are

$$\sigma = E\alpha(T_{avg} - T)$$

where

σ = axial stress (normal to cross section)

T_{avg} = average temperature or cross section

T = temperature at any circumferential location

α = coefficient of expansion

E = modulus of elasticity.

TABLE 27

48 θ STRESSES, ALUMINUM FIN

Location	T_{hot} (°F)	T_{cold} (°F)	T_{avg} (°F)	α (in./in./°F)	E (psi x 10^{-6})	σ_{max} (psi)	σ_{min} (psi)	F_{ty} (psi)
Top of cone	588	578	585	13.4	6	570	-285	1600
Mid-cone	540	520	533	13.4	6	1050	-525	1700
Mid-cylinder	465	435	455	13.2	7	1850	-925	2200

Note that the temperature distribution would be sufficiently complex to create both tension and compression on the same cross section. Relaxation would be at a variable rate circumferentially and axially (axial gradient is ≈135° F, circumferential gradient is 10 to 30° F). The stress state of the radiator would be impossible to predict, evaluate or duplicate in test. It was concluded that the fin material would be distorted ("oil canned") out of its plane, resulting in loss of structural capability for launch loads. There would be no way to predict the non-uniform axial strains and, consequently, no way to predict the out-of-plane deformations. An alternate material combination was necessary.

As cooling from a stress-free temperature to room temperature would generate tension in the aluminum and compression in the steel, the stresses over the cross section produce forces of equal and opposite magnitude. It can be seen, then, that if the forces are not concentric, there will be a couple whose magnitude depends on the degree of eccentricity of the forces, the relative coefficients of thermal expansion, the material areas, and the change in temperature. If these parameters are constant over the length of the panel, it will bow in a circular arc based on the relationship

$$\frac{M}{EI} = \frac{1}{R}$$

where

M = moment in cross section

E = equivalent modulus of elasticity

I = moment of inertia

R = radius of curvature.

The asymmetric configuration shown in Figure 58 was evaluated and found that it would bow to a 325-in. radius. Incorporating the asymmetric panels into the radiator structure would have introduced potential damaging forces on the panel splices and rings.

Several alternate designs were proposed to limit the bowing, all of which were aimed at eliminating the eccentricity. The resulting configuration, shown in Figure 58, was a symmetric cross section with as much aluminum on the inner surface as was required on the outer surface for meteoroid protection.

Launch capability is based on structural capacity compared to loads of Table 26. The structural radiator is composed of panels, each containing a tube, armor, fin and splice. The sum of these component strengths is the total for the panel. The classical relationships of strengths hold:

$$P_{cr_c} = \frac{\pi^2 EI}{L^2}$$

where

E = effective modulus of elasticity
I = moment of inertia
L = column length between rings
P_{cr_c} = load capacity of column.

This relationship applies to the tube/armor and the splice.

The fin strength is from the following:

$$P_{cr_f} = \frac{K, c, \pi^2 E A_f}{12\,(1-\mu^2)} \left(\frac{t}{6}\right)^2$$

where

K_c = buckling constant
μ = poissons ratio
t = fin thickness
b = fin effective width
A_f = fin effective area.

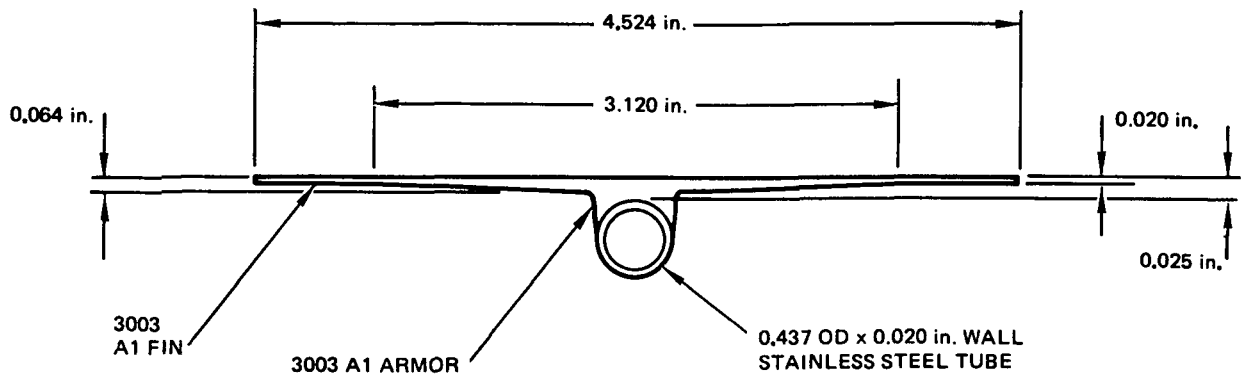

a. ASYMMETRIC CROSS SECTION

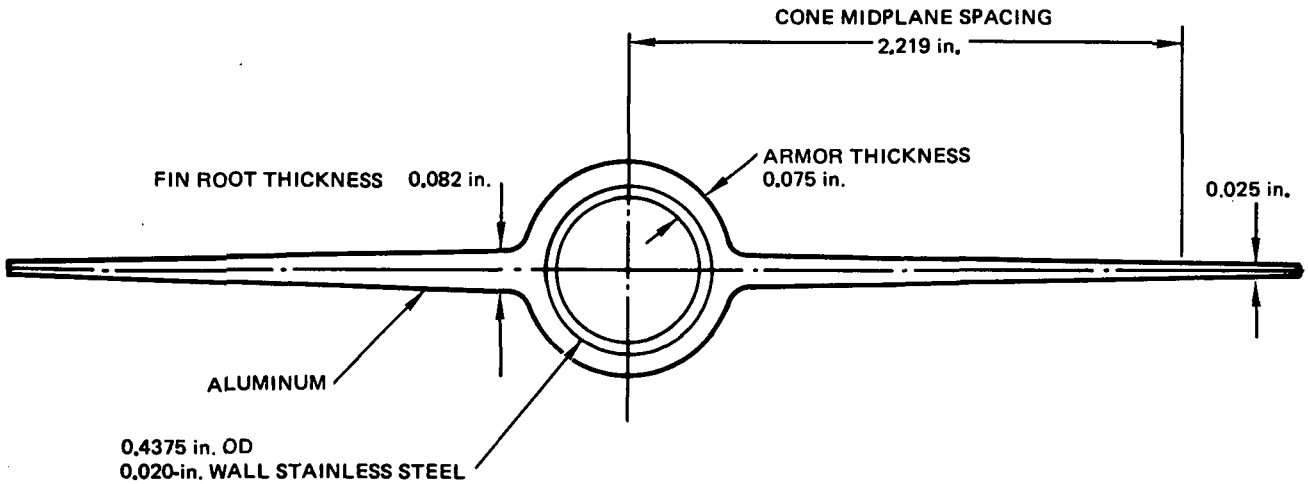

b. SYMMETRIC CROSS SECTION

6532-40147

Figure 58. Fin/Tube Cross Section

Figure 59 shows the aluminum radiator capacity compared to the maximum dynamic loading for all stations. There was more than adequate strength.

The mechanical capacity of the Lockalloy configuration exceeded the launch loads by more than 2.0 at all stations.

With beryllium as one of its constituent materials, it is natural to be concerned about the crack propagation of Lockalloy. Beryllium was notorious for its characteristic cracking at riveted joints and for its high notch sensitivity: Two basic reasons for the development of Lockalloy. The combination of ductile aluminum with beryllium was to provide a material which possessed the best properties of both. The notch sensitivity and resistance to crack propagation is significantly improved over that of beryllium but not as good as that of aluminum. It can be shown with the fracture mechanics relationships that Lockalloy 38 will not have crack propagation from rivet to rivet with the induced loads and the anticipated rivet spacing.

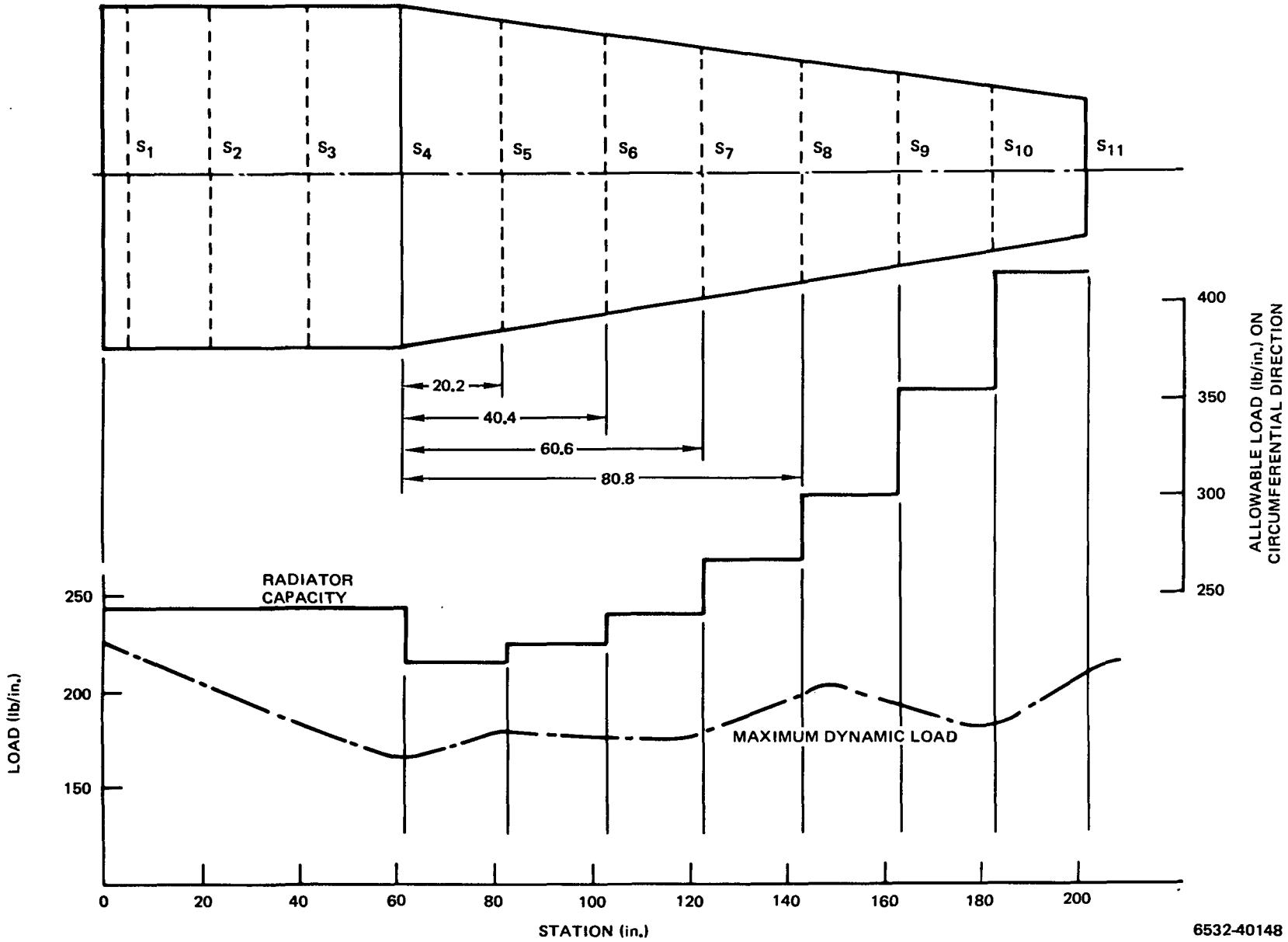

Figure 59. Load versus Capacity

VII. LIQUID METAL SYSTEMS

This section describes the primary and secondary loop NaK piping, volume accumulators and expansion joints.

A. PIPING

Figure 60 shows the system layout, emphasizing the primary loop, and Figure 61 emphasizes the secondary loop.

For the piping thermal analysis, the structural criteria of the Power Piping Code ANSI B31. 1. 0, and Section III Class 1 High Temperature Code, Case 1331. 5 of ASME BPVC Section III were considered for application to the piping systems.

Initially, the thermal analysis was performed on the primary piping system of the reference conceptual design layout. It investigated the reference design and also explored alternate design configurations. The analysis was limited to the primary piping system from the reactor to the 16 thermoelectric converters. The stress analysis was performed under idealized startup conditions (Figure 62) because this transient cycle caused the most severe differential thermal movements between the body and the piping.

After the reference design concept became finalized, a more detailed thermal stress analysis was performed on the piping systems. The primary load analysis is based on the system of loadings that would occur in space. No gravitational, seismic, support or component weight forces were considered, therefore; only the pressure thrust of the expansion joint was taken into account.

The stress analysis was performed per the MEL-21 computer program. All stress levels that were calculated at elbows and nozzles are directly related to the allowable stress range S_A per the Power Piping Code B31. 1. 0. The bulk of the stress analysis was associated with the primary loop and dealt with thermally induced stresses. Pressure (35 psi) had induced negligible stresses and was not given significant effort during the primary phase.

The coefficients of expansion of the stainless tubes and the radiator structure were very similar; and since the gradients were relatively low, the secondary system was also a low priority component during the preliminary phase.

PAGE INTENTIONALLY LEFT BLANK

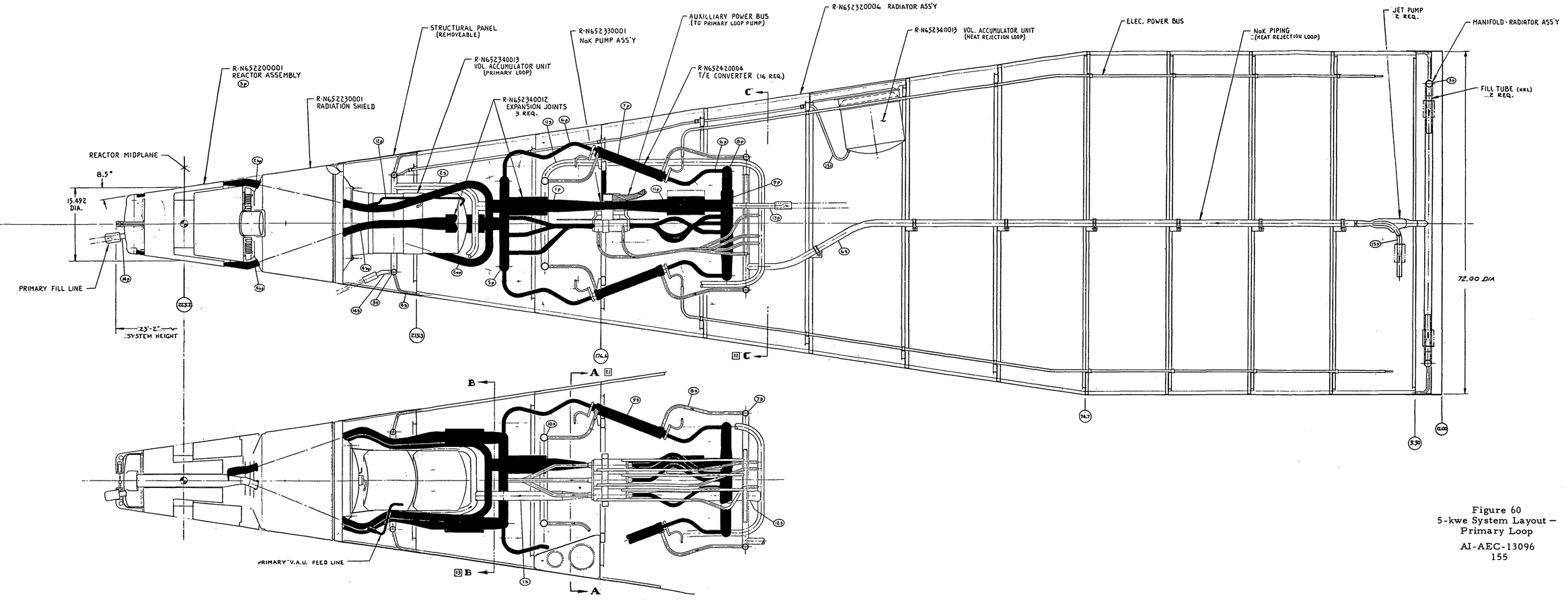

Figure 60
5-kwe System Layout –
Primary Loop

PAGE MISSING FROM AVAILABLE VERSION

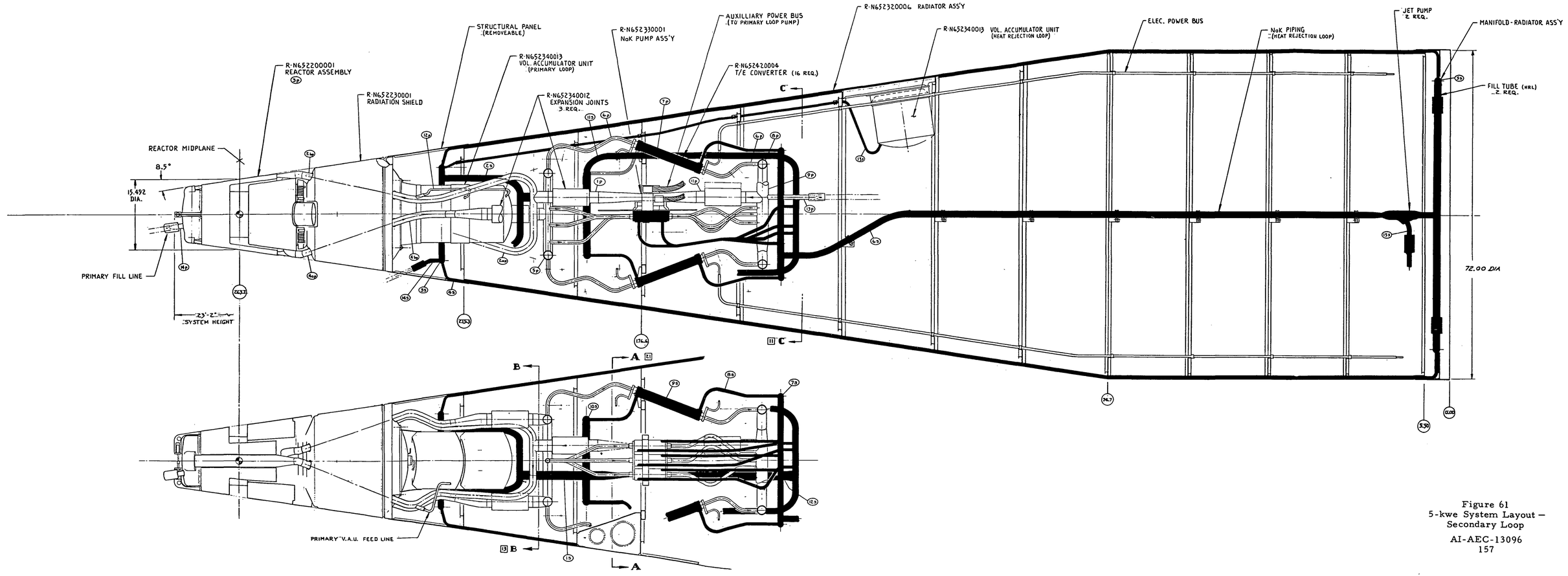

Figure 61
5-kwe System Layout –
Secondary Loop

AI-AEC-13096
157

PAGE MISSING FROM AVAILABLE VERSION

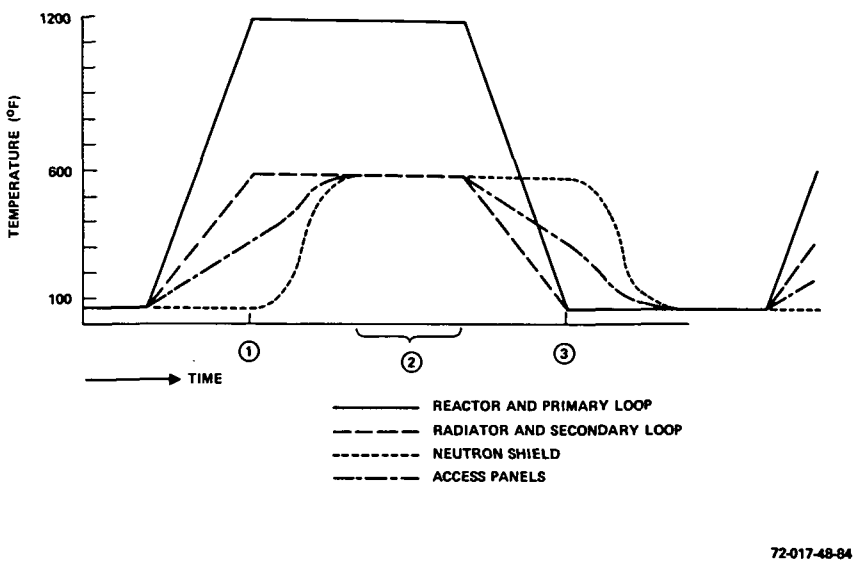

Figure 62. Idealized Transient Temperatures

The primary system, however, would reach high (1200°F) temperature while the structure to which it was attached would range from room temperature to 750° and would not be isothermal. Thus, there would be a relatively large differential in the growth of the tubes with respect to its supporting structure.

The basic sources of stresses in the piping system arise from the restraint of isothermal expansion, from thermal gradients within a component and the bimetallic expansion mismatch:

$$\sigma = E(\alpha_1 \Delta T_1 - \alpha_2 \Delta T_2) \quad .$$

In the primary loop, the differential in growth of the piping between the reactor and the support point station 176 is shown on Figure 63 for the three stages: (1) end of startup transient, (2) steady-state, and (3) end of shutdown of Figure 62.

The reference design, therefore, incorporated four bellows expansion joints. The bellows material is Inconel 718 with a 125,000 psi capability at 1200°F. The bellows are preloaded in tension to minimize the travel between startup and shutdown. Figure 64 shows the stress levels and joint loads in the primary

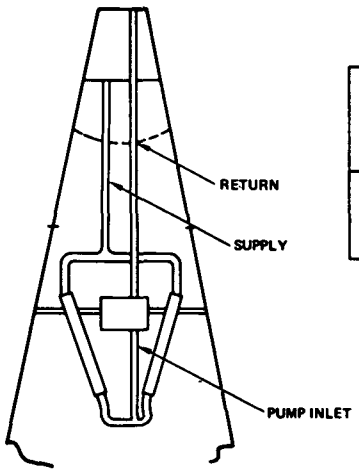

LINE	END OF LOOP TRANSIENT (STARTUP) (in.)	STEADY-STATE OPERATION (in.)	END OF LOOP TRANSIENT (SHUTDOWN) (in.)
RETURN	-0.499	-0.355	+0.144
SUPPLY	-0.589	-0.445	+0.144
PUMP INLET	-0.110	-0.110	0

72-017-48-85A

Figure 63. Primary Piping Expansions

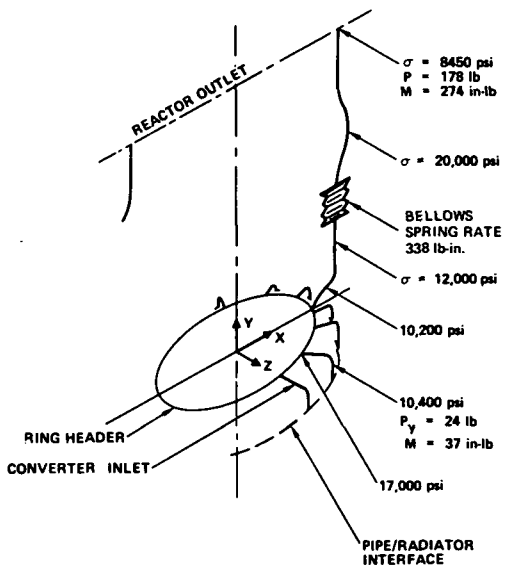

72-017-48-94A

Figure 64. Type 316 SS Pipe with Bellows

loop with a 338 lb/in. spring rate bellows. These stresses would be further reduced with a lower spring rate bellows and all stresses would be at acceptable levels.

B. EXPANSION JOINT UNITS

Four identical expansion joint units (EJU's) are utilized in the primary coolant piping loop to accommodate the expansion or contraction of the piping with respect to the components and supporting structures during the various operational phases. No expansion joint units are used in the secondary coolant piping loop inasmuch as the relatively small differential expansions of secondary coolant piping can be accommodated by the bends.

The general design requirements for the EJU's were:

1) The EJU boundary loading reaction forces imparted to the system piping shall not cause the piping stresses to exceed allowable magnitudes.

2) The EJU length and weight shall be minimized within the objectives of meeting piping loading and bellows stress limitations and EJU reliability goals.

3) To maximize the EJU reliability, the design shall utilize double containment of the NaK within the EJU.

4) The flow pressure drop through the EJU shall not exceed the flow pressure drop through an equivalent straight length of piping by more than 50%.

5) The material for the EJU detail parts shall be compatible with NaK and shall be weldable to the Type 316 SS piping of the 5-kwe system.

6) The EJU shall be designed to operate for 5 years at the pressures and temperatures of the NaK coolant piping system, after being subjected to the acceptance test and system launch conditions.

7) A common design shall be used for all EJU's in the system, if possible.

The prototype EJU was designed to be installed in four locations of the 5-kwe system primary coolant loop piping, as shown in Figure 65.

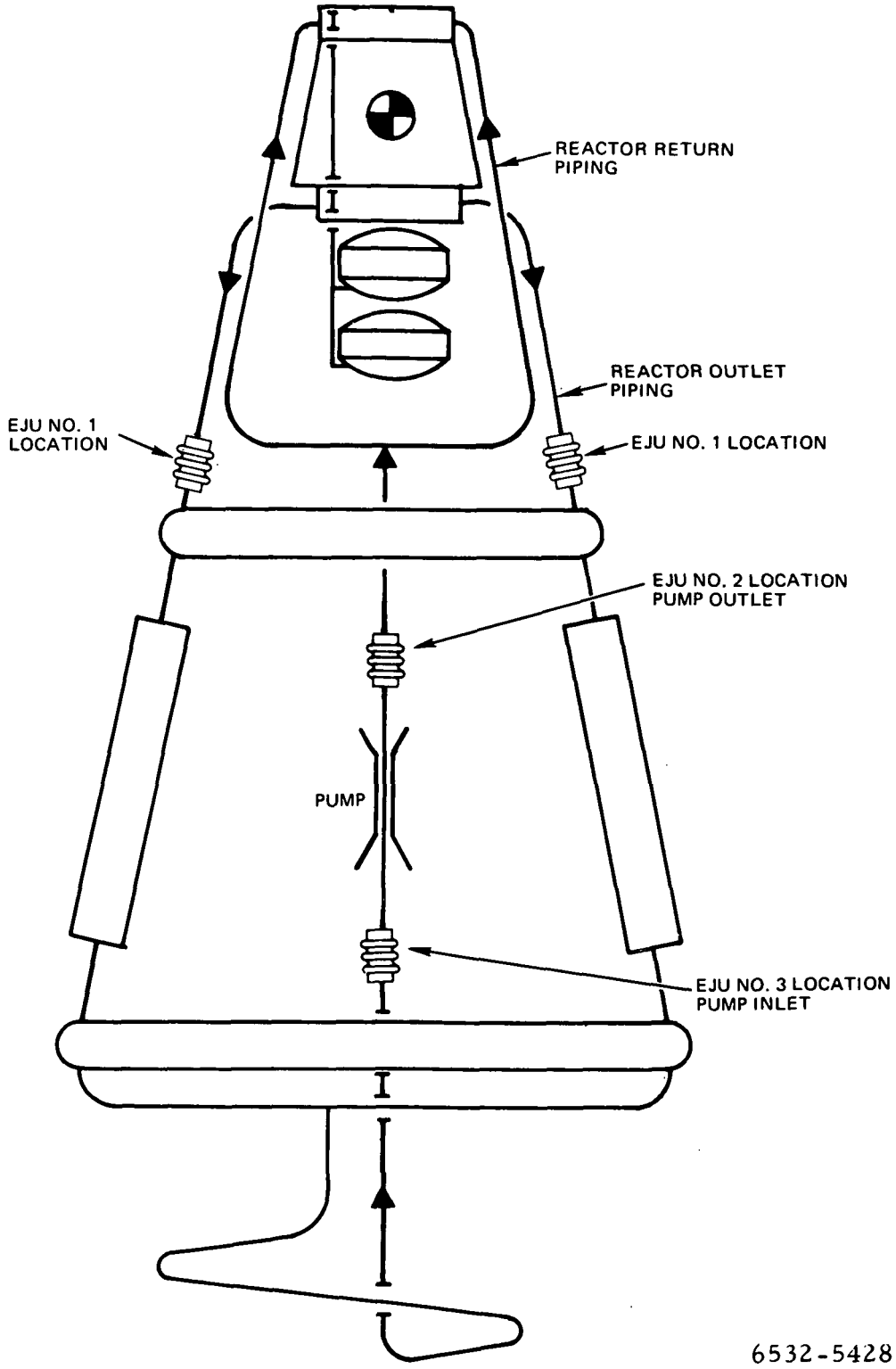

Figure 65. Expansion Joint Unit Locations for the 5-kwe Reactor Thermoelectric System

Figure 66 shows the layout of the prototype EJU. The EJU replaces a short section of the piping between rigid piping mounting to allow essentially free axial movement of the two pipe ends within the EJU. Hydroformed metal bellows provide a flexible closure between these pipe ends. The bellows spring rate and deflection determine the end reaction and, consequently, the stress levels throughout the piping loop. The bellows in contact with the loop NaK is the primary containment bellows. A second unit, called the secondary containment bellows, serves as a backup containment barrier in the event of NaK leakage through the primary containment bellows, and allows continued uninterrupted operation of the system after such an occurrence. These two bellows are identical and are placed in tandem to minimize the perturbation of the straight-through NaK flow. The bellows are a nesting-formed type and are fabricated from a single ply of 0.010-in.-thick Inconel 718.

The performance requirements for the EJU in the prototype 5-kwe system are summarized in Table 28. These requirements are based on a 50°F design margin added to the maximum expected piping temperature.

TABLE 28

EJU PERFORMANCE REQUIREMENTS

Operational Phase	Condition				
	Maximum NaK Temperature (°F)	Maximum NaK Pressure (psia)	Minimum EJU End Deflection* (in.)	Minimum EJU Offset (in.)	Maximum Axial† Load (lb)
Launch	70	46.1	0	±0.040	-
Startup Operation	1235	36.0	0.864 Contraction	±0.040	<|223|
Long-Term Operation	1300	32.0	0.766 Contraction	±0.040	<|223|
Reactor Shut Down	70	4.0	0.394 Extension	±0.040	<|223|

*Change in EJU length from initial installed length includes 0.250 in. over travel margin.

†End reaction force generated by the EJU.

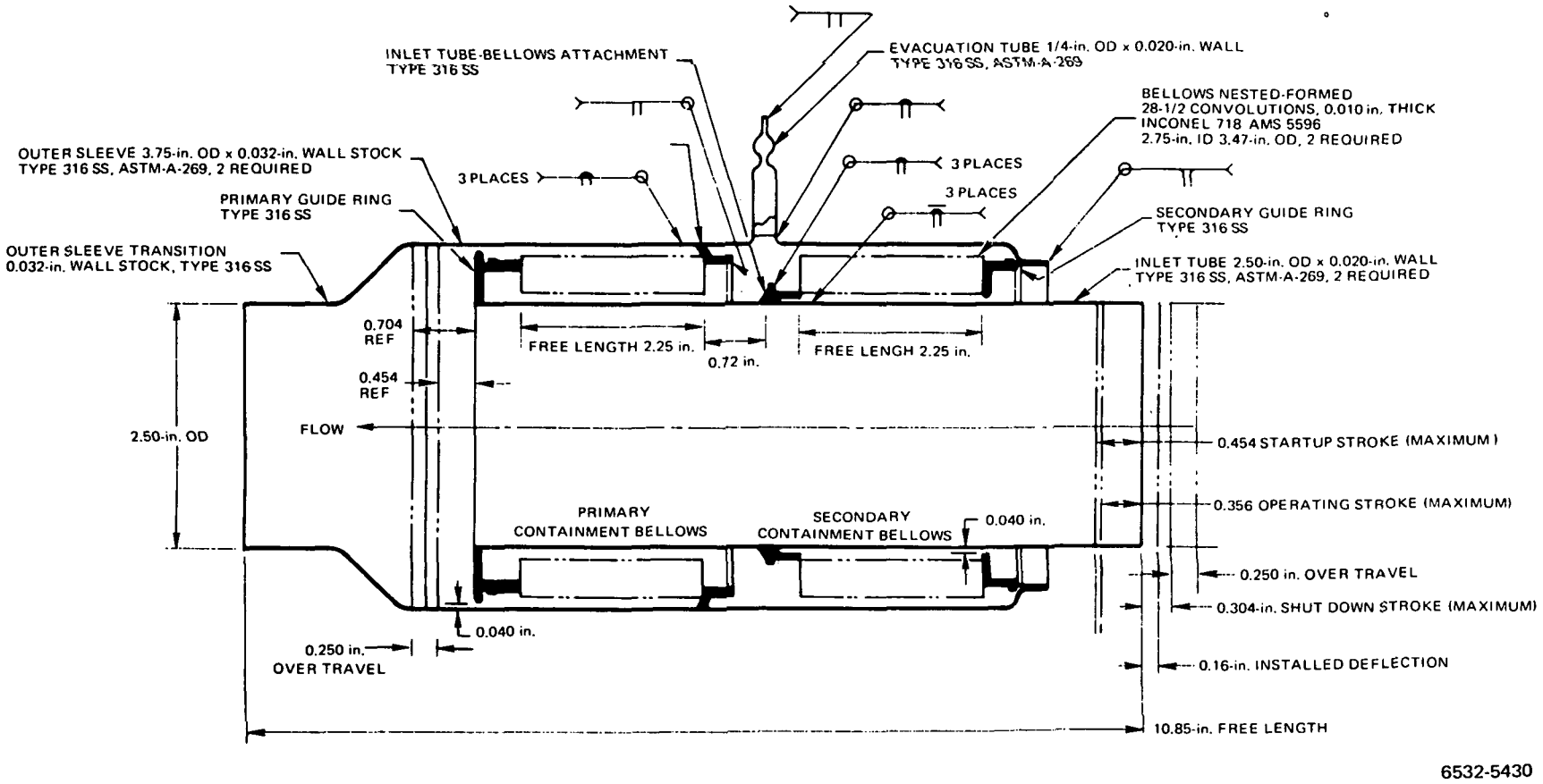

Figure 66. Layout of Prototype EJU

The prototype EJU design conforms to the following requirements:

1) Bellows Stress. The design stress of the bellows, under the startup condition, shall not exceed two-thirds of the minimum specified material yield strength.

2) Proof Pressure. When held at its free length, the EJU shall withstand internal pressure of 10^{-3} torr to 55 psig (with respect to test environment) with no permanent distortion or material yielding.

3) Burst Pressure. When held at its free length, the EJU shall withstand internal pressure of 92 psig without rupture of, or leakage through, the primary containment.

4) Buckling Pressure. Instability buckling of bellows shall not occur at an internal pressure of less than 70 psig.

5) Bellows Natural Frequency. The natural frequency of the bellows, without damping, shall be greater than 35 Hz.

The calculated performance of the EJU at each system location under the various 5-kwe system operational modes is shown in Table 29. The factors listed in the table are defined as follows:

1) End deflection (§) = Change in EJU length from initial installed length.

2) Bellows deflection = Bellows compression (+) or extension (-) from its (EJU) free length.

3) Bellows spring rate (k) - Combined spring rate of primary and secondary bellows at temperature noted.

4) Bellows spring force (K §) - Force required to compress the EJU from its free length.

5) Hydraulic force = Force due to the internal NaK pressure action on bellows and piping net area.

6) Net reaction load = Sum of bellows spring force and hydraulic force.

TABLE 29

EJU REACTION LOAD ON THE PIPING

System Condition	EJU Temperature (°F)	End Deflection (in.)	Bellows Deflection (in.)	Bellows Spring Rate (lb/in.)	Bellows Spring Force (lb/in.)	Internal NaK Pressure (psig)	Hydraulic Force (lb)	Net Reaction Load on Piping (lb)	Allowable Piping Load (lb)	Margin of Safety
Primary Outlet EJU										
Installation	70	0.0	-0.16	222	-35.5	0.0	0.0	-35.5*	-	-
Startup	1235	+0.614	+0.454	179	+81.3	36.0	101.0	182.3	223	+0.22
Operation	1300	+0.516	+0.356	176	+62.6	32.0	90.0	152.6	223	+0.46
Shutdown	70	-0.144	-0.304	222	-67.5	4.0	11.5	-56.0*	223	+3.0
Primary Return Piping										
Pump Outlet (Installation Deflection is -0.16 in.)										
Installation	70	0.0	-0.16	222	-35.5	0.0	0.0	-35.5*	-	-
Startup	1148	+0.541	+0.381	184	+70	36.0	101.0	171.0	262	+0.53
Operation	1205	+0.447	+0.287	181	+52	32.0	90.0	142.0	262	+0.85
Shutdown	70	-0.144	-0.304	222	-67.5	4.0	11.5	-56.0*	262	+3.7
Pump Inlet (Installation Deflection is 0.0 in.)										
Installation	70	0.0	0.0	222	0.0	0.0	0.0	0.0	-	-
Startup	1148	+0.12	+0.12	184	+22.1	36.0	101.0	122.1	~200	+0.64
Operation	1205	+0.13	+0.13	181	+23.5	32.0	90.0	113.5	~200	+0.76
Shutdown	70	0.0	0.0	222	0.0	4.0	11.5	11.5	~200	+16.5

*(-) Denotes tension forces imposed on piping.

7) Allowable piping load = Max. compression (+) or tensile load (-) on piping to limit piping stress within allowable values.

8) Margin of safety = $\frac{\text{Allowable load-actual load}}{\text{actual load}}$

It is seen from Table 29 that the EJU's provide a minimum piping load margin of safety of + 0.22.

Plans for fabrication of six EJU's for testing were being formulated at the time of program closeout.

C. VOLUME ACCUMULATOR UNITS

Three identical volume accumulator units (VAU's) are used in the 5-kwe system; two in the primary coolant system and one in the secondary coolant system. The VAU's are utilized to:

1) Accommodate NaK coolant thermal expansion and contraction during the 5-kwe system startup, operation, shutdown, and storage.

2) Provide void-free NaK coolant systems.

3) Provide pressure regulation of the NaK coolant systems.

The general design requirements for the VAU's were:

1) The weight of the unit shall be minimized within the objectives of meeting bellows stress limitations, volumetric capacity and pressure regulation requirements, and VAU reliability goals.

2) To maximize reliability, the design shall utilize double containment of NaK within the VAU.

3) The material for detail parts shall be compatible with NaK and shall be weldable to the type 316 SS piping of the 5-kwe system.

4) The VAU shall be designed to operate with no maintenance for 5 years at the operating conditions of the 5-kwe system, after being subjected to acceptance test and system launch conditions.

5) A common design shall be used for all VAU's in the 5-kwe system, if possible.

The prototype VAU was designed to be installed in three locations in the 5-kwe system. Two of these locations are in the primary coolant loop and the other is in the secondary coolant loop.

On the basis of the results of trade studies and bellows evaluation, it was determined that the prototype VAU would utilize two Inconel 718, nested-formed bellows in redundant arrangement, with the secondary containment volume evacuated, and the bellows force augmented by gas charge pressurization.

Figure 67 shows a design layout of the prototype VAU. All parts, except the NaK inlet tube, are fabricated from Inconel 718. The NaK inlet tube is Type 316 SS. There are three cavities in the VAU: the primary containment cavity, the secondary containment cavity, and the secondary bellows cavity. The primary containment cavity, which is formed by the NaK dome, primary containment bellows and the movable head, accommodates the NaK overflow volume from the coolant loop. The secondary containment cavity, which is formed by the primary and secondary containment bellows and the shell, is evacuated and provides secondary containment of the NaK in the event of failure of the primary containment bellows. The secondary bellows cavity, which is formed by the movable head, secondary containment bellows and gas dome, is charged with inert gas and provides the gas pressure force needed to augment the bellows spring force to obtain the desired pressure regulation of the coolant loop.

The performance requirements for the prototype VAU were:

1) NaK Volume Capacity. The VAU at 750° F shall be capable of accommodating a NaK volume increase of 337 $in.^3$ above the initial volume.

2) NaK Pressure. The combined action of the gas charge and the bellows force shall impose the following pressures on the NaK:

   a) Initial Pressure - At 100° F VAU temperature on the residual volume* of NaK in the VAU shall be 4 psia minimum.

*The NaK volume which is required to fill the primary containment cavity at 100° F with the movable head positioned 0.12 in. from the NaK dome.

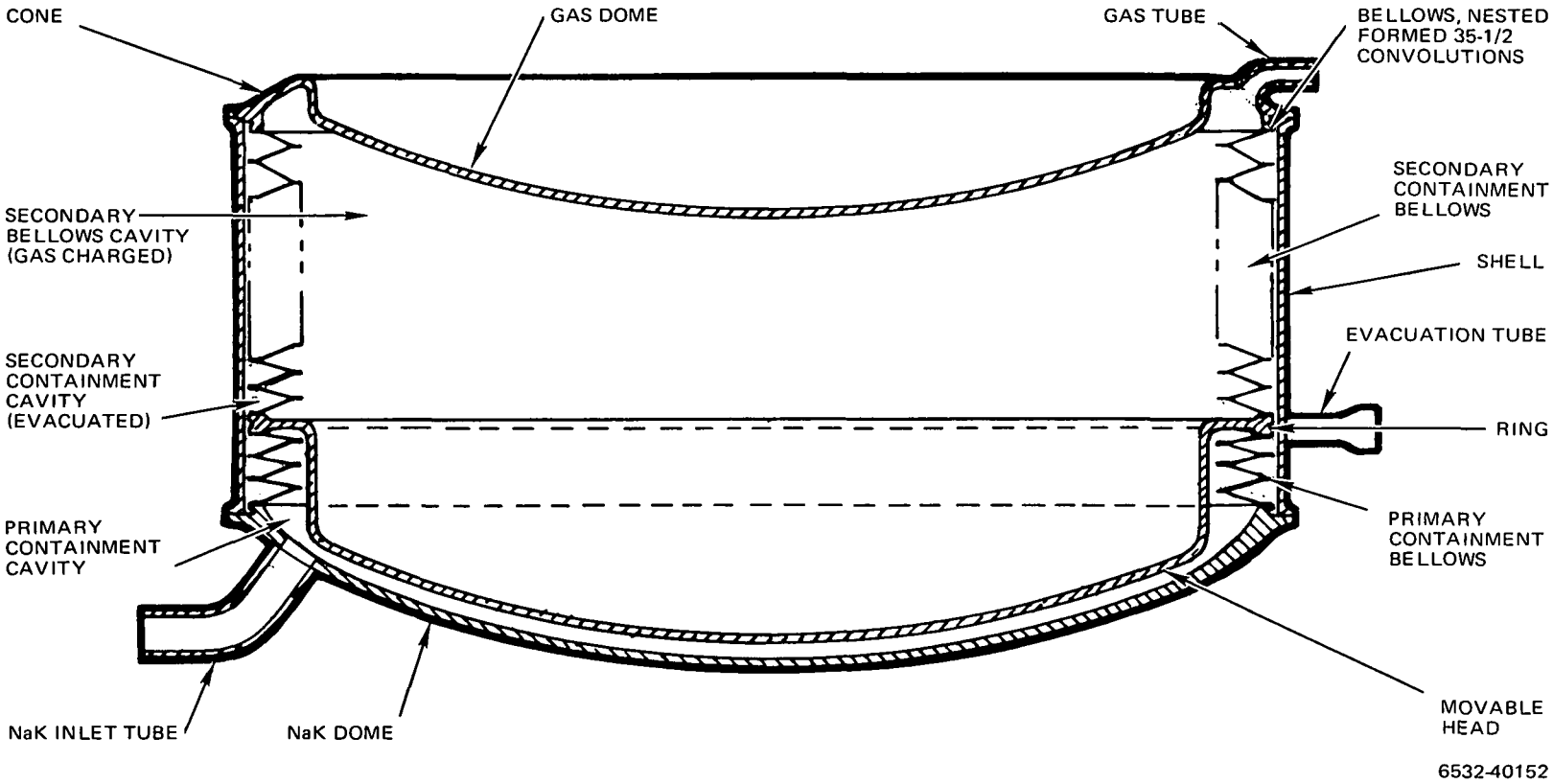

Figure 67. Prototype Volume Accumulator Unit

b) Operating Pressure - Shall be 28.0 psia maximum at 750° F VAU temperature.

c) Failed Primary Bellows - In the event of primary bellows failure, the VAU shall maintain 6 psia minimum pressure on 236 $in.^3$ plus the residual volume of NaK in the primary and secondary containment cavities. This pressure shall be maintained at 600° F VAU temperature.

3) Useful Life. The VAU shall have an operational life of 5 years after being exposed to storage environment for up to 2 years, and then to preflight through launch environment, with no maintenance.

4) Reliability. The reliability of the VAU for 5 years of operation without causing failure of the 5-kwe system shall be not less than 0.997.

The following design criteria were applied to the prototype VAU design:

1) Stress Limits. The design stress in the bellows at a NaK pressure of 36 psia pressure and 337 $in.^3$ volume change shall not exceed two-thirds of the minimum specified material yield stress.

2) Proof Pressure. The VAU at 750° F shall withstand NaK proof pressure of 10^{-3} torr to 43.2 without any permanent distortion or material yielding.

3) Burst Pressure. The VAU at 750° F shall withstand NaK burst pressure of 72 psia without rupture of the primary containment.

4) Bellows Natural Frequency. The axial natural frequency of the bellows, undamped except by atmospheric gas, shall not be less than 35 Hz.

The prototype VAU has a bellows natural frequency of 48 Hz. Each unit weighs 23.2 lb. Reliability of the prototype VAU has been calculated to be 0.99999 to 0.99998 for a 5-year operation; other performance characteristics are shown in Table 30.

Plans for fabrication of bellows capsules and prototype VAU's for testing were being formulated at the time of closeout of the 5-kwe Reactor Thermoelectric System Program.

TABLE 30

PERFORMANCE CHARACTERISTICS OF THE PROTOTYPE VAU

VAU Condition	Total NaK Volume* ($in.^3$)	NaK Pressure† (psia)		VAU Temperature (°F)	Average NaK Bulk Temperature (F°)
		Normal	Failed Primary Bellows		
Primary Loop VAU					
Over Design	344	26.9	21.4	750	-
	344	26.1	19.9	660	-
	337	26.5	21.1	750	1238
Operation	319	25.5	20.3	750	
	319	23.8	18.8	660	1188
	300	24.5	19.5	750	
	300	22.8	18.0	660	1138
Secondary Loop VAU					
Over Design	344	23.9	18.7	600	-
	344	22.4	17.6	525	-
	236	18.9	14.7	600	
	236	17.6	13.7	525	590
	190	17.1	13.2	600	
Operation	190	15.9	12.1	525	540
	180	16.7	12.8	600	
	180	15.5	11.8	525	520

*Does not include residual volume.

†Based on gas charge fill pressure of 7.05 psia at 100°F, which provides an initial NaK pressure of 4.05 psia at V = 0.

§In the primary loop VAU's, failed primary bellows is assumed in both VAU's.

VIII. RADIATION SHIELD

A. NUCLEAR ASPECTS

With a reactor source, shielding is required to reduce the radiation levels at the payload. The reactor emits two types of radiation that must be attenuated by the shield: neutrons and gamma rays. Neutrons are most effectively attentuated by light hydrogeneous materials. For gamma-ray attenuation, high density metals are the most efficient materials. The reactor shield is thus composed of a combination of a high density material and hydrogenous material.

Because shielding represents a significant fraction of the total power system weight, careful system design is required to minimize shield weight. The shield weight is a function of many variables, some of which are influenced by the system design. The primary variables of importance are the separation distance between the reactor and the dose plane, and the cone half-angle that must be shielded. The shield weight can be minimized by increasing the separation distance, and by reducing the shield cone half-angle. The allowable radiation level at the dose plane is also a key variable.

The 5-year dose limits, averaged over the dose plane, were set at the following levels:

Neutrons	10^{12} nvt ($E_n < 0.1$) Mev)
Gamma rays	10^{6} rad

These criteria are based on mid-1960 data. More recent data indicate that a factor of ten higher (or 10^{13} nvt and 10^{7} rads) dose criteria can be used for conventional aerospace electronic components that have been carefully selected. The lower values were used for design of the 5-kwe Reactor Thermoelectric System shield to make the system compatible with electronic components that have not been designed for a radiation environment. Use of the higher dose criteria, if the payload electronics permit, would result in a significant weight reduction. (The gamma-ray dose criterion of 10^{7} rad eliminates the need for a gamma shield.)

1. Shield Materials

This section describes the selection of the neutron and gamma-ray shield materials.

Lithium hydride (LiH) was selected for the neutron shield, since it has proved to be a very effective neutron shield material. It has a low density (0.72 gm/cc), and a very high effective neutron attenuation coefficient which has been confirmed experimentally. It also has a high melting point (1270° F) and a very low dissociation pressure.

The weight of the gamma-ray shield represents a significant fraction of the total shield weight. Consequently, careful selection of a gamma-ray shield material may result in significant weight savings. As the gamma-ray shield is placed immediately below the reactor core, the secondary gamma-ray generation in the shield due to core leakage neutrons is a significant factor. In addition, heat generation in the gamma-ray shield is important.

Various high density materials were considered: lead, Ta - 10 W, U - 8 Mo, tungsten alloy (95 wt % W), stainless steel, and borated stainless steel. Lead was rejected because of its very low melting point (620° F). Ta - 10 W was rejected because of its excessive weight resulting from the large capture gamma ray production in tantalum. A U - 8 Mo shield (using depleted uranium, 0.2% U^{235}) resulted in a low shield weight. However, it was rejected because of its high internal heating (due to fast fission), and its instability at high temperatures.

One-dimensional calculations were performed to compare tungsten alloy, stainless steel, borated steel (with natural and B^{10} enriched B_4C) and tungsten alloy with a thin sheet of borated steel between it and the LiH shield. The relative shield weights are given in Table 31. Further two-dimensional perturbation theory calculations using the DOT code were performed to shape the gamma-ray shield by varying its thickness and radius. Relative weights obtained from two-dimensional analysis are also presented in the table for tungsten alloy and borated steel (using natural boron). Since the shield weight using borated steel is less than that of tungsten alloy, it was selected as the reference shield material, with tungsten alloy as an alternate.

TABLE 31

GAMMA-RAY SHIELD MATERIALS COMPARISON

Shield Materials	Relative Weight	
	One-Dimensional Analysis	Two-Dimensional Analysis with Shaping
Tungsten Alloy (95 wt % W)	1.00	1.00
Stainless Steel	1.02	-
Stainless Steel + 2% B_4C	0.72	0.88
Stainless Steel + 2% $B_4^{10}C$	0.70	-
Tungsten + Stainless Steel + 2% $B_4^{10}C$	0.75	-

2. Radiation Sources

There are three primary sources of radiation at the dose plane: core, radioactive coolant, and scattering sources. The last effect occurs when neutrons and/or gamma rays scatter from materials external to the core and reach the dose plane.

The reactor core is a source of both neutrons and gamma rays. The core neutron source includes the fission neutrons, delayed neutrons and photo-neutrons. The core gamma-ray source includes prompt-fission gamma rays, fission product gamma rays, gamma rays from neutron capture (i.e., non-fission), gamma rays from neutron inelastic scattering, and decay gamma rays from neutron-activated materials in the core. In addition, gamma rays resulting from neutrons captured outside the core by the vessel and shield, for example, must be considered. Use of the DOT code with a coupled n,γ library permits these neutron and gamma-ray sources to be accounted for in a single calculation.

The use of NaK as a reactor coolant results in the circulation of radio-active isotopes in the primary coolant loop. These radioisotopes are produced by neutron interactions with the coolant material in the reactor. The most

important activation reactions in NaK involve the capture of neutrons by Na^{23} (100% isotopic abundance) to produce Na^{24}, and by K^{41} (6.91% isotopic abundance in potassium) to produce K^{42}. Na^{24} decays by beta emission with a half-life of 15.0 hr and emits one 2.75 MeV and one 1.37 MeV gamma ray per disintegration. K^{42} also decays by beta emission with a half-life of 12.4 hr, and emits a 1.52 MeV gamma ray in 18% of the disintegrations.

The radiation source level of the radioactive NaK coolant is much lower than that of the reactor core. However, in the 5-kwe Reactor Thermoelectric System design, a large fraction of the radioactive NaK loop is not shielded. Thus, the dose rate contribution from the radioactive NaK is a significant fraction ($\sim$ 20%) of the total gamma ray dose rate at the dose plane.

The NaK activity was obtained using the APC code (a buckling iteration version of ANISN). The NaK absorption in various locations is presented in Table 32. As the half-lives of both Na^{24} and K^{42} are much less than the reactor operating time and much greater than the NaK loop circulation time, the Na^{24} and K^{42} activities will reach an equilibrium level; i.e., for every absorption there will be one disintegration. The APC calculation indicated that there are 0.00331 absorptions in NaK per source neutron.[10] This corresponds to Na^{24} and K^{42} activities of 0.78 and 0.32 Ci/kwt, respectively.

Scatter sources become important only when the scattered dose rate is greater than the shielded direct dose rate. For unmanned systems, a shadow shield is used to minimize shield weight. Care must be taken not to place objects outside the shielded cone. The effect of neutron scattering from the radiator in a design in which the entire radiator is outside the shielded cone is discussed in a later section.

3. Effect of System on Shield Design

This section discusses the attenuation provided by the PCS equipment for both gamma rays and neutrons, the radiation level from the radioactive NaK coolant in the PCS and plumbing below the shield, the radiation level due to neutrons streaming through the shield penetrations, and the scatter dose rate effect if the radiator is located outside the shield cone.

TABLE 32

NaK ACTIVITY SOURCE

Source	Absorption per Source Neutron	Percent
Bottom Plenum	0.00031	9.4
Lower Grid Plate	0.00014	4.2
Core	0.00260	78.6
Upper Grid Plate	0.00007	2.1
Upper Plenum	0.00019	5.7
Total	0.00331*	100.0

*Normalized for $k_{eff} = 1.0$

a. Attenuation Provided by PCS

The attenuation provided by the PCS equipment is a very important consideration. The PCS equipment includes the thermoelectric modules, thermoelectric pumps, NaK accumulators, and the NaK coolant pipes below the shield.

The gamma-ray dose rate attenuation provided by the PCS equipment was calculated using three different methods: hand calculations, the QAD (ray tracing) code, and the DOT/SPACETRAN codes.

In the hand calculations, a single energy (2.0 MeV) gamma ray was used. The effect of holes in the PCS components was taken into account and the solid sections were homogenized.

In the case of the QAD code analysis, the gamma-ray leakage spectrum from the LiH shield was used as a source. The QAD code was used in R-Z geometry with quadratic surfaces used to simulate the PCS equipment. Eighteen energy groups were used in the analysis.

In the DOT/SPACETRAN analyses, the DOT code was used to simulate the PCS components in R-Z geometry. In this calculation, the thermoelectric modules were simulated by a series of stepped rings. The first step in the calculational sequence was a DOT code run on the reactor-shield system. The leakage from the bottom of the shield was used as input to a second DOT case, this one covering the PCS assembly. The leakage flux from the second DOT case was then fed to the SPACETRAN code. This last program then calculates the neutron flux and gamma-ray dose rate at various points on the dose plant (below the lower boundary of the DOT case).

Table 33 presents the attenuation provided by the PCS equipment for gamma rays. It may be seen that all three methods agree fairly well. Figure 68 presents the shield weight saving as a function of gamma-ray dose rate attenuation provided by the PCS equipment. The weight savings has been normalized to a factor of 3.0. If no credit were taken for the PCS attenuation for gamma rays, PCS attenuation factor = 1.0, the additional shield weight required would be about 200 lb. This illustrates the importance of including the gamma-ray attenuation provided by the PCS equipment in the analysis.

TABLE 33

PCS EQUIPMENT ATTENUATION FACTORS

Calculational Method	Attenuation Factor	
	Gamma Ray	Neutrons
Hand Calculation	3.0	1.7
QAD (ray tracing)	3.2	-
DOT/SPACETRAN	3.03	2.23

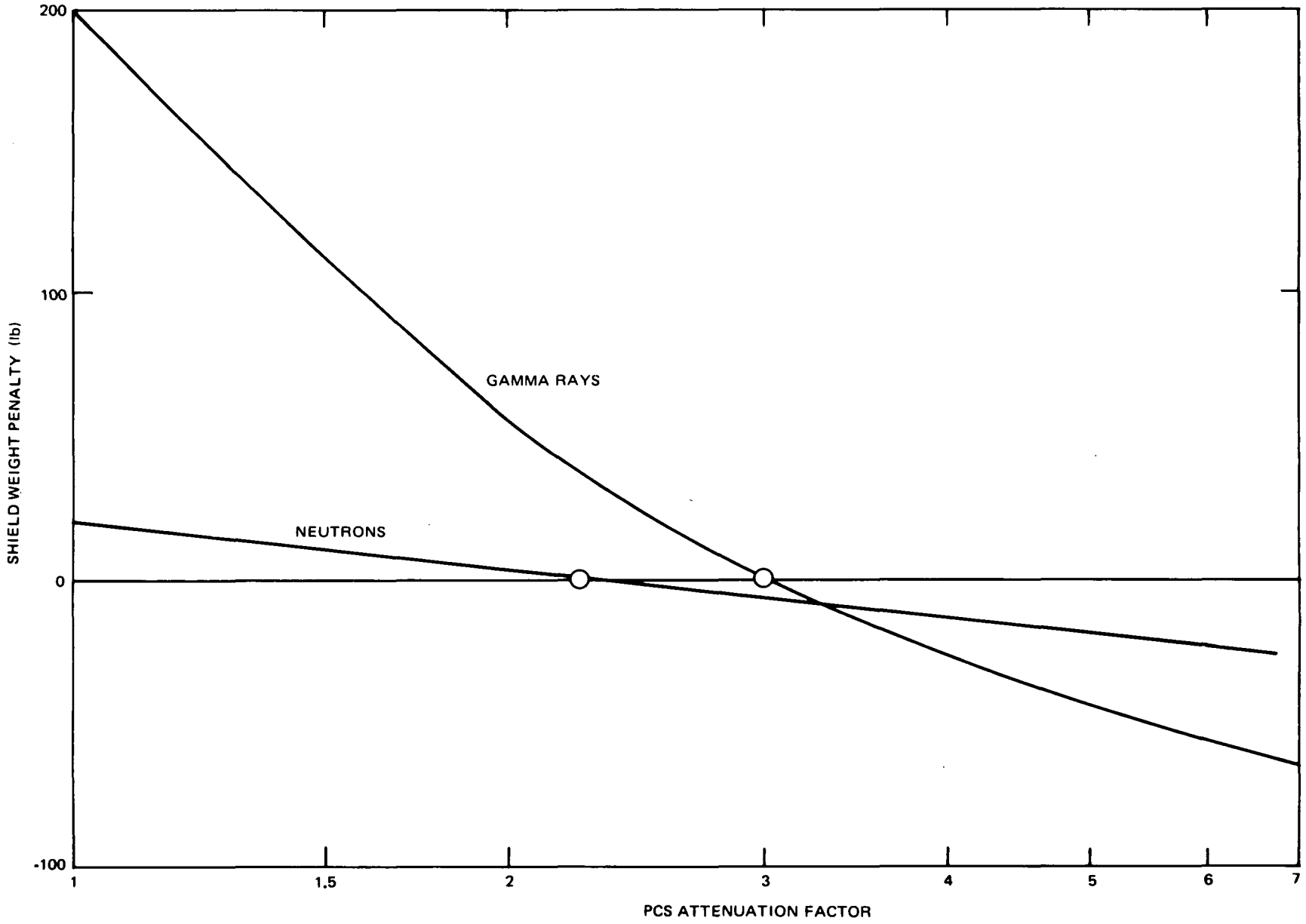

Figure 68. Shield Weight Penalty versus PCS Attenuation Factor

The neutron attenuation provided by the PCS equipment was also calculated. Both hand calculations and the DOT/SPACETRAN code cases were used. In the hand calculation, a method similar to the hand gamma-ray method was used, except that neutron removal cross sections were used rather than gamma attenuation cross sections. The DOT/SPACETRAN code case was similar to that for gamma rays presented in the previous section.

Table 33 presents the PCS equipment attenuation factors for neutrons using both hand calculations and the DOT/SPACETRAN code. Figure 68 also presents the shield weight saving as a function of PCS attenuation factor for neutrons. This curve is normalized to a factor of 2.23. If no credit were taken for the PCS attenuation for neutrons, the additional shield weight required would be only about 20 lb compared to 200 lb for not taking credit for PCS attenuation of gamma rays. This shows that the PCS attenuation is much more critical for gamma rays than for neutrons.

b. Radioactive NaK Coolant in PCS

The radioactive NaK below the shield is an additional gamma-ray source. The unshielded radiation level from 1 Ci of Na^{24} and K^{42} is 19.94 and 1.45 rad/hr-Ci at 1 ft distance, respectively. For the reactor operating at 100 kwt, the total unshielded radiation level is 1601.7 rad/hr at 1 ft. The fraction of primary NaK below the LiH shield was calculated to be 62%, and the weighted effective separation distance was calculated to be 15.2 ft from the dose plane. Thus, the unshielded dose rate at the dose plane is 4.32 rad/hr. The shielding provided by the PCS equipment for the radioactive NaK dose rate was estimated to be about 1.5. Thus, the radiation level due to the radioactive NaK coolant is 2.9 rad/hr at the dose plane.

As mentioned earlier, the shield was designed to a dose rate criterion of 10^6 rad/5 years at the dose plane. This is equivalent to 22.8 rad/hr. Since the NaK dose rate is 2.9 rad/hr, then the allowable dose rate from the reactor is the difference, i.e., 19.9 rad/hr.

c. Neutron Shield Penetrations

The LiH neutron shield attenuates the neutron flux at the dose plane by a factor of about 6×10^4. Thus, the effect of either the penetrations (for primary

NaK pipes) in the LiH shield, or of neutrons scattered off materials outside the shield cone may be important. This section discusses the effect of shield penetrations.

Detailed neutron streaming calculations through the NaK pipe penetrations in the LiH shield were performed using a combined transport and Monte Carlo code package (DOT-DOMINO-MORSE, DDM).[10]

The neutron dose criterion was set at 10^{12} nvt/5 years, and this is equivalent to a neutron flux of 6.34×10^{3} n/cm^2-sec. The shielding provided by the PCS equipment is 2.23 for neutrons. Thus, for the neutron penetration calculations, the dose criterion is 1.41×10^{4} n/cm^2-sec.

From Table 34, it may be seen that the neutron flux is 1.28×10^{4} n/cm^2-sec for the reference shield with the 2.25-in.-OD penetrations. Since this flux is within 10% of the neutron dose criterion (1.41×10^{4} n/cm^2-sec), it was decided that the reference shield would be used as it meets the desired dose criteria with a small margin of safety.

TABLE 34

EFFECT OF NEUTRON SHIELD PENETRATION ON NEUTRON FLUX AT DOSE PLANE

Method	Neutron Flux (n/cm^2-sec)	
	DOT/SPACETRAN	DDM
1. Reference Shield – No Holes	$5.4 - 5.5 \times 10^{3}$	$5.03 \times 10^{3} \pm 8\%$
2. Reference Shield + 2 in. LiH – No Holes	1.8×10^{3}	$1.85 \times 10^{3} \pm 6\%$
3. Reference Shield with 2.25 in. OD Holes		$1.28 \times 10^{4} \pm 11\%$
4. Reference Shield + 2 in. LiH with 2.25 in. OD Holes		$3.96 \times 10^{3} \pm 12\%$

d. Neutron Scattering from Radiator Outside Shield Cone

At the beginning of this study, the radiator was designed so that part of it was outside the shielded cone. Figure 69 illustrates the radiator geometry that was considered. As shown, the outermost point on the radiator is outside the shielded cone. The neutron flux leaking from the side of a 4π shielded SNAP reactor designed for manned applications is proportional to the cube of the size of the angle between the neutron path and the surface of the side shield (see Figure 69). Using this relationship, the neutron flux at the outermost point on the radiator, assuming 2 degrees outside the shielded cone coming from the reactor side shield, would be much less than the neutron flux attenuated by the bottom LiH shield (i. e., the direct neutron flux).

For unmanned systems (with no side shielding), however, the side leakage is proportional to the sine of the angle (see Figure 69) raised to only the ~ 1.5 power. Thus, for even a 2-degree angle, the neutron flux coming from the reactor side is about 65 times greater than the direct flux. This causes the neutron flux scattered from the radiator to be greater than the direct flux. It was decided, therefore, that the radiator cannot be permitted to extend beyond the shielded cone.

4. Shield Design

As mentioned in the previous section, the dose rate from radioactive NaK is 2.9 rad/hr. The dose criteria for gamma rays is 10^6 rad/5 years or 22.8 rad/hr. Thus, the dose rate from the reactor is equal to the difference, or 19.9 rad/hr. Since the NaK dose rate is less than the gamma-ray dose criteria, the primary NaK in the PCS area does not have to be shielded. Thus, a gallery to house a NaK-to-NaK heat exchanger is not necessary. It should be noted that if the gamma ray-dose criteria were reduced by a factor of 10, or if the reactor power level were increased by a factor of 10, then a gallery housing a NaK-to-NaK heat exchanger would be required.

The present design has the gamma-ray shield below the reactor, followed by the LiH shield (see Figure 70). The gamma-ray shield design was calculated using two-dimensional perturbation theory techniques in conjunction with the DOT code. The gamma-ray shield was optimized by varying the thickness as a

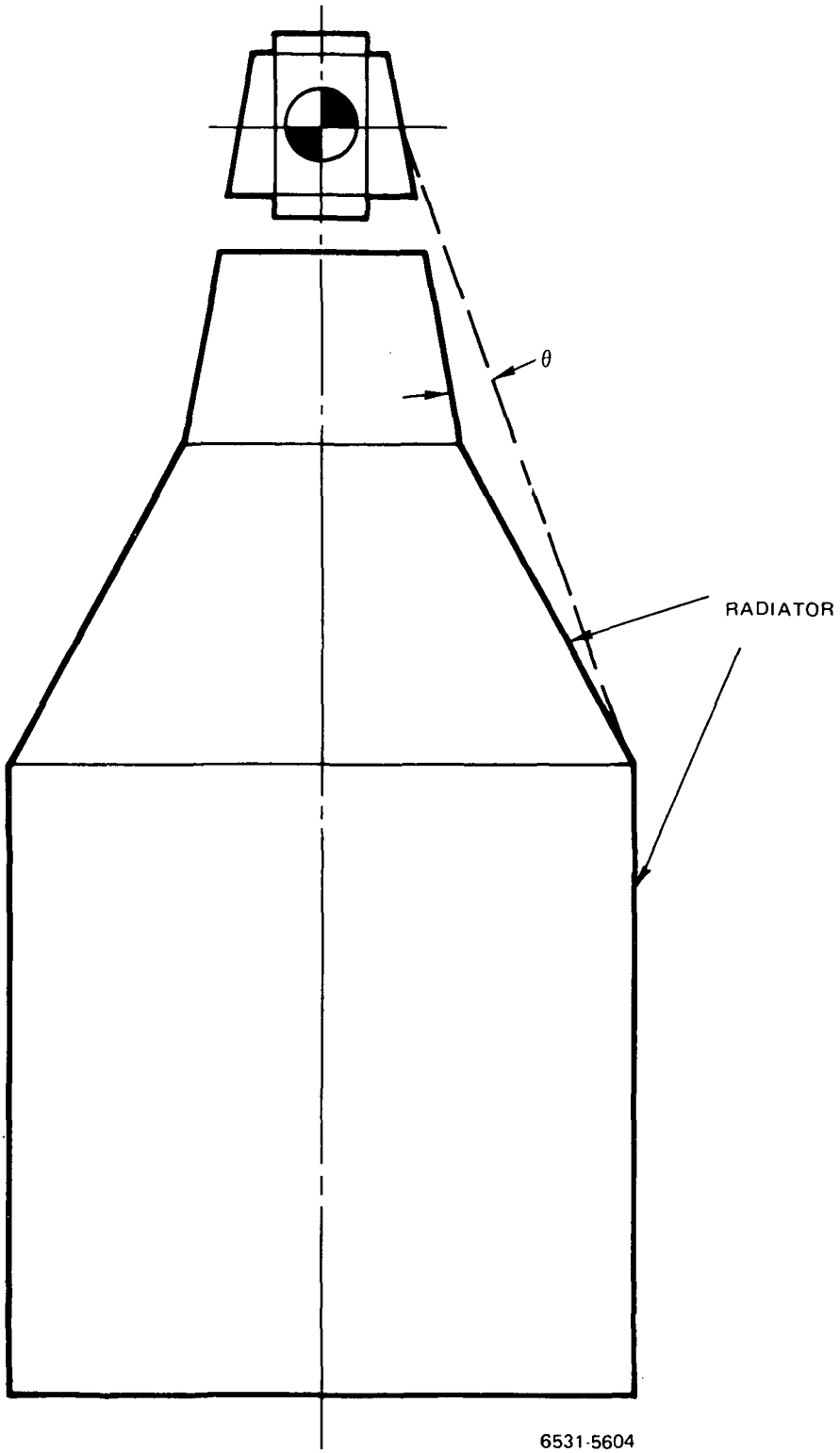

Figure 69. Design with Radiator Outside Shielded Cone

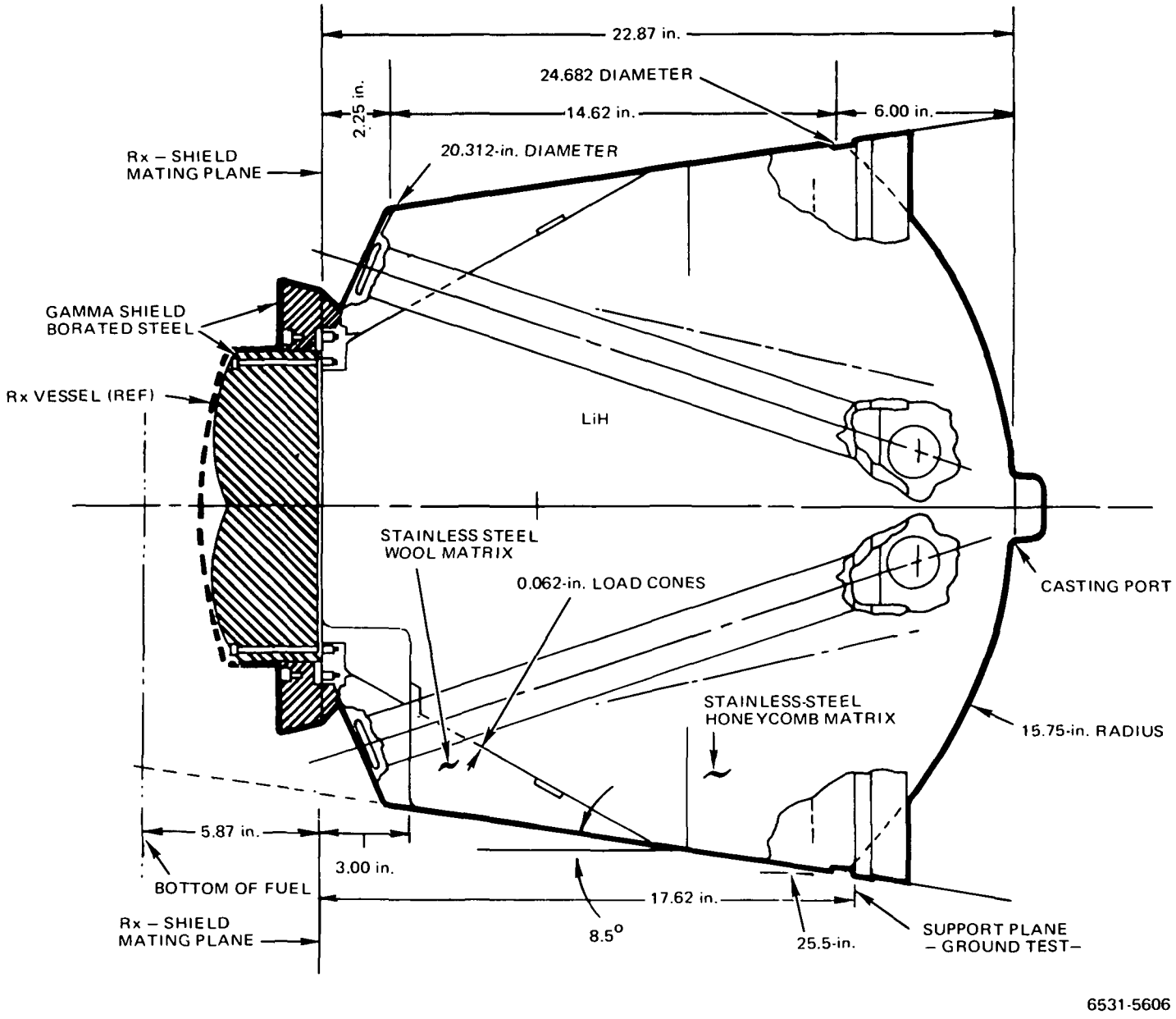

Figure 70. Reference Shield Design

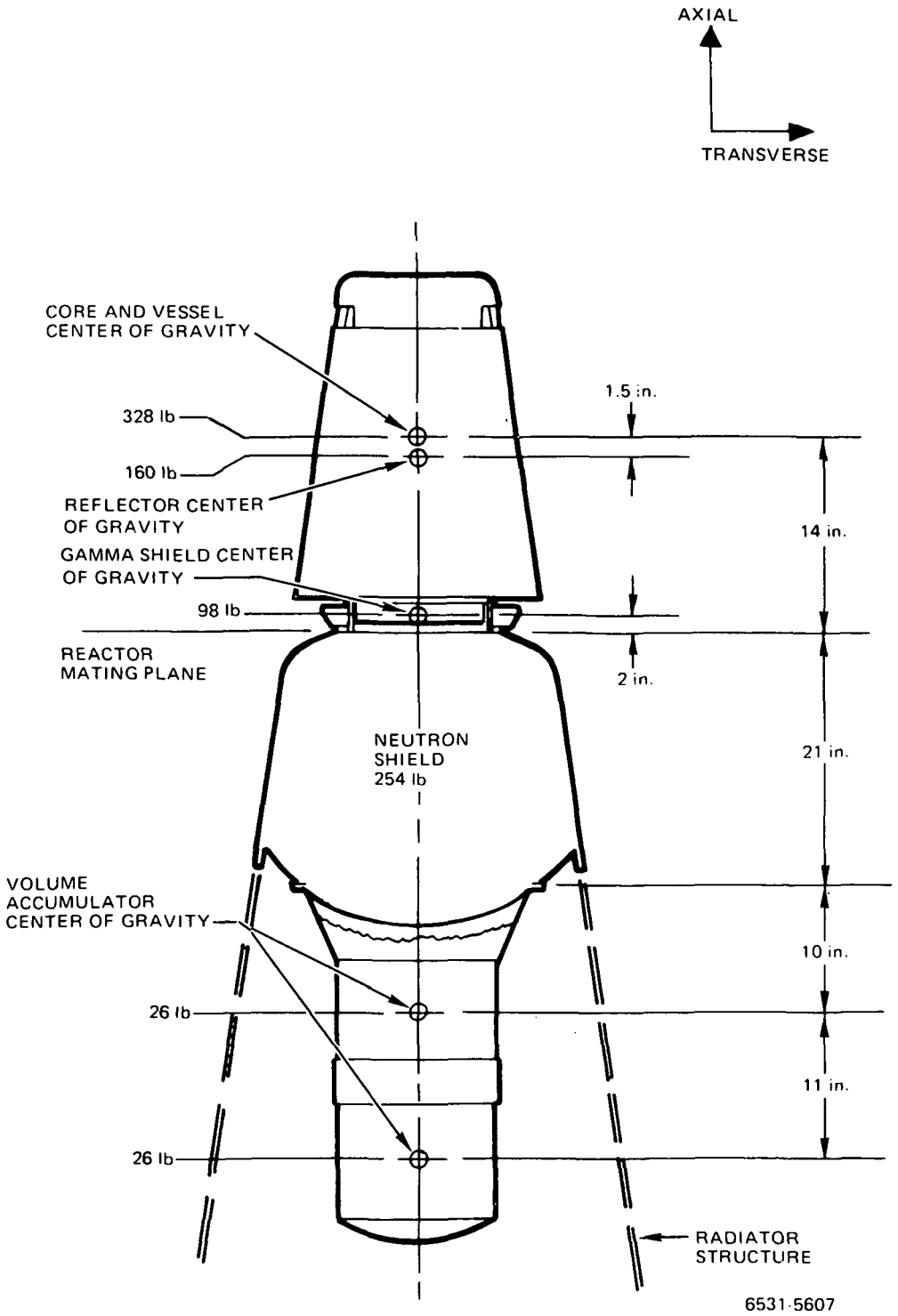

Figure 71. Shield Load Schematic

function of shield radius to yield a minimum weight shape. The shaped shield is thickest below the reactor vessel, and thinnest in the annular ring section below the reflector.

The reference borated stainless steel shield weighs 98 lb, and the LiH shield weighs 254 lb. The LiH shield includes 195 lb of LiH and stainless steel honeycomb, and 59 lb of steel casing and structure. The total shield weight is thus 352 lb.

B. MECHANICAL ASPECTS

1. Specification

In addition to its shielding functions, the neutron shield acts as an integral part of the 5-kwe Reactor Thermoelectric System structure, being attached to the radiator structure at its aft circumference and supporting the reactor at the forward end. In addition, it provides the basic support for the primary NaK system volume accumulator units (VAU's) at its aft end. Structural requirements are, therefore, an important aspect of the neutron shield design.[10]

Figure 71 is a shield load schematic showing the components supported from the shield, their weights, and center-of-gravity locations. When rotational moment of inertia of a component is required, a close estimate can be obtained by assuming the mass to be uniformly distributed over the length of the component.

Table 35 shows the launch acceleration load criteria to be used in the structural design of the shield. As the reactor and the VAU's have relatively long moment arms between their mass centers and their attachment to the shield, the transverse accelerations are the most important criteria in the structural design.

The design must be evaluated for stress in the shield structure, displacements of the supported components (interconnecting piping can be damaged if the displacements are excessive), and natural frequency. The natural frequencies of the supported components should be above the first mode fundamental frequencies of the launch vehicle so that primary low frequency resonances do not occur. The first mode fundamental frequencies for the

TABLE 35

LAUNCH LOAD CRITERIA

Condition	Expected Level – Limit (g)		Design Level – Ultimate (g)	
	Axial	Transverse	Axial	Transverse
Low Frequency, Maximum	6.0	1.6	7.5	2.0
Low Frequency, First-Stage Burnout	8.0	1.0	10.0	1.25
Thrust, Maximum Acceleration	13.0	0.5	16.25	0.625

Titan III launch vehicle are approximately 25 Hz in the axial direction and 10 Hz in the transverse direction.

A number of thermal criteria are applicable to the design of the neutron shield. The shield assembly must be capable of withstanding the thermal transients and temperature gradients that are induced by these transients, plus the temperature gradients that will exist during steady-state operation. The shield will be subjected to thermal loadings during the final step in its fabrication (casting cool-down), during system NaK loading and acceptance tests, and during orbital startup and operation. These loadings must not destroy the capability of the shield to meet its launch structural requirements and its orbital shielding requirements.

The LiH shield material must function (during long-term reactor operation) between temperature limits of 600° F and 750° F. Below 600° F the LiH swells due to its inability to reabsorb hydrogen that has been dissociated by neutron bombardment. Above 750° F the hydrogen loss resulting from thermal dissociation becomes excessive if the casing is punctured by meteoroids.

2. Design Description

The radiation shielding shown in Figure 70 consists of the gamma-ray shields, located just below the reactor, followed by the neutron shield, located

as close to the reactor as possible and configured to completely shadow the remainder of the system from the reactor.

The gamma shielding is made up of three machined segments of borated stainless steel. A center disk, 10.5 in. in diameter and approximately 3.5 in. thick is attached to the bottom of the reactor vessel and thermally isolated from the neutron shield. This disk has a profiled thickness, to meet the shielding criteria at minimum weight, and two semicircular cutouts to provide clearance for the control actuators that project slightly under the reactor. Two outer ring segments are located just below the reflectors and are attached to the reactor vessel mounting flange. They do not form a complete ring due to the presence of the control drive actuators and the reflector mounting hinge mechanisms.

The neutron shield is basically a stainless steel casing filled with LiH. The LiH is cast into a perforated square cell honeycomb matrix so that any cracking that does occur is distributed and oriented so that no direct streaming paths through the shield can develop.

The top face of the LiH shield has a flat central area surrounded by the reactor mounting surface which includes tapped holes for the reactor attachment bolts. The outer portion then slopes aft to intersect the outer wall. Two recessed pockets provide clearance for the control drive actuators. These recesses are sized to allow the actuators to move inward as the reflector-control assembly rotates 15 degrees about the mounting hinge axis at EOL shutdown.

The outer surface is a truncated cone having an 8.5-degree half angle and the aft surface is spherical, having a 15.75-in. radius and a 6-in. mid-height (see Figure 70). A mounting surface for attachment of the primary NaK system volume accumulators, and a fill port and instrument feed through assembly are incorporated in the aft surface.

A shield mounting ring is incorporated at the intersection of the side-wall and the aft surface. The ring includes a skirt extension for attachment of the shield to the radiator structure and a circumferential groove which is to be used to support the PCS during ground handling and ground test operations.

Four straight pipe ducts traverse the LiH shield from the outer areas of the forward and aft surfaces of the shield. The traverse of each duct is at an oblique angle so that the view looking forward through a duct does not "see" any part of the reactor, and the view looking aft through a duct is as far away from the payload as possible. This design minimizes the radiation dose contribution at the payload due to streaming through the pipe ducts without the complications of arcing, spiraling or dog-legging the piping through the LiH shield.

The pipe ducts are 2.180-in. ID with 0.035-in. wall. This provides for a 1.50-in.-diameter NaK pipe with a 0.125-in. insulation thickness, and allows 0.095 in. for piping thermal movement, 0.060 in. installation error in placement of the NaK pipe, 0.015 in. for duct and piping straightness deviation, plus a design contingency of 0.045 in. per side.

The reactor support loads are transmitted through the shield by an internal structural cone, 0.062-in. thick, which extends aft from the reactor attachment area with a 30-degree half angle until it intersects the side wall of the casing. The aft end of the load cone has a short flange with an 8.5-degree half angle for a spot welded connection to the casing sidewall. The reactor loads are then carried down the lower 5 in. of the casing sidewall (0.042 in.-thick) to the reactor support ring.

The entire casing is constructed of Type 316 SS. The spherical parts of the aft dome, the casing sidewall and the outer portion of the forward part of the shell are 0.042-in. thick. The two parts of the casing that form actuator recesses are formed from 0.062 in.-thick material.

The shield, as currently designed, has 16 internal thermocouples. Eleven of these were placed to monitor shield thermal performance during the system demonstration ground test. The leads are brought out of the casing through welded seals surrounding the casting port in the aft part of the casing. The remaining five thermocouples are required only during the LiH casting operation and their leads are brought out through the casting port and then cut off prior to sealing the casting port. All 16 thermocouples may be used during the LiH casting operation.

3. Design Analysis

a. Structural

(1) Reactor Support

As shown in Figure 72, the loads of the reactor and gamma shields, weighing almost 600 lb, must be transmitted through the neutron shield to the radiator structure. This must be accomplished at the acceleration levels listed in Table 35. The long moment arm (13.5 in.) between the reactor center of gravity and the top of the shield makes the high transverse accelerations the most difficult criteria to meet.

Early in the conceptual design a number of shield structure concepts were considered and two were selected for detailed evaluation. These were: an internal frame structure, very similar to the design used in the SNAP 2 DRM shield, and an internal conical shell structure. Structure designs were developed for each of the concepts, based on meeting the limit level (expected) acceleration criteria without exceeding two-thirds of the material yield strengths. The structure weights and the reactor natural frequencies, in the axial and transverse directions, were then calculated and used as the primary basis for comparison. Other factors such as fabrication difficulty and cost, shield castability, etc., were considered but not evaluated quantitatively.

The conical shell concept was selected for the shield structure. Figure 72 shows the calculated principal stresses induced in the reactor load path by the reactor and gamma-ray shield loads, under conditions of low frequency maximum g load (6.0 g axial and 1.6 g transverse acceleration). Although the stresses appear extra conservative, it should be noted that some additional stresses, not calculated during the conceptual design, will be induced by the weight of the neutron shield itself; and that the design must be capable of withstanding ultimate loads which are 25% higher. It was also felt that the thickness of the internal load cone should not be reduced below 0.062 in. because of the possibility of damage resulting from the LiH shrinkage during the casting solidification and cooling.

Plans projected for the preliminary design phase were to investigate the weight reduction potential of increasing the structural cone half-angle, which

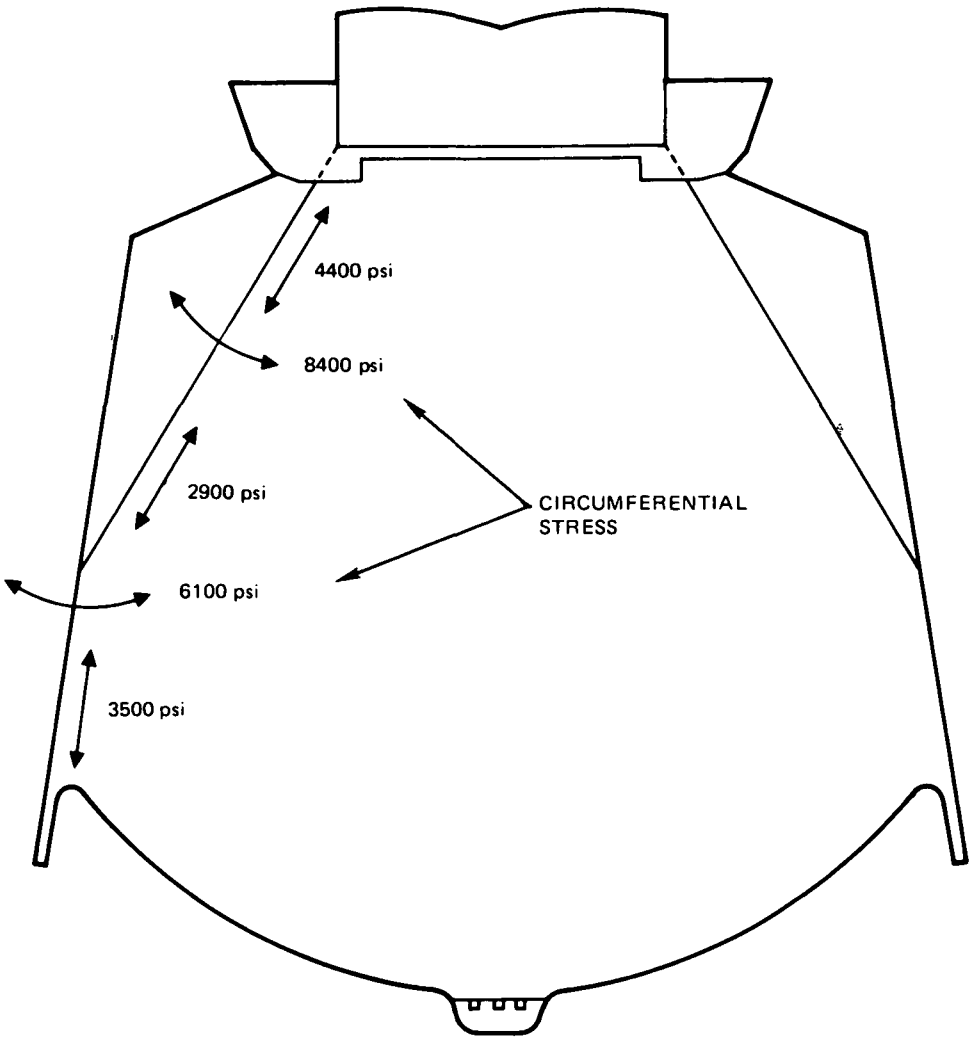

LIMIT LOAD (g)	AXIAL	TRANSVERSE
LOW FREQUENCY MAXIMUM	6.0	1.6
FIRST-STAGE BURNOUT	8.0	1.0
MAXIMUM THRUST	13.0	0.5

6531-5610

Figure 72. Shield Launch Load Stresses

would shorten the cone and transfer the load into the casing sidewall nearer the reactor. It is expected that no large change can be made because the stiffness characteristics will deteriorate rapidly as the cone angle is increased. Another area that requires detailed definition is reinforcement of the edges of the cutouts in the actuator recess area, holes for the pipe ducts, and holes to allow the LiH to flow into the volume behind the structural cone during casting.

(2) Volume Accumulator Attachment

The primary NaK system VAU assembly is supported by the bolting flange built into the aft dome of the shield casing, as shown in Figure 71. The aft dome of the shield was analyzed for the launch acceleration criteria of Table 35, assuming the VAU assembly to be a rigid body. Shell stresses were determined for the ultimate loading conditions because the failure mode is compressive instability for which any stresses above yield are not acceptable. Calculations indicated that the rigidity of the VAU support is inadequate as currently designed. The natural frequencies are essentially equal to the Titan III first-mode fundamentals (25 Hz axial and 10 Hz transverse) and there is a high probability that damaging resonances would occur. The calculated peak displacements of the VAU (0.163-in. axial and 0.232-in. transverse) at peak acceleration are excessive, and these would probably be even greater under resonant vibration conditions.

At the time of project closeout, the VAU mounting rigidity problem was not resolved. Increasing the thickness of the shield aft dome to obtain the required stiffness would require a large increase in the shield casing weight. Other options were being considered but had not been studied in detail. These options basically involved the addition of stabilizing supports, tension rods and/or struts, between the VAU assembly and the top of the radiator structure or the shield mounting ring. The potential problems associated with these options are the possibility of excessive forces generated by temperature differences between struts and other components involved in VAU support, and the extremely limited access for installation because of the presence of NaK manifolds and piping, wiring, etc., in the area.

(3) Structural Design Status

At the time of project closeout, two basic areas of shield structural analysis remained to be completed to verify the structural soundness of the design. The first is the VAU mounting stiffness problem discussed in the previous section. The second is the determination of stresses induced in the shield outer casing, internal structure, and the piping ducts by differences in thermal expansion which result from the large difference in expansion coefficient of LiH and stainless steel, and by thermal gradients that occur in the shield casting cycle and in system operating transient and steady-state conditions.

Development of the thermal model of the shield had just been completed and the initial temperature distribution data were being generated. Temperature data taken during the casting of the SNAP 2 DRM shield were being studied to evaluate the effects of the casting process on the shield structure.

b. Duct Clearance

To minimize the radiation streaming dose contribution at the payload, the diameter of the pipe ducts through the neutron shield should be as small as possible.

The size of the NaK pipes passing through the shield was set at 1.50-in. OD by a trade study which determined the optimum size based on consideration of loop pumping requirements, system weight, NaK volume, etc. A study of thermal insulations established that a 0.125-in. thickness of insulation is required between the pipe and the duct. Clearance spaces are required to accommodate piping movements, pipe position error in system construction, and straightness deviations in the pipes and the ducts.

An analysis of the movement of the pipes in the shield area showed that the mechanical forces and moments in the piping produced insignificant displacements; consequently, the relative movement between the pipe and the duct, at any point, could be established on the basis of thermal expansion only.

The calculated hot-leg thermal movements at startup, related to the pipe and duct axis, are given in Table 36. Cold-leg movements are slightly less due

TABLE 36

CALCULATED HOT-LEG THERMAL MOVEMENTS
STARTUP CONDITIONS

Location	Movement (in.)*	
At top of shield	Axial	0.008
	Lateral	0.089
At bottom of shield	Axial	0.218
	Lateral	0.095

*Axial and Lateral are related to pipe and duct axis

to the lower pipe temperature and a subtractive effect of the relative expansion of the vessel and the pipes in the reflector area.

When the shield reaches its operating temperature, the displacements are reduced to about 50% of those at startup. If the NaK piping system is cooled to 100° F with the shield at operating temperature, the displacements are about 50% of those at startup.

Allowances of 0.060 in. for installation error, and 0.030 in. for pipe and duct straightness deviations were assigned. A tabulation and addition of the dimensions and allowances are presented in Table 37, which shows that the minimum duct ID is 2.120 in. A standard tubing size of 2.25-in. OD by 0.035-in. wall (i.e., 2.180-in. ID) was selected for the duct, giving a margin of 0.030 in. per side over the minimum requirement.

c. Thermal Control

The heat source to the LiH shield is by conduction through the reactor support skirt, by radiation from the gamma shield (the underside of the reflector assembly), the four NaK pipes that pass through ducts in the shield, and by neutron and gamma ray absorption in the LiH. Heat is rejected from the shield by radiation to space from part of the top and all of the sidewall surface of the LiH shield casing. The aft dome of the shield faces the VAU and the interior of the heat rejection radiator, both at an average temperature of approximately 600° F.

TABLE 37

DUCT ID REQUIREMENT

NaK pipe radius (in.)	0.750
Insulation thickness (in.)	0.125
Lateral pipe movement	0.095
Installation error	0.060
Duct and piping straightness	0.030
Duct inside radius, minimum (in.)	1.060
Duct ID, minimum (in.)	2.120

When LiH is subjected to radiation, some of the hydrogen is dissociated. At temperatures below 600°F, this hydrogen will not be reabsorbed by the lithium, and the LiH swells due to the pressure of this free internal hydrogen.

The basic method available for control of shield operating temperature is by selection of surface emissivities between the gamma-ray shields and the top of the neutron shield, and between the NaK pipes and the pipe ducts for control of heat input, and on the aft dome and the areas of the casing facing space for control of heat rejection.

Shield temperature calculations were performed with the DEAP computer code, which determines the steady-state solution for the nodal networks in the shield. Nodes representing the reactor outlet plenum, space, the radiator interior, and the NaK pipes through the shield ducts were attached to the shield network and fixed at specified temperatures.

Nuclear heating of the shield materials was not included in the program because the data were not available. However, a review of previous shield analyses at the same thermal power showed that nuclear heating does not have a large effect on the LiH shield temperatures.

Thermal calculations showed that the size of fractures in the LiH shield (due to shrinkage in the casting process) had no effect on the temperature of the LiH shield.

To meet the design objective of a shield temperature of 600° to 750° F, thermal calculations indicated that the emissivities at a few surfaces were critical. Table 38 presents the preliminary recommendations.

TABLE 38

RECOMMENDED EMISSIVITIES

From	To	Emissivity
LiH shield casing	Radiator interior	0.10
LiH shield casing	Space	0.10
LiH shield casing	Gamma-ray shield	0.05
NaK pipes	Piping ducts	0.05

Additional analysis, using the thermal model that has been developed, is required before a final selection of the parameter values that control shield temperature can be made. A specific requirement is a more detailed evaluation of the sensitivities of effective emissivities, i. e., from the NaK pipes to the piping ducts, from the shield casing to the radiator interior, and from the shield casing to space. The objective is to select a combination of emissivity values that are realistically attainable and that give the least sensitivity to error between the selected value and attained value, or to change in value during system lifetime.

IX. CONTROL SYSTEM

The control system for the ground test reactor adjusts the thermal output of the reactor by varying the position of two sliding segments in the radial beryllium reflector. Movement of the reflector segments changes reactivity by increasing or decreasing the size of the window in the reflector at the axial midplane of the core, thus changing the neutron leakage. The reflector window varies from completely closed to 4 in. open, and this provides approximately $8 of reactivity control. The position of each segment is adjusted by means of an electrical actuator driving a screw in a ball-nut anchored to the movable segment. The actuator is a reluctance stepping motor with four stator phases; rotation is produced by sequentially flowing current through each phase coil. The direction of rotation is determined by the order in which the coils are supplied power.

The segments are driven in discrete steps corresponding to a single cyclic activation of the four phase coils. This cyclic activation produces a rotation of the actuator rotor of 7.2 degrees, resulting in a segment movement of 0.0054 in. When not being driven in this manner, the actuator is locked against rotation by means of an internal spring-loaded toothed brake. This brake must be released before rotation begins and must be set at the end of the rotary motion.

The control system consists of the automatic control system, the manual control system, the computer control system, which controls the reactor under all normal conditions, and the safety system, which provides protection against hazardous operating conditions.

The automatic control system consists of a prototype flight controller and would demonstrate the performance of the flight control system for startup and steady-state operation. The manual control system provides the reactor operator with direct control of the reflector segment actuators. The computer control system permits testing of variations in the programmed automatic startup sequence by simulating the automatic controller. The computer control system also serves as a backup to the automatic controller for long-term operation.

Design objectives for the automatic controller have been established on the basis of operational requirements, engineering analyses of the system, and safety guides and standards. These objectives are:

1) Startup time less than about 5 hr.

2) Temperature rise through the core limited to less than 150°F.

3) Rate of temperature change in the inlet plenum limited to less than 150°F/min.

4) Accommodate uncertainties in reactivity and reactivity coefficients.

5) Shutdown margin (cold) in the range of -$0.50 to -$3.00.

6) Maximum reliability as needed to meet lifetime requirements.

7) Minimum number of required flight qualified items and minimum number of items to operate near reactor.

8) Operating lifetime of 5 years at power, surviving average payload radiation dose with no additional shielding.

9) Shelf life of 2 years.

10) Adjustment of reactor power to produce electrical power within ±2.5% at 5 kw.

11) Minimum power overshoot at end of rise to power.

12) Ease of modification to meet changes in performance details.

To limit the complexity of the flight system, it was intended to use the minimum of instrumentation to guide the operation of the automatic controller. Thus, no segment position sensors would be provided, nor would monitoring of the reactor power by neutron or gamma-ray detectors. The automatic controller is to operate on the basis of a pre-established program with a minimum of information that may be easily obtained from existing instrumentation or simple additions of instrumentation.

The design of the automatic controller has relied upon digital computer simulation of the reactor system. The simulation program used was written in the IBM CSMP modeling language. A schematic diagram of the system, as modeled in the program, is shown in Figure 73. Each block represents a lumped temperature node.

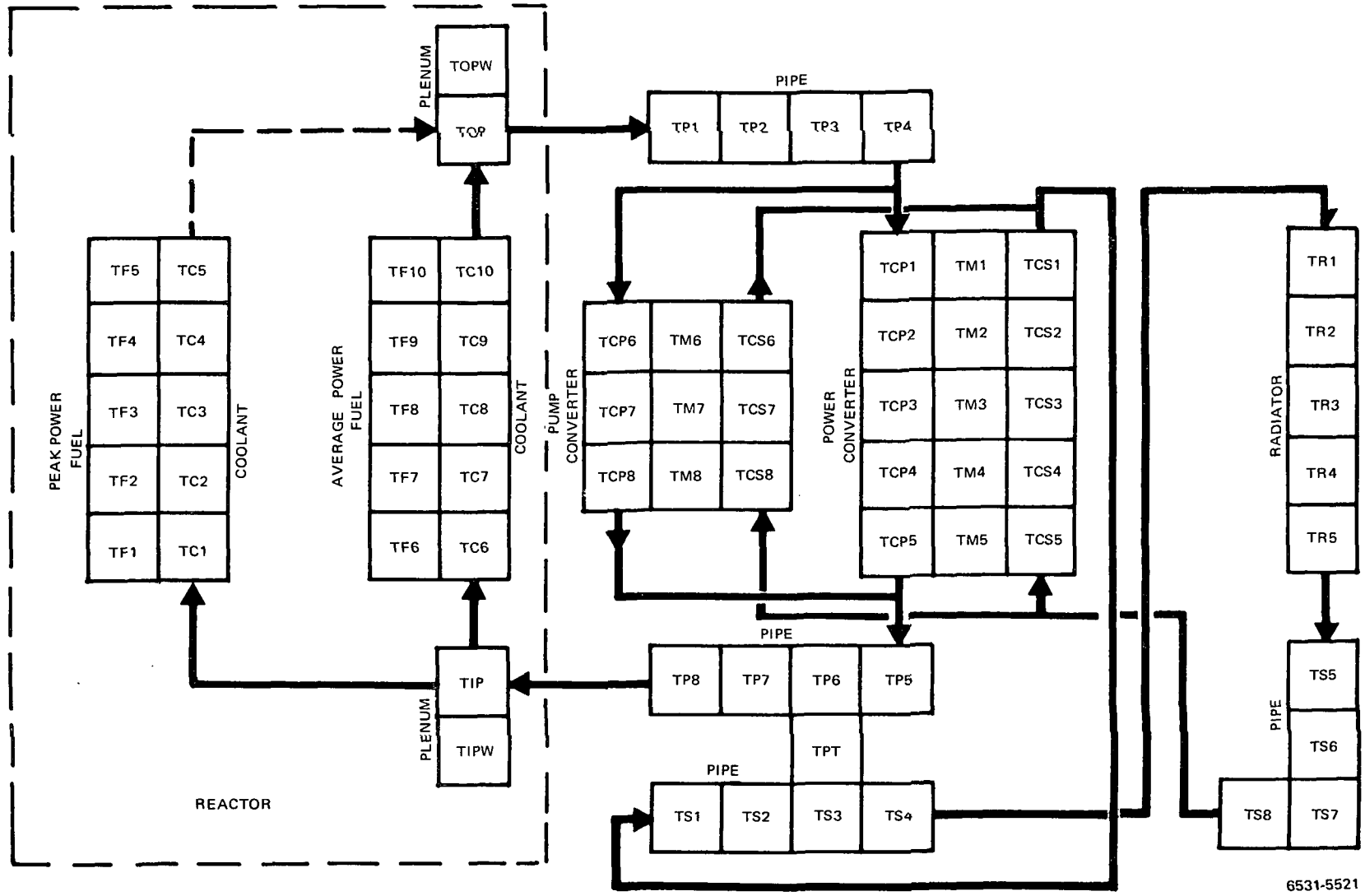

Figure 73. Simulation Model for 5-kwe Reactor Thermoelectric System

This simulation model was used to investigate various startup sequences chosen from three basic approaches: (1) the single reactivity insertion rate, (2) the single rate with hold above critical, and (3) the multiple insertion rate. The multiple insertion rate was the only method that completely met the design objectives.

A functional block diagram for the automatic control system is shown in Figure 74. A pair of coupled oscillators supplies the basic pulse sequence used to initiate control operations. During startup, pulses from the oscillators are passed by the startup blocks (subject to conditions established by the position, temperature, and current indicators) to the delay block and then to the alternator, where the pulses are alternately passed to one or the other of the phase sequencers. The active phase sequencer produces a series of pulses that turn on the power switches, in order, passing current to the actuator brake release coil and the four actuator phase coils. At the completion of the cycle, the brake is reset.

The startup blocks determine the segment insertion rate by dividing the pulse rate from the oscillators. The insertion rate is selected according to the segment position and the primary NaK system temperature. The segment position relative to the starting position is determined by counting current pulses to two of the phases of each actuator. The order of these pulses identifies the direction of the actuator step.

The segments are inserted rapidly until 45¢ has been added, and then slowly until the primary system temperature (at the EM pump, for example) increases by 100° F. At this point, a moderate insertion rate is used to raise the reactor power to the desired operating level. The startup blocks are then switched off and the operating blocks control the segment positions to maintain the output of the thermoelectric generator at 5 kw.

Segment drive commands originating in the startup or operating blocks pass to the delay block where they are inhibited unless 1 sec has elapsed since the previous command was passed. This insures that adequate time elapses for completion of an actuator step before a subsequent drive command is received.

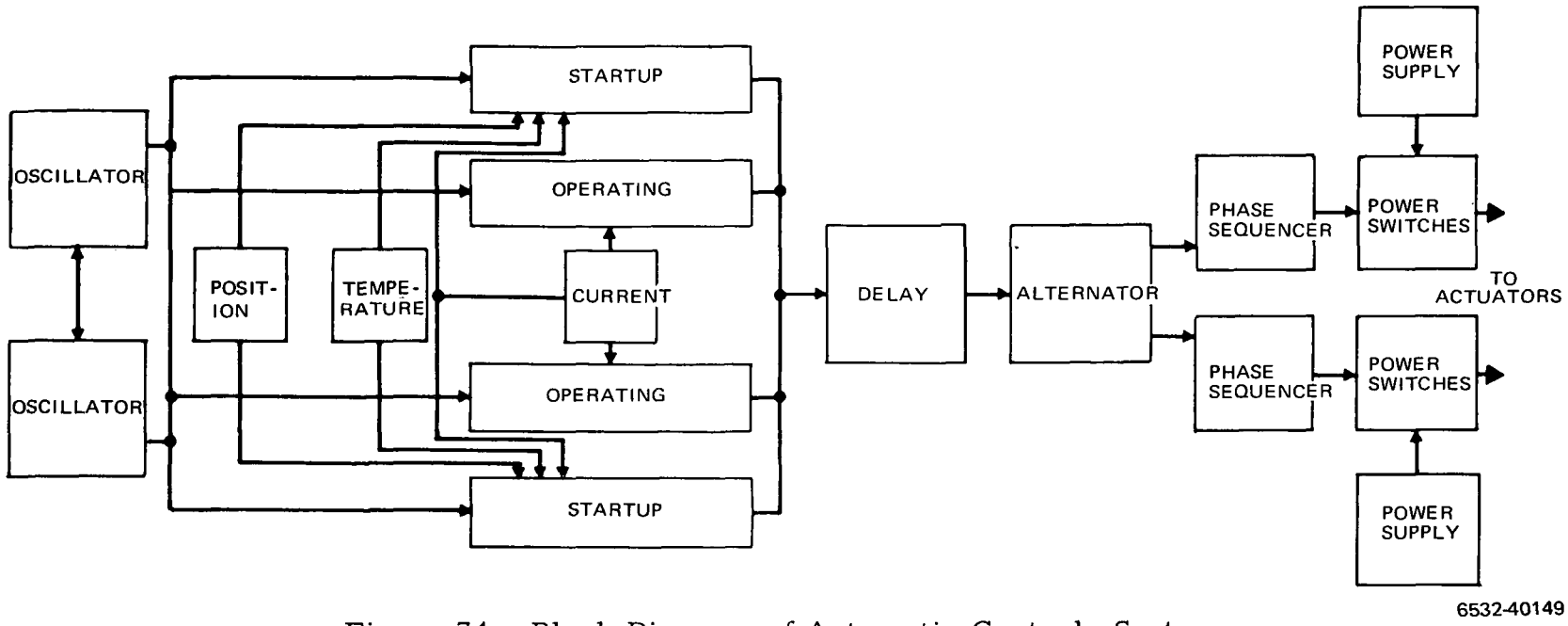

Figure 74. Block Diagram of Automatic Control System

The alternator functions to share insertion and withdrawal commands equally between the two segments. So long as segment motion is maintained in one direction, each segment is stepped alternately. If the motion is reversed, the segment to be stepped first is the one that had just been stepped.

The phase sequencer that is selected by the alternator generates a series of phase signals whose order is determined by the drive direction required. These signals initiate release of the actuator brake and control the sequential application of current to the four stator phase coils in the actuator.

The phase signals operate transistor switches in the power switches block to pass current to the appropriate actuator coils to release the brake, provide for one cycle rotation of the actuator, and reset the brake.

Flight reactor performance, from prelaunch to EOL, is shown in Figure 75. For this sequence, it is assumed that the reactor is installed in the launch vehicle with the segments fully retracted, keeping the reactor subcritical by $3 relative to the 0-power (cold) critical configuration. As the countdown proceeds successfully towards launch, the segments are inserted, by ground command and using ground support electrical power, to add $2.50, which leaves the reactor an estimated 50 ¢ sub-critical.

Following a successful launch and injection into an acceptable orbit, a startup command will be directed to the automatic control system. This signal starts the programmed startup sequence which begins by inserting 45 ¢ rapidly, to bring the reactor to the neighborhood of 0-power critical configuration. As the uncertainty in the estimated 50-¢ subcriticality at the beginning of startup is expected to be ± 10¢, this insertion leaves the reactor between 15¢ subcritical and 5¢ supercritical. Reactivity is then added by inserting the segments at a very slow rate until the temperature in the primary NaK system increases by 100° F. At this event, the battery supplying power to the primary and secondary EM pumps is disconnected. This is necessary since the battery-supported flow in the secondary system is backwards, and this reverse bias at the pump hinders transition to the normal operating conditions. This event also signals the automatic controller to begin reactivity insertion at a faster rate. This rate is still slow enough, however, to allow the negative temperature feedback to modify the rate of power increase.

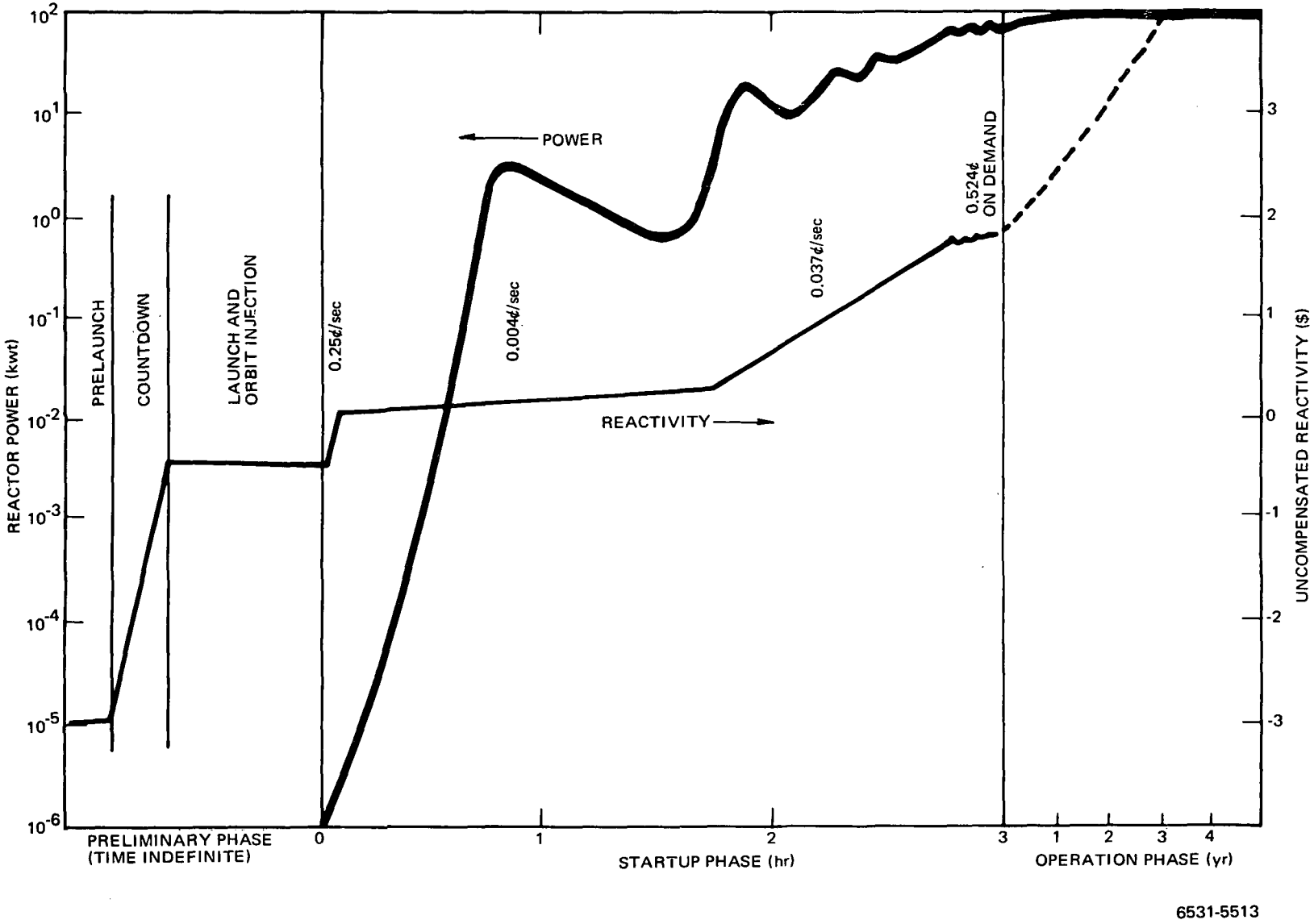

Figure 75. Reactor Power and Inserted Reactivity During Preliminary, Startup, and Operation Phases

The reactor power is forced to increase in this manner until the output of the thermoelectric generator reaches the desired level, 5 kw. The automatic controller is switched from the startup mode to the operating mode. In this mode, segment insertion or withdrawal is directed in response to the signal from the current monitor. Segment steps are supplied on demand if the current falls below or rises above the lower or upper control limits, respectively, but the maximum rate is limited to allow the system time to respond to each step.

The results calculated by the simulation program for some of the system characteristics for such a startup are shown in Figure 76. (The final proposed startup sequence differs somewhat from that used in this simulation and so the results shown here should be regarded as only representative.) The elapsed time from initiation of startup to production of 5 kw by the thermoelectric generator actually would range from 2.3 hr to 3.6 hr due to the effect of the ± 10¢ uncertainty in the reactivity of the system in orbit.

The response of the thermoelectric generator output to a single segment step, as would occur after stabilization in the operating mode, is shown in Figure 77. It is clear from comparison of the small power excursion with the width of control deadband, that oscillation induced by the control limits is unlikely to occur. The system is inherently more stable than is necessary for the desired power regulation.

The reactivity addition required to maintain the full electrical power output for 5 years, after the initial operating adjustment, is estimated to be about $1.83. This requires approximately 350 segment steps or about 1 step every 5 days.

Two methods of shutdown are available for the flight configuration reactor. One is by the irreversible release of the radial reflector halves. This is the intended EOL shutdown, controller by a timer. This shutdown method may also be utilized by means of a ground control signal. The other method is to drive both segments out, part or all the way, to achieve the desired degree of subcriticality.

This second method does not preclude restart, nor does it interfere with subsequent use of the EOL shutdown mechanism. The possible need for reversible shutdown and restart has been considered. Because of the wide variety

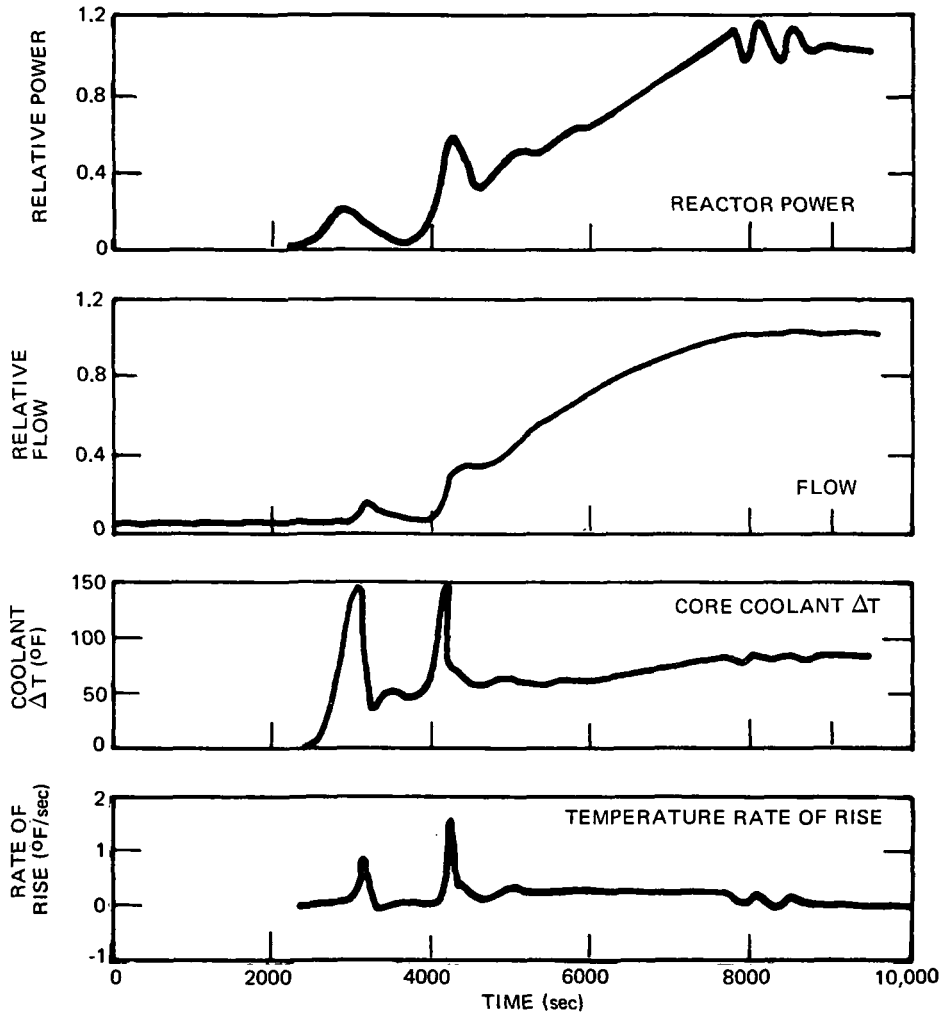

72-017-48-178A

Figure 76. System Characteristics for Reference Startup

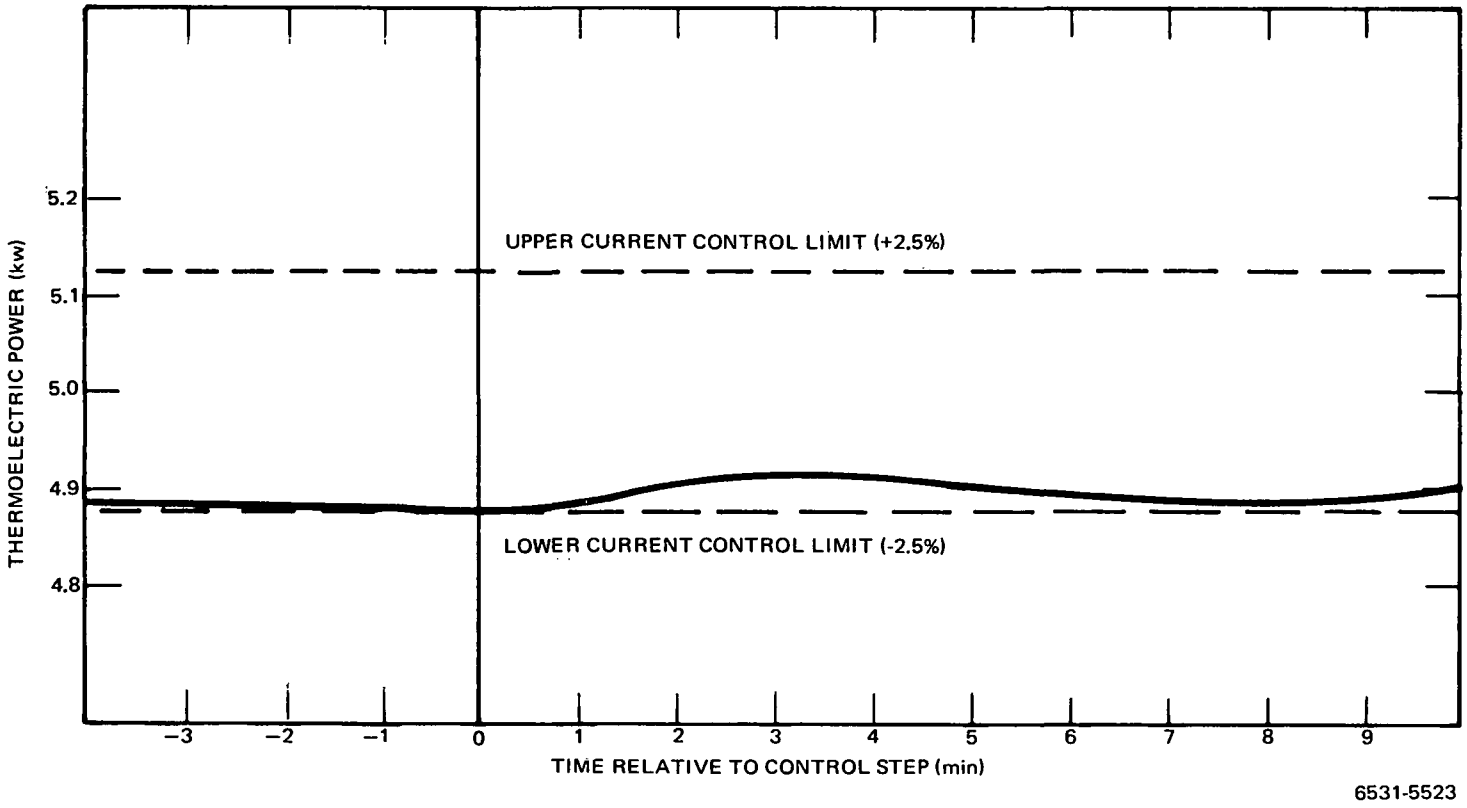

Figure 77. Generator Power Response to Single Control Step of +0.524¢

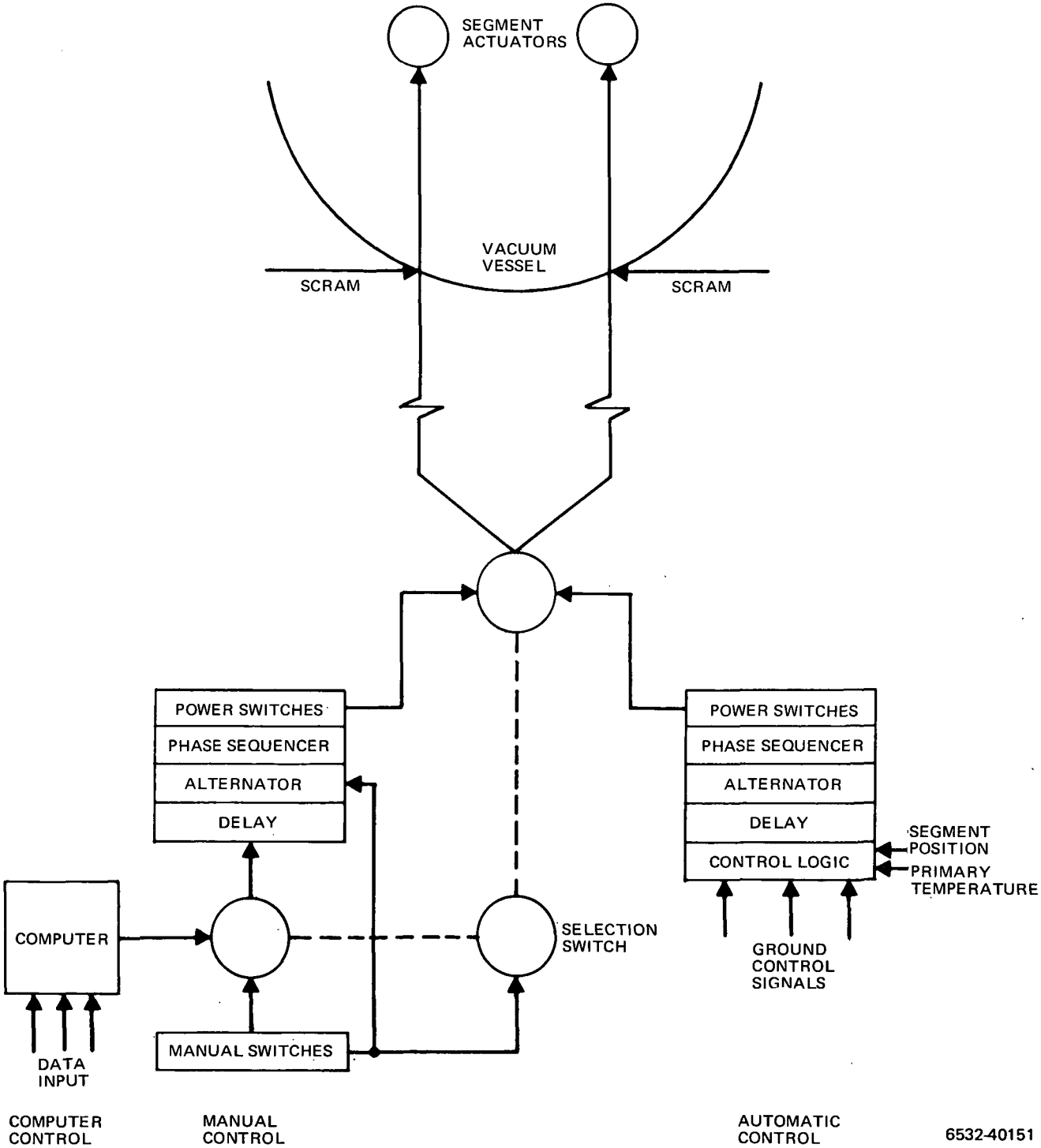

Figure 78. Ground Test Control System

of conditions that may exist following shutdown, it is difficult to plan an optimum method to restart the reactor. The ranges of available reactivity, shutdown margin, temperature, and flowrates are wide, and depend on the operating and shutdown history. For this reason, no provision for restart capability has been specifically designed into the automatic controller. However, restart can be accomplished using the normal operating function to insert reactivity at a very slow rate until the lower current limit is satisfied. The details of such a startup have not been investigated and would depend upon the operating history, and post-shutdown conditions. The fission product decay heat amounts to a few hundred watts for several months after shutdown, fading to about 10 w at 2 years after shutdown. At some time this power would no longer be sufficient to prevent freezing of the NaK in cold spots and thus could no longer provide circulation in the primary and secondary systems.

It appears likely that restart might be possible even with a partially frozen system. A restart from 0° F would require insertion of reactivity at the slow rate for approximately 30 hr, at the end of which time the reactor would be at 1200° F and at a power level determined by the heat rejection existing at the time. Heat transfer by conduction and thermal radiation would probably suffice to melt frozen regions during the restart so that circulation would be normal when operating temperature is reached. Thermal shock and temperature differences may be severe following a melt-through that permits circulation. Clearly, a more detailed analysis of this startup would be required.

The control system for use in the ground test program must be considerably more versatile. The objectives of the ground test control system are: (1) provide for flexible operation of the reactor by means of manual control, (2) to test and demonstrate the performance of the automatic controller, and (3) to afford the opportunity to utilize an on-line computer for testing various automated startup and control methods. The interrelation of these three systems in the ground test control system is shown in a conceptual block diagram in Figure 78. The three systems are grouped to form two independent lines of control: one consisting of the automatic controller alone, the other consisting of the manual controls and the computer, sharing some equipment in common.

The system to control the segment positions is chosen by means of a three-position selector switch. Selection of either the automatic or computer control systems is immediately revoked by operation of a manual segment drive switch, with control reverting to the manual system. The selector switch must be repositioned to return control to the automatic or the computer control system in this event.

The manual control system provides the reactor operator with the ability to independently adjust segment positions as required to obtain the desired reactor system conditions. In concept, it consists of two manually operated switches, one for each segment that request drive signals, in or out, depending upon the direction the switch actuator is pressed. A push-it-in, pull-it-out analogy would be used for the switches to aid the operator in associating with the segment actuation. The drive signals are generated by a phase sequencer and associated power switches after being passed by delay and alternator blocks, as in the automatic controller.

Operation of a single segment manual switch bypasses the alternator function and drives only the selected segment. Similarly, if one segment manual switch is pushed in and the other pulled out, the segments will be driven in the selected directions. Actuation will alternate step by step between the two segments as long as both switches are in operation. If both switches are operated in the same direction, the alternator performs the same function as in the automatic control system to share insertion and withdrawal commands equally between the two actuators.

The maximum segment drive rate is limited by the delay block to 1 step/sec to allow completion of the actuator cycle for each command before a subsequent command is received. Slower rates are easily achieved by intermittent operation of the switches. The maximum rate is sufficiently slow that the segments may be driven in discrete steps as required.

Segment steps would be sensed and counted in the same manner as for the automatic controller, by detecting current pulses to the actuators, but would be done independently of the automatic control system. The position of each segment would be displayed digitally.

While the manual control system uses portions of the automatic controller (all but the control logic) no further details have been prepared.

The computer control system is even less well defined at the present time. It would use a small on-line computer to control movement of the segments by comparing reactor operating data with program values to achieve a desired operating condition. The computer could be programmed to act like the automatic controller and thus facilitate testing of variations of the automatic startup plan. Reduced-time startups could also be investigated by supplying the computer with more complete reactor data and utilizing the speed and preciseness of response of the computer to approach closely, but not exceed, the established startup limits.

Integration of the three control systems in the ground test operating system has not been developed in much detail, in part because design of some of the systems has not progressed very far. The three systems interface with the segment drive system by means of the mode selector switch, which places the segment actuators under the control of the automatic controller, the computer, or the reactor operator. The operating information required by the automatic controller and the computer are supplied to these systems regardless of the position of the mode selector switch so that either system can be switched in at any time without generating inappropriate control commands.

Operation of the manual segment drive switches would automatically return complete control to the manual system. This facilitates the operator's actions should it be necessary to make corrections while off manual control. Manual adjustments could be made while remaining under automatic control by using the ground control telemetry input to the automatic controller.

In addition to the ground test operating system, for use under all normal circumstances, a ground test safety system is provided to rapidly remove reactivity if any of a variety of operating parameters exceed established limits. The ground test safety system is shown schematically in Figure 79.

Two different mechanisms are designed for rapid shutdown of the reactor. One of these is the normal scram, consisting of withdrawal of both segments at 5 steps/sec, resulting in a reactivity removal rate of -5.24¢/sec. Six means of initiating a normal scram have been designated and are shown in the figure.

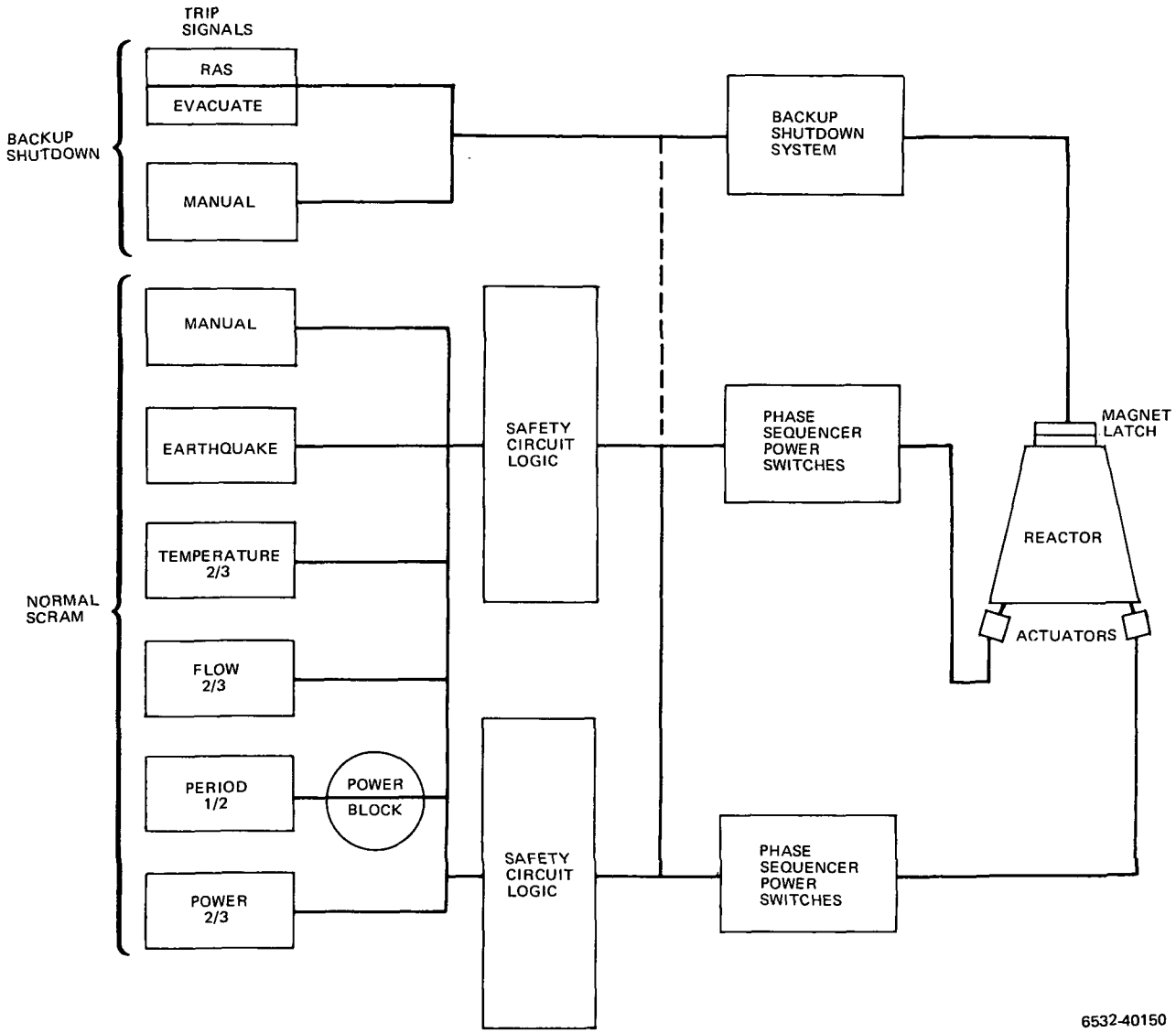

Figure 79. Ground Test Safety System

The manual scram switch provides the reactor operator with the ability to scram the reactor in anticipation of a hazardous condition or in case the appropriate automatic scram did not function quickly enough.

The earthquake switch provides a scram if the local ground motion becomes excessive. This trip point is level VII on the modified Mercalli scale.

High reactor outlet temperature is a symptom of several types of malfunctions which might lead to rupture of fuel cladding. Coincidence of two out of three channels is required to prevent spurious scrams resulting from sensor or instrument failure. This trip point has been tentatively set at 1250°F.

Partial or complete loss of primary system NaK flow can lead to the generation of unacceptably high fuel temperatures. A scram based on two-fold coincidence of three flowmeters is used to halt continued operation with inadequate flow. The minimum acceptable flowrate is a function of reactor power and has not yet been determined.

A short period is indicative of too rapid a power rise, which could lead to a power excursion or to severe thermal shock and gradients. Either of two channels provides a trip signal, but this is blocked at low power, where the normal reactor and instrument noise generates many false period signals, and also at high power, where the period trip offers little advantage over the power level trip. The recommended trip point is 10 sec in the power range of 10 w to 10 kw.

The power-level trip uses a two-fold coincidence of three reactor neutron power monitors. Setting the trip point at 125% of full power provides adequate maneuvering room for power and operating condition adjustments, so as to avoid inadvertent scrams, but sufficiently low to provide effective response to a power rise.

In the event of a scram, triggered by any of these causes, the segments are rapidly driven out by the actuators, powered by the scram controllers. The scram controllers are phase sequencer-power switch units adapted from the comparable units used in the control system. The modifications consist of: a faster cycle rate, providing 5 steps/sec instead of 1/sec; the capability to drive the actuators in one direction only; and the continuation of the sequence cycling until receipt of a termination signal. In addition, the scram controllers are

self-checking to provide immediate indication of failure in a unit. Periodic testing of each unit would be performed to check the units more thoroughly.

The backup shutdown system, which is an additional safety system intended for use only as a backup for the normal scram, is based on the EOL shutdown device of the flight configuration reactor. It consists of releasing magnetic latches that hold the radial reflector halves in place, and swinging the reflector halves 15 degrees away from the reactor. This removes $18 of reactivity in about 0.2 sec.

Prior to startup of the ground test system, each reflector half would be driven into position against the core by means of an air piston. Each reflector half would be held in position by two electromagnets, each one capable of holding the reflector against the gravitational and spring forces tending to swing the halves away. The driving piston would then be retracted. Release of the reflector halves would be caused by interrupting current to the holding coils.

It is expected that this mode of shutdown would be used only under circumstances so severe as to require evacuation of the facility and which would therefore not permit observation of reactor shutdown. The backup shutdown would be initiated by pressing a Manual Shutdown switch or the Evacuate switch. Activation of the Radiological Alarm System (RAS), which responds to excessive radiation levels in the facility, will also cause release of the reflector halves.

The backup shutdown mechanism has been reserved for this purpose because the more rapid reactivity removal provided has not been shown to be needed in the accidents that have been studied, and its use may generate undesirable mechanical stress in some of the components. Simulations have shown that the thermal stress following use of the backup shutdown mechanism is not significantly different from that following a normal scram. As shown by the dotted line in the schematic diagram (Figure 79), the backup shutdown mechanism may be connected to the automatic scram system, if necessary to provide adequate independence and redundancy in the safety system, for example.

REFERENCES

1. R. V. Anderson, "Performance Modeling of the 5 kwe Reactor TE, System," AI-AEC-13058 (April 3, 1973)

2. L. D. Felten and E. Moody, "Fuel Element and Core Bundle, 5-kwe Reactor Thermoelectric System," AI-AEC-13077 (June 1973)

3. A. H. Lillie, "ZrH Fuel Element Performance Characteristics," AI-AEC-13084 (June 1973)

4. W. J. Anderson, "Irradiation Creep Evaluation," ER-095-211-001 (April 1972)

5. "Compact Thermoelectric Converter System Technology, Quarterly Progress Report, November 1972-January 1973," (February 12, 1973)

6. "NaK Pump and T/E Converter Assembly Layout (Prototype)," R-N652330001A (May 1973)

7. "Environmental Design and Test Requirements for 5-Kwe ZrH Reactor Thermoelectric Space Power System," SS-652N170001A (June 1972)

8. "Space Nuclear System TE NaK Pump Development Summary," AI-AEC-13091 (June 1972)

9. "TE Pump Performance Analysis Computer Code," AI-AEC-13095 (May 1972)

10. V. Keshishian, et al, "Radiation Shielding for ZrH Reactor Systems," AI-AEC-13081 (June 1973)

NASA Supplementary Report Distribution List for
AEC Contract No. AT(04-3)-701
LERC Order Nos. C21029 and C-21030

NASA Lewis Research Center
21000 Brookpark Road
Cleveland, Ohio 44135
Attention: Martin J. Saari (15)
M. S. 60-6

NASA Lewis Research Center
21000 Brookpark Road
Cleveland, Ohio 44135
Attention: Leonard W. Schopen (1)
M. S. 500-206

NASA Lewis Research Center
21000 Brookpark Road
Cleveland, Ohio 44135
Attention: Norman T. Musial (1)
M. S. 500-113

NASA Lewis Research Center
21000 Brookpark Road
Cleveland, Ohio 44135
Attention: Librarian (2)
M. S. 60-3

NASA Lewis Research Center
21000 Brookpark Road
Cleveland, Ohio 44135
Attention: P. E. Foster (1)
M. S. 3-19

NASA Lewis Research Center
21000 Brookpark Road
Cleveland, Ohio 44135
Attention; G. Mervin Ault (1)
M. S. 3-5

NASA Lewis Research Center
21000 Brookpark Road
Cleveland, Ohio 44135
Attention: Robert E. English (1)
M. S. 500-201

NASA Lewis Research Center
21000 Brookpark Road
Cleveland, Ohio 44135
Attention: Henry O. Slone (1)
M. S. 501-6

NASA Lewis Research Center
21000 Brookpark Road
Cleveland, Ohio 44135
Attention: Donald Packe (4)
M. S. 500-201

NASA Lewis Research Center
21000 Brookpark Road
Cleveland, Ohio 44135
Attention: B. T. Lundin (1)

NASA Lewis Research Center
21000 Brookpark Road
Cleveland, Ohio 44135
Attention: B. Lubarsky (1)
M. S. 3-3

NASA Lewis Research Center
21000 Brookpark Road
Cleveland, Ohio 44135
Attention: Samuel J. Kaufman (3)
M. S. 49-2

NASA Lewis Research Center
21000 Brookpark Road
Cleveland, Ohio 44135
Attention: V. F. Hlavin (1)
M. S. 3-10

NASA Lewis Research Center
21000 Brookpark Road
Cleveland, Ohio 44135
Attention: Neal T. Saunders (3)
M. S. 105-1

NASA Lewis Research Center
21000 Brookpark Road
Attention: Report Control Office
Cleveland, Ohio 44135
Attention: A. P. Dill (1)
M. S. 5-5

NASA Scientific and Technical
Information Facility
Acquisitions Branch
Post Office Box 33
College Park, Maryland 20740 (10)

National Aeronautics and
Space Administration
Washington, D. C. 20546
Attention: P. R. Miller (3)
Code RNP

National Aeronautics and
Space Administration
Washington, D. C. 20546
Attention: D. S. Gabriel (2)
Code NS 2

Jet Propulsion Laboratory
4800 Oak Grove Drive
Pasadena, California 91103
Attention: Library (1)

National Aeronautics and
Space Administration
Geo. C. Marshall Space Flight Center
Marshall Space Flight Center,
Alabama 35812
Attention: Library (1)

NASA Flight Research Center
P. O. Box 273
Edwards, California 93523
Attention: Library (1)

NASA Ames Research Center
Moffett Field, California 94035
Attention: Library (1)

NASA Goddard Space Flight Center
Greenbelt, Maryland 20771
Attention: Library (1)

NASA Langley Research Center
Langley Station
Hampton, Virginia 23365
Attention: Library (1)

NASA Manned Spacecraft Center
Houston, Texas 77058
Attention: Library (1)

Atomics International Division
Rockwell International

P.O. Box 309
Canoga Park, California 91304